MICHAEL CHARLES HAROLD McKUBRE

An Impedance Study of the Membrane Polarisation Effect in Simulated Rock Systems

Submitted for the degree of
Doctor of Philosophy in Chemistry
at the Victoria University of Wellington,
November, 1976.

Contents

Figures

Tables

Appendices

Section

I

Introduction

CHAPTER 1 ABSTRACT

Work is reported on the development of a high precision, low frequency impedance bridge, and the use of impedance measurement in characterising the induced polarisation effect of unmineralised material.

Impedance spectra for a variety of laboratory model clay/rock/electrolyte systems are analysed in terms of an equivalent circuit. By measuring the dependence of the parameters of this circuit, on such variables as electrolyte type and concentration, temperature and pore geometry, an electrochemical model for membrane polarisation has been developed. Polarisation is considered to arise from diffusional limitation of cations at the membrane/electrolyte interface of clay aggregations in rock pores, and this is found to be amenable to a Warburg diffusional impedance analysis.

CHAPTER 2 INTRODUCTION TO THESIS

2.1 INDUCED POLARISATION

2.1.1 Introduction

The purpose of this thesis is to examine the electrical mechanism of a geophysical phenomenon known as induced polarisation, or the "I.P." effect. This effect appears in the frequency domain as a frequency dependence of the "resistance" of soils and rock strata. In more conventional terms the electrical impedance between two points on the ground surface contains a significant reactive component. In the time domain, I.P. is characterised by the decay of a secondary voltage between one pair of electrodes, following the interruption of a ground current passed through adjacent electrodes. Although a time constant is often assigned, this secondary decay is not exponential and attempts have been made to fit empirically the voltage-time curves (197,104). The phenomenon is observed to occur over times of the order of seconds or tens of seconds.

Provided the medium is linear (130), time and frequency domain observations are mathematically equivalent, through the Fourier Transform.

This polarisation effect was known to Schlumberger (177) as early as 1912, and called by him "provoked polarisation". When attempting to use this effect to prospect for metallic ores he believed to be responsible for it, Schlumberger found that the effect of wet soils interfered substantially with the effect he expected from metallic sulfides. In conformity with this observation, two distinct mechanisms are known to be responsible for induced polarisation.

2.1.2 Electrode Polarisation

The most pronounced I.P. effect in geologic materials is the polarisation which occurs in rocks containing disseminated metallic or semi-conducting minerals. An electrode reaction is considered (129) to occur at the interface between pore blocking grains of electron

conductive material* and the pore electrolyte, giving rise to the observed polarisation.

Induced polarisation is a powerful prospecting tool and has been used since about 1950 primarily to prospect for metallic sulfide bodies. While the electrochemical mechanism is far from comprehensively understood, individual grains are considered to behave as polarised electrodes having an associated Warburg diffusional impedance and double layer capacitance, from which the measured impedance dispersion or secondary voltage decay, arise.

2.1.3 Membrane Polarisation

The polarisation process which arises in moist soils is found to be virtually ubiquitous (134) but is rarely of the same order of magnitude as the I.P. effect of commercially significant metallic sulfide bodies. Mayper (134) has shown that the background or "normal" effect of non-mineralised regions is associated with the presence of clays. Marshall and Madden in a series of papers (127,128,129,130,131) have demonstrated that the I.P. effect of clay-electrolyte systems results from their membrane properties, and that commercial ion exchange resins can be made to display an I.P. effect which is larger than but similar in form to that of clays.

Despite substantial experimentation over a period of decades, a satisfactory electrochemical model for the polarisation effect of clay-containing soils has yet to be proposed and experimentally justified. It is the purpose of the present work to study exclusively the membrane polarisation phenomenon associated with clay/rock/electrolyte model soil systems, in an attempt to elucidate the electrochemical mechanisms.

---

* Electron conductors include not only metallic sulfides but also graphite, magnetite and pyrolusite, which are all observed to give a similar I.P. effect (130).

2.2 GEOPHYSICAL PARAMETERS

2.2.1 Introduction

A number of parameters have been evolved to describe both frequency and time domain data. Each describes a particular property of the response of a system, although none accurately describes the I.P. effect. Nevertheless single valued parameters are used exclusively in geophysical prospecting and in the geophysical literature, and a brief description of the most common must be given.

2.2.2 Time Domain

The I.P. effect observed in the time domain has the form shown in Figure 2.1.1, and is associated with three parameters

1) The ratio of the secondary voltage at time $t = t_o$, to the primary voltage; expressed in milli-volts per volt (mV/V).
2) The ratio of the area under the decay curve to the primary voltage. This is known as the polarisability and is expressed in milli-volt seconds per volt (mV-s/V).
3) Despite the non-exponential form of the decay, a time constant is often assigned, being the time taken for the secondary voltage to reach 1/e of its value at t_o.

2.2.3 Frequency Domain

The precise form of the impedance dispersion is not known, however at the limits of both high and low frequency the reactance tends to zero (see Figure 2.1.2).

$$R_{High} = |Z|_{f\to\infty},\ R_{Low} = |Z|_{f\to 0}$$

$$R_{High} < R_{Low}$$

Three parameters are commonly derived from these limiting resistances.

FIGURE 2.1.1 Time Domain I.P. Effect

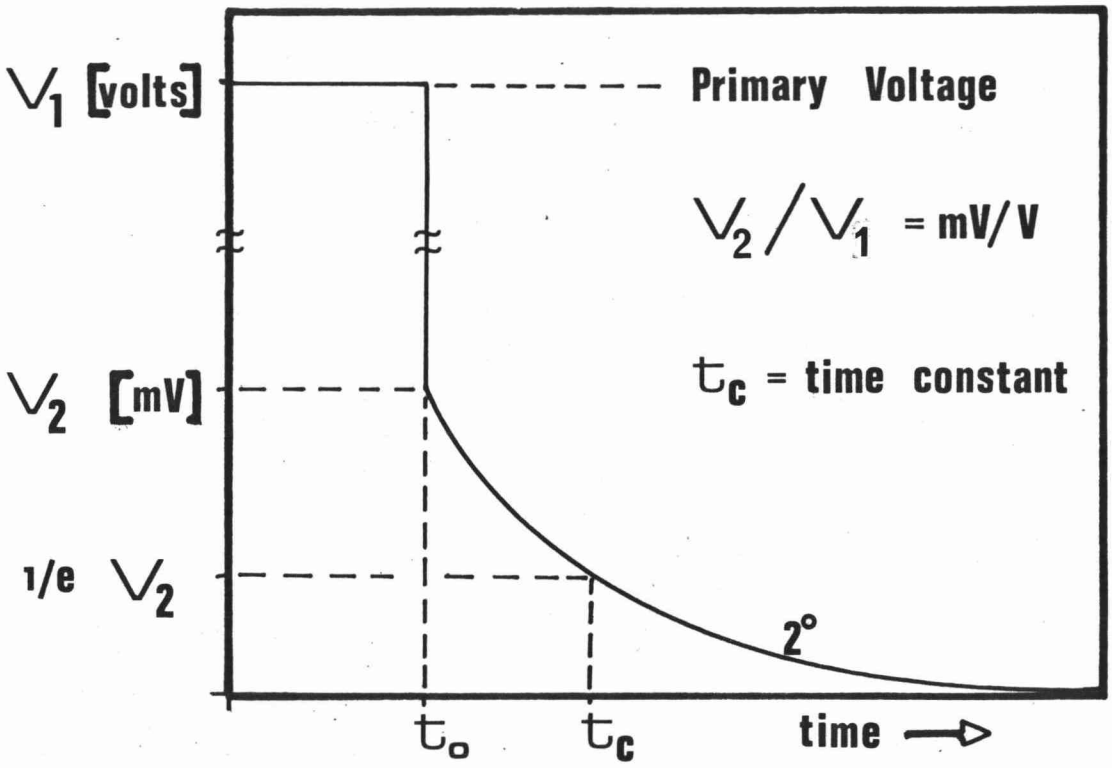

FIGURE 2.1.2 Frequency Domain I.P. Effect

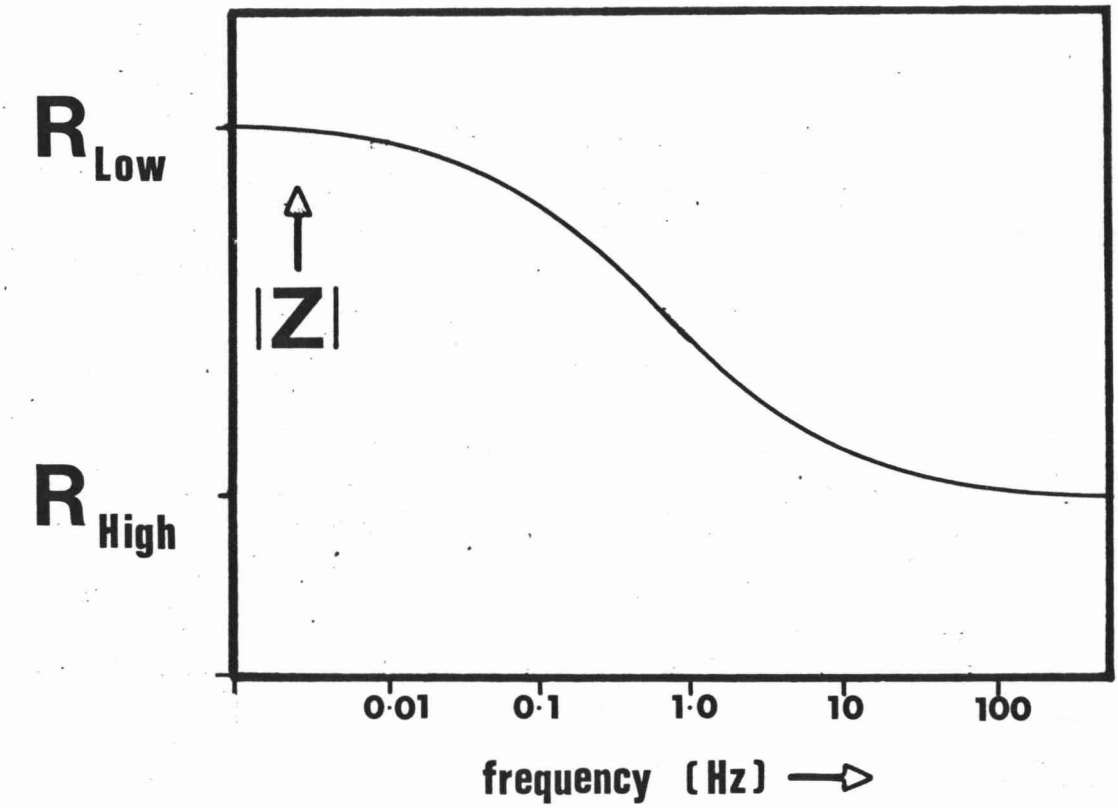

1) The "frequency effect", defined as,

$$F.E. = (R_{Low}-R_{High})/R_{Low}$$

In practice the "resistances" are often measured at two frequencies for which the impedance need not have a limiting value.

2) The percentage frequency effect defined as the decrease in the impedance at frequency f, from the limiting low frequency value. Thus,

$$\% \text{ F.E.} = 100(R_{Low}-|Z_f|)/R_{Low}$$

3) The frequency effect and % F.E. have the significant disadvantage of being dependent on the shunt electrolyte resistance of unblocked pores. The metal factor is defined to decrease this dependence.

$$\begin{aligned} M.F. &= 2\pi x10^5 \ (G_{High}-G_{Low}) \\ &= 2\pi x10^5 \ (R_{Low}-R_{High})/(R_{Low})(R_{High}) \\ &= 2\pi x10^5 \ (F.E.)/R_{High} \end{aligned}$$

where $G = 1/R$

2.3 GEOPHYSICAL LITERATURE

2.3.1 Introduction

A comprehensive historical bibliography of the literature relating to laboratory investigations of the electrical properties of clays, and of the membrane polarisation effect of clay and model clay systems has been previously published (McKubre 1972). The material covered in that review is of little more than historical significance since, without exception, workers in this field have attempted to characterise the observed induced polarisation using single valued parameters.

There is however a substantial body of work. Many models have been proposed, and the dependence of a variety of parameters on physical variables examined. In order to place the present work within the context of previous studies it is intended to examine briefly the models that have been proposed for the induced polarisation of non-metalliferous materials. A large body of material relating to clay

membranes, clay resistance and self potential is of only peripheral interest and has been discussed previously (137).

2.3.2 Models for Induced Polarisation

These divide naturally into two categories according to whether the models are associated with the presence of clays (models 4 to 8), or not (models 1 to 3). In an attempt to distinguish between these categories, several models which do not require the presence of clay were adumbrated by Mayper (134), as follows.

1) "Surface Conduction" due to distortion of lattice potentials and hence electron band conduction at the surface of solids could, according to Mayper, lead to electrodic over potentials.

2) The Electrokinetic Effect of Air Bubbles was observed by Mayper to produce "erratic" relaxation phenomena.

3) The Poor Conductor Hypothesis is based on the assumption that the electronic conductivity of minerals usually regarded as insulators is actually sufficient to create overpotentials.

Mayper found that the I.P. effect was strongly correlated with the presence of clay minerals. The I.P. response of clay-containing core samples was found to become unmeasurably small after firing, and Mayper was not able to measure any relaxation having a magnitude corresponding to the I.P. effect of clay-containing core samples, for specimens which did not contain unfired clay. These results strongly support field observations that the I.P. effect is exclusively associated with the presence of electron conducting particles or moist clays (106). Thus, by confining the region of interest to effects of geophysical significance it is not unreasonable to reject models (e.g. 1 to 3) which do not associate membrane polarisation with the presence of clays.

4) The Ion Exchange Disequilibration Model was advanced by Vacquier *et al* (197) and by Schufle (179), and was favoured by Mayper (134) simply on the basis that it required the presence of clay. It is assumed that the passage of current through a clay/rock/electrolyte system electrodialyses the clay - that is causes the exchange reaction

of cations on exchange sites with cations from the electrolyte. This reaction may be written as

$$M^+(\text{exchange site}) + N^+(\text{electrolyte}) \rightleftharpoons N^+(\text{exchange site}) + M^+(\text{electrolyte})$$

In the time domain, a steady state condition is approached which differs from the initial equilibrium condition, so that when the current is interrupted, the relaxation of the system to equilibrium gives rise to potentials which are observed as induced polarisation.

This model requires the presence of two different cations, and thus a system containing homo-cationic clay and electrolyte ($M^+ = N^+$), should not display an I.P. effect. However, Vacquier measured a significant time domain I.P. effect for the homo-cationic system, hydrogen form kaolinite/quartz sand/HCl, which he attributed unjustifiably* to clogging of the kaolinite exchange positions by Al^{3+} ions (197). Both Schufle (179) and McKubre (137) have observed appreciable I.P. effects for homo-cationic ion exchange resin/electrolyte systems, which are inconsistent with Vacquier's model.

5) The Dipole Layer Relaxation Model advanced by Henkel and Collins (91) postulates a layer of oriented dipoles (the nature of which is not specified) on the surface of the clay. Rotation of the dipoles within this layer results in a form of localised dielectric dispersion (see section 3.4), and Henkel and Collins have developed a mathematical expression for the resultant polarisation. This derivation is based on an unreasonable assumption of reversibility for the dipole orientation process, but the prime objection to this model is that any rotational polarisation which occurs in a fluid medium (such as the diffuse double layer) will display a characteristic frequency greater than 1 M Hz, and thus outside the frequency range of the I.P. effect.

Measurement of the time domain I.P. response of soil samples by Henkel and Collins yield results which do not support their model.

---

* Vacquier's results require about 33% of the exchange sites to be occupied by Al^{3+}, but according to Mukherjee *et al* (148) kaolinite is only "slightly" susceptible to clogging of its exchange site.

6) The Elementary Clay Conductor Model. Henkel and Collins proposed a second model in which they treat the problem on a macroscopic scale. They consider clay to be an "electrical conductor" and that electrolyte saturated earth plugs represent two conduction paths. One path lies within the electrolyte and the other in the clay but having an interface with the electrolyte (92 , 211). The latter path is arbitrarily considered to involve a 90° phase shift of the current at the electrolyte-clay interface. Polarisation results from the effective charge storage in the imaginary component of the current.

The origin of a 90° phase shift is not specified and is difficult to account for electrochemically. Even supposing the existence of a large double layer capacitance, resistive shunts within the double layer would reduce the phase angle from 90°. In fact the model does not explain the mechanism of induced polarisation but merely characterises the effect in terms of an oversimplified two element equivalent circuit.

7) The Coupling of Flows. Dakhnov (55) proposed a model for the I.P. effect in unmineralised bodies based on coupling of the flows of electrolyte and electric current (electro-osmosis). Polarisation originates (in the time domain) as a streaming potential created by the inertia of the moving electrolyte. Mayper (134) dismisses this model because "the time constants would be far too long to explain the present phenomenon". Marshall and Madden (128, 130) have systematically evaluated the coupling of flows employing a set of phenomenological equations based on the coupling of heat, solvent and ion flows under the driving forces of temperature, pressure and electrochemical potential gradients. From the calculated coupling coefficients they conclude that only diffusion coupling could produce polarisation of the magnitude observed for I.P. The coefficients for electro-osmotic and thermo-electric coupling are calculated to be too small, thus ruling out Dakhnov's model.

Recently Mehran (139) has re-examined the correlation between electro-osmosis and the electrical dispersion observed for compacted illite and kaolinite systems equilibrated with NaCl electrolyte. Electrical measurements were conducted in the frequency domain and a "conductivity" dispersion* was observed to occur in the frequency range

---

* The conductivity dispersion parameter is defined by Mehran as $1-G_{High}/G_{Low}$, where G_{High} and G_{Low} are the limiting high and low frequency conductivities.

10^3 to 10^7 Hz. This is four orders of magnitude higher than the effect observed for moist soils but the dispersion is observed to have a form compatible with induced polarisation. Mehran uses the phenomenological approach of irreversible thermodynamics to derive an expression for the conductivity dispersion based on electro-osmotic coupling. From separate measurements of the electrical and electro-osmotic properties he concludes that for systems as microporous as compressed clays, the contribution of electro-osmotic coupling to the electrical dispersion is significant. However, for clay/rock/electrolyte systems having a relatively open pore structure, the contribution of such a coupling of flows to the effect known as induced polarisation, is probably negligible.

8) Alternating Transference Zones. Based upon their conclusion that only diffusional coupling could account for the I.P. effect, Marshall and Madden and coworkers (127, 128 , 129 , 130 , 131) proposed the model shown in Figure 2.2.1. Polarisation results from the difference in cation transport number (t_+) between zones I containing electrolyte ($t_+ \approx 0.5$) and zones II which are cation selective ($t_+ \approx 1$), pore blocking clay zones. Using the formalism of irreversible thermodynamics these authors develop a mathematical expression for the impedance assuming all selective zones to have identical properties (length, t_+, cation diffusion coefficient), and all non-selective zones to have identical properties. The expression is extremely complicated (137) and contains four independently adjustable parameters relating to the membrane phase (II), which are operationally defined by the model itself, and are therefore indeterminate.

Fredricksberg (73) and Keller *et al* (5, 103, 104, 105, 106) have separately proposed a similar model based on the presence of selective transference zones. Rather than the cation selectivity arising within a pore completely blocked by clay, both consider the anion mobility to be reduced in regions where constrictions in the rock pores cause the double layers on opposing walls to overlap. Keller considers this to arise from the double layer of clay particles adhering to the rock, and Fredricksberg considers the origin to be the double layer of the rock itself (see Figure 2.2.2). Anions cannot enter the double layer because of the coulombic repulsion force of fixed negative charge, and after a prolonged unidirectional current a

FIGURE 2.2 Alternating Transference Zone Models

2.2.1 MARSHALL and MADDEN

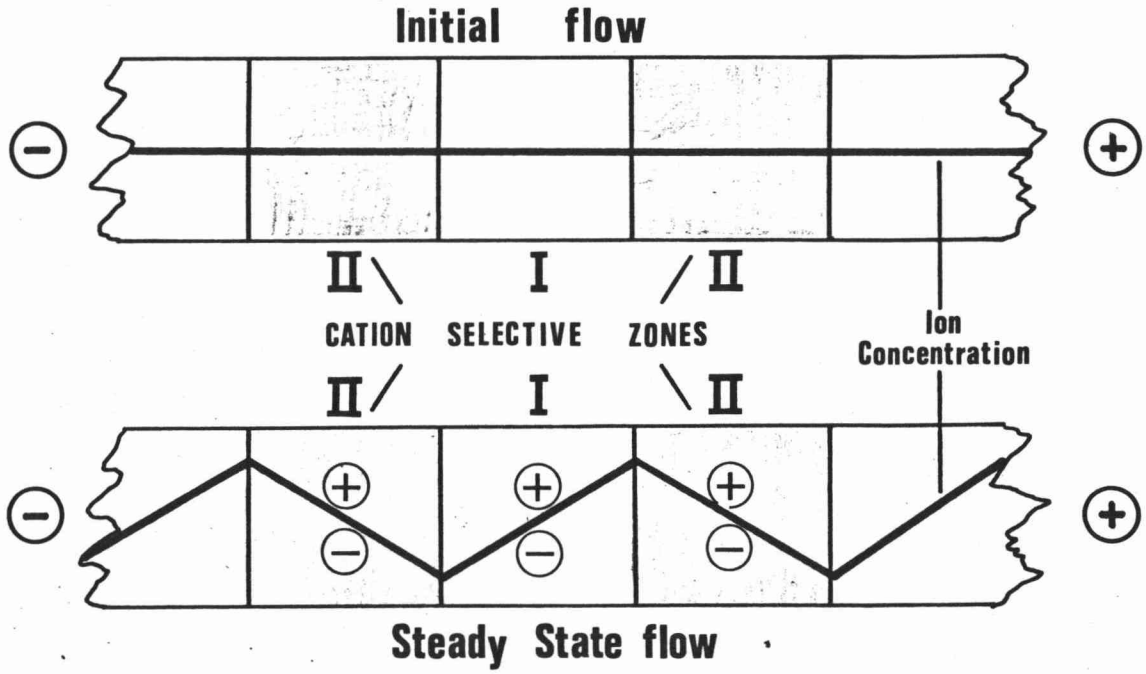

2.2.2 KELLER and FREDRICKSBERG

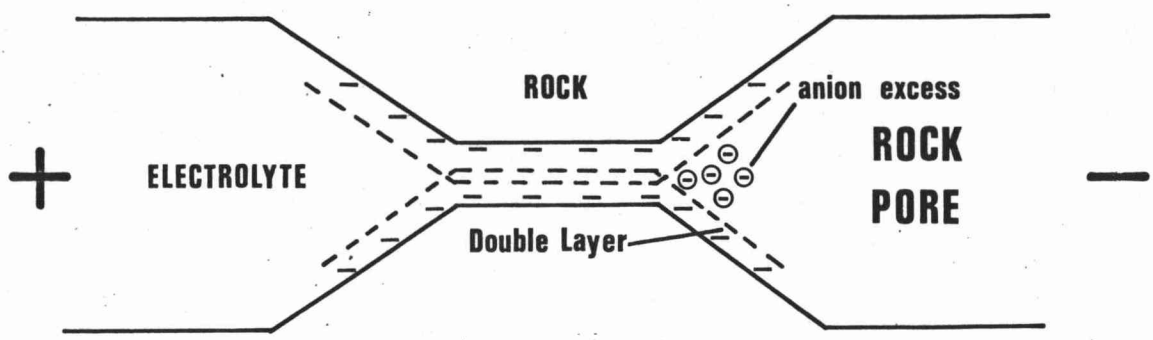

In Keller's model the double layer arises from clay adhering to the rock pore walls. Fredricksberg ascribes the double layer to the rock itself.

concentration excess will arise. When the current is interrupted this concentration excess will relax, accompanied by a secondary voltage decay. Both authors develop mathematical expressions for the time domain I.P. effect, and Mohomed (143) has demonstrated from measurements of the polarisability of sandstone samples that Fredricksberg's model is not inconsistent with experimental results.

Models based on double layer overlap require an effectively complete blockage of some pores so that anions cannot immediately diffuse around the double layer periphery, and a concentration excess can arise. Since the diffuse double layer is likely to be of the order of 10^{-7} m thick (50), such a constriction within a rock pore is not unreasonable, however a major limitation of the models of Keller and of Fredricksberg is that they fail to predict the I.P. effect observed for beds of spherical ion exchange resin particles up to 10^{-3} m in diameter saturated with electrolyte. Large I.P. effects have been observed for such beds (130, 137, 179), in which the pores are very large with the double layer likely to occupy only a small fraction of the pore cross sectional area, and for which the effective reduction of anion transport number due to double layer overlap will be insignificant. This criticism does not apply to the model proposed by Marshall and Madden and for a bed of ion exchange resin particles, an effective reduction of anion transport number can occur in a manner similar to that proposed for pore-blocking clay zones. Since anions are excluded from within cation exchange resin particles (i.e. they are cation selective), all paths which involve conduction within both the electrolyte and resin phases fulfill the condition of alternating transference zones required by Marshall and Madden's model.

2.3.3 Discussion

Sufficient information is available from the literature to justify laboratory experimentation on carefully selected model clay systems, in order to elucidate the mechanism of the membrane I.P. effect. However, the models described in this section, which have been proposed to describe the I.P. effect, contribute little to the understanding of the underlying mechanism and may be grouped under two general categories.

A) Models found to be inconsistent with experiment

1) Surface Conduction
2) The Electrokinetic Effect of Air Bubbles
3) The Poor Conductor Hypothesis
4) The Ion Exchange Disequilibrium Model
5) The Dipole Layer Relaxation Model
7) The Coupling of Flows

B) Models which cannot be tested because of mathematical inexactitude

6) The Elementary Clay Conductor Model
8) Alternating Transference Zones

The purpose of a model is to allow the prediction of properties of interest from the known behaviour of a system. Clearly none of the above fulfil this basic requirement, the models being too vague and imprecise in their prediction. However, the models listed under category B will be discussed in Chapter 10 with reference to results of the present study. While it would be possible, at this stage to propose an indefinite number of further electrochemical models, without a basis of experimental observation, this process is not useful.

2.4 STRUCTURE OF THESIS

In order to study the mechanism of membrane polarisation it is necessary to employ simple systems and to observe the dispersion over a wide range of frequencies (or times). Unless an equivalent circuit is known, the single valued parameters used to describe the I.P. effect have no significance.

This thesis is therefore of an exploratory nature, and the development of an electrochemical model will be based on the results of a large number of experiments measuring the effects of physical variables on the induced polarisation. This approach is reflected in the structure of the thesis. Experimental results are presented to develop a model rather than to prove one, and it is not intended mathematically to examine the parameters of the equivalent circuit developed further than is necessary to show this to be physically reasonable.

The thesis is divided into four parts as follows.

Section I contains introductory material.

Section II contains the primary objectives of this work. Simple laboratory clay and model clay systems were developed which display an effectively identical membrane polarisation effect to that observed in moist soils. In addition a system was developed capable of measuring and accurately characterising the membrane polarisation of these cells.

Section III involves the development of an equivalent circuit by which the membrane polarisation effect may be described. From this, information may be obtained about the dependence of the I.P. effect on electrolyte type and concentration, particle size, clay type, and temperature.

Section IV provides a basis from which the ultimate objective of this research may be obtained. That is to develop a comprehensive electrochemical model which describes the effects of all physical variables on the membrane polarisation effect, not only of laboratory systems but of the real earth.

2.5 PRACTICAL JUSTIFICATION

Apart from a fundamental electrochemical interest in this phenomenon, an understanding of the membrane polarisation effect is of significance in the field of exploration geophysics for several reasons.

1) Present I.P. mineral prospecting techniques cannot differentiate between electrode (mineral) and membrane (clay) polarisation. If the mechanisms are different then it may be possible to remove the background effect due to the presence of clays. This would effectively increase the sensitivity of I.P. surveys and allow hitherto undetectable mineral deposits to be prospected for.

2) I.P. surveys have been successfully conducted to find ground water (197, 143), utilising the observation that wet clays have a considerably larger I.P. effect than dry clays. A greater understanding of the origin of this polarisation would aid in prospecting for water and for clays.

3) As stated in section 2.4, in the absence of an equivalent circuit, the significance of the parameters conventionally used to describe the I.P. effect, is limited. Such a circuit should therefore be developed.

4) The properties of a hydrothermal zone which make it suitable for power production are high temperature and high porosity. In addition the ground water has a high salt content and thus resistivity surveys are highly suitable as a method of prospecting for such zones (89). If a model for the I.P. response of clay/electrolyte systems could be extended to temperatures and pressures of the order of those found in geothermal regions, it is possible that a significant impetus could be given to prospecting for exploitable steam reservoirs.

CHAPTER 3 ELECTROCHEMICAL POLARISATION

3.1 INTRODUCTION

A number of electrochemical systems are known to display a conductance which is not independent of the applied frequency. This variation or dispersion of an electrical property may be mathematically represented by defining an impedance having variable real and imaginary components; and by using a variety of techniques (10, 80) this impedance may be measured as a function of frequency.

The first step in the elucidation of an electrochemical mechanism from a measured impedance dispersion is generally to postulate an electrical circuit with the same impedance spectrum as the system under test. All circuit representations, even those from which prediction of measurable results is possible, only fulfill the role of an equivalent circuit, and are not a description of the physical mechanisms involved. For any electrical circuit it is possible to describe the impedance as a function of frequency and thus determine circuits having equivalent electrical properties, but it is not possible to define uniquely the combination of electrical circuit elements which constitute the circuit under test by making two terminal impedance measurements. For electrochemical systems the situation is further complicated since the charge carriers may be ions and not electrons. Ions may carry a positive or negative charge and may be multivalent, and ionic transport is influenced by chemical as well as electric field gradients. It is possible therefore that an electrochemical impedance be composed of electrically non-ideal circuit elements.

Nevertheless, no case has been found for which the equivalent circuit concept has been demonstrated to be fallacious (85). By measuring the dependence of the parameters of an equivalent circuit on physical and chemical properties, a mechanistic significance may be placed on such a circuit, and a variety of polarisation mechanisms are known to operate in electrochemical systems.

Specifically, polarisation relates to a storage of charge, and thus any system in which the current (i.e. the ion flux) lags or leads the potential gradient may be said to polarise, and a dispersion of

impedance will arise. Polarisation may arise within a homogeneous material, because of inhomogeneities within the bulk of a material, or at a macroscopic discontinuity or phase boundary. There are three distinct categories of polarisation known to be significant within electrolyte systems.

1) Electrode Polarisation
2) Membrane Polarisation
3) Dielectric Polarisation

These will be discussed in turn as mechanisms possibly contributing to the I.P. effect observed in clay/rock/electrolyte systems.

3.2 ELECTRODE POLARISATION

Experimentally, the most familiar form of polarisation in electrochemical systems arises at a metallic electrode/electrolyte interface when current is passed across such an interface. In the steady state D.C. case, the potential ε of an electrode through which current flows differs from the equilibrium potential ε_o established when no current passes through the electrode. The difference between these potentials

$$\Psi = \varepsilon - \varepsilon_o$$

is described as the overvoltage (40 , 201) and opposes the applied E.M.F. thus increasing the effective cell impedance.

Electrode polarisation is of significance when considering the I.P. effect of non-mineralised as well as mineralised rock/electrolyte systems, and will be discussed briefly.

A number of separate mechanisms contribute to the phenomenon known as electrode polarisation, and these have been comprehensively described by Grahame (85) and others (169, 120), and reviewed by Vetter (201). Very briefly, electrode polarisation arises because the electrode reaction by which current flows from ionic carriers in the electrolyte phase to electronic charge carriers in the metallic electrode phase, cannot occur instantaneously. Any of a number of processes may impede the flow of charge resulting in the current lagging the potential gradient, and thus polarisation. The most familiar of these are,

1) Diffusion of material to or from the electrode,
2) Reaction at the electrode,
3) Transfer of charge to the metallic phase.

The electrode impedance is commonly represented by an equivalent circuit of the form shown in Figure 3.1, although others have been proposed (119,120).

Figure 3.1 Electrode Impedance

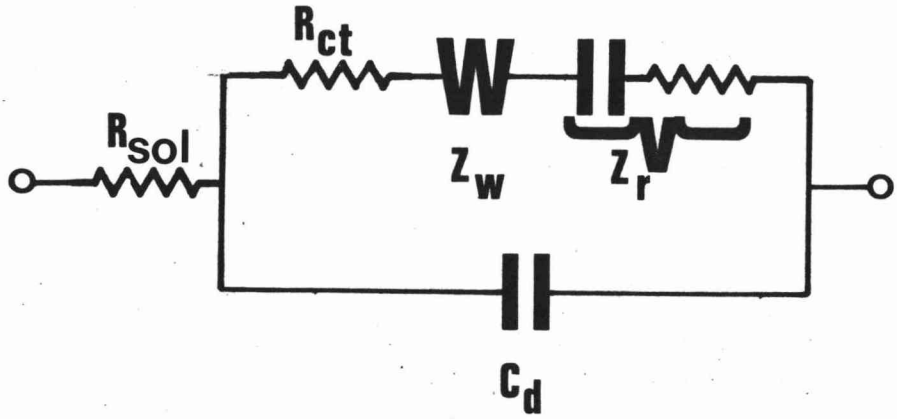

The impedances arising from diffusion (Z_w), reaction (Z_r) and charge transfer (R_{ct}) appear in series, shunted by the double layer capacitance (C_d) which arises because of the effective separation of charge in the electrical double layer at the electrode/electrolyte interface. R_{sol} is simply a term for the (ohmic) migration resistance within the bulk electrolyte phase. Of these impedances only R_{ct} and Z_r cannot contribute to the impedance dispersion associated with the I.P. effect of clay/rock/electrolyte systems,* and Z_w and C_d will be considered in detail in subsequent chapters.

---

* A membrane I.P. effect has been observed for systems containing homoionic clay (or ion exchange resin) and electrolyte for which no chemical reaction, and thus no charge transfer, can take place (130, 137, 179).

3.3 MEMBRANE POLARISATION

3.3.1 Introduction

Investigations of the resistance and capacitance of biological materials as early as 1910 (96) have indicated that these materials display a dispersion of impedance not dissimilar to electrode polarisation. Measurements on materials as diverse as Muscle Tissue (75) and Frogs Eggs (47), and those by Cole *et al* on the biologically significant Squid Giant Axon (43, 44 , 45), have all indicated a similar dispersion. The equivalent circuit shown in Figure 3.2 was proposed by Cole (42) to describe the observed electrochemical impedance, but the underlying mechanism was not apparent to these authors.

Figure 3.2 Biological Membrane Impedance

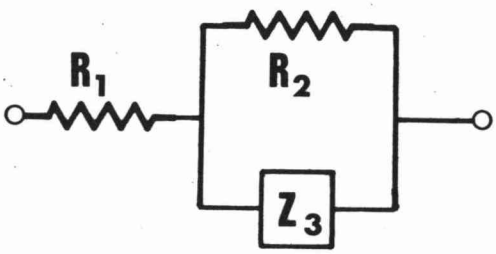

$Z_3 = R + jX$

$-X/R$ = a positive constant

More recently studies on ion selective electrodes, both glass (31 , 32 , 37 , 38 , 39) and liquid ion exchanger (30 , 31), have indicated a similar form of impedance dispersion to that displayed by biological membranes. For both systems the impedance locus* has the form shown in Figure 3.3, of a distorted semi-circle with centre below the real axis.

The systems displaying this impedance dispersion may be collectively described as membranes, and all consist of a phase containing fixed charges of one sign together with mobile counter ions, separating electrolyte phases. These systems will thus exhibit membrane and Donnan potentials (65 , 201) and will display the membrane property of semi-permeability due to exclusion of the co-ions from the membrane phase.

---

* The real plotted against the imaginary component of the impedance.

FIGURE 3.3 · Impedance Locus for Glass Electrodes after BUCK and KRULL

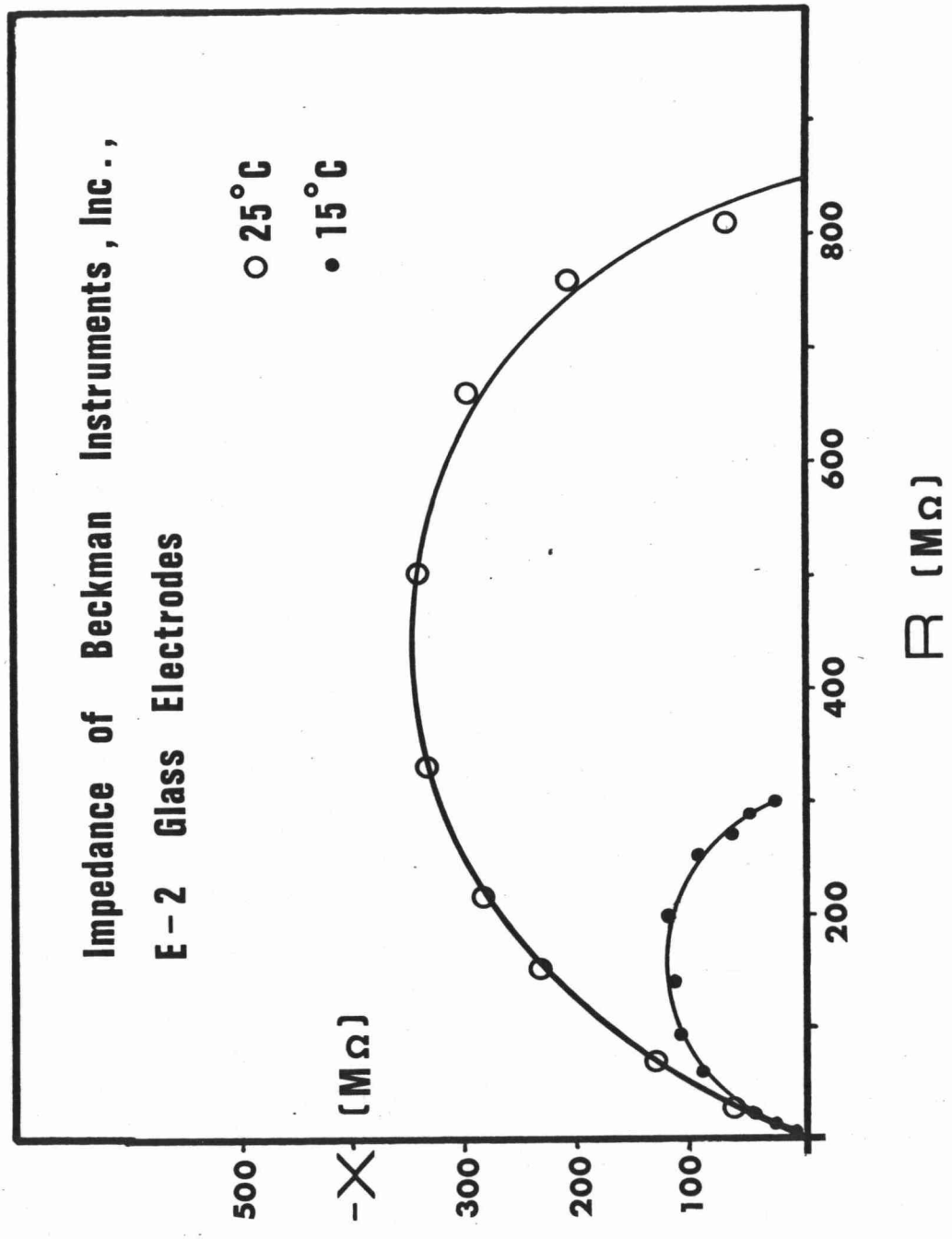

3.3.2 Equivalent Circuit

On the basis of impedance measurement the equivalent circuit shown in Figure 3.4 was proposed by Buck (38 , 39), for the bulk glass impedance (excluding the hydrated surface layer) of glass electrodes

Figure 3.4. Glass Electrode Impedance

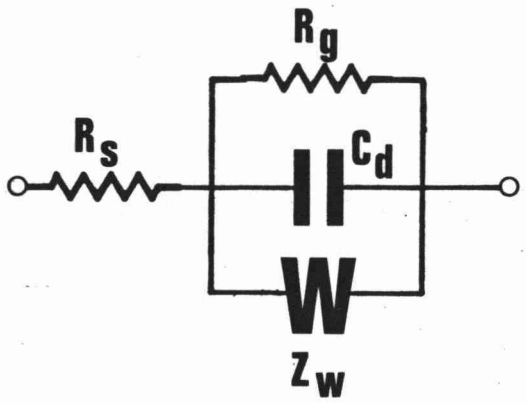

R_s is the solution resistance and R_g the limiting low frequency glass resistance. C_d is the double layer capacitance and Z_w a Warburg diffusional impedance, as for electrode polarisation (Fig. 3.1).

A similar circuit was found by Brand and Rechnitz (31, 32) to apply to a variety of glass electrodes, but for liquid-membrane electrodes (30) these authors found that the frequency dependent component did not show a Warburg-like impedance behaviour (85). The latter effect is possibly due to stray or double layer capacitive effects which Brand and Rechnitz ignore, however their data is of insufficient precision adequately to characterise an equivalent circuit.

Buck in a subsequent publication (173) observed two distinct dispersion processes for glass electrodes. One he attributes to "a slow surface process", and the other to a relaxation mechanism within the glass phase characterised by a distribution of RC time constants (see section 3.4). Buck maintains that a Warburg diffusional impedance is not observed at frequencies down to 0.01 Hz, but purports to base his model on the theoretical considerations of MacDonald (119, 120) in which a diffusional impedance is considered to be of significance particularly at high frequency. Buck loosely described an equivalent circuit based on MacDonald's (119, 120) theoretical considerations for

Electrode Polarisation and on empirical fit of impedance locus plots to the model of Dielectric Polarisation proposed by Cole (48). He does not however, adequately consider the implications and limitation of applying these theories to an essentially membrane system, and the experimental justification is far from conclusive.

In a previous attempt to describe the membrane polarisation effect of glass electrodes, Buck (48) considered the membrane phase to be composed of a concentration of fixed anionic sites and mobile cations from the glass and electrolyte phases. Using the Nernst-Planck equations he determines the transient potential-current-time profiles after the manner of Helfferich (90). A general analytical solution is not given except under certain simplifying conditions, and a strict transform into the impedance domain has not been performed. Neither is the impedance data of sufficient precision to accurately describe an equivalent circuit, and the mechanism for this form of polarisation is far from understood.

There is some evidence to suggest that ion exchange resins display a similar impedance dispersion (23, 156), but comprehensive studies have not apparently* been performed.

3.4 DIELECTRIC POLARISATION

3.4.1 Relaxation Processes

The forms of polarisation so far discussed arise primarily because of the presence of a phase boundary, or discontinuity of a transport property. Dielectric polarisation however is a bulk property of matter and originates because atoms or molecules in an electric field alter their mean electric configuration to oppose the applied field. In addition to the current due to the flow of free charge, current flows in a dielectric material because of the oscillation of the electrical configuration of the constituent atoms or molecules. The extent of the contribution to the total current due to bound charge is determined by the permittivity (or "dielectric constant") ε. This oscillation however

---

* These studies have been made in Russia, and information regarding experimental techniques and results, is limited.

is a relaxation process occurring with a characteristic relaxation time constant (or characteristic frequency), and ε is not a constant for a particular material, but is markedly frequency dependent. This is best explained by considering the mechanisms which contribute to dielectric polarisation.

1) Debye: The rotation of polar molecules results in a polarisation. This was first treated by Debye (59), who assumed the rotation of spherical polar molecules in an A.C. field to be opposed by the effects of thermal agitation and viscous damping. In order to express the resultant frequency dependence, a complex permittivity was defined

$$\varepsilon = \varepsilon' + j\varepsilon'' = \varepsilon_\infty + (\varepsilon_o - \varepsilon_\infty)/(1+j\omega\tau_o) \qquad [1]$$

where ε_∞ and ε_o are the limiting high and low frequency permittivities

τ_o = relaxation time

ω = angular frequency

2) Debye-Falkenhagen: Upon application of an A.C. field the ionic atmosphere about a central ion will oscillate. Dielectric polarisation resulting from this was treated first by Falkenhagen (69).

3) Maxwell-Wagner: The Debye and Debye-Falkenhagen effects relate to homogeneous materials, but dispersion can also occur in an inhomogeneous dielectric. Such a dispersion occurs in a double layer dielectric if the ratio of the conductivities and permittivities of the two separated phases, are not equal. Wagner (205) has mathematically treated the case of spheres dispersed in a uniform dielectric medium. The resultant complex permittivity has the same form as equation [1].

4) Non Localised Diffusion: In addition it has been pointed out recently (147) that there are electrical relaxation effects associated with long-range ionic diffusion processes which may lead to an observable dispersion in the permittivity. This process has been called Non Localised Diffusion (in contrast to Maxwell-Wagner dispersion which is a localised diffusion process) and is divided into two relaxation phenomena, NLD I and NLD II, which occur at low and high temperatures respectively (152,153).

NLD involves the movement of free charges and is associated with a leakage current. In contrast Maxwell-Wagner, Debye and Debye-Falkenhagen

dispersion represent purely localised translational or rotational relaxation. In the classical sense a dielectric material supports an electric polarisation vector due to the presence of oscillating fixed charge, and it is difficult to see why NLD should be treated as a dielectric process.

In highly fluid materials all these relaxation processes occur at high frequencies ($>10^6$ Hz) and are thus of no interest in this work. In solids and viscous liquids however relaxation has been observed with time constants greater than one second, and much research has been carried out to characterise dielectric relaxation processes particularly in glasses of varying composition (95, 121, 152, 153, 167), low temperature electrolytes (121, 147), ice (47, 48, 58, 82), organic solvents (82, 146, 207) and organic solids (47, 149, 184). Relaxation processes in these materials may occur at very low frequencies, and Namikawa (152, 153) has identified NLD and Maxwell-Wagner relaxation occurring in oxide glasses with τ_o as large as 10^2 or 10^3 seconds.

It is important to distinguish between the observed dielectric dispersion process which occurs in dry glasses, and the membrane polarisation phenomenon which occurs for glass electrodes. In the former, the ions which relax rotationally or translationally are the cationic components of the glass quasi-lattice, and the phenomenon occurs throughout the bulk of the glass. For glass electrodes, conduction is primarily by cations from the electrolyte phase which enter the glass (or membrane phase) and diffuse normal to the interface. In this case the dispersion process is not a bulk property of the glass, and the relaxational process is expected to be associated with the diffusion of electrolyte derived cations within a region of limited thickness. Both these dispersion processes occur with characteristic frequencies of the same order of magnitude as those observed for the I.P. effect of clay/rock/electrolyte systems, and may be significant contributary mechanisms to such polarisation.

3.4.2 Equivalent Circuit

The equivalent circuit for dielectric dispersion is shown in Figure 3.5.1, which is a circuit representation of equation [1].

Figure 3.5.1

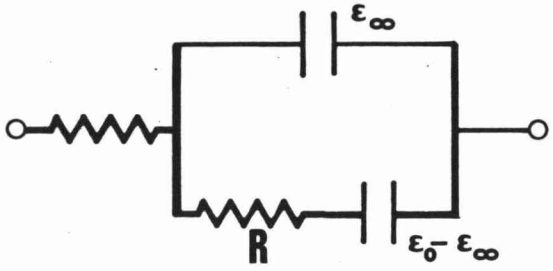

$R = \tau_o/(\varepsilon-\varepsilon_o)$

Figure 3.5.2

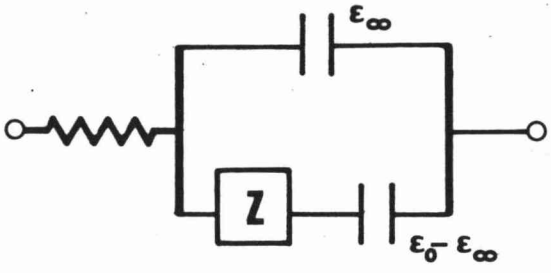

$Z = \tau_o(j\omega\tau_o)^{-\alpha}/(\varepsilon_o-\varepsilon_\infty)$

The real and imaginary components of the permittivity may be determined from equation [1],

real $\quad \varepsilon' = \varepsilon_\infty + (\varepsilon_o-\varepsilon_\infty)/[1+(\omega\tau_o)^2]$

imaginary $\quad \varepsilon'' = \omega\tau_o(\varepsilon_o-\varepsilon_\infty)/[1+(\omega\tau_o)^2]$

and the conventional method of plotting complex permittivity data is in the form of a "Cole-Cole" plot (ε' versus ε''). From equation [1], the expected form of such a plot is a semicircle with centre on the real axis (see Figure 3.6.1). From experiment the general form is that shown dotted in Figure 3.6.1, with centre below the real axis characterised by the angle $\alpha > 0°$.

The discrepancy between the measured dielectric dispersion and the form expected for equation [1] is shown more clearly in Figure 3.6.2, from which it may be seen that the experimentally observed dispersion is broader and flatter than the theoretical.

3.4.3 Distribution of Time Constants

The observed broadening of the dispersion spectrum is explained on the basis of a distribution of time constants. Each molecular dipole relaxes with a slightly different characteristic time, and the bulk material permittivity is considered to represent the summation of a distribution of relaxation times. A variety of mathematical forms have been proposed for this distribution, and these are discussed by

FIGURE 3.6 . DIELECTRIC DISPERSION

3.6.1 "COLE – COLE" PLOT

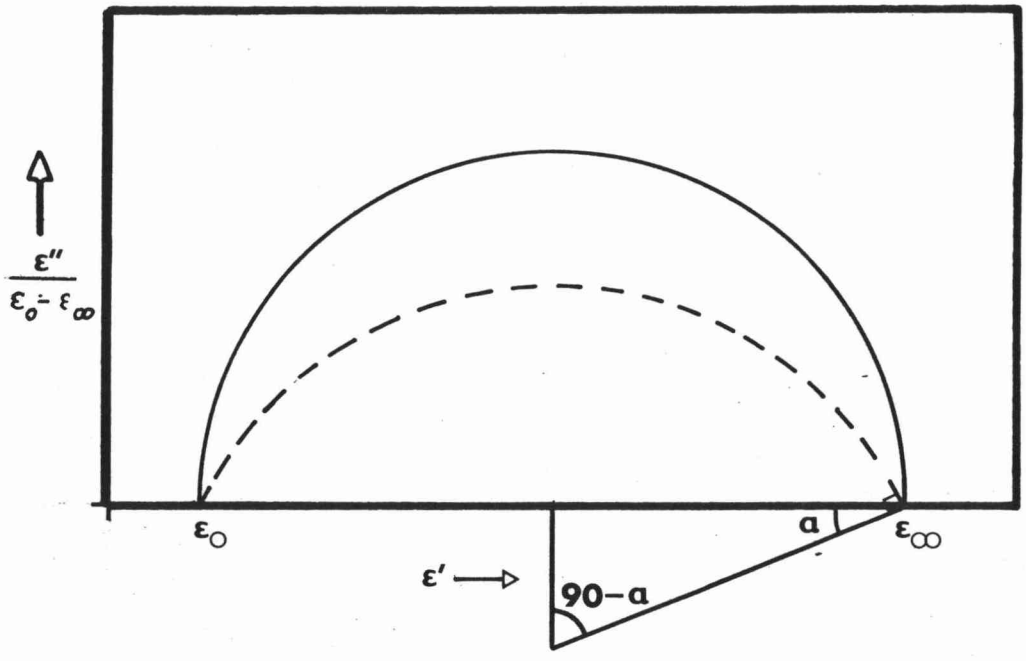

3.6.2 FREQUENCY DEPENDENCE of the IMAGINARY COMPONENT

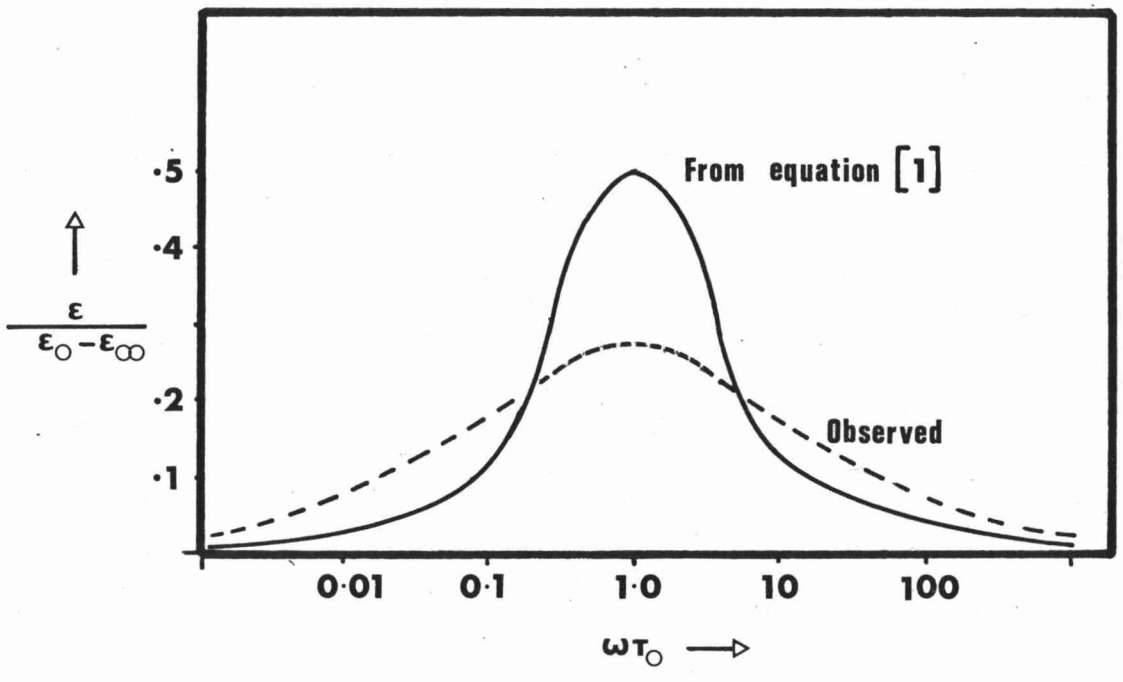

Cole (47 , 48) and in an excellent review of dielectric relaxation in glass by Owen (161). There is however no theoretical basis for any particular distribution function, and the observed experimental best fit has resulted in a phenomenological modification to the proposed equivalent circuit, to give the form shown in Figure 3.5.2.

3.4.4 Dielectric Dispersion in Geologic Materials

The interpretation of the electrical behaviour of clay/rock electrolyte systems which display a frequency dependent conductance has been widely based on the formalism of a lossy dielectric (78,80,105,204). This has been the subject of much debate since the magnitude and time constant of "dielectric dispersion" in geological material, are many orders of magnitude larger than for such dispersion processes in electrolytes. However, the dispersion observed in non-mineralised geological systems is not inconsistent with NLD dielectric dispersion observed in glasses or viscous electrolytes.

Fuller and Ward (80) consider geological materials to be homogeneous dielectrics, and attempt to determine theoretically the transfer function between the electromagnetic field (input) and current (output). These authors define a complex conductivity and permittivity and, making use of the time dependent Maxwell's equations and Fourier transform techniques, obtain equations for the frequency dependent permittivity and conductivity which they demonstrate to be not inconsistent with experimental results.

This approach however is purely phenomenological and is not a basis for concluding that the I.P. effect arises from the same translational and rotational relaxation processes as does dielectric polarisation. Indeed the complex dielectric formalism merely provides a means of describing two variables in one equation - just as the impedance formalism does. There would seem to be little justification therefore in using the concept of permittivity unless the material being examined fulfills the classical requirement of a dielectric, for which the oscillation of fixed charge only contributes to the polarisation vector, and thus ε. Clearly also, clay/rock/electrolyte systems are macroscopically inhomogeneous, and the concept of a permittivity which is a bulk property of the system, is not totally adequate.

Throughout this work the measured electrical dispersion will be expressed quantitatively and discussed, in terms of a complex impedance, which requires no assumption regarding the causal electrochemical mechanism.

3.5 PROPOSED COURSE OF RESEARCH

The models discussed in Chapter 2 are those which have been proposed to account for the I.P. effect of clay/rock/electrolyte systems. In no case can the experimental evidence be shown to be in accord with the models proposed, specifically because the evidence is limited and imprecise.

The polarisation models discussed in Chapter 3 are those known to occur in electrochemical systems. With the exception of Membrane Polarisation and NLD Dielectric Polarisation, the mechanisms for these are well understood, but the applicability of any or all of these to the effect known as Induced Polarisation, is not known.

It is hoped to extend the conclusions of this thesis beyond the phenomenological determination of an equivalent circuit for the I.P. effect, and obtain information about the underlying electrochemical mechanisms. To this end the models and mechanisms of polarisation discussed contribute no more than possible avenues of exploration, since no mechanism or equivalent circuit has been shown unambiguously to represent the I.P. effect. The method by which this problem will be approached is as follows.

1) To make precise, wide frequency band impedance measurements on laboratory model clay/rock/electrolyte systems.
2) To determine a simple two terminal equivalent circuit which describes the electrical properties of such systems.
3) To determine the dependence of the parameters of this equivalent circuit on such physical properties as are readily adjustable (e.g. electrolyte type and concentration, pore size, temperature, clay type etc.).
4) From the physical dependence, to determine an electrochemical model which may be used to make quantitative predictions about the I.P. effect of geological systems.

The culmination of this work must necessarily involve wide frequency band impedance measurement of real earth systems, in order to examine the predictions of an electrochemical model. This however is beyond the scope of the present study.

Section

II

Experimental

CHAPTER 4 THE MEASUREMENT OF IMPEDANCE

4.1 PRELIMINARY EXPERIMENTATION

4.1.1 Introduction

Observations of the Induced Polarisation effect may be made in the time or frequency domains. Field studies are most commonly conducted in the time domain, frequency domain observations being limited to "resistance" measurements at two discrete frequencies.

There are however, significant practical advantages to be gained from conducting laboratory investigations in the frequency domain. The most important advantage is that the electrical parameter obtained in the frequency domain, the impedance, is associated with a well defined and understood formalism. In addition techniques for bridge measurement of impedance have been highly developed, and the precision with which such measurements can be made, is significantly greater than for comparable time domain measurements.

It was decided to conduct measurements in the frequency domain. Since the characteristic frequency for the I.P. effect ranges from 0.1 to about 10 Hz, it was necessary to devise a system to measure the impedance from effectively D.C. to perhaps 1 k Hz. The first technique employed, involved determining the magnitude of the impedance $|Z|$, and the phase angle between the current and voltage ϕ, since

$$Z = R + jX,$$
$$R = |Z| \cos \phi,$$
$$X = |Z| \sin \phi.$$

This was accomplished initially using a twin beam oscilloscope to compare the magnitude of the voltage drop across the cell $|V_{cell}|$, and across a non-reactive resistance (R) in series with the cell $|V_R|$.

$$|Z| = |V_{cell}| R / |V_R|$$

ϕ can be determined directly from the phase difference between the two traces.

This technique was limited by the resolution of the oscilloscope, however sufficient information was obtained to conclude that a four terminal configuration is imperative, as electrode polarisation effects completely masked any membrane polarisation present.

4.1.2 Four Terminal Measurement

With a four electrode cell*, the measurement of impedance was improved by using a two channel chart recorder (Kipp and Zonen BD 9) to observe $|V_{cell}|$ and $|V_R|$ below 1 Hz, and a digital multimeter (Fluke 8000 A) above 10 Hz. The phase angle was measured by using the zero crossing points of V_{cell} and V_R to gate an electronic counter (Heath EU-805). This system has a precision of 0.1% for R and 1% for X between 10^{-3} and 10^{2} Hz, the limitation being measurement of ϕ at high frequency.

A number of measurements were made on ion exchange resin, and clay four terminal cells. While resins showed a considerable impedance dispersion (a reactive component of a few hundred ohms in a total impedance of a few thousand ohms), clay cells displayed only one tenth or one hundredth of this dispersion. For the clay cells a large non-reactive resistance appears in series with the frequency dependent impedance. This non-reactive component being 10 or 100 times as large as the component of interest, the precision with which the reactive component can be measured is significantly reduced. It was also clear, particularly for clay cells, that the impedance dispersion is not complete at 100 Hz and a greater bandwidth is required.

The limitations of bandwidth and precision together with the fact that impedance data was not available from the chart recorder above 1 Hz and from the digital voltmeter below 10 Hz, thus leaving a very important decade unmeasured, prompted the search for an improved measuring system.

---

* The two pairs of electrodes were Ag/AgCl which are reversible to chloride, and platinised platinum which are known to polarise little (99). In a two terminal configuration however, Ag/AgCl electrodes polarised significantly (more than 1%) above 100 Hz and platinised platinum electrodes polarise below 500 Hz. In a four terminal configuration, platinised platinum was used for the current electrodes, and Ag/AgCl for potential.

FIGURE 4.1 · BERBERIAN – COLE Low Frequency Admittance Bridge

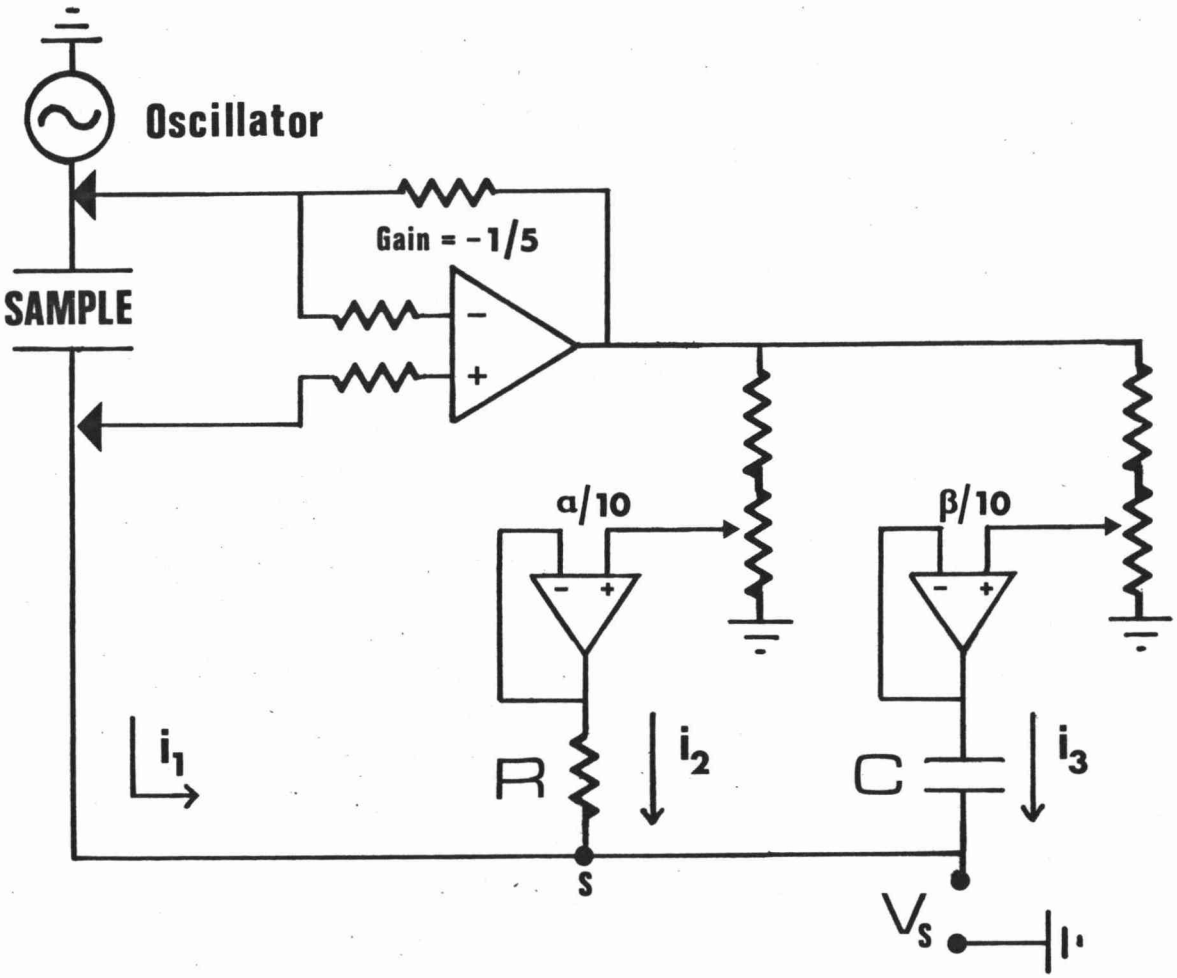

Basic Operation

At all times the sum of the current flowing into any node is zero, thus at the summing point (S)

$$i_1 + i_2 + i_3 = 0$$

At balance, $V_s = 0$, and

$$i_1 = i_{sample}$$

$$i_2 = -(\alpha/10)(V_{sample})/R$$

$$i_3 = -(\beta/10)(V_{sample})(j\omega C)$$

Thus,

$$i_{sample} = (V_{sample})(\alpha/10R + j\omega C\beta/10)$$

But,

$$i_{sample}/V_{sample} = 1/Z_{sample} = Y_{sample}$$

and the real and imaginary components of the unknown sample admittance (Y_{sample}), may be determined from the values of α and β at balance.

It should be noted at this point that neither conventional nor transformer ratio bridge measurement can be made directly on a four terminal cell. Also, there are no commercial systems for impedance measurement in this low frequency range, and systems of limited precision have appeared in the literature only in the last few years (10 , 18 , 19 , 30 , 39, 67 , 68). None of the systems reported meet the criteria of bandwidth (better than 0.01 to 10^3 Hz) and resolution (better than 0.1% for R and X) necessary to characterise adequately an equivalent circuit for clay/rock/electrolyte systems. The system proposed by Berberian and Cole (19) and modified by Gammell (81) however, proved to be very successful after extensive development.

4.2 BASIC THEORY OF A BERBERIAN-COLE BRIDGE

The complex admittance* measuring system proposed by Berberian and Cole (**19**) in 1969 differs from a conventional bridge in that active circuits are used as bridge elements. The system can be described as a bridge only in the sense that resistive and capacitive standards are varied in order to produce an output null, and at this null the values of the resistive and capacitive standards have some fixed mathematical relationship to the sample R and C.

The operation of a Berberian-Cole bridge is shown in Figure 4.1. Briefly, the voltage developed across the sample is inverted and one fraction ($\alpha/10$) fed through a resistor to the summing point (s) and another fraction ($\beta/10$) fed through a capacitor to s, to be combined with the unknown sample current. Balance is obtained by varying the real ($\alpha/10$) and orthogonal ($\beta/10$) fractions until the summing point voltage, $V_s = 0$. Berberian and Cole use a tuned amplifier and an oscilloscope as a null detector, and a picoammeter and filter at low frequency. The bandwidth stated is from 0.01 to 1 k Hz.

---

* The complex admittance vector,

$$Y = A + jB$$

is the reciprocal of the complex impedance

$$Z = \frac{1}{Y} = \frac{1}{A+jB} = \frac{A-jB}{A^2+B^2} .$$

This system is subtle but suffers from a number of significant disadvantages which result in a resolution much worse than the 0.1% required.

1) Since the summing point is at ground potential only at balance, the current through the sample varies with α and β.

2) All four terminals of the cell must be floated at large resistances from ground with resultant noise problems.

3) The resolution is significantly limited by taking the reading from the bridge as the setting of two potentiometers, because of the limitations of linearity and reactivity of even 10 turn helipots.

4.3 A MODIFIED BERBERIAN-COLE IMPEDANCE BRIDGE

With the limitations of the Berberian-Cole system in mind, a number of modifications were proposed and over a period of two years three bridges were constructed with increasing bandwidth and resolution.

Limitation (1) above is basic, and a simple modification to provide an invariant cell current to the summing point is to use a second amplifier to observe the voltage across a non-reactive resistor in series with the cell and to drive a voltage to current converter (a second non-reactive resistor) to the summing point. This procedure allows one of the cell current electrodes to be connected to ground (see (2) above). The first bridge constructed used this system. Resolution of the potentiometers was increased by using a 1 k Ω 10 turn helipot in series with a 9 k Ω resistor as a voltage divider. This proved to be unsatisfactory as a number of range switches must be employed which cannot be maintained internally calibrated to 0.1%. Bridge 2 used external decade resistance and capacitance standards as voltage to current converters and this proved very satisfactory. Bridge 3 operates in a similar fashion but the amplifier gains were made variable to allow a wider range of impedance to be measured.*

The bridge to be described in the following sections is the final modification (Bridge 3 Mark II), and it is with this bridge that

---

* An additional design criterion is the range of impedance to be measured. The cells used in this study have impedances between 100 Ω and 100 k Ω, with a maximum reactive component of about 10%.

all impedance determinations reported in this work were made.

The bridge operates as shown in Figure 4.2.

From Figure 4.2

$$Z = \left(\frac{R''}{R'}\right)\left(\frac{B}{A}\right)\left(\frac{1+j\omega CR_1}{1+(\omega CR_1)^2}\right)R_1 \qquad [1]$$

thus the impedance is proportional to R"/R', B/A and R_1, as well as being dependent on C and ω. It is imperative therefore that R_1, R' and R" be non-reactive, and Sullivan 0.1% non-reactive resistances were used throughout. For R_1 two Sullivan non-reactive decade boxes were used connected in series to span 8 decades of resistance. The calibration for these decade boxes is shown as Appendix 4.1. The resistive and capacitive components of R' and R" were measured at 1592 Hz (using a Wayne-Kerr B331 Autobalance Bridge), and the resistor discarded if the resistance or reactance was more than 0.05% from the prescribed value. For the capacitance standard a Hewlett Packard 4440B capacitance decade box was calibrated (see Appendix 4.2) and used.

Since the gains, A and B, appear as a ratio in equation (1), it is desirable that the amplifiers A and B be identical, and that R" is the same magnitude as Z_{cell} so that the input voltages to the two amplifiers are similar. It should be noted that while amplifier B may have one terminal connected to ground, amplifier A cannot. Also, the input impedance to both terminals of A must be high (greater than about 10^9 Ω) so as not to load the probe electrodes.

Amplifiers A and B are the most critical components of the bridge, and the frequency and temperature dependence of B/A will determine the accuracy with which impedance can be determined. The device ultimately chosen for A and B was the Analog Devices Instrumentation amplifier AD520K, and these have proved most satisfactory. Pertinent specifications are included in Appendix 4.3.

Figure 4.2 is grossly oversimplified and in order to construct a practical bridge the following factors must be considered.

The cell to be tested is invariably enclosed in a constant temperature bath (see section 4.5.1) which necessitates the use of relatively long leads to connect the cell to the bridge. Two problems arise as a consequence of this.

FIGURE 4.2 · Modified BERBERIAN-COLE Impedance Bridge

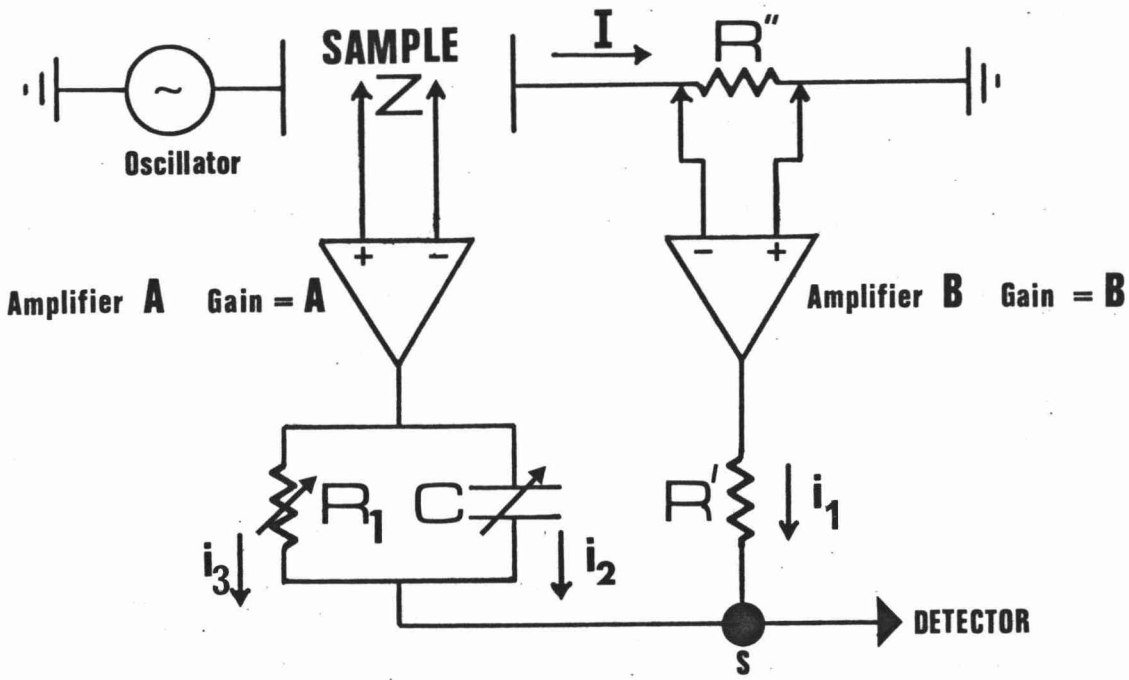

Basic Operation

At all times, $i_1 + i_2 + i_3 = 0$

At balance, $V_s = 0$, and

$$i_1 = B\, V_B/R' \qquad (V_B = IR")$$

$$i_2 = -A\, V_A\, j\omega C \qquad (V_A = IZ)$$

$$i_3 = -A\, V_A/R_1 \qquad (V_A = IZ)$$

Therefore, at the summing point,

$$\frac{BIR"}{R'} = \frac{AIZ}{R_1} + AIZ\,(j\omega C)$$

Removing I and solving for the unknown impedance, Z,

$$Z = \frac{R"B}{R'A}\,\frac{R_1(1-j\omega CR_1)}{1+(\omega CR_1)^2}$$

1) Noise pick-up - primarily 50 Hz mains.

2) Capacitive coupling. A variety of capacitive couples are possible - chief amongst these being coupling between the probe electrodes, coupling between each of the probe electrodes and the bath wall, and coupling between the inputs to amplifier A and the inputs to amplifier B.

The result of (1) above is to reduce the precision available, as the sensitivity of the null is ultimately determined by the noise present at the summing point. The result of (2) above is to reduce the accuracy at high frequencies* and hence to reduce the bandwidth. To reduce the effects of stray capacitance and noise is the only major difficulty in the utilisation of this form of bridge.

Two techniques eventually employed to achieve a reduction were,

i) to use input voltage followers** within the constant temperature bath as close as possible to the cell, to drive the cable to the bridge, and

ii) to make extensive use of double coax*** cable and connectors.

Using these techniques it was possible to reduce the noise at the summing point by an order of magnitude, and to increase the practical upper limit of impedance measurement from 2 k Hz to above 10 k Hz for a typical cell (Z = 10 k Ω).

It is necessary also to employ voltage followers after the outputs of amplifiers A and B in order to reduce coupling between the bridge circuit elements, and to reduce errors in the voltage to current conversion across these elements caused by the relatively high output impedance of 2 Ω (see Appendix 4.3) of the AD520K. Figure 4.3 incorporates these modifications.

---

* For a capacitor

$$Z = -j/\omega C, \quad \omega = 2\pi \times \text{frequency}$$

As frequency increases capacitive shunts reduce the apparent cell impedance and couple the inputs of amplifiers A and B.

** A voltage follower is a unity gain amplifier having a high input impedance and low output impedance.

*** This cable has two coaxial sheaths, insulated from each other and from the central conductor. It is often referred to as triaxial.

FIGURE 4.3 · Schematic Diagram of Bridge Circuitry (Bridge 3 Mark II)

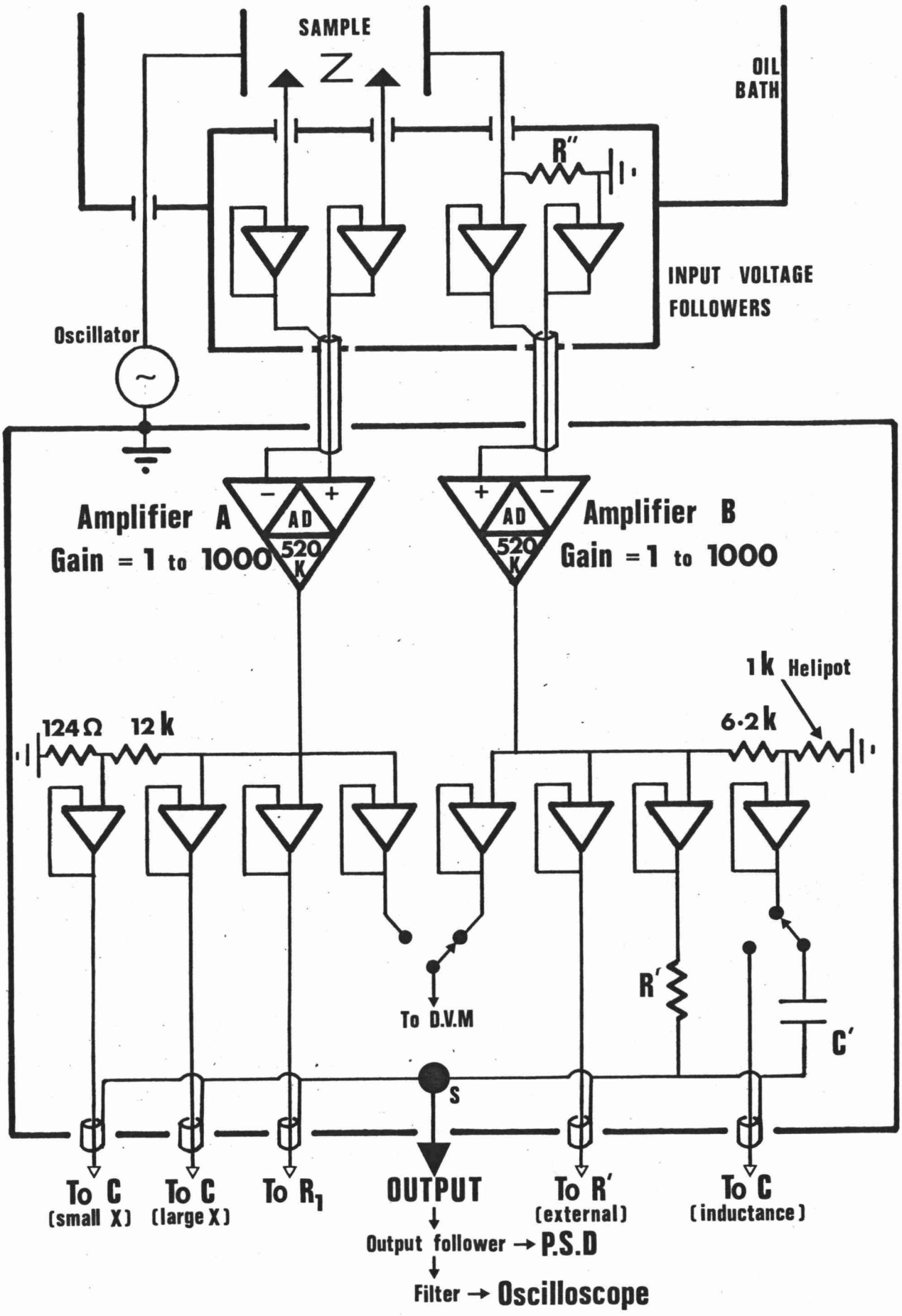

4.4 DESCRIPTION OF BRIDGE

4.4.1 Input Followers

The four input followers and R" were enclosed within a die cast alloy box and placed inside the grounded constant temperature bath. Short (approximately 10 cm) leads connect the probe electrodes of the cell with one pair of input followers. The inputs of the other pair of voltage followers are connected to each side of R" which is mounted on the same circuit board as the voltage followers. Each pair of followers drives the central conductor and first sheath of a 1 m double coax (Suhner GO3332) cable which terminates at the bridge. The outer sheaths of both cables are connected to the metal box enclosing the followers, and to the ground of the bridge itself. Double coax connectors* (Suhner 11-BNT-50/23-BNT-50) were used at both ends of the 1 m double coax cables, and also for the oscillator input in order that the oscillator could be isolated from the bridge ground if necessary.

4.4.2 Bridge Circuitry

The double coax cables from the voltage followers terminate at the chassis of the bridge and coax is carried inside the chassis to the inputs of the instrumentation amplifiers. This system significantly reduces noise pick-up - primarily because the cables are driven from a very low impedance source, but also because the inputs to A and B are coaxial from the voltage followers and noise induced on either cable will sum to zero at the output of the differential amplifier.

All circuits within the bridge were constructed as plug-in modules for ease of modification and to reduce coupling between the various groups of elements.

All voltage followers are 14 pin dual in line National LM310D integrated circuits (see specifications Appendix 4.3). This device has a bandwidth at least 100 times as wide as the instrumentation amplifiers and a typical gain of 0.9999, thus the use of this voltage follower does

---

* These connectors will henceforth be referred to as BNT plugs or sockets. The T stands for the misnomer "Triax".

not degrade the performance of the bridge significantly. The circuitry associated with the voltage followers is as shown in reference (154). 1 k Ω Braun "helitrim" potentiometers were used throughout to allow a precise D.C. offset voltage adjustment.

The bridge circuitry is housed within a silver plated 16 gauge brass box which contains partitions for extra rigidity and to provide additional shielding (see Figure 4.4). Gammell (81) who has constructed a high precision Berberian-Cole bridge, stressed the importance of a rigid chassis and has stated: "Any movement of the conductor will cause interference, and such vibrations will be within the frequency range of the measurements."

In order for the chassis to function as an electrostatic shield, it must be a good conductor and have a very good surface conduction to ground. Silver plated brass fulfills the criteria of conductivity and rigidity well, and proved far more satisfactory than 16 gauge aluminium which is not rigid and for which it is extremely difficult to obtain a reliable ground.

The power supply to the bridge is a ±15 V regulated D.C. supply. It was found necessary to mount the voltage regulator on a separate chassis and to keep it well separated from the bridge in order to reduce 50 Hz A.C. pick-up. Feed through capacitors to ground are used within the bridge D.C. entry compartment.

4.4.3 Instrumentation Amplifiers

The connection diagram for one AD520K is shown in Figure 4.5. Amplifiers A and B are identical in all respects. Four gains (1, 10, 100, 1000) are independently switchable for each amplifier using two Beckman 4 pole 5 position thermocouple switches. Gain is set initially by adjusting the resistors in the switched resistance networks. With the exception of the variable resistances which are Braun helitrims of values stated, all resistors in these networks are 1% metal oxide resistors - chosen for their low reactivity and relatively low temperature coefficients.

Figure 4.6 shows a calibration of the gain for amplifiers A and B as a function of frequency and output voltage.

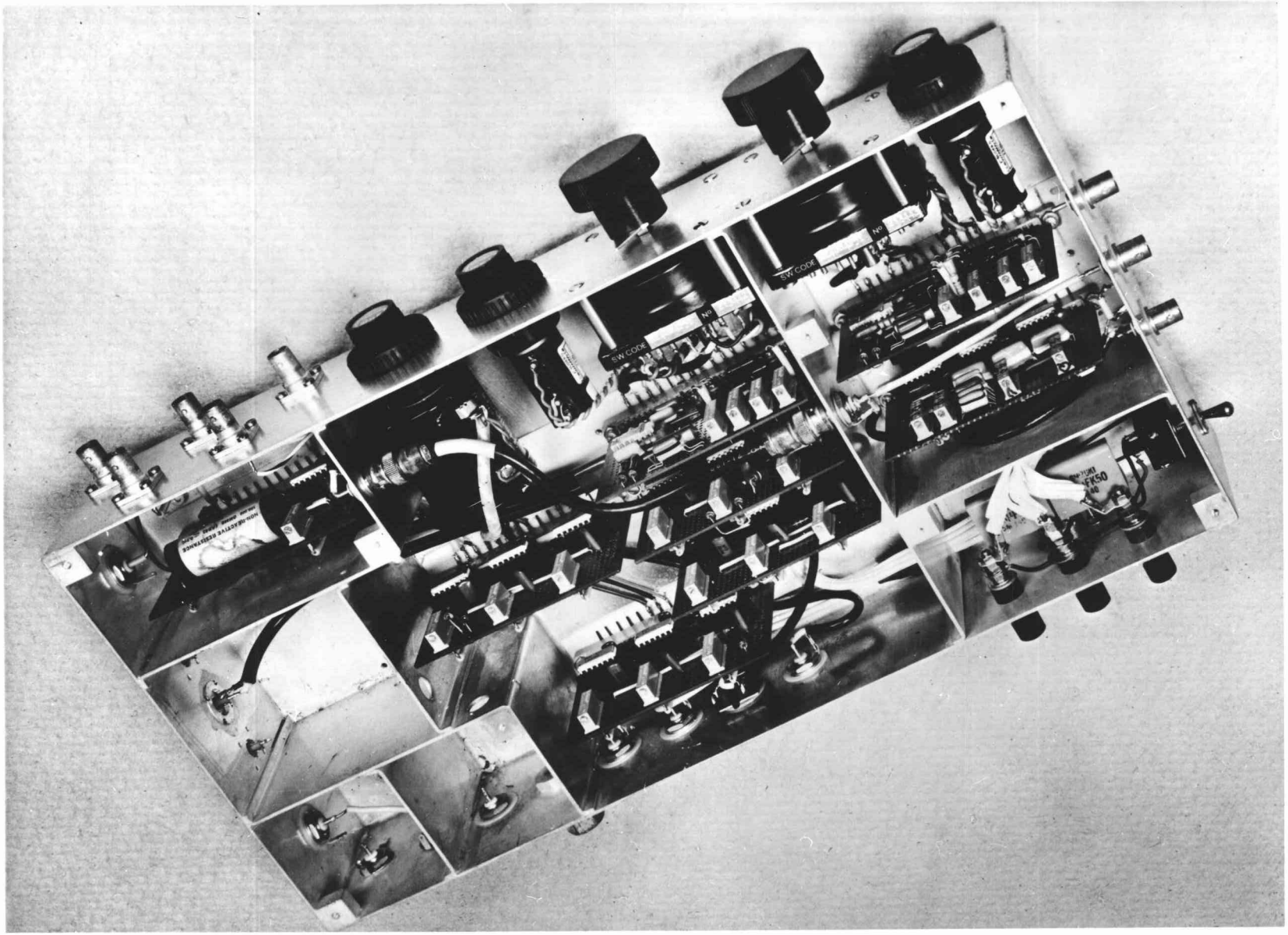
SW CODE
SW CODE
FK50

FIGURE 4.4 Impedance Bridge

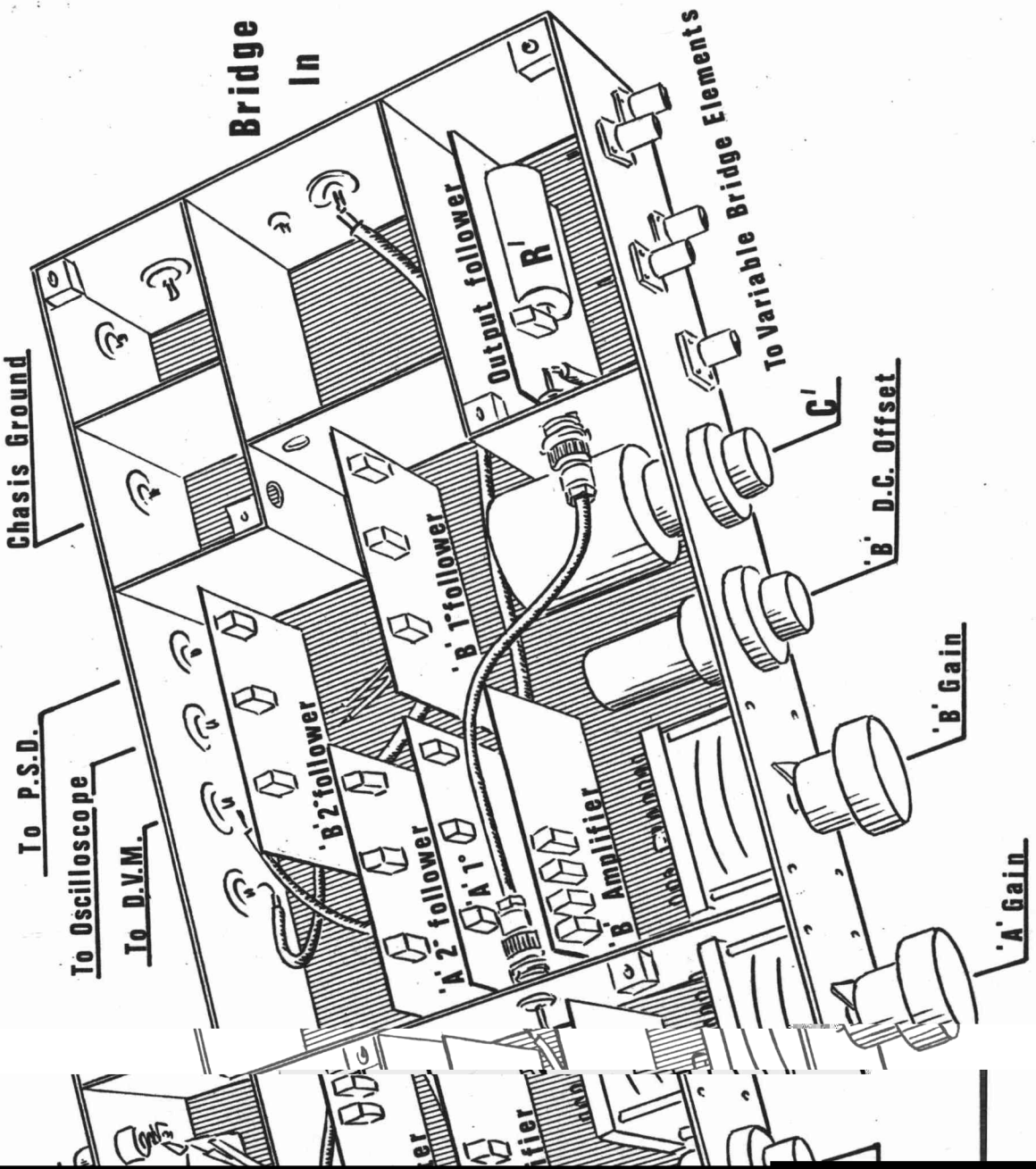

FIGURE 4.5 · Connection Diagram AD 520 K

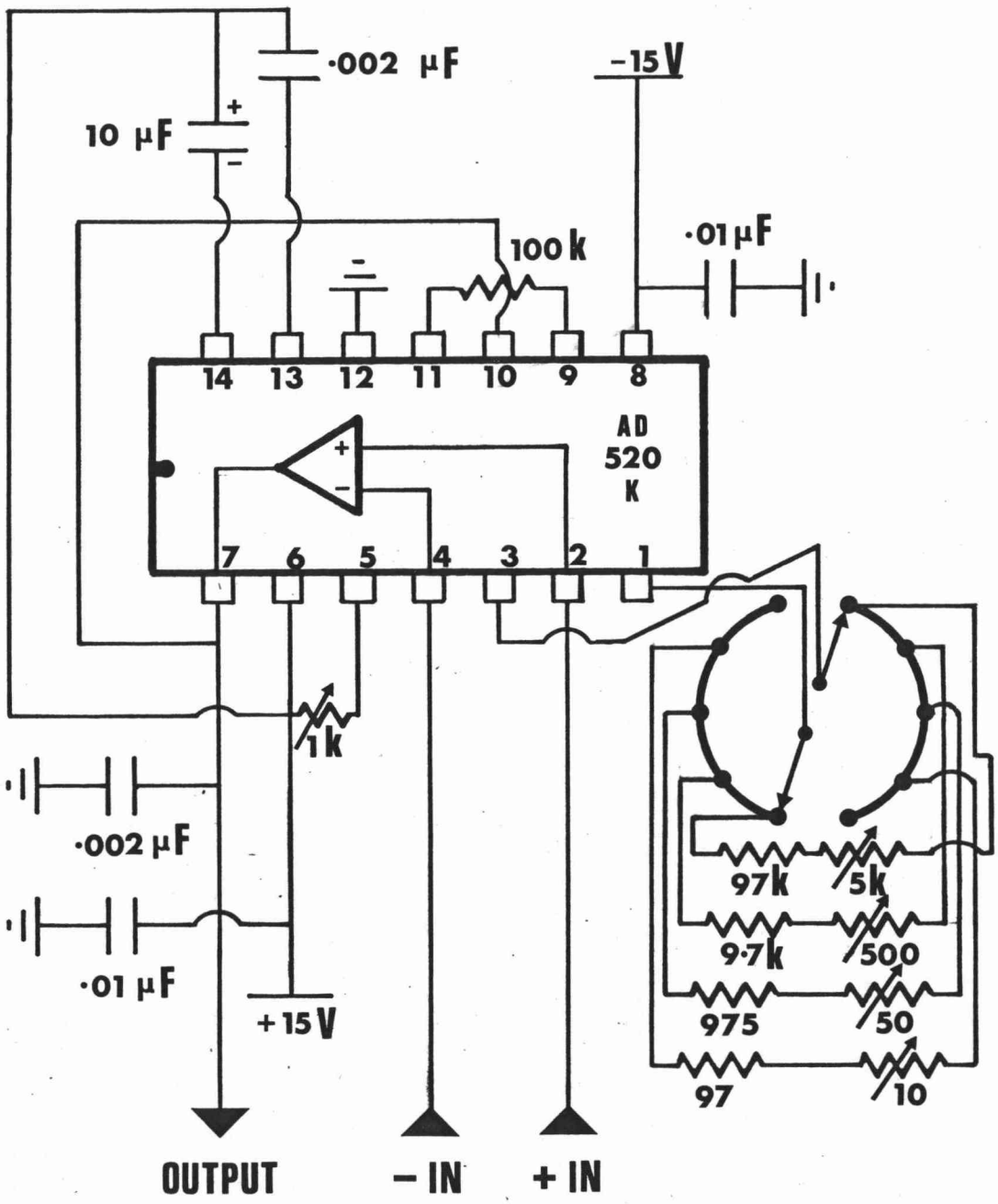

All fixed resistors are Metal Oxide ± 1%.

All variable resistors are Braun 10 turn "Helitrim".

The switch shown is a Beckman 4 pole 5 position Thermocouple Switch.

Figure 4.6 Calibration of Bridge Gain

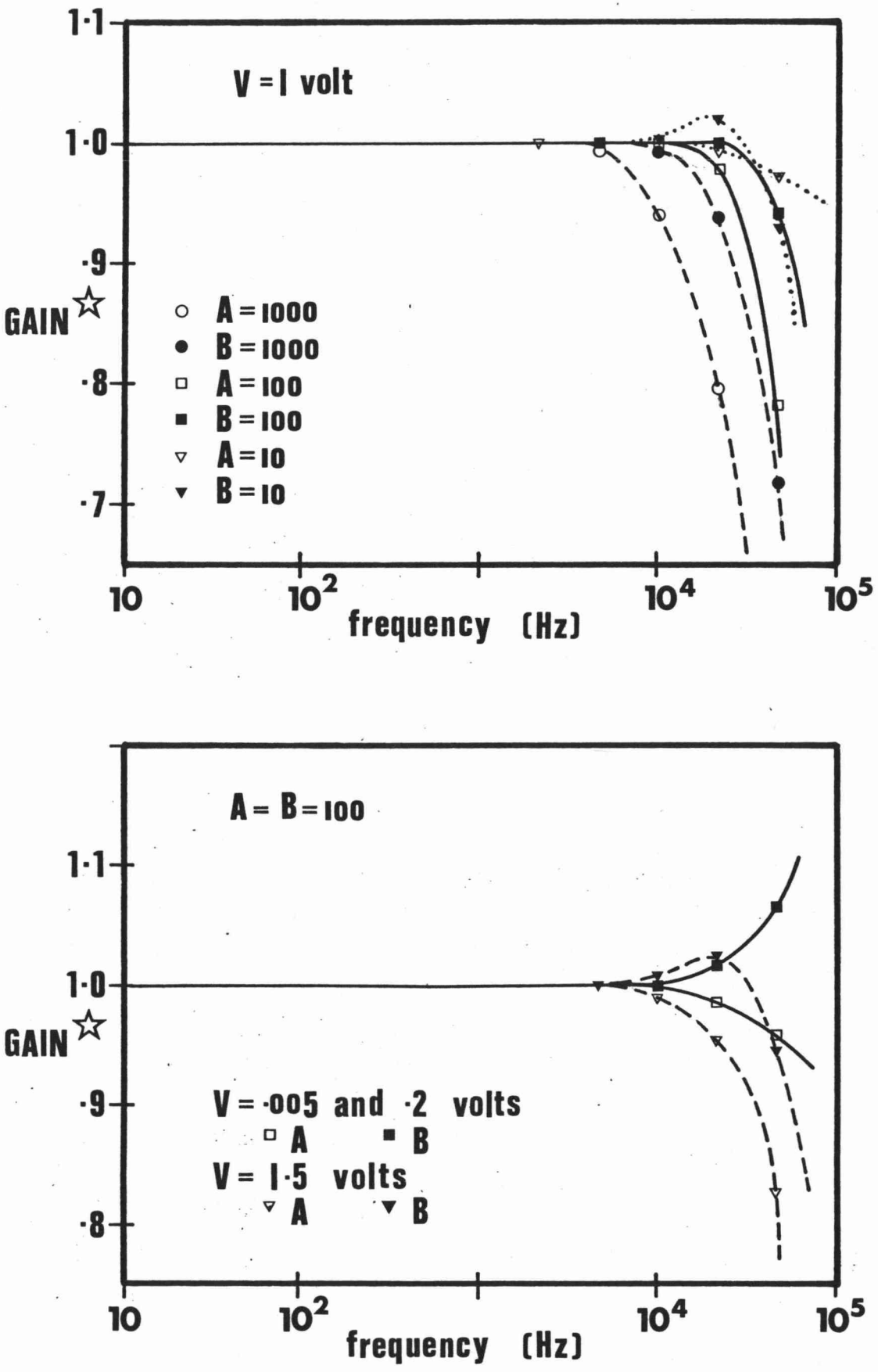

☆ MEASURED / NOMINAL

4.4.4 Primary Voltage Followers

Two groups of voltage followers follow the output of both A and B. The first group (primary followers) provide signals for the fixed and variable bridge elements R_1, C, R' and C'. R_1 and C are driven from the followed output of A and are connected to the front panel of the bridge via double coax cables and connectors in a three terminal configuration. High potential is the central conductor, low potential (the current return path) is the first sheath, and the outer sheath is connected in each case to the chassis of the variable bridge element and to the bridge ground. In addition to the two double coax front panel outputs having a potential identical to the output of A, a further output having a potential of 0.01020 A is provided by using a simple voltage divider network (using 1% metal oxide resistors) and following the fractional voltage to provide a low impedance output. This output is primarily utilised in measuring very small capacitances - in this case C is connected to the reduced potential output.

Three primary voltage followers also follow the output of B.

1) The first of these drives R' which is a 100 k Ω 0.05% non-reactive Sullivan resistance mounted on the output follower card.

2) The output of the second voltage follower is a continuously variable fraction of 0.1389 B produced from a voltage divider consisting of a 4.2 k Ω metal oxide resistor in series with a Beckman 1 k 10 turn Helipot. The fraction is read out on a Braun three figure digital duodial, and

$$\text{Voltage follower output} = 1.389 \times 10^{-4} \text{ B x dial reading}$$

This output is controlled by an internal switch and either drives a front panel double coax connector, or a fixed 1027.26 pF* polystyrene capacitor. The bridge normally operates in this latter mode, and the product of the attenuation and the capacitance is known as C'. C' is used to offset the cumulative effects of stray capacitance at high frequencies (see section 4.6.2).

---

* As measured at 1592 Hz on a Wayne-Kerr B331 Autobalance bridge. Polystyrene was selected because of the very low leakage current in this material.

3) The third primary B follower drives the last of 5 front panel double coax connectors. This terminal is used to measure large inductances (see Figure 4.3).

4.4.5 Secondary Voltage Followers

A group of secondary followers provide auxiliary outputs for a variety of purposes associated with bridge balance (see Figure 4.3).

4.4.6 Output Voltage Follower

The bridge out of balance signal is taken from the summing point which corresponds to the low potential side of the bridge elements R, C, R' and C'. As such the central sheath of the 5 front panel double coax sockets are connected together and to the low potential side of R' and C' at the high impedance input of the output voltage follower. This circuitry together with R' and C', and the C'/front panel switch comprise the output follower module which is mounted within a partition and isolated from the rest of the bridge. Since at balance the summing point is at ground potential, it is not necessary to take particular precautions with the connecting cable, but it is advisable to employ an output follower to follow V_s (the summing point voltage) to reduce the possibility of noise pick-up along the cables to the detectors.

4.4.7 Combination Output Filter

Despite extensive precautions to reduce noise, for a typical cell and using gains of 100 for A and B, the output follower signal at balance is composed of up to 2 mV of 50 Hz A.C. pick-up and a similar amount of high frequency noise (see section 4.5.7). To alleviate this problem a 50 Hz regenerative notch filter together with a 2 pole 12 db/octave Butterworth low pass filter was employed (see Figure 4.7). This 3 db point for the low pass filter was adjustable from 5 to 15 k Hz, with the high frequency roll-off normally set to occur outside the frequency range to be measured.

FIGURE 4.7 Combination Output Filter

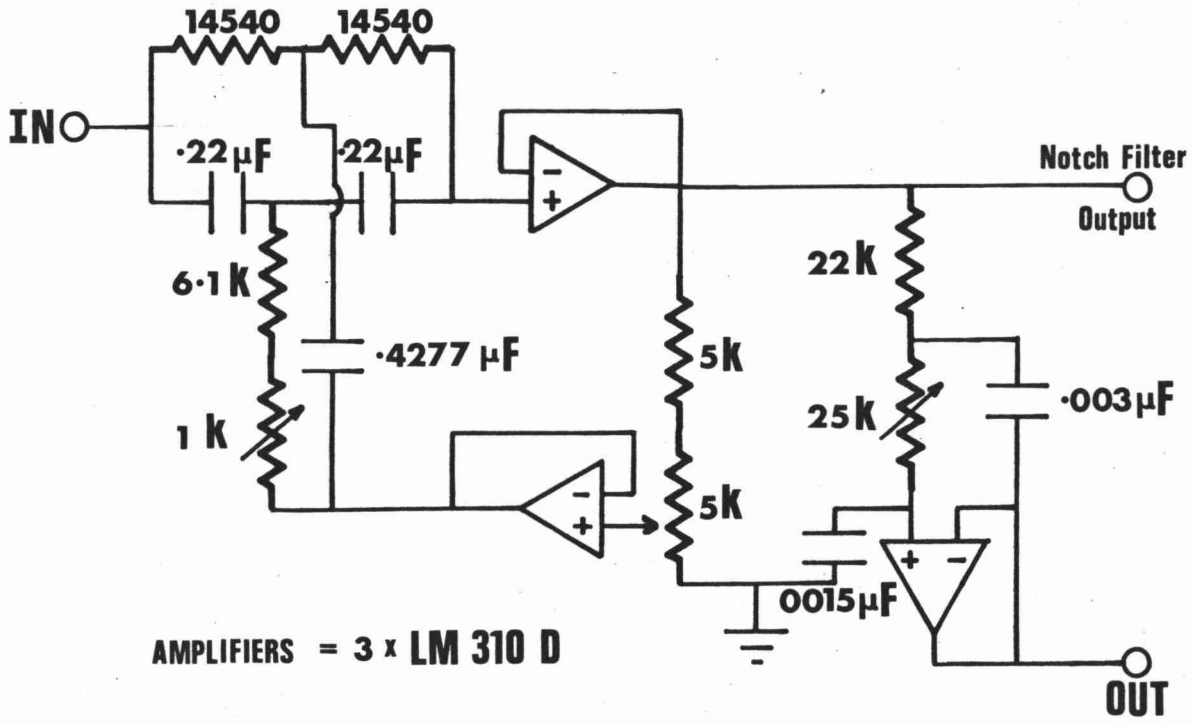

Notch Calibration

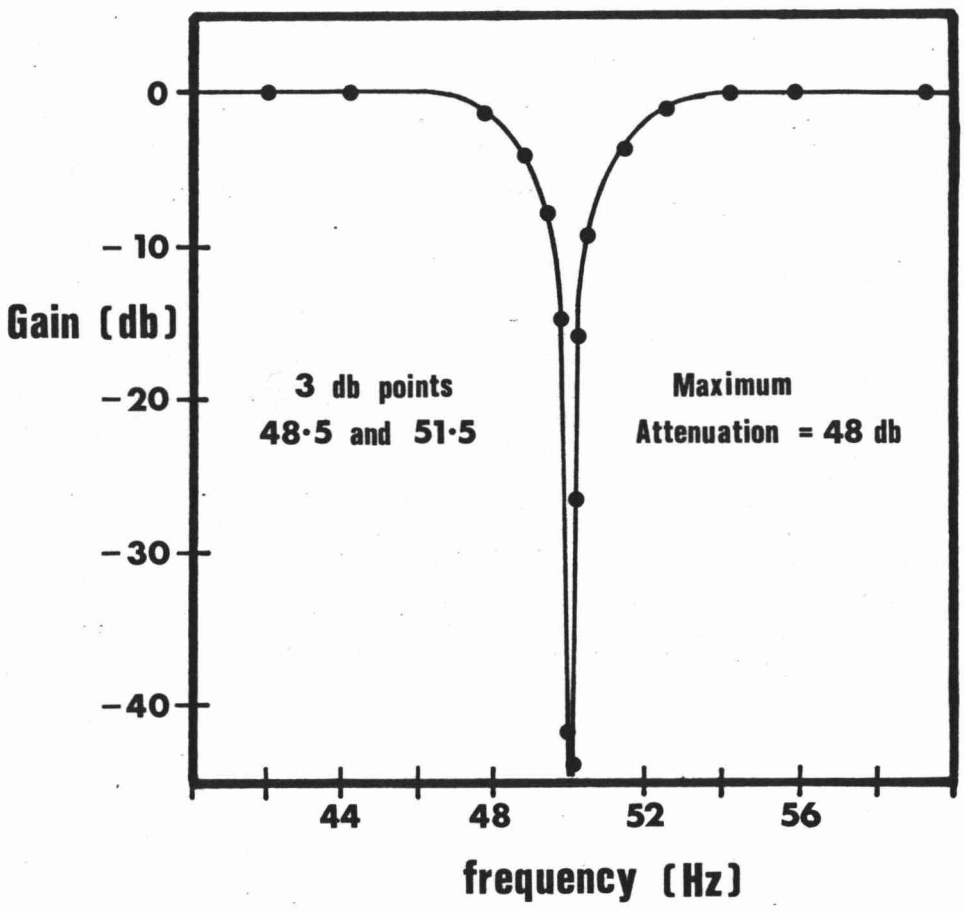

4.5 AUXILIARY INSTRUMENTATION

4.5.1 Constant Temperature Bath

The temperature coefficient of the resistance of a range of clay and resin cells was observed in the vicinity of 30°C and found to conform roughly to a 2.5% decrease in resistance per K. Thus if a precision of ±0.01% is to be achieved, temperature must be stable to within ±0.004 K.

A Tamson constant temperature bath was utilised to thermostat all cells, using Tellus 11 light hydraulic oil as a bath fluid. This oil has a flash point of 94°C.

Two modifications to this bath were necessary in order to obtain adequate long and short term temperature stability.* The first modification was to employ a large volume centrifugal pump for additional mixing - the stirrer provided in the bath being inadequate for the oil which is relatively viscous (6 centipoise) in the vicinity of 30°C. The second modification was to thermally protect the mercury contact regulator thermometer by pumping oil from the thermostat bath through a specially constructed enclosing cylinder. In addition a 16 gauge aluminium top was constructed to complete the electrostatic shielding of the cell.

The combined effects of Joule heating from the bath stirrer and auxiliary pump, and good lagging in the bath, make cooling necessary when operating below 35°C. This cooling was normally provided by passing a regulated flow of mains supply water through a cooling coil installed in the bath. By judicious control of the flow of cooling water and the power available to the control heating element, long term stability (days or weeks) of better than ±0.005°C, and short term stability (hours) of better than ±0.002°C was easily obtained.

4.5.2 Function Generator

The device chosen to provide a sine wave to the cell for impedance measurement was a Brookdeal type 471 Signal Source. This device is essentially a conventional function generator coupled with a tracking

---

* Measured using a Wayne-Kerr B331 Autobalance bridge and a calibrated platinum resistance transfer standard.

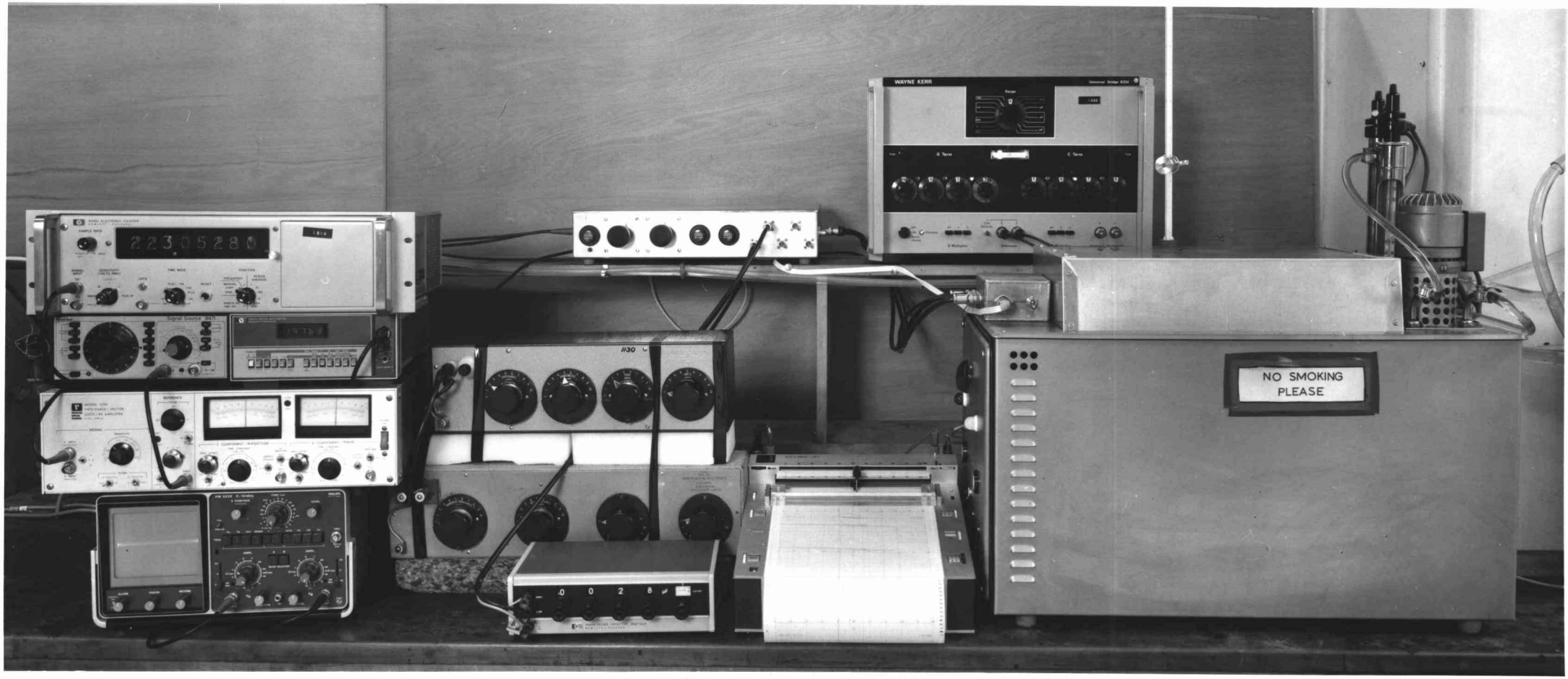
WAYNE KERR
NO SMOKING
PLEASE

Band Pass filter. The purpose of this filter is to reduce second and higher order harmonics which normally are a significant component of a sine wave produced by shaping a triangular waveform. This feature is of some significance since the Phase Sensitive Detector used as a null detector (see section 4.5.7) provides no rejection of odd order harmonics and serious displacement of the balance point can result if the harmonic content is high. Brookdeal states (34) that the total harmonic distortion is less than 0.05% between 1 Hz and 10 k Hz.

The signal source has a total bandwidth (with increased distortion) of 0.001 Hz to 11 M Hz. It also provides a 14 position precision attenuator with continuous vernier between ranges up to 3.16 V R.M.S., can provide output sine or square waves, and operate in a grounded or floating mode. In the "EXTERNAL" mode the signal source is voltage controllable.

4.5.3 Counter

An electronic counter (Hewlett Packard model 5245L - 8 digit) was used to measure the frequency accurately. The counter is used in a period average mode and the frequency is determined as 10^6/(period in micro-seconds). In view of the stated accuracy of the crystal oscillator (0.02 ppm - ref. 93) calibration was not necessary.

4.5.4 Decade Resistance and Capacitance Standards

R_1 consists of the series resistance of two Sullivan 0.1% non-reactive decade boxes, which combined cover a resistance range of 1.1 M Ω with 0.01 Ω resolution. C is determined as the setting of a Hewlett Packard 4440B decade capacitance with a capacitance range from 40 pF to 1.2 μF, with 2 pF resolution.

Calibrations for R_1 and C are presented in Appendices 4.1 and 4.2. The relatively large (0.5%) reactive error for large value of R_1 shown in Appendix 4.1, is effectively removed by the operation of C' (see section 4.6.2).

4.5.5 Digital Multimeter

A Hewlett Packard 3465A, 4½ digit multimeter was utilised in conjunction with a double pole double throw switch on the back panel of the bridge to observe the A.C. and D.C. components of A and B. This device has a maximum sensitivity of 1 μV D.C. and 10 μV A.C.

The initial setting up procedure for the bridge utilises this meter extensively in order to set the D.C. offset voltage for each of the voltage followers and the four gains for each instrumentation amplifier, to their prescribed values.

4.5.6 Oscilloscope

Two techniques were used to determine bridge balance. A Lissajous Figure null using an oscilloscope was used as a coarse adjustment because of the speed and visual simplicity with which this could be done. The oscilloscope used was a Philips PM 3232 twin beam with maximum sensitivity 2 V/cm.

4.5.7 Phase Sensitive Detector

The fine adjustment to a position of final bridge null is performed using a Phase Sensitive Detector (P.S.D.) as a null device. The instrument chosen was the Princeton Applied Research (P.A.R.) Model 129A, two phase/vector lock-in amplifier.

Since the P.S.D. is the central component of the null detection system it is worthwhile briefly investigating the operation of this device in order to understand its utility in such an application, and its limitations.

A P.S.D. functions by modulating the input signal with an external reference. This modulation can be considered to function by multiplying the input signal by +1 when the reference input is "high" and by -1 when the reference is "low". For an input signal of the same frequency as the reference the result is shown in Figure 4.8 for in phase and quadrature signals. If the time average is taken by passing the modulator

output through a low pass filter, the result will be a positive D.C. voltage for an in phase signal, but the out of phase signal will time average to zero. An A.C. signal of the same frequency as the reference is known as synchronous, and the D.C. output from a P.S.D. is proportional to the R.M.S. value of the in phase component of a synchronous signal applied to the input.

The real power of phase sensitive detection is however in its treatment of asynchronous (noise) signal, of which there are two broad categories.

1) Random Noise

a) White noise is generated by the motion of electrons in a resistor. This is known as Thermal Noise and is the least amount of noise that can accompany any signal. Its value in volts R.M.S.is given by

$$E_N = (4\ k\ T\ B\ R_s)^{\frac{1}{2}}$$

where k = Boltzmanns constant

T = Temperature

B = Bandwidth of measuring system

R_s = Source resistance

To this, each amplifier contributes noise according to its noise factor (NF, usually quoted in db), and the total thermal noise is given by

$$E_t = \Sigma[(4\ k\ T\ B\ R_s)^{\frac{1}{2}} \times 10^{NF/20}]$$

for all amplifiers in series.

Since the output of the bridge is derived from three LM 310D's (B = 20 M Hz), one AD 520K (B = 150 k Hz) and a variety of resistors (and capacitors) in series, in addition to the noise generated within the P.S.D. itself (Ref.166, p. IV-8), this noise is of some significance.

b) A second type of random noise is known as flicker noise or 1/f noise and has a noise power proportional to the reciprocal of frequency. This noise is of some significance therefore for low frequency measurements.

2) Spurious A.C. Noise

a) The most common form of A.C. noise is 50 Hz mains pick-up which may be of the order of hundreds of millivolts superimposed upon a

test signal, unless major efforts are made at shielding and ground loop supression.

b) The other common form of A.C. noise is harmonic distortion originating in the function generator or caused by non-linearity in the system under test or subsequent amplifiers.

Since the D.C. component of random noise and asynchronous A.C. noise is zero, the effect of the synchronous modulator and low pass filter combination is to reduce the effects of such noise (theoretically) to zero. The one exception to this is the effect of odd order harmonics, since the modulator output for these does not time average to zero (see Figure 4.8).

The P.A.R. Model 129A P.S.D. used in this study simultaneously measures the in phase (real) and quadrature (imaginary) components of an input voltage. This is accomplished by generating a reference signal at 90° to the input reference, to drive the quadrature synchronous modulator (and low pass filter).

This instrument is an exceptional null detector. Using output time constants of the order of 1 to 10 seconds, full scale sensitivities of 10 μV were routinely available without the use of input filtering. Input filtering was sometimes required however to prevent overloading of the inputs. Such filtering can also be employed to lessen errors caused by the presence of odd order harmonics.

The stated bandwidth is 0.5 Hz to 100 k Hz, but reliable measurements have been made down to 0.2 Hz. P.S.D. nulls down to below 0.1 Hz were accomplished using a Brookdeal 9412 P.S.D. with a stated bandwidth (34) of $<$0.1 Hz to 3 M Hz. This device will measure only one component and in phase and orthogonal reference signals must be switched to adjust the real and imaginary components of the bridge output voltage to zero. Due to the settling time of the P.S.D. this technique takes much longer to find a bridge null. In addition the sensitivity of the Brookdeal P.S.D. is much less than the P.A.R. device.

4.5.8 Two Channel Recorder

A Kipp and Zonen BD 9 two channel chart recorder was invariably used in order to balance the smoothed D.C. output from the P.S.D. to zero.

FIGURE 4·8 Operation of a Phase Sensitive Detector

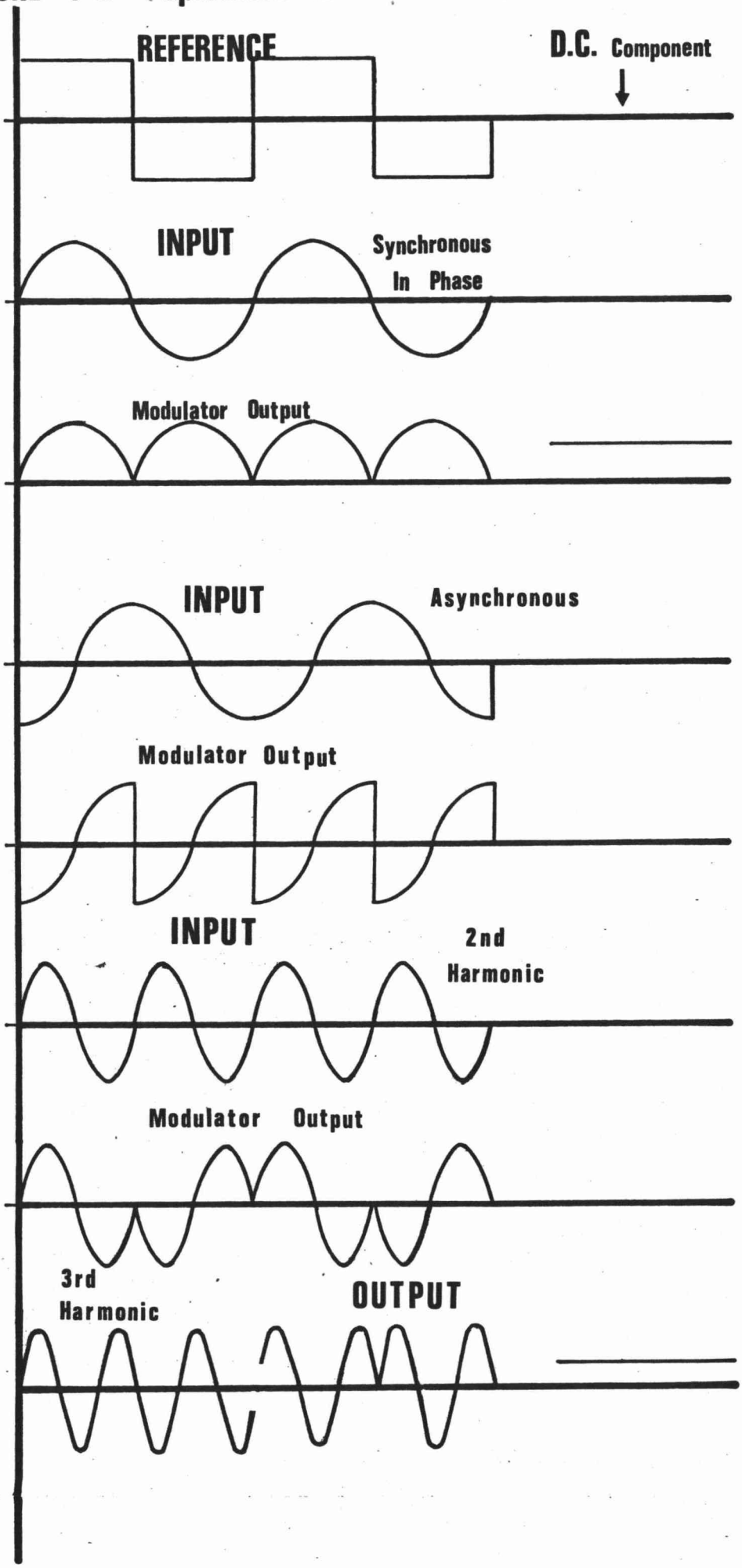

One channel was used for each of the real and imaginary components of the out of balance signal. This technique is imperative particularly when operating the bridge at low frequencies and hence with long output smoothing time constants (10 to 100 seconds).

This chart recorder was also utilised for direct measurement of the magnitude of the impedance (see section 4.1.2) at frequencies below 1 Hz. To do this the output of amplifier A is fed into channel A of the chart recorder, and the output of amplifier B to channel B. The peak-to-peak voltage on the chart recorder can be determined to within 0.1%, and thus

$$V_A = A\ I\ |Z| \qquad\qquad V_B = B\ I\ R''$$

where A and B are the gains of amplifiers A and B respectively.

$$|Z| = \frac{A\ V_A}{B\ V_B} R'' \pm 0.2\%$$

The phase angle ϕ can also be determined directly from the chart, but with a precision not less than 1° (i.e. $\pm 0.5\%$).

4.6 FOUR TERMINAL IMPEDANCE MEASUREMENT

4.6.1 Introduction

The description of the bridge to this point has contained a great deal of emphasis on resolution, bandwidth and noise, but little quantitative information has been conveyed as to what limits of these are necessary or acceptable. The reasons for this are twofold. Firstly the bridge described in detail is the result of some two years development, this particular bridge having had two less sophisticated predecessors. Preliminary measurements have been made using these bridges to observe the impedance of four terminal cells containing ion exchange resins, clay and electrolyte, as well as dummy RC combinations. These measurements have indicated the need for a greater bandwidth, more resolution and less output noise without indicating any quantitative constraint.

The second reason is more fundamental, and is also the reason why the bridge and its peripherals have been described in such detail. Research into low frequency membrane polarisation is essentially open

ended. Once a satisfactory equivalent circuit has been developed for the impedance dispersion of membrane systems then impedance measurements may be made to obtain information regarding ion movement, ion-ion interaction, double layer structure, ion exchange etc., in these systems. This information can only be obtained by making high precision, wide bandwidth, low frequency measurements, and the limits of precision will determine the limits to which electrochemical systems having relatively long relaxation times can be understood.

The types of system that can be subjected to low frequency impedance analysis are large in number and in importance, and include most dielectric processes in solids (47, 48 , 95 , 121 , 167) and viscous liquids (82, 146, 207) as well as many Faradaic electric processes (6, 7, 8, 9, 10, 67, 68, 119, 120).

Because of the significance of this technique, the development of a high precision, low frequence impedance bridge has been treated as a major part of this thesis.

4.6.2 Technique

In order to determine the impedance dispersion of a sample in a four terminal cell, the following procedure is employed.

1) Current: A variety of cells including resin, clay, latex and electrolyte only, were tested to determine the effect of cell current on the potential drop across the cell. These cells displayed an essentially ohmic behaviour up to current densities as high as 1 mA cm^{-2}. Field IP surveys,however,utilise current densities of the order of 10^{-9} to 10^{-8} A cm^{-2} (204), and Scott and West (181) have shown the upper limit of linearity in geological materials to be 10^{-5} to 10^{-6} A cm^{-2}. As such the current has been kept below 2×10^{-6} A cm^{-2} wherever possible, to ensure linearity, and in an attempt to conform approximately to field conditions.

Using the digital multimeter to measure A.C. volts the current is set to the desired value by observing V_B*.

---

* $V_B = B\ I_{cell}\ R$".

2) Gain: Because the bandwidth decreases and the common mode rejection increases with increasing frequency (see Appendix 4.3), the bridge performance is maximised if A = B = 100. However, if the cell impedance is outside the range 1 to 10 k Ω, the gains must be adjusted to keep $V_A \approx V_B$ ($\lesssim$2 V R.M.S.).

3) D.C. Balance: After the current and gain have been adjusted, the multimeter is set to D.C. volts and used to observe the D.C. component of V_A and V_B alternately. These are adjusted to zero using the bridge front panel potentiometers (Figure 4.4), and are kept at 0±1 mV during a run.

4) Stray Capacitance Balance: As stated in section 4.4.4 stray capacitances are balanced out using C' at a high frequency (normally 11 k Hz) above which the impedance dispersion of the sample is assumed to be zero. With C disconnected the bridge is balanced by adjusting the real and imaginary out of balance signals to zero using C' and R_1. This determination is not used as a data point but R_1 and C' are recorded to check for subsequent drift. Frequency is recorded from the counter as the average period in micro-seconds (i.e. $10^6/f$).

5) A.C. Balance: C is now connected and data points obtained by balancing the bridge using C and R_1 at the frequencies of interest. C' is not touched. Data is normally obtained at 1/6th decade intervals, corresponding to frequencies of $(1.5, 2.1, 3.1, 4.5, 6.5, 9.5)\times10^n$, where n = -1, 0, 1, 2, 3. After six determinations C is disconnected and the frequency returned to the high frequency limit, where the bridge is re-balanced using R_1 and C', to check for drift.

4.6.3 Conversion from Bridge Data to Impedance

The condition of bridge balance is derived in Figure 4.2 and must be used to determine the cell impedance from the bridge data (R_1, C and $10^6/f$).

$$Z = \frac{R''B}{R'A} \frac{R_1 - j\omega C R_1^2}{1+(\omega C R_1)^2} \qquad [2]$$

Thus

$$R = \frac{R''B}{R'A} \cdot \frac{R_1}{1+(\omega CR_1)^2} \qquad [3]$$

$$-X = \frac{R''B}{R'A} \cdot \frac{CR_1^2}{1+(\omega CR_1)^2} \qquad [4]$$

This conversion is normally conducted point by point as the run proceeds using a Hewlett Packard HP 65 programmable calculator to determine R, -X and ω. In the first instance -X is plotted versus R, the form of this complex impedance plane diagram being a semicircle with centre below the real axis for all systems displaying a dispersion of impedance.

4.7 BRIDGE PERFORMANCE

4.7.1 Introduction

In specifying the performance of an instrument it is necessary to define two general criteria.

1) Accuracy - used to denote the degree of systematic error by which a measured value differs from the "true" value, (17).
2) Precision - used to denote the degree of random error in a measurement (17).

For an impedance bridge these criteria must be specified for both the real and imaginary components, and both are necessarily non-simple functions of the limitations of the bridge components and input/output devices.

4.7.2 Accuracy

From equations [3] and [4], R and X may be seen to depend on the fixed and variable bridge elements (R_1, R', R" and C), on the instrumentation amplifier gains (A and B), and on the angular frequency (ω). Thus the combined systematic error or error in calibration of these components, will determine the accuracy with which R and X may be determined.

The bridge elements have been calibrated and these are presented in Appendices 4.1 and 4.2. Since it is possible to determine ω to eight

places if required (section 4.5.3), the errors in this term are vanishingly small. The calibration of A and B is readily accomplished to within ±0.01% at any frequency, however since these are active devices, gain is a function of both frequency and output voltage because of variable amplifier bandwidth and slewing rate (Appendix 4.3). However, since A and B appear as a ratio and are identical devices, amplifier non-linearities are partially compensated.

The most satisfactory way of specifying the accuracy of an impedance measuring device is to make measurements on samples of known impedance. This has been done and the results are presented in sections 4.7.4 to 4.7.6.

Bridge accuracy is also determined by the magnitude of the impedance being measured, for two reasons.

1) A and B are adjustable only over a range of 1 to 1000 (with reduced accuracy at gain G = 1000). Thus if R is large, R_1 must be large*, which results in a decreased accuracy because of poor calibration of R_1 in the higher ranges (Appendix 4.1).

2) The differential (and common mode) input impedance of the bridge is of the order of 10^{12} Ω (Appendix 4.3). Thus in order to maintain an accuracy of, say, 0.1%, the impedance being measured must be less than 10^9 Ω** to prevent errors due to the amplifier input impedance forming a resistive shunt.

In practice the first limitation is more significant and limits the range of impedance measurement to about 10^6 for the bridge circuit shown in Figure 4.3. The lower limit of impedance measurement is determined by the bridge precision.

4.7.3 Precision

Two major factors contribute to the precision with which R and X may be measured.

1) The bridge resolution is directly determined by the resolution of the variable bridge elements R_1 and C. However, the maximum resolution of

---

* R' and R" are fixed resistances which may be adjusted only by replacing these elements with further non-reactive resistances.

** This value is effectively independent of frequency up to 10^5 Hz (154).

1 part in 10^8 for R_1, and 2 parts in 10^6 for C, seldom impose any limitation on bridge operation.

2) The major limitation is the precision with which the bridge null can be determined. This is determined by

a) the ratio of the bridge out of balance voltage ($V_A + V_B$), to the sensitivity of the null detector, and

b) the total asynchronous bridge output voltage (or noise - see section 4.5.7) observed at the detector.

The two null detectors used are an oscilloscope (section 4.5.6) and a P.S.D. (section 4.5.7). Since an oscilloscope is a wide-band device, the effective noise rejection is small and the available precision is consequently reduced. The P.S.D. however has an excellent noise rejection and is capable of tracking a synchronous signal in 100 db of asynchronous noise (166). Using the P.S.D. as a null detector the precision available is of the order of

1 part in 10^4 for R between 1 and 10^4 Hz.
1 part in 10^3 for R between 0.1 and 1 Hz.
1 part in 10^4 for X between 1 and 10^3 Hz.
1 part in 10^3 for X between 0.1 and 1 Hz.
1 part in 10^3 for X between 10^3 and 10^4 Hz.*

For very low cell impedances, the cell voltage (for a particular current) is small, but the noise which primarily originates within the bridge is not correspondingly reduced. This effectively imposes a lower limit of impedance measurement for which the precision is greater than the accuracy, of about 10 Ω for R, and 0.1 Ω for X.

4.7.4 Non-Reactive Dummy Cell

Measurements of the four terminal dummy cell shown in Figure 4.9 were performed in order to determine the accuracy of bridge measurement as a function of frequency, input voltage and amplifier gain.

---

* Since $X \propto \omega C$ (see equation [4]), at high frequencies the precision is limited by (1) above.

Figure 4.9

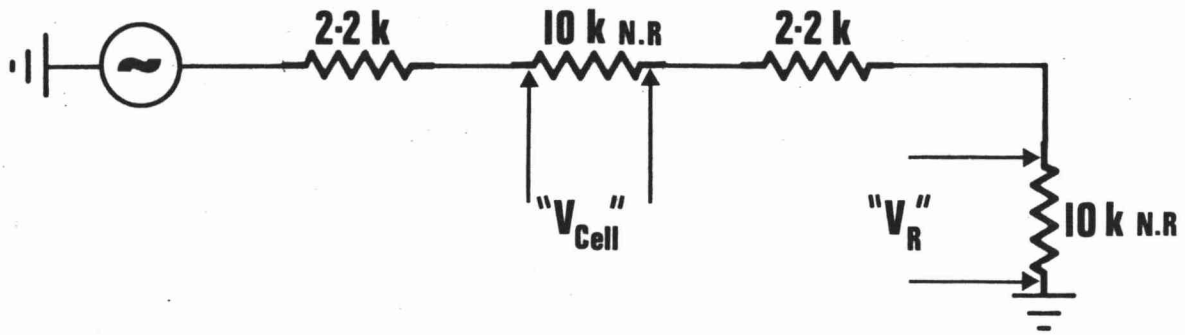

The results are most conveniently expressed graphically, and are shown in Figures 4.10 and 4.11 as a percent deviation from the prescribed value of $|Z_{cell}| = 10^4\ \Omega$ for R and X. Bridge measurements were performed as described in section 4.6.2.

4.7.5 Reactive Dummy Cell

A more representative dummy cell was constructed to approximate the expected reactive properties of clay and resin cells. Bridge impedance measurements were performed as described in section 4.6.2. The results are given in Figure 4.12 together with the dummy circuit and its expected response, and show an accuracy for R and X up to 2 k Hz of better than 0.1%.

4.7.6 Non-Reactive Cells

Before data can be utilised from impedance measurements made on cells containing model clay/rock/electrolyte systems, it is necessary to demonstrate that any impedance dispersion observed is not an artifact of the measuring system, or of the cells used. This may be accomplished by making bridge impedance measurements on cells containing materials for which a dispersion of impedance is not expected. A number of such measurements were made on cells containing

FIGURES 4.10 and 4.11 Bridge Measurements on Non-Reactive Dummy Cell (Gain Error)

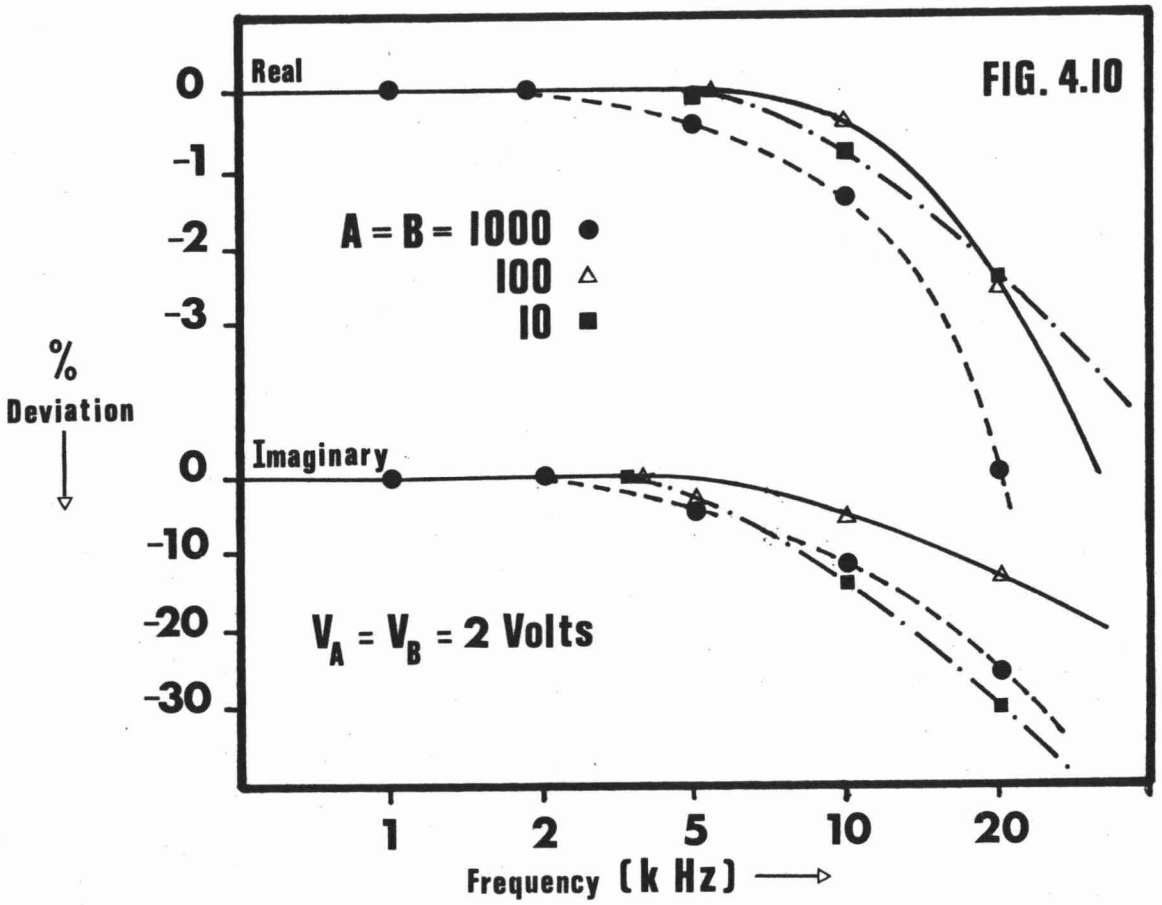

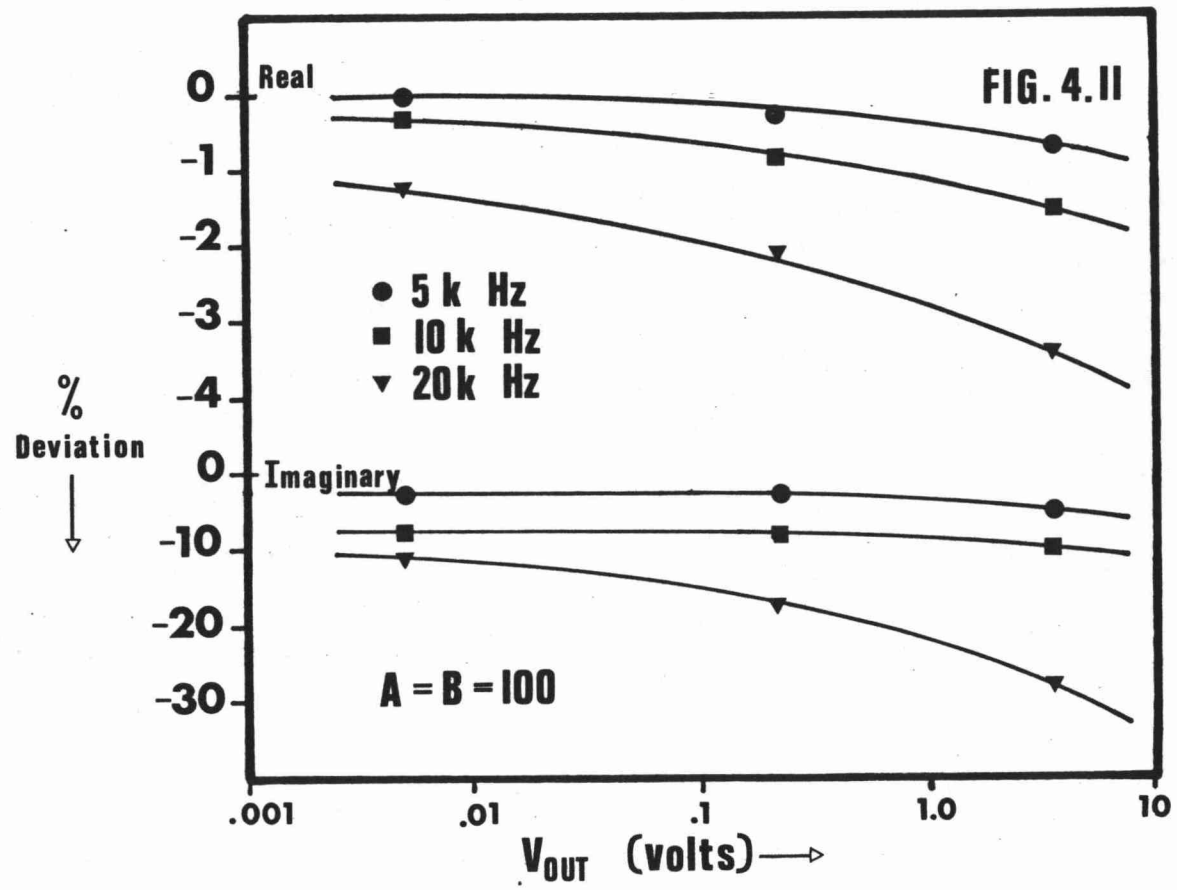

FIGURE 4.12 Reactive Dummy Circuit

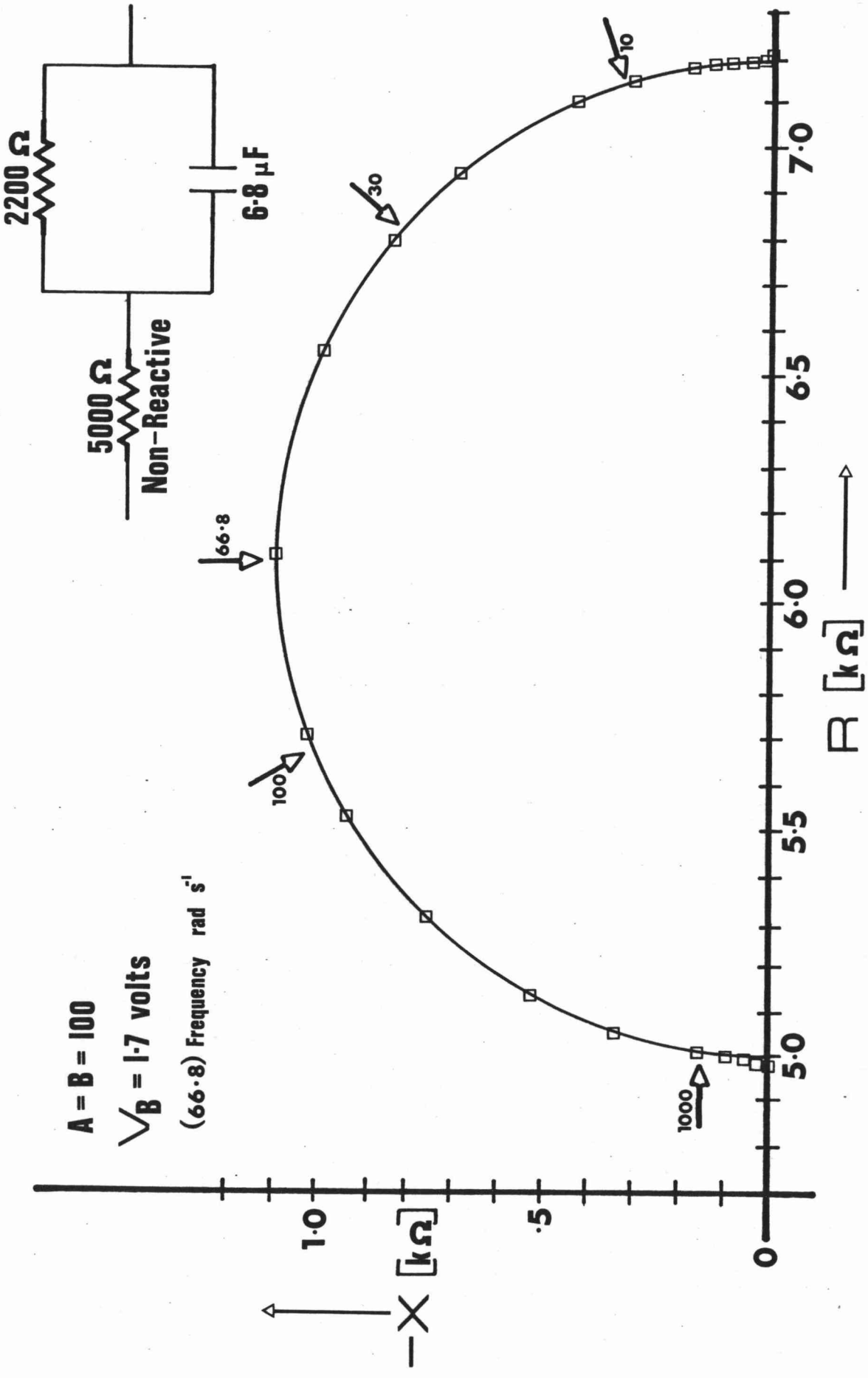

1) Electrolyte alone.
2) Electrolyte/ground glass.
3) Electrolyte/glass spheres.
4) Electrolyte/plastic spheres.

At frequencies below 10 k Hz these systems all behaved non-reactively within the accuracy of the bridge (Table 4.1), provided C' was employed (sections 4.4.4 and 4.6.2). If C' was not used the reactance was observed to be positive at frequencies above 2 k Hz, increasing to as much as 30% of the total impedance at 10 k Hz.

In addition measurements made on a number of systems expected to display an impedance dispersion indicated a reactance only within the limits of bridge accuracy. These include

1) Clay dispersed in electrolyte.
2) Plastic clay containing about 50% electrolyte.
3) Uncemented clay/glass/electrolyte systems (see section 5.1.5).

These results clearly indicate that any impedance dispersion observed in model clay/rock/electrolyte systems, is a property of the system and not of the measurement technique.

4.8 BRIDGE SPECIFICATIONS

The considerations discussed in section 4.7, together with more obvious electrical properties of the bridge, are summarised in Table 4.1.

Table 4.1 Specifications of Impedance Bridge (Bridge 3 Mark II)

4.1.1 Electrical Properties

Power Supply	±15 to 18 V D.C.
Current Requirements	100 mA
Input Impedance	10^{12} Ω (Differential)
	10^{12} Ω (Common Mode)
Output Impedance	0.7 Ω
Voltage Gain	1, 10, 100, 1000 V/V

4.1.2 Impedance Measurement

	Real	Imaginary	Units
Range of Measurement	10 to 10^6	0.1 to 10^4	Ω
Precision			
0.1 to 1 Hz	0.1	0.1	%
1 to 1 k Hz	0.01	0.01	%
1 k to 10 k Hz	0.01	0.1	%

Bandwidth*

A	B	V_B	(0.1%)	(1%)	(0.1%)	(1%)	
10	10	1 V	1	11	1	3	k Hz
10	100	1 V	2	10	**	**	"
100	100	1 V	2	11	2	3	"
1000	1000	1 V	2	8	1	3	"
100	100	0.005 V	3	13	3	7	"
100	100	0.17 V	2	10	2	3	"
100	100	1.6 V	1	8	2	3	"

* At the specified accuracy (%)

** Error in reactive balance due to missadjustment of C'.

CHAPTER 5 MODEL CLAY/ROCK/ELECTROLYTE SYSTEMS

5.1 HISTORICAL

In selecting a laboratory model system from which to gain information about induced polarisation in the earth it is desirable that,

1) the system chosen displays a large and reproducible impedance dispersion, and

2) the type of model cell is realistic in terms of the known physical structure and impedance dispersion of non-metalliferous bodies.

Mayper (134) has demonstrated that the "normal" induced polarisation effect is due to the presence of clays in rock pores and a number of different types of laboratory clay model systems have been employed by workers in this field.

5.1.1 Core Samples

Induced polarisation studies on clay-containing core samples have been made by Collet (49), Henkel and Collins (91), Keller (5 , 103, 104, 105), Mayper (134), Mohomed (143) and Fraser *et al* (72). With the exception of Fraser *et al*, all these studies have been conducted in the time domain and the I.P. effect observed is very similar to that observed in the field, both in magnitude and characteristic relaxation time. Fraser *et al* (72) observed in the frequency domain a small but similar I.P. effect.

Core samples however are subject to two major limitations which make them far from suitable as model systems in a study concerned with determining a mechanistic model for induced polarisation.

1) There is no control over the type and situation of clay, or the pore geometry.

2) Electrode polarisation effects arising from very small amounts of metallic contaminant may produce large induced polarisation errors (204).

5.1.2 Compressed Clays

Clays compressed to reduce the water content have been the subject of a limited number of studies. Marshall and Madden (127, 128,129,130,131) studied the time and frequency domain response of kaolinite compacted at pressures of from 1 kg cm^{-2} to 2.75 kg cm^{-2}. Mehran (139) has observed the frequency domain I.P. effect of illite kaolinite, and a mixture of 50% kaolinite and 50% silica flour consolidated at unspecified pressures, from 100 Hz to 100 k Hz. Arulanandan (12) observed the frequency domain response of consolidated illite grundite and montmorillonite from 2 M Hz to 70 M Hz. In all three cases conductivity dispersion occurs at much higher frequencies than is observed in the field. Mehran observed a characteristic frequency of 10^{6} Hz for kaolinite and Arulanandan about $2x10^{7}$ Hz for montmorillonite, compared with 10^{-1} to 10 Hz observed in the field.

Compressed clay systems thus do not display a similar impedance dispersion to that of non-metalliferous bodies, the observed characteristic frequencies being much too high, however it is probable that they are simply a limiting case of the system described in 5.1.5 (see section 2.3.2).

5.1.3 Clay Dispersions

A number of workers have studied the impedance dispersion of colloidal clays in a range of electrolytes. Arulanandan (12), Fricke and Curtis (76), Olsen (157), Schwan and Schwartz (180) have observed the dispersion of conductivity and dielectric constant down to as low as 10 Hz for a range of dispersed clay/electrolyte system. As with compressed clays, dispersion occurs at higher frequencies than are found in the field for induced polarisation. It is also highly unlikely that a significant amount of clay would be in a dispersed phase under the conditions of electrolyte concentration typical for rock pores.

5.1.4 Clay Membranes

A type of clay membrane was initially prepared by Marshall (126) and has been developed by Bose (24), Adhikari (2) and Pain and Mukherjee (162). The technique involves evaporating a clay suspension to dryness. The clay is then cut into disks and heated to a temperature as high as 600°C. The membrane that results is cation selective, although not specific, and has properties similar to ion exchange resin membranes and glass membranes (2). Impedance studies have not been made on such a system but it is highly probable that an impedance dispersion would be observed and that this would correspond to an induced polarisation effect.

The obvious limitation of this technique is the need to fire the membrane which might seriously alter the electrical properties of the clay, and Mayper (134) observed that the I.P. effect of clay-containing core samples became unmeasurably small upon firing. However, Marshall (126) observed that the membrane potential for a "membrane prepared from calcium-saturated Wyoming bentonite showed little or no effect with heat treatment from 300-600°C."

5.1.5 Clay Bonded to an Inert Matrix

In an attempt to simulate the assumed distribution of clay in a rock pore network, Vacquier (197) formed a system of clay adhering to a quartz sand by drying a kaolinite/sand slurry, and rewetting. The result was an open pored sand matrix cemented with clay, and with clay adhering to the matrix surfaces. Vacquier made time domain measurements of kaolinite/sand systems in a number of electrolytes, the results of these being entirely consistent with field I.P. surveys.

A slightly more sophisticated technique was used by Wright (137, 209) who dried clay onto a sintered glass matrix mounted within a pyrex conductance cell, in order to make time domain induced polarisation measurements.

The situation of clay in a glass matrix corresponds closely to that expected for clay in a rock pore, and the I.P. response of such a system is consistent with that observed for non-metalliferous bodies. It was proposed therefore to model clay/rock/electrolyte systems by

bonding clay onto an inert framework which can be perfused with electrolyte.

5.2 THE CHOICE OF CLAY

Hypotheses for the origin of induced polarisation in non-metalliferous bodies rely heavily on the fact that clays have an extensive electrical double layer. It is reasonable therefore to select a clay with a large surface area and ion exchange capacity to maximise electrical effects (79). Furthermore the clay should be well characterised and its important properties (cation exchange capacity, cation preference, zeta potential, particle size, etc.) known.

Two types of clay were chosen. Preliminary studies were conducted using Wyoming bentonite and later studies using laponite CP.*

5.3 THE PROPERTIES OF CLAYS OF THE WYOMING BENTONITE-LAPONITE TYPE

5.3.1 Structure

Wyoming bentonite is a montmorillonite and laponite is a synthetic hectorite type clay. Both are three layer clays having proposed structures (86) similar to pyrophyllite for which magnesium, sodium and lithium have been substituted for aluminium in octahedral sites (see Figure 5.1). The central layer consists of these octahedrally coordinated metal ions linked by bridging oxygen atoms to tetrahedrally coordinated silicon atoms in the outside layers. The layers are continuous in the a and b directions (Figure 5.1) and are stacked one above the other in the c direction. Montmorillonite is dioctahedral since only two out of every three octahedral sites is occupied, while laponite is trioctahedral as essentially all octahedral sites are occupied.

---

* Trade name for a synthetic material marketed by Laporte Industries Ltd, Redhill, Surrey, England.

FIGURE 5.1 Pyrophylite Structure

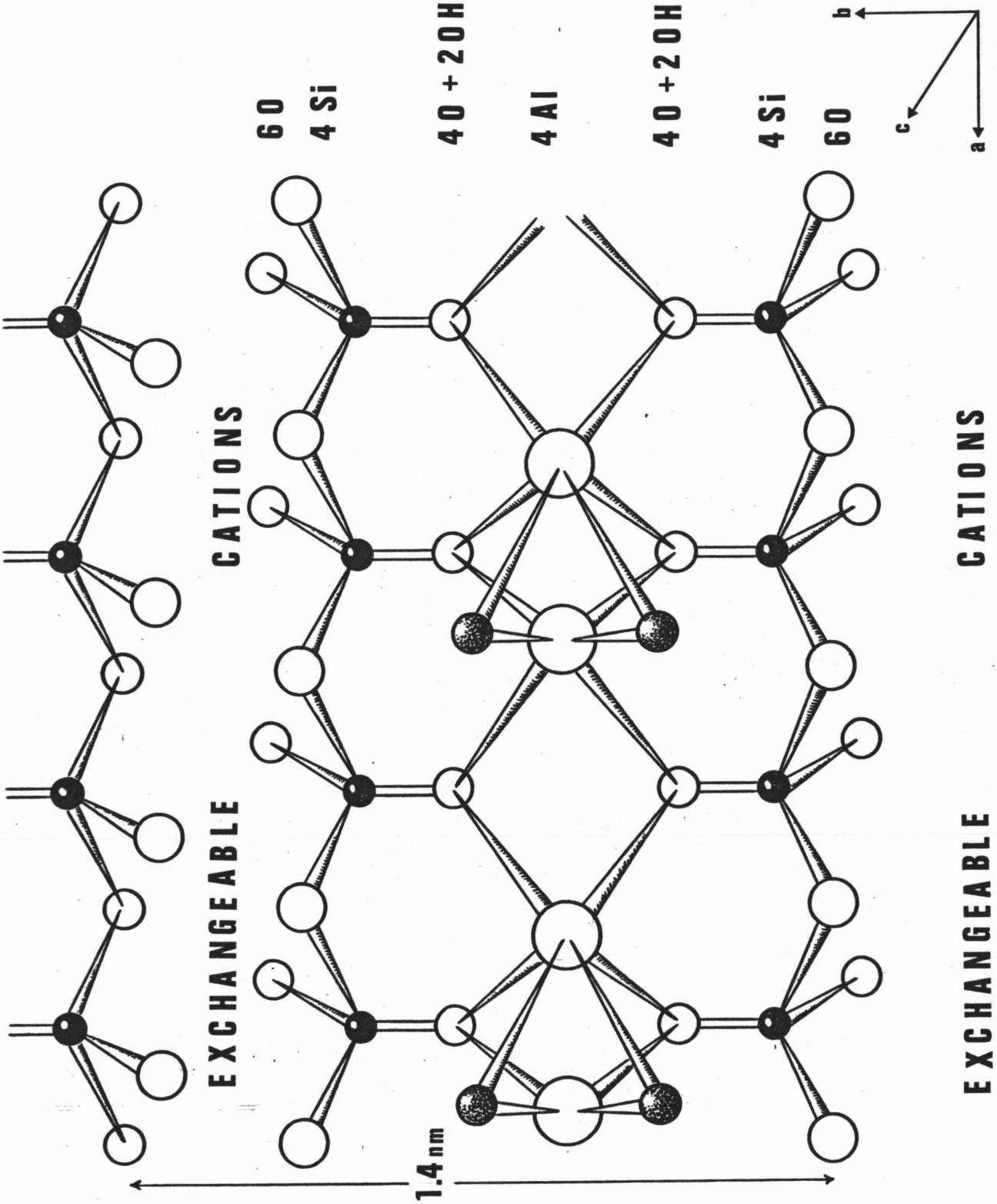

The exposed basal face of three layer clays consists of oxygen atoms each bonded to two silicon atoms within the lattice

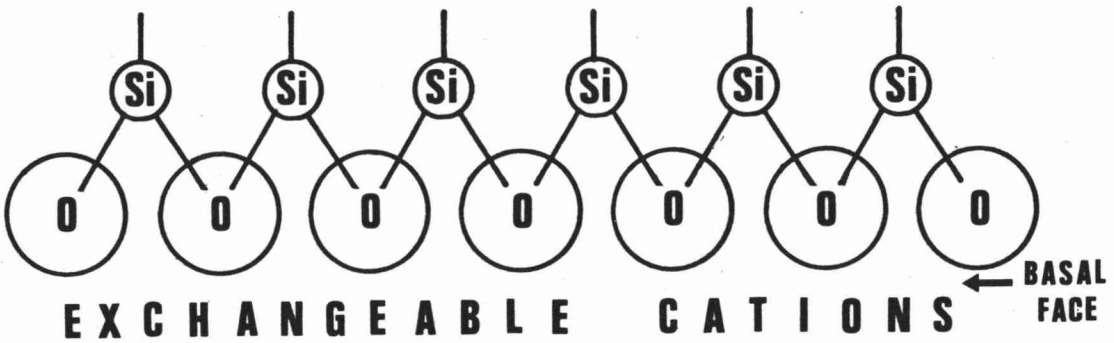

5.3.2 Exchange Capacity

Clays invariably have exchangeable cations associated with their exposed basal surfaces, and with the broken edges of the unit layers. These exchangeable cations are present to compensate for a charge deficit within the lattice which arises primarily as a consequence of substitution of Al^{3+} for Si^{4+} in tetrahedral sites, and M^{n+} for $M^{(n+1)+}$ in octahedral sites.

Grim (86) ascribes the majority of the cation exchange capacity for montmorillonites to substitution within the lattice of Mg^{2+} for Al^{3+} and to a lesser extent Al^{3+} for Si^{4+}. Broken bonds at the particle edges account for about 20% of the exchange capacity while exchange of the hydrogen of exposed hydroxyl ions is not considered important.

Perkins *et al* (164) consider the exchange capacity of laponite to arise from substitution of Li^{+} and H^{+} for Mg^{2+}.

Movement of aluminium from the lattice to exchange positions reduces the exchange capacity of montmorillonite clays. This is in part due to clogging of the exchange positions by Al^{3+}. Grim (86) points to unpublished work by Michelson as suggesting that this movement is facilitated by drying.

A sample of Wyoming bentonite analysed by Grimshaw (87) had a total cation exchange capacity (c.e.c) of 76.5 meq/100 g* with

---

* Milli equivalents of exchangeable ion per 100 grams of dry clay.

exchangeable cations present in the following percentages.

Ion	Ca^{2+}	Mg^{2+}	Na^{+}	K^{+}	H^{+}	Total
%	23.2	19.4	50.7	4.3	2.5	100.1%

Grim (86) quotes a figure of 77 meq/100 g determined at neutrality and states that Wyoming bentonite carries Na^{+} as the dominant ion.

Neumann (155) has observed the c.e.c. of laponite to be 79 meq/100 g.

The exchangeability of various cations is important in producing a clay of known type. The preference of exchange site for laponite and montmorillonite is observed (192, 86) to be generally as follows

$$Mg^{2+} > Ca^{2+} > K^{+} > Na^{+} > Li^{+}$$

5.3.3 Swelling

For a dry clay the unit layers are weakly bonded in the c direction (Figure 5.1) with a spacing of about 0.96 nm for montmorillonite. When swelling clays (of which Wyoming bentonite and laponite are good examples) are hydrolysed however, water molecules enter between the unit layers causing the lattice to expand.

According to Grim (86) after drying at room temperature a montmorillonite with Na^{+} as the exchange ion frequently has one molecular water layer and a C-axis spacing* of about 1.25 nm. With calcium-montmorillonite there are frequently two molecular water layers and a C-axis spacing of about 1.55 nm. As the clay is hydrated successive layers of water molecules enter the interlayer regions and Bradley *et al* (28) have observed four discreet hydrates for Wyoming bentonite having C-axis spacings of 1.24 nm, 1.54 nm, 1.84 nm and 2.14 nm.

Experiments by Mering (140) and by Bradley (29) with montmorillonite in the presence of large quantities of water suggest that with Na^{+} as the exchangeable cation the unit layers separate completely, but with Ca^{2+} and H^{+} the separation is not complete. This effect is a probable explanation for the observation made in this work

---

* That is unit layer thickness plus interlayer spacing.

that Wyoming bentonite will adhere to glass in the calcium form, but in the presence of excess electrolyte sodium-Wyoming bentonite slakes off the glass and forms a dispersion. The phenomenon was also observed by Vacquier (197) for kaolinite on quartz sand.

5.3.4 Electrophoretic Mobility

There is some evidence to suggest that clay particles are negatively charged on the basal surfaces, but positively charged at the broken edges of unit layers. Matijevic has measured the electrophoretic mobility as a function of pH for sodium montmorillonite (193) and laponite CP (164). As pH increases both clays show a constant mobility with a sudden increase to a second constant mobility at some value of pH. For laponite this occurs at about pH 6 and for sodium-montmorillonite at pH 9. Matijevic attributes the sudden increase in electrophoretic mobility to an interaction between hydroxyl ions and the positive edges of the platelets rendering them neutral or slightly negative.

This expected variation of surface charge with pH might well be important in theoretically treating induced polarisation data and the pH was monitored for clay cells using a Radiometer GK2321C combination pH electrode. The pH's measured for Wyoming bentonite and for laponite cells were all between pH 7 and pH 8.5*, over which range the electrophoretic mobilities of laponite particles are constant at -3.1 cm s^{-1} V^{-1} (164) and sodium-montmorillonite particles constant at -2.0 cm s^{-1} V^{-1} (193).

5.3.5 Surface Conduction

Surface conduction occurs in hydrated clays due to ionic migration of diffuse layer/exchangeable cations primarily within the interlayer regions expanded by water molecules. The thickness of this region in a fully

---

* The increase in pH invariably observed is thought to be due to partial conversion of the clay to the hydrogen form - thus reducing the concentration of hydrogen ions in the bulk electrolyte.

hydrated calcium-montmorillonite is not more than a few times the hydrated diameter of calcium ions (86) and conductivity in this region is on a molecular scale. Phenomenological models which assume water to have its bulk properties are inapplicable to this microscopic environment and workers employing such models are obliged to postulate an increased viscosity (109,110,115,116,117),decreased dielectric constant (60), increased dissociation constant (77) and decreased density (3, 4 , 145) for the first few layers of water adsorbed on a clay surface, in order to explain the observed surface conduction.

The foregoing notwithstanding the theories and concepts of surface conduction have application in this work not only to conduction observed for clay cells (Chapter 8) but to ion exchange resin cells and polystyrene latices (Chapters 7 and 8).

The theoretical calculation of the electrical conductivity of heterogeneous systems has frequently been attempted and numerous equations have been proposed for various particle geometries (53,187). For a system composed of (assumed) non-conducting particles surrounded by a surface double layer and immersed in electrolyte, the conductivity is considered to be composed of two terms. The first is a solution conductivity in electrolyte unmodified by the presence of the electrical double layer, and reduced from the electrolyte-only value by the presence of non-conducting particles. The second is the surface or excess conductivity occurring within the double layer.

Cremers (52, 53, 54) utilises an equation of the following form to describe surface conductivity.

$$K = K_s/f + K_\sigma$$

where K = observed conductivity

K_s = electrolyte conductivity

K_σ = surface conductivity.

The formation factor, f, is essentially the ratio of the solution to the observed conductivities in the absence of surface conduction. Plots of K versus K_s as a function of electrolyte concentration are observed to have a linear region at high concentrations for many materials (54,136,187), from which f and K_σ can be calculated.

The value of K_σ is a function of a geometric factor and the concentration and equivalent conductivity of mobile ions in the double layer. Assuming a Gouy type diffuse layer, then the equivalent surface conductivity (57),

$$\lambda_\sigma = -(2\varepsilon RTc/\pi F^2)^{\frac{1}{2}} \lambda \sinh(F\zeta/2RT)$$

where ε = dielectric constant

R = gas constant

T = temperature

F = Faraday constant

λ = equivalent conductivity of mobile ions

ζ = zeta potential

and

$$K_\sigma = \lambda_\sigma S/f\phi$$

where S = surface of solid per unit volume

ϕ = porosity = volume fraction of liquid.

Correlation between the observed surface conductivity and the above theory has been made for a number of particulate dispersions (51 , 52 , 53, 56, 57,187,199) and electrolyte saturated porous plugs (136, 175, 208), with moderately good agreement. Specifically, Cremers (54) obtained a value of K_s for a suspension of sodium-Wyoming bentonite in 0.02 M NaCl of $(1.75\pm.25)\times10^{-9}\ \Omega^{-1}\ cm^{-1}$ from which he calculated the following parameters.

$\sigma = 1.10\times10^{-7}$ meq cm^{-2} (surface charge density)

$\ell = 0.42$ nm (distance of plane of shear from clay surface)

$\zeta = -78$ mV (potential of plane of shear).

The value of ℓ obtained from K_σ would imply at least two partially hydrated adsorbed layers within the Stern region and is larger than is commonly assumed (192). The variation of ζ from the electrokinetically determined value of -33 mV (section 5.3.6) is considerable, and Cremers suggests an increased viscosity or decreased dielectric constant as possible explanations. It is probable however that this failure of the theory is on a molecular scale for which the concepts of viscosity and bulk dielectric constant are inapplicable.

In addition to excess surface conductivity, Cremers and Thomas (53) utilise the concept of excess diffusion coefficient, defined similarly, and determined from self diffusion measurements. For Na^+ in sodium-montmorillonite/0.025 M NaCl the excess diffusion coefficient is determined to be $D_\sigma = (0.388 \pm .007) \times 10^{-5}$ cm^2 s^{-1}, which is a little under half of the bulk electrolyte value (168).

Values of K_σ and D_σ are not available for laponite or hectorite.

5.3.6 The Zeta Potential

The zeta potential (ζ) is the potential of the plane of shear outside which an electrolyte carrying diffuse ions of one sign may flow with respect to a surface carrying the opposite charge. The zeta potential within the interlayer region will be different from ζ for a dispersed particle because the structure of the double layer will be different. The former however is not measurable.

The zeta potential of clays is determined by measuring the electrophoretic mobility of the dispersed phase colloidal particle and using the Smoluchowski equation (87),

$$\mu = \varepsilon\zeta/4\pi\eta$$

where ε = dielectric constant

ζ = zeta potential

η = viscosity of electrolyte

μ = electrophoretic mobility

Stone (186) calculated the zeta potential by this method for three samples of Wyoming bentonite and obtained a value of -33±1 mV at pH 8.8 Touret and Vestier (196) measured the electrophoretic mobility from pH 2 to pH 11 and found the zeta potential to be essentially constant at a value of -33±3 mV.

It should be noted that the zeta potential data of Touret and Vestier (196) are not consistent with those of Swartzen-Allen and Matijevic (193) who find the electrophoretic mobility (and thus ζ) to increase sharply for sodium-montmorillonite at a pH of about 9. This discrepancy is puzzling but may be associated with the difficulty in

measuring the pH of an inhomogeneous system, and ascribing this pH to the layers of relatively immobile water adjacent to the clay platelet surfaces (192).

Utilising the data of Perkins *et al* (164), the zeta potential of laponite for pH greater than 7 may be calculated from the Smoluchowski equation as

$$\zeta = -44 \pm 2 \text{ mV}.$$

5.3.7 Particle Dimensions

The shape and size of montmorillonite particles is rather poorly characterised. According to Grim (86) electron micrographs of this material "show irregular fluffy masses of extremely small particles". Some of the individual particles appear to be about 2 nm thick - that is of the order of thickness of the unit layer (Figure 5.1). Grimshaw stated that "the larger proportion of particles are 50 nm (long), and that those over this size are probably agglomerates."

Laponite particles are much more regular, and Neumann (155) describes the particles as being platy, lath-shaped having approximate dimensions 40x10x1 nm, and having an area (determined by nitrogen adsorption) of 354 m^2/g.

The basic particles of montmorillonite and laponite are thus of similar size and since the densities are approximately the same one would expect the area's to be similar. However because of the presence of agglomerates the area of montmorillonite is not simply determined, and the value obtained depends upon the technique chosen to measure it. Nitrogen adsorption gives a very low value (27-71 m^2/g, Ref.192) presumably because N_2 molecules are unable to penetrate between unit layers and adsorb onto the interlayer basal faces. Adsorption of water and of ethylene glycol which are known to penetrate between unit layers give more realistic values of 400-440 m^2/g (145, 178) and approximately 700 m^2/g (178). The latter is a commonly excepted value.

5.3.8 Chemical Purity

While the dominant clay-mineral component of bentonite is montmorillonite, other clay minerals particularly illite and kaolinite are usually present as are non-clay minerals notably cristobalite and silica (**86**). As such,an extensive purification process was employed to remove soluble and non-colloidal impurities (137) from Wyoming bentonite before it was used in this work.

A significant advantage of laponite is that it can be prepared reproducibly in rather pure form, and as such is free from various contaminants commonly encountered in natural clays (**155**). According to Neumann (155) "Apart from traces of soluble sulphate and carbonate it is free from detectable impurities."

5.3.9 Summary of Data for Wyoming Bentonite and Laponite Type Clays

Table 5.1

Property		Symbol	Bentonite	Laponite	Units
Structure			3 layer Dioctahedral	3 layer Trioctahedral	
Particle Dimensions:	Length	x	50	40	nm
	Breadth	y		10	nm
	Thickness	z	2	1	nm
	Surface Area	A	400-700	354	$m^2\ g^{-1}$
Cation Exchange Capacity		c.e.c	77	79	meq/100 g
Electrophoretic Mobility (pH=7)		μ	-2.0	-3.1	$cm\ s^{-1}\ V^{-1}$
Zeta Potential (pH=7)		ζ	-33	-44	mV
Surface Conductivity		K_σ	1.75×10^{-9}		$\Omega^{-1}\ cm^{-1}$
Surface Diffusion Coefficient		D_σ	0.388×10^{-5}		$cm^2\ s^{-1}$
Surface Charge Density		σ	1.10×10^{-7}		meq cm^{-2}

5.4 PREPARATION OF CLAY CELLS

5.4.1 Introduction

Cells of the type used by Wright (see section 5.1.5) were prepared and an attempt made to observe a frequency domain I.P. effect, however extreme difficulty was encountered in bonding sufficient clay to the sinter to produce a measurable impedance dispersion (137). A technique similar to that of Vacquier (197, see section 5.1.5) was then employed using ground pyrex or soda glass spheres instead of quartz sand.

This latter technique involves dry mixing clay and glass, mixing this with water and then drying. Under suitable conditions the clay cements the glass particles and this matrix may be perfused with electrolyte without slaking of the clay.

5.4.2 Preparation of Materials

Pyrex was prepared by grinding and sieving and soda-glass spheres by sieving, and the glass was then washed and dried. It was necessary to remove impurities from Wyoming bentonite but laponite was considered to be sufficiently free from impurities (see section 5.3.8). The clays were exchanged to the required cationic form using an ion exchange resin. All these techniques have been described previously (137).

Initial wetting was performed using double distilled water and all electrolytes were prepared from Analar reagents and double distilled water.

5.4.3 Determination of Clay:Glass Ratio

Experiments were conducted to determine a suitable clay:glass ratio from which to construct cells for impedance measurement. Quantities of clay and glass were mixed with water in a 5 ml beaker, and dried. For mixtures containing between 5 and 10% clay this technique produced a rigid framework of glass cemented with clay, which when rewetted with electrolyte could be subjected to some

mechanical stress. For mixtures containing less than 5% clay there was no apparent cementation after rewetting with electrolyte, and when lightly stirred the clay slaked off the glass surface forming a dispersion. For clay/glass mixtures containing greater than 10% clay, when rewetted with electrolyte the clay swelled and filled the pores in the glass framework, and the system behaved much like a gritty clay.

The limits of 5 and 10% depend somewhat on the glass grain size and type, and no cementation could be observed for Wyoming bentonite with soda-glass spheres. The cationic form of the clay and the nature of the rewetting electrolyte also are important and sodium-Wyoming bentonite matrices rewetted with 0.01 M NaCl resulted in slaking of the clay from the glass surface, while calcium-Wyoming bentonite rewetted with 0.01 M $CaCl_2$ produced a stable matrix. This effect has been described previously (section 5.3.3) and is probably due to the fact that the double layer is compressed by multivalent ions and clay-clay (and clay-glass) electrostatic repulsion terms are overcome. A consequence of this is that reliable measurements cannot be easily made on sodium Wyoming bentonite cells.

5.4.4 Practical

To prepare a cell for measurement the following technique was employed. Appropriate weights of cleaned, exchanged clay and sieved, cleaned glass were mixed together dry, then wet with double distilled water and mixed to a thick paste. This was forced into the central section of the conductivity cell (see section 5.7) using a funnel, and the whole dried in air under a heat lamp for two days and then in an oven at 80°C* for four days. The cell was then assembled, perfused with electrolyte and placed in the thermostat bath to equilibrate for two days.

After measurements had been made it was possible to re-equilibrate laponite cells with a new electrolyte concentration by passing electrolyte

---

* Temperatures greater than 80 C were not used in order to prevent complete and irreversible dehydration of the clay lattice (86), and to prevent movement of Al^{3+} into exchange positions (see section 5.3.2).

through the clay/glass matrix. For Wyoming bentonite cells however attempted repercolations invariably resulted in clay eluting with the electrolyte, and reproducible determinations were not possible.

5.5 FOUR TERMINAL IMPEDANCE CELLS

5.5.1 Requirements

The experiments which prompted the use of a four electrode configuration have been described (section 4.1) and the requirements of such a cell are as follows.

1) The cell must be capable of being placed within a thermostat bath.
2) It must contain a chamber in which clay/glass matrices and other model systems can be placed.
3) The current electrodes should not contribute to the series impedance of the cell.
4) The potential electrodes must be non-polarisable, and be placed within, or close to, the system under test.

5.5.2 Electrodes

Only the last of these requirements is restrictive and after some experimentation (137) Ag/AgCl electrodes were selected as non-polarisable potential electrodes. These electrodes are reversible to chloride ions and restrict measurements to systems in which chloride ions are present. The most important asset of Ag/AgCl electrodes is that they are small, compact, can be used in any orientation, and do not usually significantly contaminate any medium in which they are immersed (99). They are not difficult to prepare, and using a series plating technique (Appendix 5.1), asymmetry potentials of the order of 0.1 mV can be obtained. A significant defect of these electrodes is an aging effect having a much longer time constant than that discussed by Janz (Chapter 4, 99). Over a period of weeks or months Ag/AgCl electrodes were observed to change colour from a deep purple-brown to light yellow-brown, accompanied by an increase in asymmetry potential between pairs of electrodes from ±0.1 mV to as high as ±5 mV.

It is imperative therefore to provide within the cell for replacement of Ag/AgCl electrodes periodically.

Platinised platinum was used for the current electrodes since these electrodes were also used for two terminal A.C. bridge conductivity measurements. Platinisation of the electrodes was performed as described in Appendix 5.1.

5.5.3 Cells

Cells were constructed in five parts as shown in Figure 5.2. Potential electrodes (1 and 2) were constructed by chloridising (Appendix 5.1) a 1 mm dia. silver wire passed through 35 mm of 7 mm dia. PTFE* rod machined at one end to a 1 in 10 taper to fit a 5/13 pyrex socket. The main advantage of this system over a conventional silver/glass electrode is the greater mechanical strength of silver/PTFE. In order to pass silver through pyrex it must be joined to platinum and then tungsten and the glass flowed over these two welds. This junction was found to be susceptible to damage, particularly when removing the chloride layer and cleaning an old electrode (using several grades of emergy paper) before re-chloridising. The PTFE/pyrex conical joint also does not require greasing. The PTFE/Ag/AgCl electrodes produced were found to give stable and reproducible results and electrode potentials were not apparently affected by any capillary creep of electrolyte between the silver wire and the PTFE rod which might have occurred.

Current electrodes (3 and 4, see Figure 5.2) consist of 1 cm squares of platinised platinum foil (0.1 mm thick) and these were mounted to connect to the central chamber using a 19/26 conical ground glass joint. PTFE sleeves were used instead of grease for the joints. For one set of electrodes a fifth platinised platinum wire electrode (1 mm dia.) was included with the current electrode (Figure 5.2.1) in order that conductivity measurements could be made of the electrolyte in order precisely to determine electrolyte concentration.

The central chamber (5) contains the system to be studied, confined between glass sinters. A number of these were constructed

---

* Poly(tetrafluoro-ethylene). Teflon.

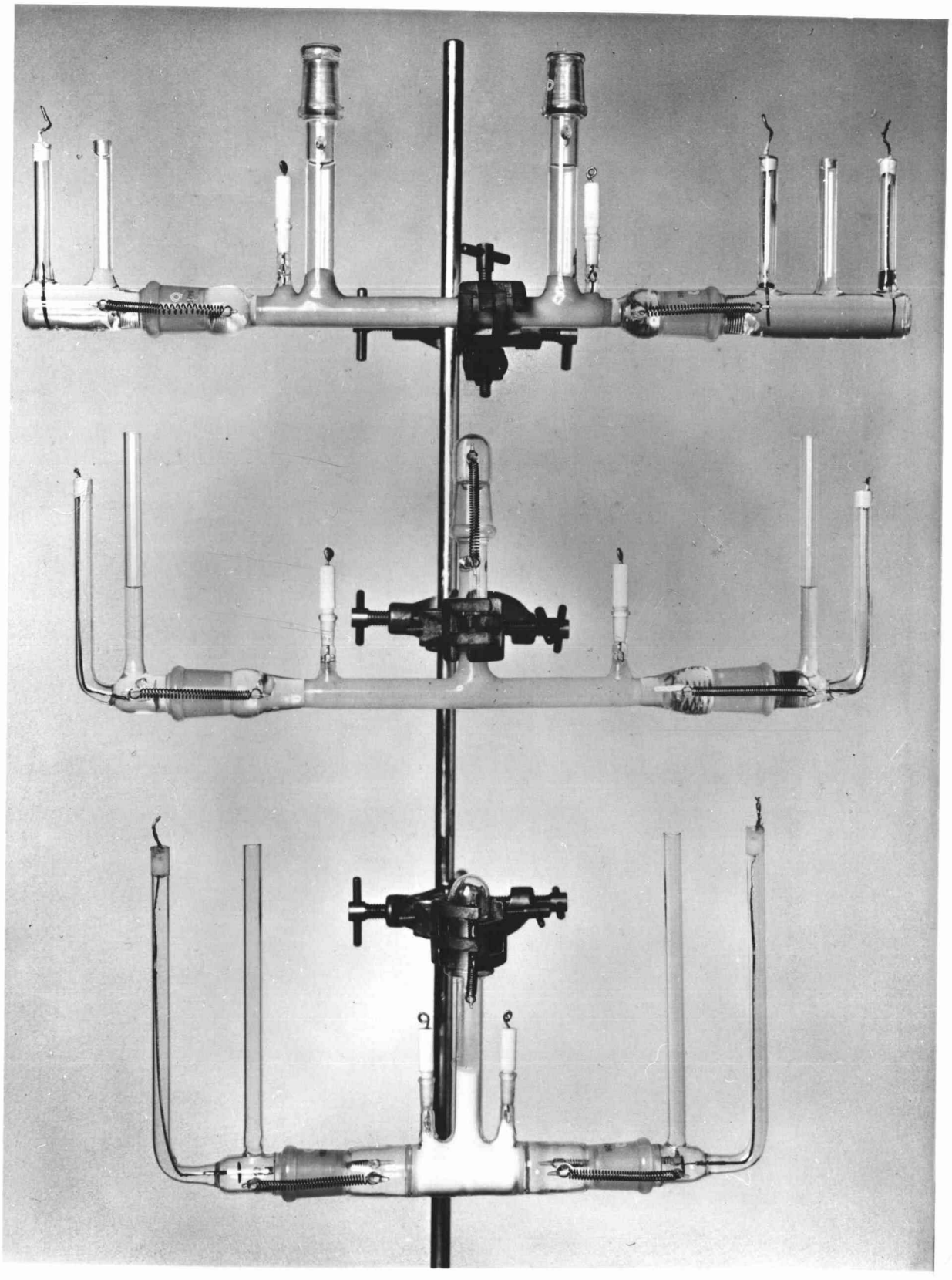

FIGURE 5.2.1

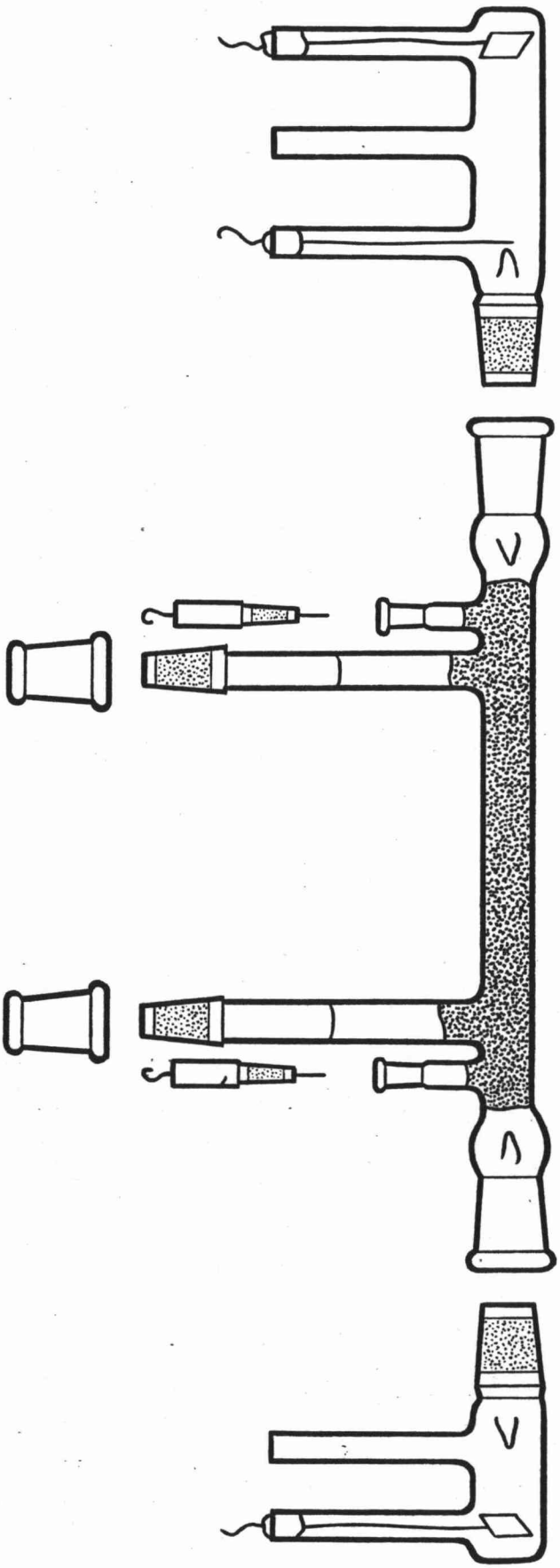

Scale 1:2

FIGURE 5.2.2

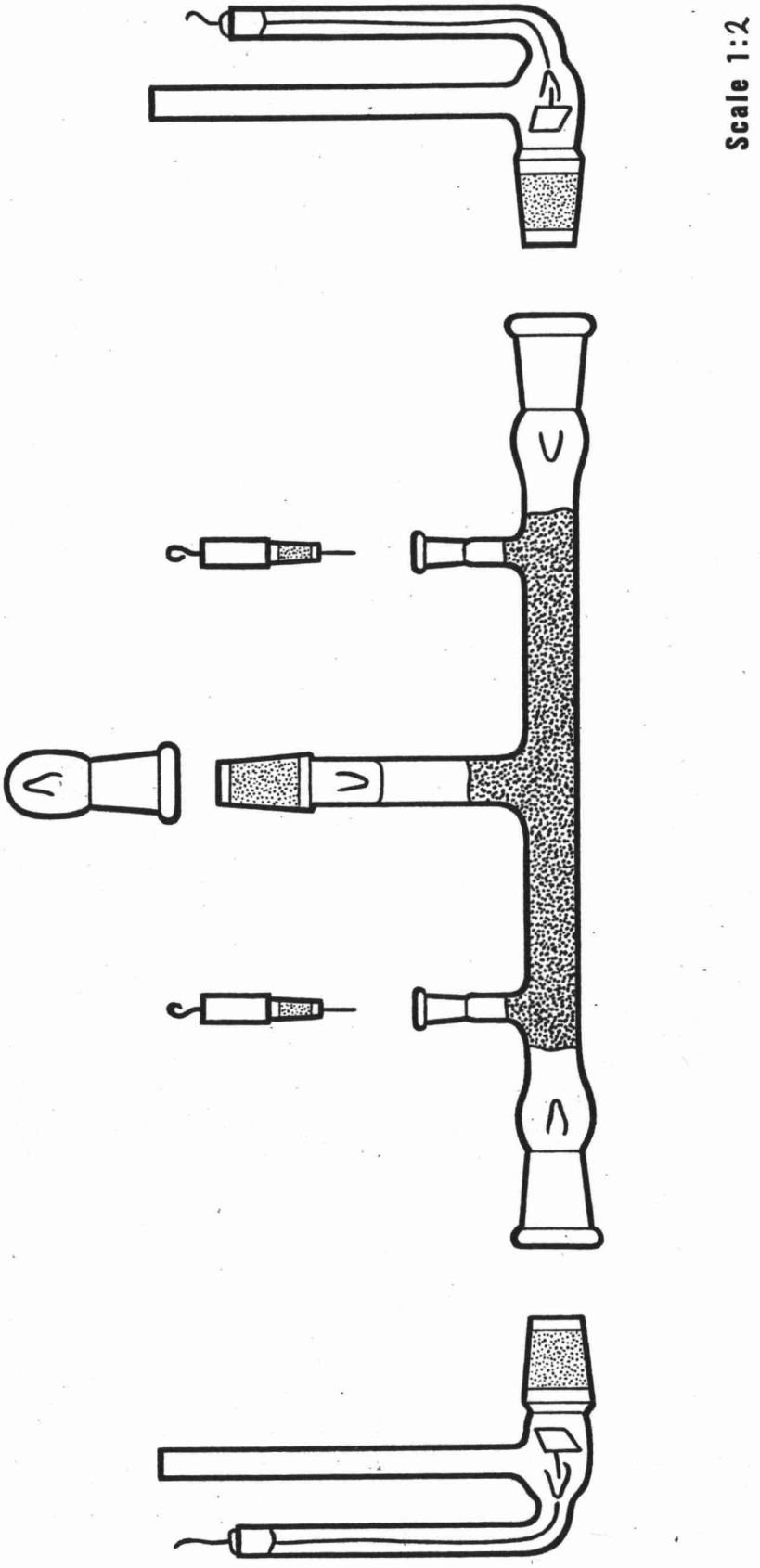

Scale 1:2

FIGURE 5.2.3

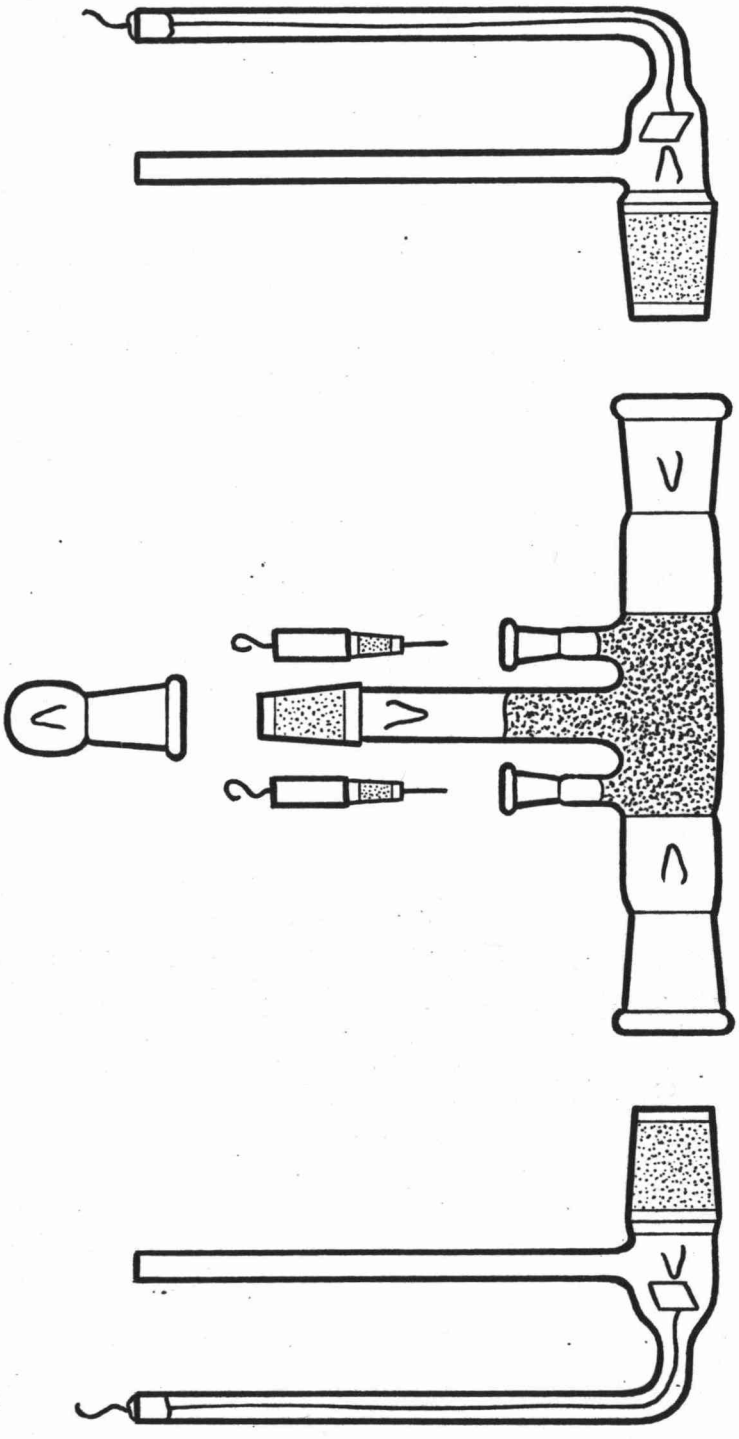

Latex Cell

Scale 1:2

for different purposes having one or two filling tubes and different porosity sinters, but the length between potential electrode sockets and the diameter of the chambers was standardised at 130 mm and 10 mm respectively. The only exception to this was a cell constructed to contain polystyrene latex (Figure 5.2.3 and see section 6.3).

CHAPTER 6 FURTHER MODEL SYSTEMS

6.1 INTRODUCTION

In order to determine the mechanism of membrane polarisation it is necessary to conduct impedance studies over a range of electrolytes and electrolyte concentrations, as well as temperatures and possibly pressures. As such the clay cells described in the previous chapter have a number of serious drawbacks. These cells are difficult to prepare* and, particularly for Wyoming bentonite, each new electrolyte or concentration requires a new cell with a resultant change in bed geometry. To facilitate research into the effects of electrolyte type and concentration two systems were used to simulate clay in a rock-pore/electrolyte environment. Synthetic ion exchange resin beads were used extensively in packed beds, and a dispersed phase polymerised polystyrene latex was used to a lesser extent.

6.2 ION EXCHANGE RESINS

6.2.1 Advantages of Resins

The advantages of resins over clay systems are as follows.

1) Resin particles are essentially spherical (21) and beds of resin or mixed beds of resin/glass spheres have a considerably greater reproducibility of pore structure than is expected for clay/glass matrices.

2) Ion exchange resins are available in a range of particle sizes and therefore pore size is easily modified.

3) Resins are much easier to handle and exchange than clays, and because they form a stable matrix they may be exchanged in situ - that is without removal from the impedance cell. This is significant as the pore geometry can be kept constant from one electrolyte to another, while the distribution of clay in a glass pore matrix is unknown and unstable.

---

* Each cell takes at least two weeks from the initial grinding of glass to the final impedance measurement.

4) For resins the exchange processes are well characterised (21, 25, 114, 150) while those for clays are not well defined.

5) The ion exchange resins used in this work had a cation exchange capacity of 5 meq/g (21) compared with 0.7 meq/g for Wyoming bentonite. This large cation exchange capacity was expected to, and did result in a large impedance dispersion.

6) The highly stable, well characterised, simple structure of resin bead beds facilitates mathematical treatment of the data.

6.2.2 Historical

Several earlier investigators used ion exchange resins as model soil systems. McKelvey *et al* (136) and Wylie *et al* (211) used cation exchange resins in a study of electrical resistance with regard to well logging. Schufle (179), and Madden and Marshall (129) observed the time and frequency domain I.P. response of resins, respectively. In none of these studies was a rigorous attempt made to justify either experimentally or theoretically the use of resins in a model system. The tacit assumption which underlies their use as model clays in I.P. investigations is that the phenomenon is caused exclusively by the presence of bound negative sites on an otherwise inert matrix. It is these sites which, if situated in a suitable pore system, give both clays and resins their membrane property of semipermeability.

6.2.3 Properties of Resins

For clays, exchange occurs on the surface, however it has been demonstrated by Kunin and Myers (113) that the cation exchange capacity of various sulphonic acid cation exchange resins may be quite accurately accounted for by the sulphur content of these resins. This indicates that the exchange of ions takes place throughout the whole gel structure of the resin and is not limited merely to the surface. Ion exchange resins may thus be considered to be gel-like particles with exchange groups randomly distributed throughout each particle (27, 113, 150), and the overall exchange process may be divided into five distinct steps.

1) Diffusion of ions through the solution to the surface of the exchange resin particle,
2) Diffusion of the ions through the resin phase to the exchange sites.
3) The exchange of these ions with those already on exchange sites.
4) Diffusion of these displaced ions out through the gel.
5) Diffusion of these latter ions away through the solution.

The work of Boyd *et al* (27) and Adamson (1) indicates that the exchange rate is diffusion controlled, and Boyd *et al* have distinguished between two diffusion processes. At concentrations less than about 0.003 M, the diffusion of ions through the film of solution about each particle is considered to be rate determining. At concentrations greater than about 0.1 M the diffusion of ions through the gel becomes rate determining.

The impedance of a matrix of ion exchange spheres homoionic with the pore electrolyte will include a term for conduction through the electrolyte and a term for conduction through resin particles. This latter term will depend upon the diffusion processes in 1 to 5 above but not on 3, and thus should be controlled by the same cationic diffusion processes observed by Boyd *et al* for ion exchange.

The resins used in this work were manufactured by Bio Rad* and were cation exchange resins consisting of a copolymer matrix of polystyrene chains cross-linked with divinylbenzene. The terminology is as follows. AG50W-X12 100-200 mesh denotes an analytical grade (AG) resin with sulphonic acid exchange groups (50W) having 12% cross-linkage (X12) and having a nominal size range 100-200 U.S. standard wet mesh.

Bio Rad (21) give the order of selectivity of monovalent cation as

$$Ag > K > Na > H > Li$$

which is very similar to that observed by Mattson (133), Jenny (101), and Weigner (206) for clays and silicates.

---

* Bio Rad Laboratories, 32nd and Griffin Ave, Richmond, California.

6.2.4 Preparation of Resin Cells

Ion exchange resins were exchanged (137, Chapter 3) in a column, then placed in the central chamber of one of the cells described in section 5.7.3 and the cell assembled. The cell was then percolated with 2 dm^3 of the electrolyte of interest and placed in the thermostat bath for 24 hours to equilibrate. This procedure could be repeated as often as desired, the cell being percolated with 2 dm^3 of a different electrolyte concentration, re-equilibrated then the impedance observed.

6.2.5 Limitations of Resin Systems

There are certain physical differences between an assemblage of ion exchange resin spheres and the assumed distribution of clays in rock pores. For a bed of ion exchange resin spheres, the cation selective phase occupies most of the available volume, and thus the predominant conduction process (at least for low electrolyte concentrations) will be within this phase. In addition, resins have fixed anionic sites on which exchangeable cations are localised, and resin phase conduction must occur by a site "hopping" mechanism. In contrast, the predominant conduction processes in clay/rock/electrolyte systems are likely to be electrolyte conduction, and surface conduction within the double layer of clay aggregations.

Nevertheless, it appears from the limited and imprecise two terminal measurements of Madden and Marshall (129) that the impedance dispersion of resins is similar to that observed for clay systems, but that it occurs over a much narrower frequency range. This conclusion is supported by the experimental results of Schufle (179), and previous experiments by this author (137) on the I.P. effect of resin systems, and it is unlikely that the polarisation mechanisms for clay and for resin systems are fundamentally different. However, a first objective of the present study must be to decide whether ion exchange resins are useful model systems.

In view of the possible limitations of ion exchange resins, impedance measurements were also made on polystyrene latices as a further model system.

6.3 POLYSTYRENE LATICES

6.3.1 Introduction

Styrene monomer can be polymerised in the dispersed phase in the absence of surfactants to produce chemically clean, spherical particles having a narrow distribution of particle diameters, but covering a wide range of particle sizes (111, 84). Such polymer lattices have, within the last decade, become extremely important in the field of Colloid Science as model systems for the study of fundamental phenomena (16,158,159), and closely resemble clays in that they possess a surface double layer. Being spherical and having essentially no conductivity within the particle, the pore structure of a compacted bed of polystyrene latex is extremely well defined and reproducible.

6.3.2 Preparation

Approximately 40 g of polystyrene latex having a particle size of 1000 nm was prepared by the method of Goodwin *et al* (84) with the following reaction conditions.

Concentration of monomer	0.87 mol dm^{-3}
Concentration of potassium persulphate	2.22×10^{-2} mol dm^{-3}
Concentration of sodium chloride	4.33×10^{-2} mol dm^{-3}
Total volume	0.80 dm^3
Temperature	60.5°C
Reaction Time	24 hours
Percent yield of latex	62%

The precautions taken by Goodwin *et al* with respect to monomer and initiator ($K_2S_2O_8$) purity were found to be fully justified. Cleaning of the latex by dialysis was also performed just as described (84).

Particle size was determined by electron microscopy, and Fig. 6.1 shows the particles to be extremely spherical and of uniform size, having a mean diameter of 1250±50 nm.

FIGURE 6-1 Electron Micrographs of Polystyrene Latex Spheres

Magnification 5000

Marker 4000 nm

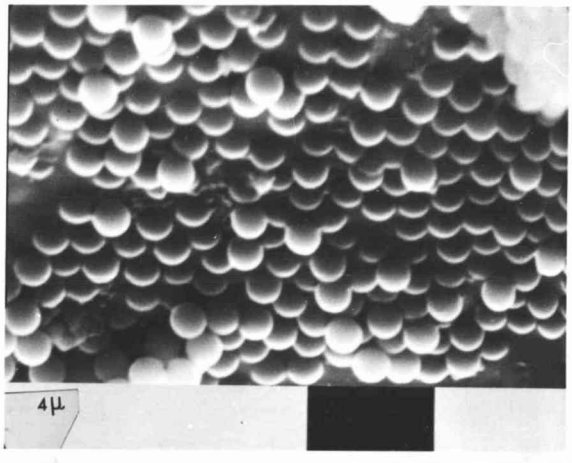

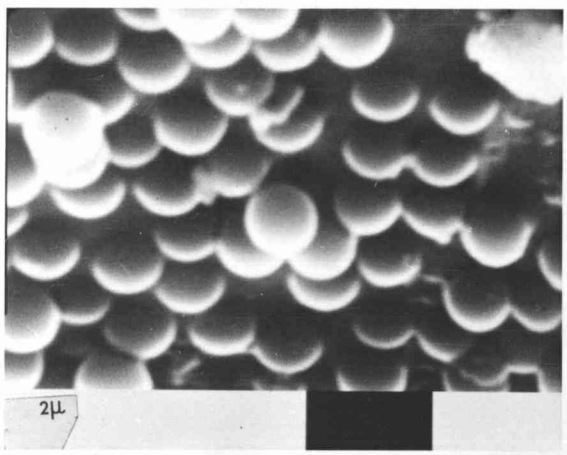

Magnification 10,000

Marker 2000 nm

Magnification 20,000

Marker 1000 nm

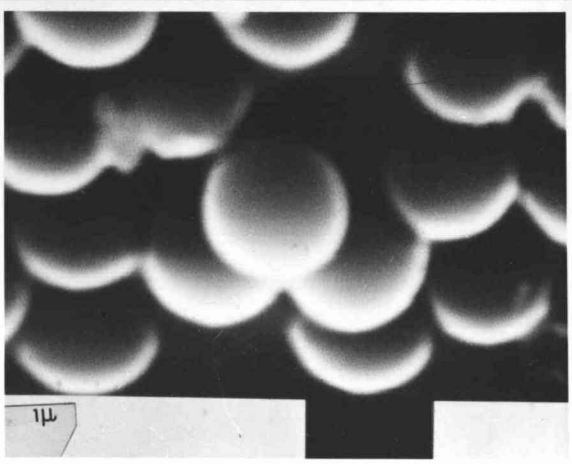

Section

III

Results

CHAPTER 7 "THE IMPEDANCE DISPERSION OF ION EXCHANGE RESIN BEDS"

7.1 DETERMINATION OF AN EQUIVALENT CIRCUIT

7.1.1 Introduction

The impedance measured by the technique described in Chapter 4 represents the equivalent two terminal impedance of that portion of the cell contents between the potential (Ag/AgCl) electrodes. This region is in no case homogeneous and the impedance observed as a function of frequency will normally represent a series-parallel combination of a very large number of resistive and reactive zones for which an effectively infinite number of equivalent circuits may be drawn; no one being more significant than another, and none precisely representing the electrochemical processes from which the impedance arises.

The form of the impedance dispersion invariably observed for resin cells is that of an arc of a circle with centre below the real axis, when data is represented as a complex impedance locus (Figure 7.1). Cole (42) has stated that a system containing any number and arrangement of resistances with one and only one variable impedance element can be reduced to one of two simple networks containing two resistances and one variable impedance element (Figure 7.2).

Figure 7.2.1

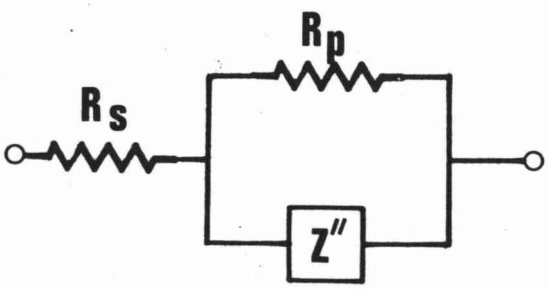

Figure 7.2.2

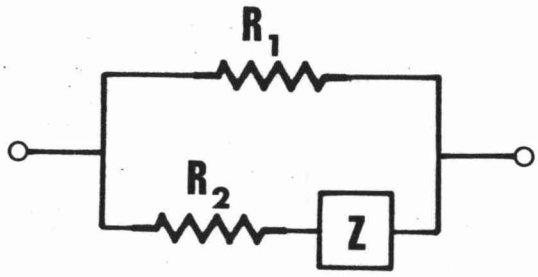

Provided there exists only one frequency dependent component, then either circuit may be used. When considering impedances however the series representation (Figure 7.2.1) is more convenient and although attempts were made to fit data to both circuits the series form was found to be the most amenable in solving for Z". The circuit shown in Figure 7.2.1 will thus be discussed exclusively.

FIGURE 7.1 Impedance Locus for Resin Cell Data

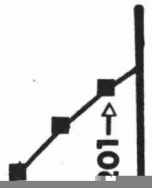

Cole shows that provided the variable impedance element (Z") has a constant phase angle then the locus of the impedance of Figure 7.2.1 is

$$R^2 + X^2 - (R_p+2R_s)R + mR_pX + R_p(R_p+R_s) = 0$$

where $m = \text{Tan}\ (1/\phi)$.

ϕ = phase angle of Z".

and Z = measured impedance = R + jX

This is the equation of a circle having its centre at the point $(R_p/2+R_s)$, $(-mR_p/2)$ and radius $(R_p/2)(1+m^2)^{\frac{1}{2}}$.

Since this corresponds exactly to the impedance loci observed for resin cells, a simple equivalent circuit may be deduced which has more significance than would generally be the case, the arguments in the first paragraph notwithstanding.

7.1.2 Frequency Independent Components

It is clear from the impedance locus (Figure 7.1), that the imaginary component tends to zero at the limits of high and low frequency; R_s being simply the high frequency intercept. Because of the observed close fit of resin data to an arc of a circle, R_s is normally determined by fitting R and X data to a circle three points at a time, and taking the mean of the high frequency intercepts.

Once R_s has been determined the reduced admittance is calculated

$$Y' = 1/(Z-R_s) = A + jB$$

and a plot of A versus B is observed to be a straight line of slope very nearly 1 and intercept on the real axis $1/R_p$ (see Figure 7.3).

7.1.3 Frequency Dependent Components

The impedance Z" which remains when R_s and R_p have been removed from the measured impedance is frequency dependent and its analysis requires frequency information. Plots of the real and imaginary

FIGURE 7.3 Admittance Locus for Resin Cell Data

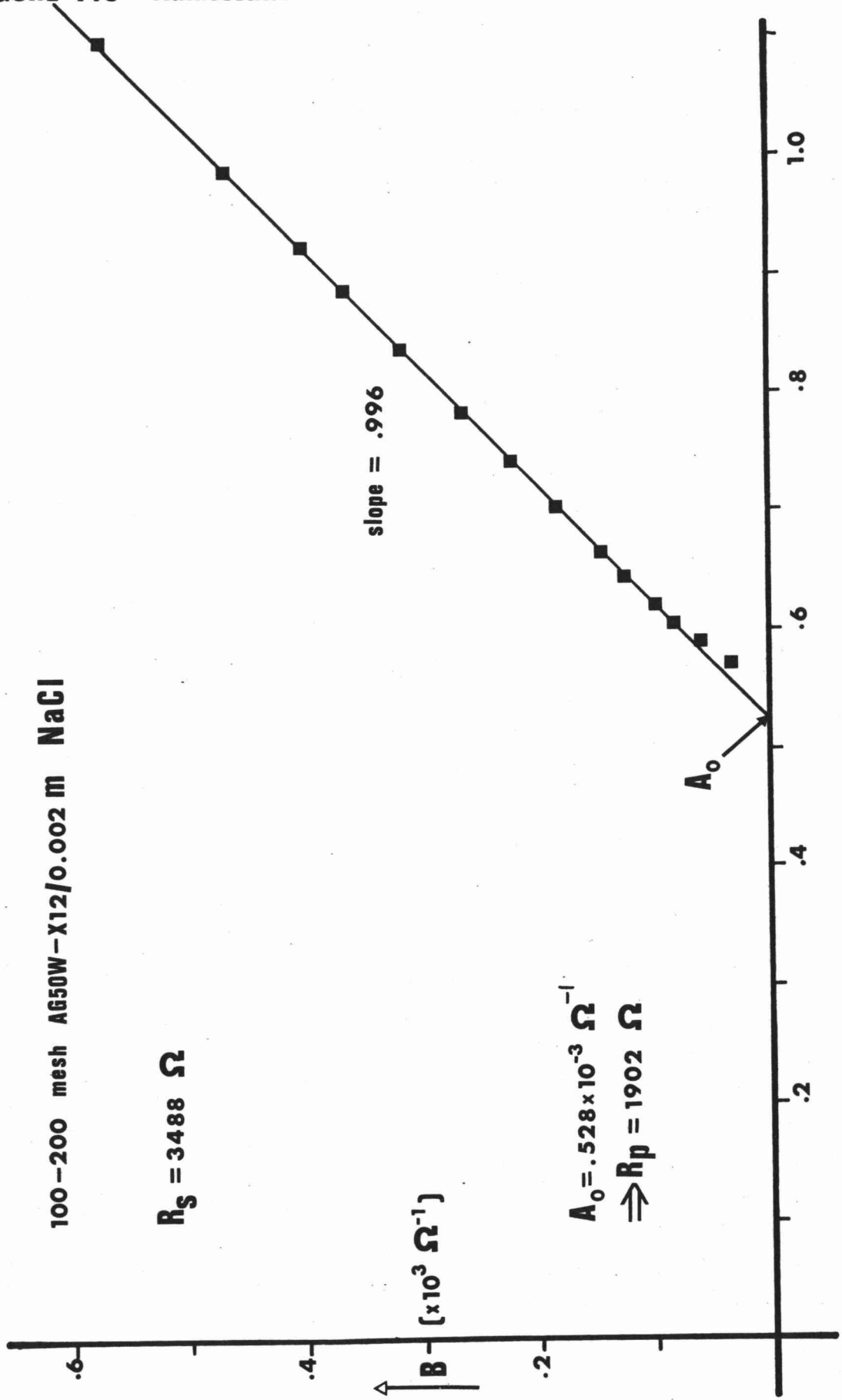

FIGURE 7.4 Z'' versus $\omega^{-1/2}$

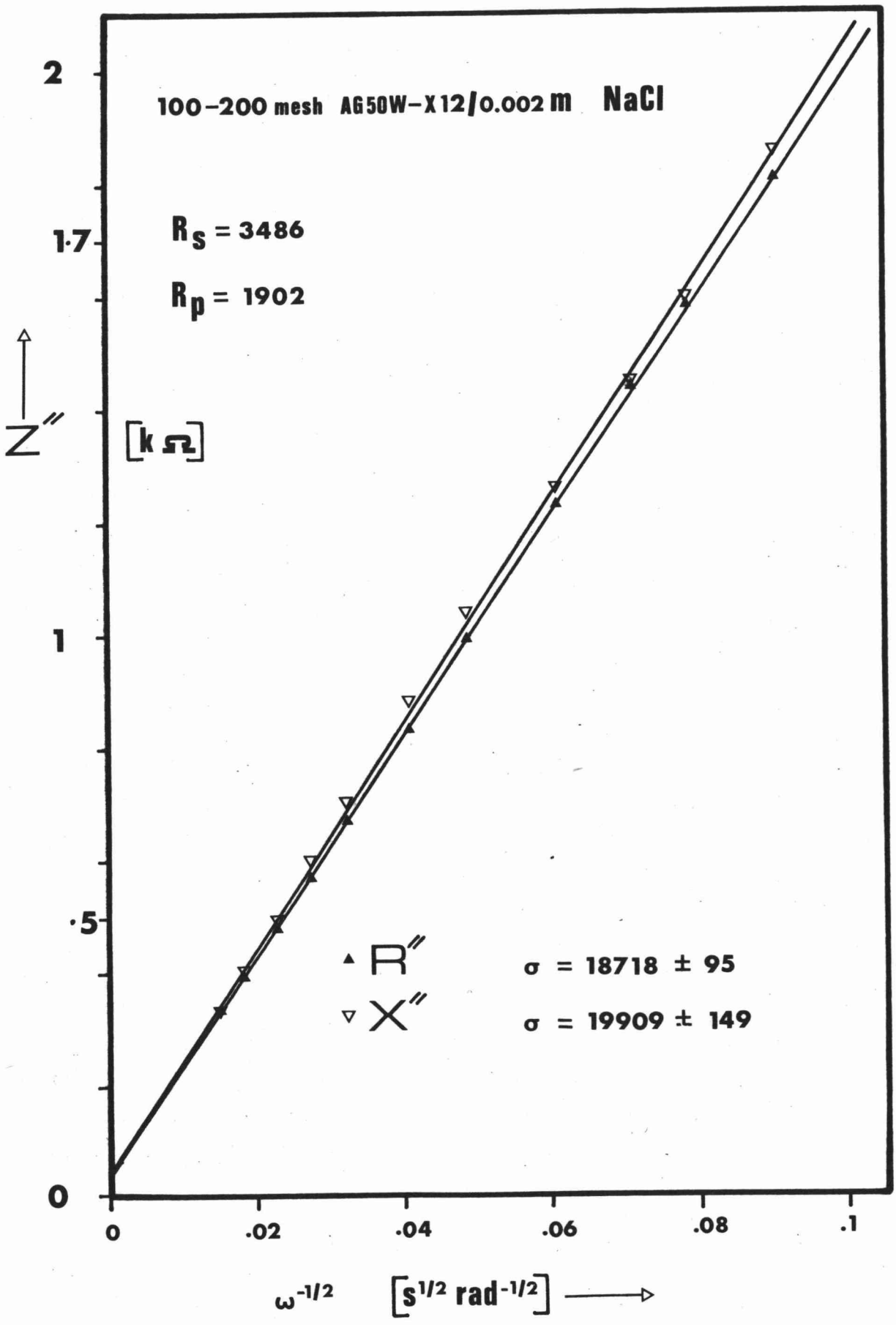

components of Z" versus $\omega^{-\frac{1}{2}}$ are found to be straight lines passing through the origin - the real and imaginary slopes being very similar (see Figure 7.4). This is exactly the form expected for a Warburg diffusional impedance (85 , 169 , 201), Z_w.

$$Z_w = \sigma(1-j)\omega^{-\frac{1}{2}}$$

where $\sigma = (RT)(n^2F^2AC)^{-1}(2D)^{-\frac{1}{2}}$

R = gas constant = 8.314 J K^{-1} mol^{-1}.

T = temperature K.

n = number of equivalents per mole.

F = Faraday = 9.649×10^4 C mol^{-1}.

A = area of diffusing zone cm^2.

C = concentration mole cm^{-3}.

D = diffusion coefficient cm^2 s^{-1}.

The phase angle for Z" is $\phi = Tan^{-1}$ (X"/R") at any frequency.

Since $R'' = a\,\omega^{-\frac{1}{2}}$

and $X'' = -b\,\omega^{-\frac{1}{2}}$

then $Tan\ \phi = -b/a$ for all frequencies.

For resin cells ϕ is observed to be very close to 45° (see Table 7.1), and for a Warburg impedance the phase angle is exactly 45°, since $\sigma = a = b$.

7.1.4 Resin Cell Data

Figure 7.5 represents the routine used to calculate the cell impedance from the bridge data and to transform this impedance into the parameters of the equivalent circuit shown in Figure 7.2.1. A tabulation of the parameters so determined is given in Table 7.1 which is a summary of determinations made on resin cells using the bridge described in Chapter 4.

The parameters R_p, a and b are determined by a linear regression and the errors accompanying these in Table 7.1 are derived from the standard errors in the regression coefficients. To demonstrate the

Table 7.1 Resin Data AG50W-X12

7.1.1 Preliminary Experimentation

Resin	Electro-lyte Type	Concen-tration (Molar)	T (°C)	R_s (Ω)	R_p (Ω)	a ($\Omega s^{-\frac{1}{2}}$)	b ($\Omega s^{-\frac{1}{2}}$)	ϕ (deg.)
20-50	$CaCl_2$	0.01	26.9	6535	1333	410	384	43.1
100-200	NaCl	0.001	26.7	4550	3138	21800	20400	43.3
"	"	0.01	26.7	1823	987	6892	7093	45.8±.1
"	"	"	47	1154	623	5575	5743	45.9±.3
200-400	"	0.001	26.7	6700	3478	53600	51600	43.9±.4
"	"	0.01	"	1750	808	8690	8593	45.3±.5
"	"	0.1	"	875	167	747	814	47.5±.2
"	"	"	45	544	104	642	760	49.8
"	"	1.0	26.7	329	8	6.7	22.8	74
"	$CaCl_2$	0.01	"	4050	1270	2975	3773	52
"	"	"	"	4033	1425	3400	3400	45±1
"	HCl	0.001	"	2168	386	7929	7915	45.0±.1
"	"	0.01	"	736	126	2058	1976	43.8±.2
"	"	"	"	683	113	1359	1406	46.0±.2
"	"	0.1	"	324.8	22.5	109	125	48.9±.1

7.1.2 Concentration Dependence, 100-200 Mesh Resin/NaCl

Concentration	T (°C)	R_s (Ω)	R_p (Ω)	a/r^{2*} ($\Omega s^{-\frac{1}{2}}$)	$-b/r^{2*}$ ($\Omega s^{-\frac{1}{2}}$)	ϕ (degrees)	G_E ($x10^6 \Omega^{-1}$)
0.0002	26.72	9210±	1330±	14960/.99994	15145/.99992	45.4	11.56
0.0005	"	6960±10	2029±10	21149/.99991	21137/.99991	45.0	26.75
0.001	"	5350±20	2226±10	20911/.99992	20964/.9998	45.1	51.87
0.001	"	5081±10	1912± 5	17498/.99998	17380/.9996	44.1	51.39
0.0015	"	3723±10	1782± 5	15060/.99997	14760/.9998	44.4	91.03
0.002	"	3565± 5	1965± 2	15830/.9995	15530/.9990	44.5	-
0.002	"	3488± 5	1902± 2	16785/.99989	16889/.99941	45.2	99.42
0.005	"	2066± 5	1193± 1	8441/.99993	8256/.99992	44.4	245.3
0.01	"	1418± 5	763± 1	4538/.99996	4478/.99995	44.6	483.8
0.02	"	1030± 3	480± 1	2445/.99989	2418/.99996	44.7	953.5
0.05	"	750± 1	249± 1	896.3/.99995	896.3/.99999	45.0	2255
0.10	"	607± 1	144± 1	391/.99997	384/.99998	45.5	4330
0.20	"	494± 1	80.1± 7	165/.9994	169/.9998	45.7	8188
0.50	"	461± 1	64.7± 5	115/.9994	122/.9998	46.6	-

* $Z'' = R'' + jX'' = (a-jb)\omega^{-\frac{1}{2}}$. r^2 values are the coefficients of determination for a and -b versus $\omega^{-\frac{1}{2}}$.

7.1.3 Temperature Dependence, 100-200 Mesh Resin/0.001 M NaCl

Concentration	T (°C)	R_s (Ω)	R_p (Ω)	a/r^{2*} ($\Omega s^{-\frac{1}{2}}$)	b/r^{2*} ($\Omega s^{-\frac{1}{2}}$)	ϕ (degrees)	G_E ($x10^6 \Omega^{-1}$)
0.001	6.37	7650±10	3824±5	22938/.99995	22830/.99988	44.9	35.48
"	14.55	6264±10	3090±5	20903/.99998	20779/.99997	44.8	41.55
"	21.12	5090±10	2477±5	18810/.99988	18640/.99995	45.3	47.70
"	26.59	4397±10	1786±5	15314/.99993	15083/.99989	44.6	54.25
"	26.63	4783±10	1902±5	17449/.99993	17754/.99992	45.5	51.48
"	35.0	3638±10	1246±5	12810/.99994	12691/.99996	44.7	60.87
"	43.1	2915±10	985±5	10677/.99999	10521/.99988	44.6	70.61
"	50.1	2433±10	768±5	9321/.99991	9238/.99991	44.7	79.50
"	61.0	2035±10	647±5	8241/.9997	8364/.99987	45.4	92.36
"	69.6	1729±10	555±5	7475/.99987	7220/.99984	44.0	103.93

* $Z'' = R'' + jX'' = (a-jb)\omega^{-\frac{1}{2}}$. r^2 values are the coefficients of determination for a and -b versus $\omega^{-\frac{1}{2}}$.

FIGURE 7.5 Impedance Data Reduction Procedure

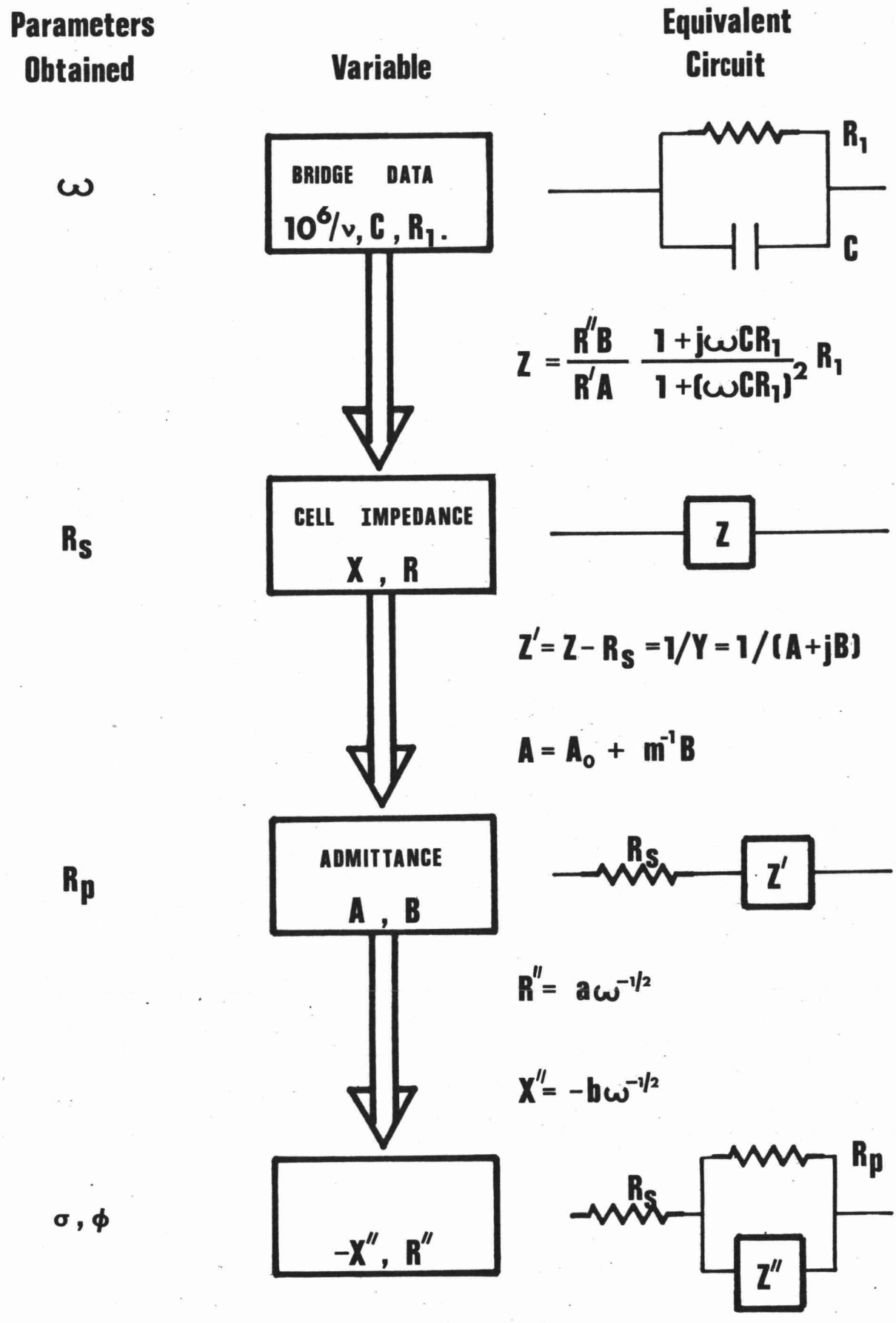

precision with which the routine shown in Figure 7.5 can be used the coefficients of determination r^2* (94) of the lines -X" and R" versus $\omega^{-\frac{1}{2}}$ are shown with a and b.

R_s is less easily and less accurately determined since it is not easy to "best fit" a circle, but more importantly because R_s must be determined at high frequencies where errors due to non-linearity within the bridge are largest (see section 4.7).

7.2 SIGNIFICANCE OF THE EQUIVALENT CIRCUIT

7.2.1 Introduction

It can be seen from Table 7.1 that Z" is well represented by an equation of the form $Z'' = \sigma (1-j)\omega^{-\frac{1}{2}}$.

To demonstrate that σ has the form predicted for a Warburg impedance will require further experimental evidence. However, the form of Z" is well defined and characteristic and may be used to calculate the expected impedance dispersion of the assumed equivalent circuit.

7.2.2 Characteristic Frequency

For a circuit of the form shown in Figure 7.2.1 the frequency dependence of the impedance will be unaffected by R_s and will be due only to the parallel combination of R_p and Z", for which the impedance is

---

* r^2 can be interpreted as the proportion of the total variation about the mean determined by the regression. For $r^2=1$ we have a perfect fit to the regression line for which the coefficients (in this case a or b) are applicable.

$$Z' = \frac{\sigma(1-j)\omega^{-\frac{1}{2}}R_p}{\sigma(1-j)\omega^{-\frac{1}{2}} + R_p}$$

$$= \frac{R_p^{\,2}\sigma\omega^{-\frac{1}{2}}(1-j) + 2\sigma^2 R_p\omega^{-1}}{R_p^{\,2} + 2\sigma\omega^{-\frac{1}{2}}R_p + 2\sigma^2\omega^{-1}}$$

$$-X' = \frac{\sigma\omega^{-\frac{1}{2}}}{1 + 2\sigma\omega^{-\frac{1}{2}}R_p^{-1} + 2\sigma^2\omega^{-1}R_p^{-2}} \qquad [1]$$

$$R' = \frac{\sigma\omega^{-\frac{1}{2}} + 2\sigma^2 R_p^{-1}\omega^{-1}}{1 + 2\sigma\omega^{-\frac{1}{2}}R_p^{-1} + 2\sigma^2\omega^{-1}R_p^{-2}} \qquad [2]$$

For -X' as a function of frequency the impedance rises to a maximum and falls, and we can define the characteristic frequency ω_o of the circuit as the frequency for which -X' is a maximum.

Thus $$\frac{d-X'}{d\omega} = 0 = -\left[\frac{\omega^{\frac{1}{2}}}{\sigma} + \frac{2}{R_p^{\,2}} + \frac{2\sigma}{R_p^{\,2}\omega^{\frac{1}{2}}}\right]^{-2}\left[\frac{\omega^{-\frac{1}{2}}}{2\sigma} - \frac{\sigma\omega^{-3/2}}{R_p^{\,2}}\right]$$

$$\frac{\omega^{-\frac{1}{2}}}{2\sigma} - \frac{\sigma\omega^{-3/2}}{R_p^{\,2}} = 0$$

$$\omega_o = 2\sigma^2/R_p^{\,2} \qquad [3]$$

7.2.3 Frequency Dependence of Z'.

Substituting [3] into [1] and [2] results in the following reduced, dimensionless forms of X' and R'.

$$-\frac{X'}{R_p} = \frac{(\omega/2\omega_o)^{\frac{1}{2}}}{1 + (2\omega/\omega_o)^{\frac{1}{2}} + \omega/\omega_o} \qquad [4]$$

and

$$\frac{R'}{R_p} = \frac{(\omega/2\omega_o)^{\frac{1}{2}} + 1}{1 + (2\omega/\omega_o)^{\frac{1}{2}} + \omega/\omega_o} \qquad [5]$$

Figure 7.6 shows $-X'/R_p$ and R'/R_p plotted against the logarithm of the reduced frequency ω/ω_o. Both X' and R' are log symmetric and at the characteristic frequency ($\omega/\omega_o = 1$), $R' = R_p/2$ and -X' has reached its maximum value of 0.2071 R_p.

R_s and σ may also be determined at the characteristic frequency since,

$$R_p = -X'_{\omega_o}/0.2071$$

and from equation [3],

$$\sigma = R_p(\omega_o/2)^{\frac{1}{2}}$$

and

$$R_s = R_{\omega_o} - R_p/2$$

When the proposed equivalent circuit (Figure 7.2.1) is applicable therefore, the parameters R_p, R_s and σ may be determined from a single observation at the characteristic frequency.

7.2.4 Characteristic Width

The reduced frequency at which $-X'/R_p$ drops to say 2/3 of its maximum value is also a characteristic of the circuit chosen. As an example the reduced form of the simplest proposed equivalent circuit for dielectric polarisation is shown also in Figure 7.6. Dielectric polarisation is a commonly proposed mechanism for the observed impedance dispersion of electrochemical and geological systems (see Section 3.4). However, the reduced impedance form is significantly different from that observed in this work to characterise the impedance dispersion of ion exchange resin systems. Not only is the expected maximum reactive component greater for dielectric dispersion than is observed for resin cells, but the 2/3 width is significantly less. This particular parameter will be discussed more fully in Chapter 8.

FIGURE 7.6 REDUCED IMPEDANCE PLOTS

SHUNTED Z_W AND C

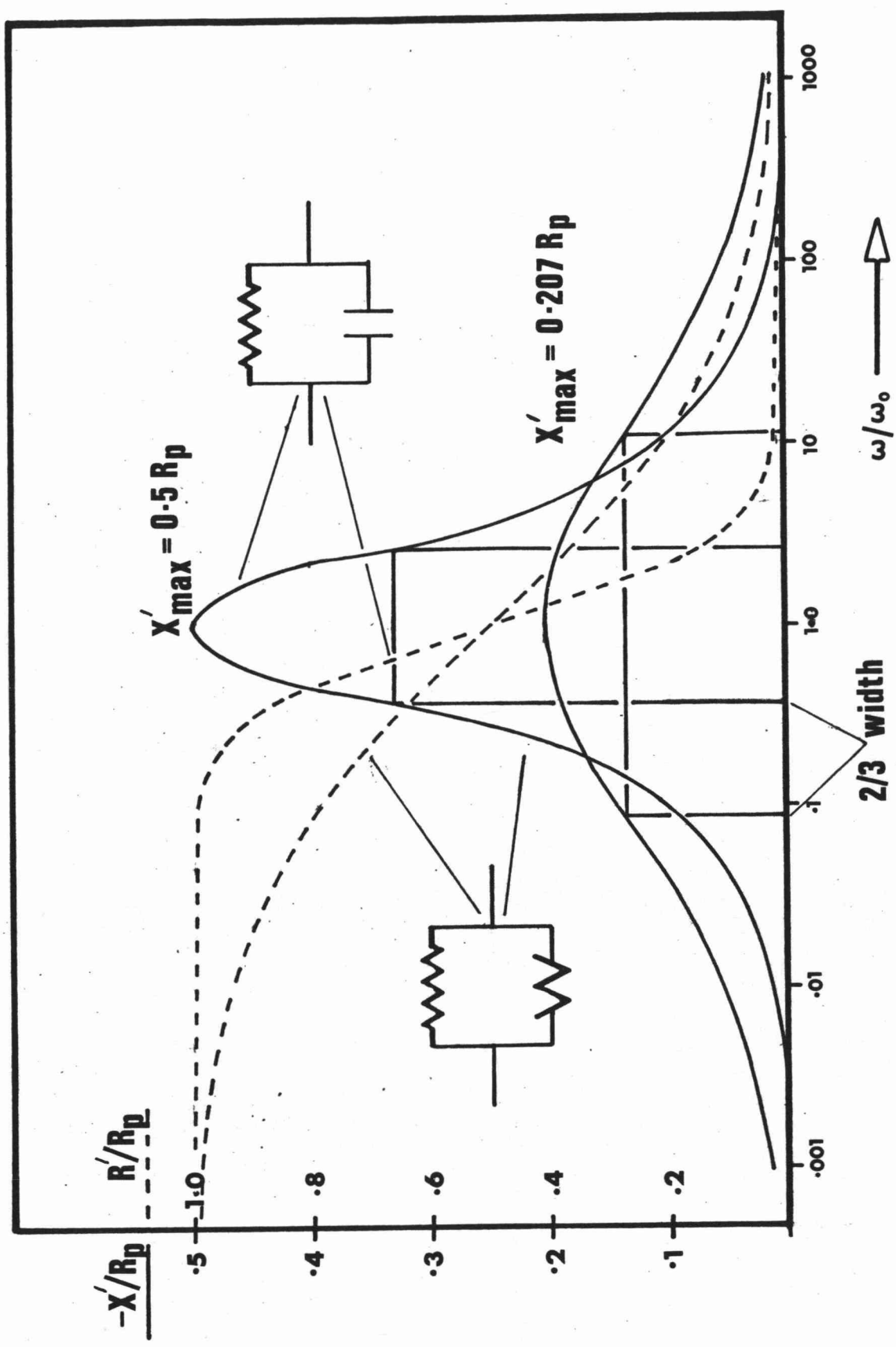

7.2.5 Conclusions

This type of analysis can be very usefully applied to test the adequacy of the proposed equivalent circuit. Resin data plotted in this reduced form are found to correspond closely to that expected for a shunted Warburg impedance and the crosses shown in Figure 7.6 represent data for a typical resin cell (shown asterisked in Table 7.1).

7.3 PHYSICAL PROPERTIES OF THE EQUIVALENT CIRCUIT PARAMETERS

7.3.1 Introduction

Having proposed an equivalent circuit the next step is to determine what physical significance its parameters have and what predictions can be made from these.

The parameters of the equivalent circuit are essentially R_s, R_p, σ and ω_o. The dependence of these on temperature and electrolyte concentration, and to a lesser extent cation type and resin particle size, have been observed and the results are summarised in the following sections. No analysis has been made of the dependence of the impedance on cell shape and size, or on the degree of packing of resin particles. To provide some conformity between cells the potential electrode spacing was standardised at 13 cm and the internal diameter at 1 cm, but the effects of resin sphere packing remain a significant uncontrolled variable.

The most precisely controlled variables are temperature and external electrolyte concentration for a single cell. A comprehensive examination of the effects of changing these variables has been made for a cell containing 100-200 mesh AG50W-X12 resin in the sodium form, equilibrated with NaCl electrolyte (Table 7.1.2 and 7.1.3). For each of the parameters of the proposed equivalent circuit, the observed temperature and concentration dependence is shown to be more generally applicable by referring to less comprehensive data for 20-50 and 200-400 mesh resin obtained during preliminary investigations (Table 7.1.1).

7.3.2 Concentration Dependence of R_p and R_s

7.3.2.1 100-200 Mesh AG50W-X12/NaCl (Table 7.1.2)

R_p and R_s were determined at 12 concentrations between 0.0002 and 0.5 Molar at a temperature of 26.6°C. In addition the conductance of the external electrolyte, G_E, was measured allowing an accurate determination of the concentration to be made. From data in Robinson and Stokes (168) for NaCl, the expected (literature) conductance G_L was calculated using the following equation

$$G_L = \Lambda c/b \qquad [6]$$

where b = cell constant = $(2.483\pm.004)\times10^{-3}$ cm^{-1}.

Λ = equivalent conductivity.

Concentration values were interpolated from a plot of log G_L versus log C using the measured values G_E. Figure 7.7 shows plots of the logarithm of G_E, G_p (= $1/R_p$) and G_s (= $1/R_s$) versus the logarithm of the interpolated concentrations.

From the slopes of the lines in Figure 7.7, the power of the concentration dependence of G is found to be,

$$G_E \propto C$$
$$G_p \propto C^{3/4}$$
$$G_s \propto C^{1/2}$$

and employing a linear regression the following lines are obtained, for data up to 0.1 M.

$$G_E\ (\times10^{-6}\ \Omega^{-1}) = 9\pm3 + (45000\pm150)C \qquad r^2 = .9999$$
$$G_p\ (\times10^{-6}\ \Omega^{-1}) = 40\pm70 + (38400\pm700)C^{3/4} \qquad r^2 = .9990$$
$$G_s\ (\times10^{-6}\ \Omega^{-1}) = -20\pm10 + (6930\pm140)C^{1/2} \qquad r^2 = .997$$

For G_E this form is just what would be expected for an electrolyte having a Kohlrausch dependence of Λ on C (168), since

$$\Lambda = \Lambda^\circ - A\,C^{1/2} \qquad [7]$$

FIGURE 7.7 Concentration Dependence

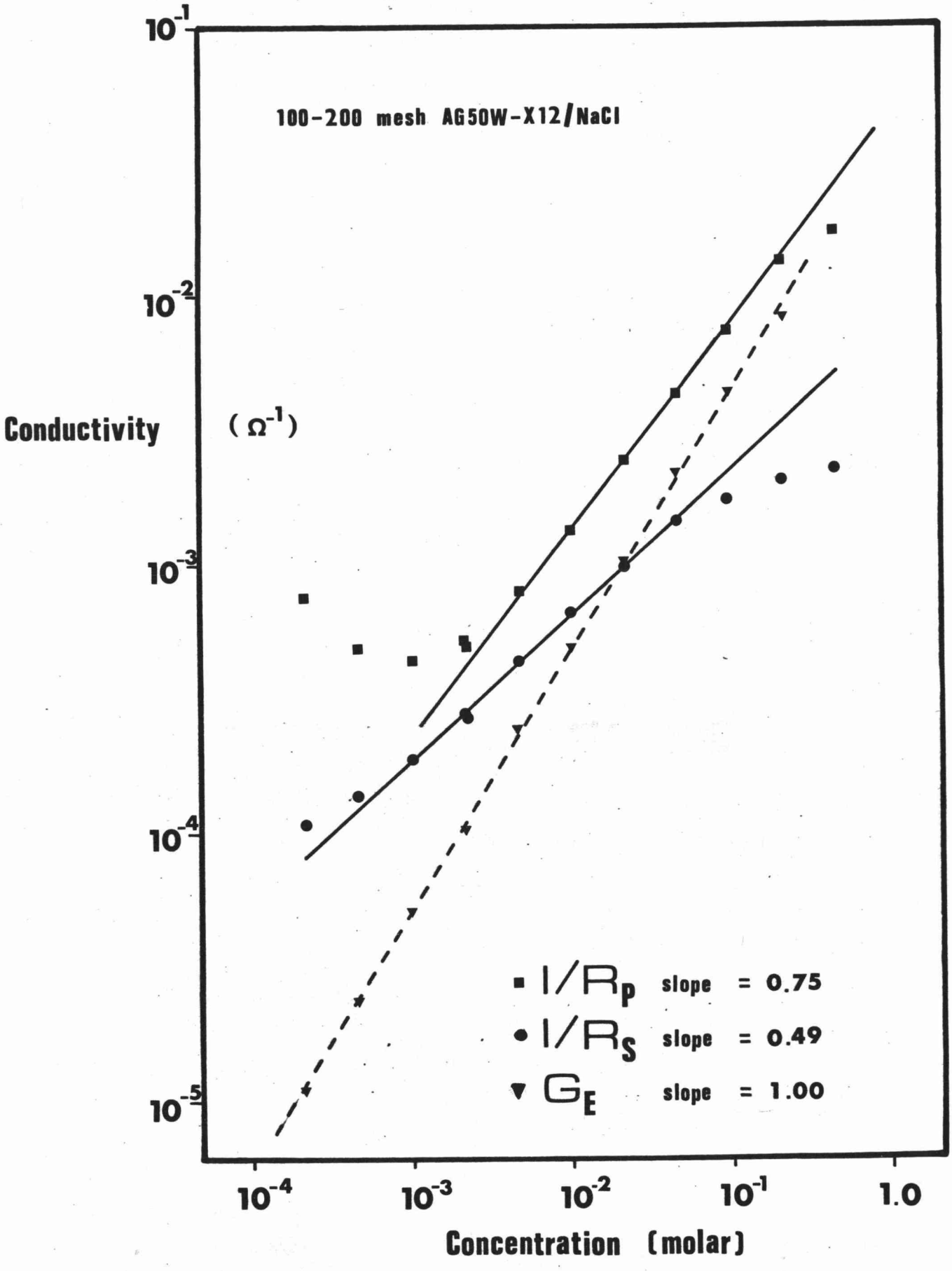

and from [6], $G_L \propto C$ at low concentrations and $G_L \propto C^{3/2}$ at higher concentrations.

In terms of equation [7] the concentration dependence of G_p and G_s are clearly anomalous, both being significantly less influenced by C than is the electrolyte conductance. Figure 7.8 is a plot of G_p versus $C^{\frac{1}{2}}$, $C^{2/3}$, $C^{3/4}$ and C, and verifies the proposed form for the parallel conductance.

7.3.2.2 Preliminary Measurements (Table 7.1.1)

The form of the concentration dependence observed above is not confined to 100-200 mesh resin or NaCl, and data for 200-400 mesh AG50W-X12 resin homoionic with the electrolyte for NaCl and HCl gives similar results.

In Figure 7.9, data for G_p and G_s versus C is presented in a logarithmic form and shows G_p to be proportional to $C^{3/4}$ and $G_s \propto C^{\frac{1}{2}}$. Excluding the 1.0 M data, a linear regression results in the following lines.

200-400 Mesh AG50W-X12/NaCl/27°C

$$G_p \ (\times 10^{-6}\ \Omega^{-1}) = 15\pm5 + (3290\pm50)C^{3/4} \qquad r^2 = .9998$$

$$G_s \ (\times 10^{-6}\ \Omega^{-1}) = 13\pm13 + (330\pm70)C^{\frac{1}{2}} \qquad r^2 = .989$$

200-400 Mesh AG50W-X12/HCl/27°C

$$G_p \ (\times 10^{-6}\ \Omega^{-1}) = 119\pm30 + (24320\pm30)C^{3/4} \qquad r^2 = .9999$$

$$G_s \ (\times 10^{-6}\ \Omega^{-1}) = 40\pm30 + (880\pm140)C^{\frac{1}{2}} \qquad r^2 = .992$$

The observed fit of G_p is particularly good and the results are strong evidence for a general dependence of G_p and G_s on the concentration of the external electrolyte, of the form

$$G_p = 1/R_p = nC^{3/4}$$

$$G_s = 1/R_s = mC^{\frac{1}{2}}$$

While the form of this dependence is immediately clear, its significance is not, and will be discussed further. It is apparent however that, at least at concentrations up to 0.1 M, neither G_p nor G_s

FIGURE 7.8 Concentration Dependence of $1/R_p$

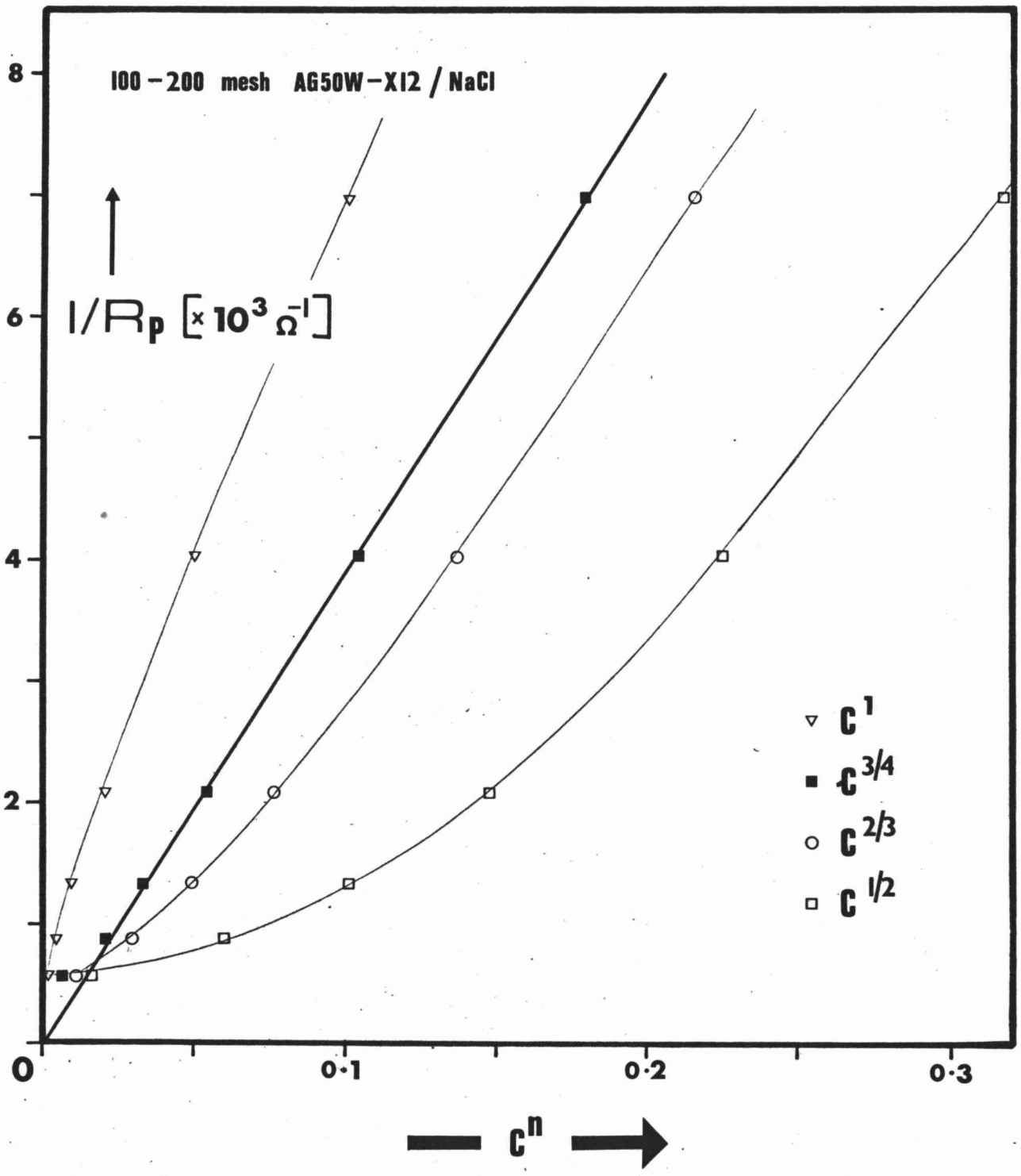

FIGURE 7.9 Concentration Dependence

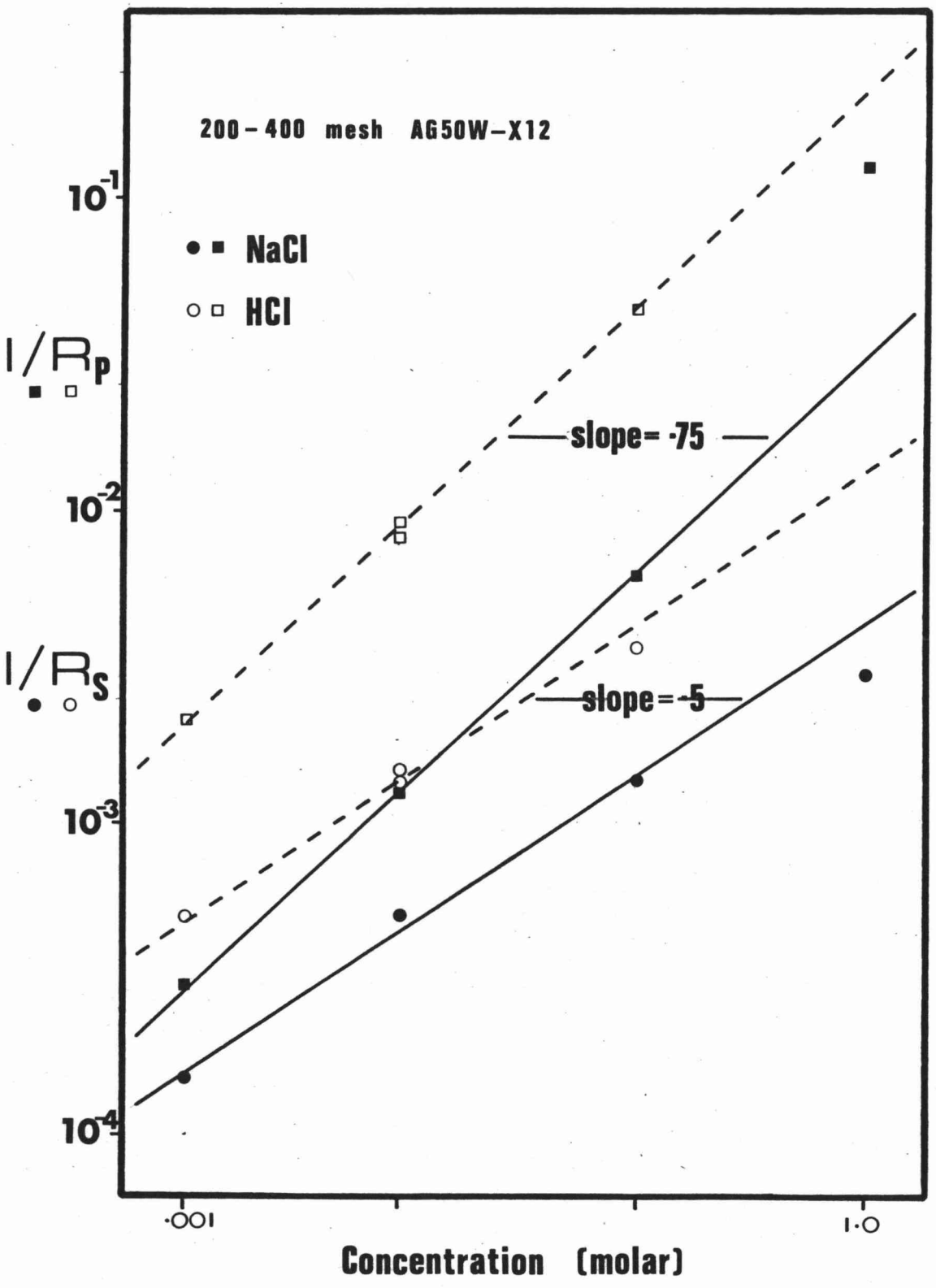

represent an electrolyte conductance in the bulk external electrolyte.

7.3.3 Concentration Dependence of σ

If one assumes Z" to be a Warburg diffusional impedance then

$$\sigma = \frac{RT}{n^2F^2AC(2D)^{\frac{1}{2}}} \qquad [8]$$

and assuming D to be independent of concentration over the range of C studied*, then $1/\sigma \propto C$.

Plots of 1/a and 1/b (i.e. $1/\sigma$ determined from R" and X" respectively) are in fact observed to be linear below 0.2 M. For the three systems discussed in section 7.3.2, a linear regression analysis gives the following equations.

100-200 Mesh AG50W-X12/NaCl

$1/a = -0.0002 \pm .0001 + (0.0305 \pm .0013)C \qquad r^2 = .999$

$1/b = \ 0.0002 \pm .0001 + (0.0299 \pm .0011)C \qquad r^2 = .997$

$\sigma = \underline{(33 \pm 1)C^{-1}}\ \Omega\ s^{-\frac{1}{2}}\ mol\ dm^{-3}$

200-400 Mesh AG50W-X12/NaCl

$1/a = -(6 \pm 13) \times 10^{-6} + (0.01344 \pm .00022)C \qquad r^2 = .9997$

$1/b = \ (1 \pm 10) \times 10^{-6} + (0.01227 \pm .00012)C \qquad r^2 = .9999$

$\sigma = \underline{(78 \pm 4)C^{-1}}\ \Omega\ s^{-\frac{1}{2}}\ mol\ dm^{-3}$

200-400 Mesh AG50W-X12/HCl

$1/a = -(7 \pm 12) \times 10^{-5} + (0.0924 \pm .0020)C \qquad r^2 = .9995$

$1/b = -(2 \pm 7) \times 10^{-5} + (0.0801 \pm .0013)C \qquad r^2 = .9998$

$\sigma = \underline{(11.7 \pm .8)C^{-1}}\ \Omega\ s^{-\frac{1}{2}}\ mol\ dm^{-3}$

---

* From 0.001 to 0.1 M NaCl, D varies from 1.585 to $1.483 \times 10^{-5}\ cm^2\ s^{-1}$ (168) for the bulk electrolyte.

The good fit of the observed concentration dependence to the form expected for a Warburg impedance suggests that Z" is in fact a Warburg impedance. Further analysis of the coefficients of σ versus C^{-1} will be performed in Chapter 9, in order to determine the parameters of equation [8].

7.3.4 Temperature Dependence of R_p and R_s

7.3.4.1 100-200 Mesh AG50W-X12/0.001 M NaCl (Table 7.1.3)

The impedance dispersion of this cell was measured for nine temperatures from 6.37 to 69.6°C. R_s and R_p were determined and G_E measured, and Arrhenius plots were found to be straight lines with least squares fits as follows (see Figure 7.9a).

$$\log (1/G_E) = 1.885\pm.054 + (717\pm17)/T \qquad r^2 = .9963$$

$$1/G_E = (177\pm20)\exp[(13.8\pm.2)/RT]$$

$$\log R_s = 0.0858\pm.0055 + (1068\pm17)/T \qquad r^2 = .9988$$

$$R_s = (2.8\pm.5)\exp[(20.5\pm.2)/RT]$$

$$\log R_p = -1.97\pm.18 + (1570\pm55)/T \qquad r^2 = .9938$$

$$R_p = (0.025\pm.006)\exp[(29.9\pm.9)/RT]$$

The activation energies for conduction are,

	$1/G_E$	R_s	R_p	
E_A	13.8±.2	20.5±.2	29.9±.9	kJ mol^{-1}

The value determined for $1/G_E$ is exactly that expected for 0.001 M NaCl (168), but clearly the activation energies for R_s and R_p are significantly greater than for electrolyte conduction.

FIGURE 7.9a Arrhenius Plots for Resin Cell Data

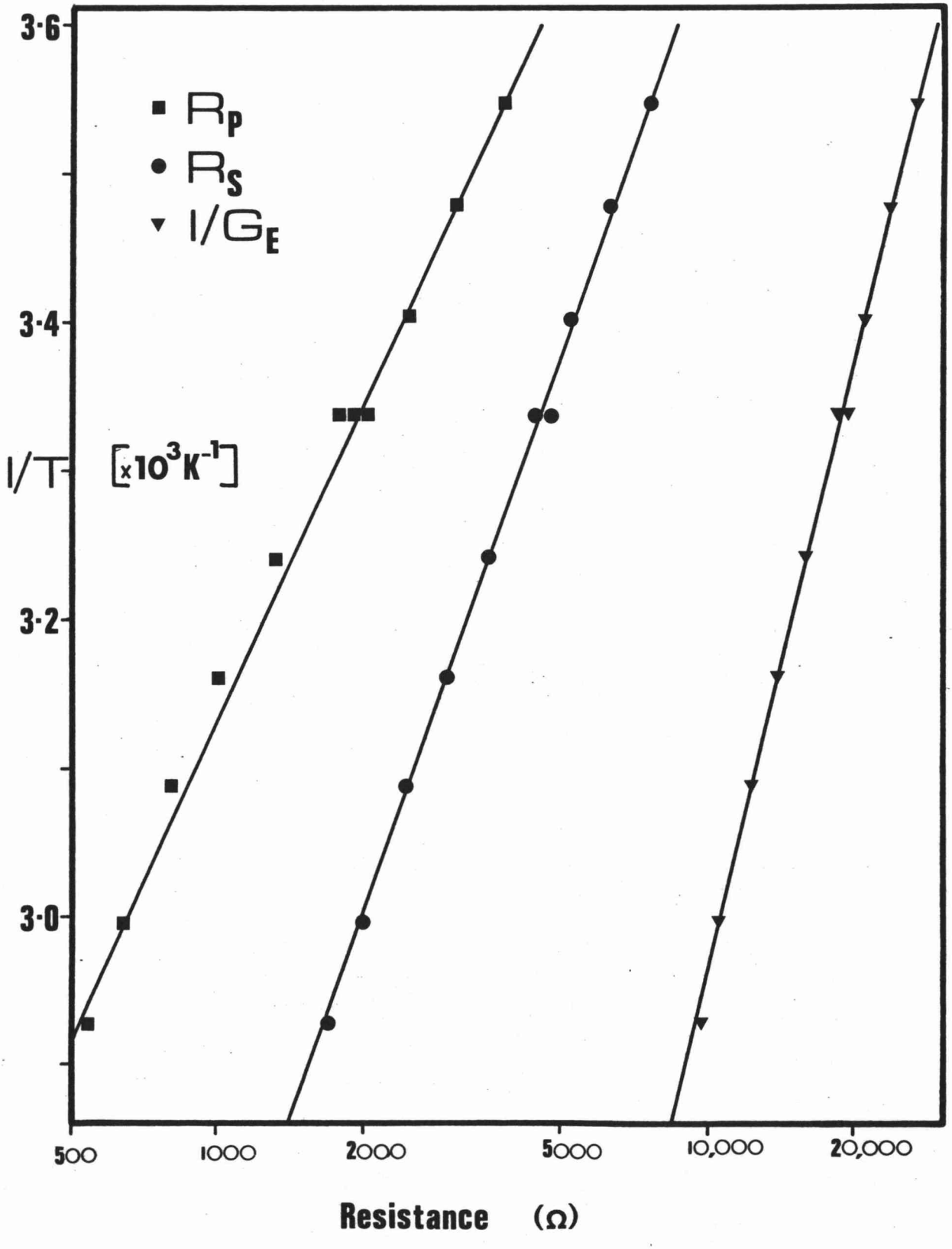

7.3.4.2 Preliminary Measurements (Table 7.1.1)

Determinations from a single elevated temperature have produced the following values for E_A.

T_1	T_2	Resin/Electrolyte	R_s	R_p
27°C	47°C	100-200 AG50W-X12/0.01 NaCl	E_A = 18.4	18.2 kJ mol^{-1}
27°C	45°C	200-400 AG50W-X12/0.1 NaCl	E_A = 21.0	21.0 kJ mol^{-1}

The values of E_A obtained thus support the conclusion drawn in section 7.3.2 that an electrolyte conduction path cannot account for R_p or R_s.

7.3.5 Temperature Dependence of σ

If Z" can be represented as a Warburg impedance, then from equation [8], and assuming A to be temperature independent, will vary with T $(D)^{-\frac{1}{2}}$. Using the Nernst-Hartley relation for a 1:1 electrolyte (168)

$$D = \frac{2RT}{F^2} \Lambda^\circ t_+^\circ t_-^\circ \left(1+ \frac{d \ln \gamma_\pm}{d \ln C}\right) \qquad [9]$$

where t_+° = limiting cation transport number.

t_-° = limiting anion transport number.

$\gamma_\pm$ = mean activity coefficient.

For 0.001 M NaCl the term in brackets can be ignored*, and since $n^2 = 1$,

$$\sigma = \frac{R^{\frac{1}{2}}}{2FAC} \frac{T^{\frac{1}{2}}}{(\Lambda^\circ)^{\frac{1}{2}}(t_+^\circ t_-^\circ)^{\frac{1}{2}}}$$

$$(\Lambda^\circ)^{-1} = 4\,\sigma^2\,F^2A^2\gamma^2\,(t_+^\circ t_-^\circ)/RT \qquad [10]$$

---

* From data in Robinson and Stokes (168) Appendix 8.9 for 0.002 M NaCl, $(d \ln \gamma)/(d \ln C) = -0.007$, and the temperature dependence of $1+(d \ln \gamma)/(d \ln C)$ between 15 and 45°C is 4 parts in 10^5.

The temperature dependence of $(t_+^\circ . t_-^\circ)$ is small*, and assuming an Arrhenius form for Λ°, a plot of log (σ^2/T) versus 1/T should be linear and have a slope $(-E_A/2.303R)$.

Using data from Table 7.1.3 for 100-200 mesh AG50W-X12/0.001 NaCl, a straight line is in fact obtained and has the following equation.

$$\log (\sigma^2/T) = -1.35 \pm .24 + (2184 \pm 75)/T \qquad r^2 = .9965$$

The activation energy for Λ_o calculated from this equation is 41.9 kJ mol^{-1} which is large compared with that for the electrolyte ($E_A \approx 14$ kJ mol^{-1}), and larger than that calculated for the resistive shunt, R_p ($E_A = 30$ kJ mol^{-1}) for the same set of experiments. The value obtained is however of the expected magnitude and the coefficient of determination (r^2) is sufficiently close to unity to justify the analysis.

7.3.6 The Effect of Particle Size

The dependence of R_p, R_s and σ on resin particle diameter is difficult to determine quantitatively because of the lack of control over packing density and bed geometry, between cells filled with different mesh resins. A limited amount of information is available from preliminary studies and the results of the one study specifically designed to test this variation are as follows.

Table 7.2

Resin (Mesh)	Electrolyte (Molar)	R_p (Ω)	R_s (Ω)	σ ($\Omega S^{-\frac{1}{2}}$)
20-50	0.01 $CaCl_2$	1333	6535	397
200-400	0.01 $CaCl_2$	1425	4033	3400

* From data in Robinson and Stokes (168) Appendix 6.2 for NaCl, $(t_+^\circ . t_-^\circ) = 0.238$ at 5°C and steadily increases to 0.241 at 55°C, a temperature dependence of 0.007% K^{-1}.

R_s decreases with decreasing particle size while R_p increases slightly. Similar results have been observed qualitatively during earlier experimentation using NaCl.

The coefficient σ increases approximately 10-fold with a 10-fold decrease in particle mesh size. Since $\sigma \propto 1/A$ (equation [8]), this is consistent with the characteristic area for Z" being associated with single resin particles. Thus, the membrane zones would appear to be individual resin spheres. Z" however, is derived from the macroscopic two terminal cell impedance, and the impedance (and thus characteristic area) of individual membrane zones cannot be determined without making an assumption about the microscopic electrical properties of the resin beds. This analysis is performed in detail in Chapter 9.

7.3.7 Summary of Results

Table 7.3 contains a summary of the measured effects of temperature, concentration and resin particle size on R_s, R_p and σ. While the results of only a small fraction of resin cell measurements have been discussed in this chapter, the forms of dependence shown in Table 7.3 are general, and no exceptions have been observed.

Table 7.3 Physical Dependence of Parameters

Parameter	Concentration	Temperature	Increasing Particle Size
R_s	$C^{-\frac{1}{2}}$	Arrhenius, $E_A \approx 20$ kJ mol^{-1}	increases
R_p	$C^{-\frac{3}{4}}$	Arrhenius, $E_A \approx 30$ "	little change
σ	C^{-1}	Arrhenius, $E_A \approx 42$ "	decreases $\propto 1/A$
Electrolyte	C^{-1}	Arrhenius, $E_A \approx 14$ "	decreases*

* For a bed of spherical particles/electrolyte the electrolyte resistance decreases with increasing particle size (61). This is due to a decreased tortuosity (176) and because the electrolyte represents a greater fraction of the total volume (i.e. greater porosity) for larger spheres.

7.4 DISCUSSION

7.4.1 Introduction

From the characteristic form of the impedance locus and reduced impedance versus frequency plots, an equivalent circuit has been determined which may be used to describe the impedance dispersion of ion exchange resin/electrolyte systems. This circuit comprises a frequency dependent element $Z'' = \sigma(1-j)\omega^{-\frac{1}{2}}$, associated with a series and parallel resistance. The impedance of resin cells can be well characterised by the parameters R_p, R_s and σ over a wide range of frequencies and varying experimental conditions.

The dependence of R_p, R_s and σ on a limited number of experimental variables has been observed and certain quantitative and qualitative relationships found, which are summarised in Table 7.3. These data may be utilised to elucidate a physical or electrochemical model for resin cells.

7.4.2 The Warburg Diffusional Impedance

From the observed concentration and temperature dependence of σ, it is clear that Z'' behaves just as a Warburg diffusional impedance, however the precise origin of this impedance is obscure. From the dependence of σ on resin particle size it may be concluded that the diffusional impedance is associated with the surfaces of ion exchange resin particles.

Buck (38) and Brand (30 , 31 , 32) have postulated the presence of a Warburg impedance for glass and for liquid-exchanger ion selective electrodes, but this type of impedance is historically associated with a metal-electrode/electrolyte interface. The impedance arises as a consequence of diffusional limitation to an imposed A.C. current in the electrical double layer adjacent to an electrode, at which one or more ionic species are being depleted. For electrodes, this depletion occurs by reaction. For an ion exchange resin particle depletion presumably occurs as cations cross the electrolyte/resin gel interface into the resin phase.

7.4.3 R_s and R_p

The physical structure of an ion exchange resin bed is essentially of uniformly sized conducting spheres, closely packed, having all voids filled with conducting electrolyte. Several conduction mechanisms are possible.

1) Conduction may occur in the electrolyte filled voids between resin particles at a sufficient distance from these particles to be in an effectively bulk electrolyte environment.
2) When resin particles are immersed in electrolyte some of the exchangeable cations on anionic sites within the resin gel move into the electrolyte phase setting up an electrical double layer at the resin gel/electrolyte interface. There are two possible conduction processes which arise as a consequence of the concentration of mobile cations in this double layer. One, normal to the interface will increase the transport of cations from the electrolyte into the resin. The other is the phenomenon of surface conduction (see section 5.3.5) occurring parallel to the interface and representing the excess conduction over the electrolyte phase due to the presence of mobile double layer cations.
3) Conduction may also occur within the resin particles. Since this is a membrane phase having a concentration of anionic sites, anions are excluded (201) and the transport number of the cations will be close to unity. Sulfonic acid ion exchange resins such as those used in this work are known to take up water (21 , 191) as well as cations (and to a lesser extent anions) from the electrolyte. Measurements of the self-diffusion coefficient of cations within the resin gel phase (189) have indicated that the mobile species are hydrated cations originating both from exchange positions and from the external electrolyte. The conduction mechanism within the membrane phase is expected to consist of site "hopping" between fixed anionic exchange grouping (37 , 63 , 122).

It is clear from the dependence of R_p and R_s on temperature, electrolyte concentration and resin particle size (Table 7.3), that the contribution to the conductance of the electrolyte phase (1), is small.

For (2) and (3) the major part of the current is carried by cations ($t_+ \simeq 1$) which are in an excess over mobile ions by the total cation exchange capacity (c.e.c) of the resin present in the cell. For the resins used in this work the c.e.c of a water saturated bed is 2.3 meq/cm^3 (21), and thus the total excess cation concentration is 2.3 equivalents dm^{-3}.

The component of conductance due to surface conduction can be assessed from the surface conductivity (see section 5.3.5).

$$K_\sigma = \lambda_\sigma S/f\,\phi \qquad [11]$$

where S = surface of solid per unit volume.
ϕ = porosity or volume fraction of liquid.
f = formation factor (see section 5.3.5).
λ_σ = equivalent surface conductivity.

$$\lambda_\sigma = \sigma_d\,\lambda_+/F \qquad [12]$$

where σ_d = surface charge density.
λ_+ = surface conductivity.*
F = Faraday constant.

For a 100-200 mesh resin bed, the mean particle diameter $\approx$0.01 cm, c.e.c = 5 meq/g and density $\approx$2. S, ϕ and f may be estimated as 408, 0.7 and 100 respectively. Assuming all fixed charges to contribute to the surface charge density, then

$$\sigma_D = (2)(5\times10^{-3})(4/3)(\pi r^3)/(4\pi r^2)$$
$$= 1.7\times10^{-5} \text{ eq cm}^{-2}$$
$$K_\sigma = \frac{(1.7\times10^{-5})(89)(408)}{(96500)\quad(100)(0.7)} = 9.1\times10^{-8}\ \Omega^{-1}\ \text{cm}^{-1}$$
$$G_\sigma = K_\sigma\, b, \text{ where } b = \text{cell constant} = 16.55\ \text{cm}^{-1}$$
$$= 5.5\times10^{-9}\ \Omega^{-1}$$
$$(R_\sigma = 1/G_\sigma = 1.8\times10^{8}\Omega).$$

---

* For Na^+, $\lambda_+ = 89\ \Omega^{-1}\ \text{cm}^2\ \text{eq}^{-1}$, including a term for electro-osmosis (57).

The expected surface conductance is thus four orders of magnitude smaller than the conductance processes necessary to produce the measured values of R_p or R_s for any resin cell. Clearly surface conduction parallel to the double layer does not contribute significantly to the cell conductance, however it is possible that R_p represents a shunt to the Warburg impedance normal to the interface.

A plot of the parallel conductivity ($K_p = 1/b\ R_p$) versus electrolyte conductivity ($K_E = G_E/b$) is found to have the form expected for excess electrolyte conduction (see section 5.3.5).

$$K_p = K_E/f + K_{d\ell}$$

where $K_{d\ell}$ is the excess double layer conductivity.

Figure 7.10 shows conductivity data for 100-200 mesh AG50W-X12 as a function of NaCl concentration (Table 7.1.3). The four highest concentration points are colinear, with the following least squares fit.

$$K_p = 0.0129\pm.005 + (0.00955\pm.00004)K_s \qquad r^2 = .9999$$

and one can determine

$$f = 104.8\pm.5$$
$$K_{d\ell} = (12.9\pm0.5)\times10^{-3}\ \Omega^{-1}\ cm^{-1}$$

Assuming that for individual resin particles R_p is due to conduction normal to the interface having a conductivity $K_{d\ell}$, and that the area for which this mechanism operates is the surface area of individual resin spheres, then the characteristic length ℓ over which this mechanism operates can be calculated.

$$R_p = \ell/(K_{d\ell})(A) \approx 100\ \Omega$$

thus,
$$\ell = (100)(12.9\times10^{-3})(\pi)(0.01)^2$$
$$= 4.1\times10^{-4}\ cm$$

This value is only 1/25th of the resin particle diameter, but is roughly 50 times the maximum expected thickness of a diffuse double layer (50). This result suggests that R_p may more readily be associated with the diffusion layer (see section 10.1.6) in which the Warburg impedance is determined.

FIGURE 7.10 Parallel versus Electrolyte Conductivities

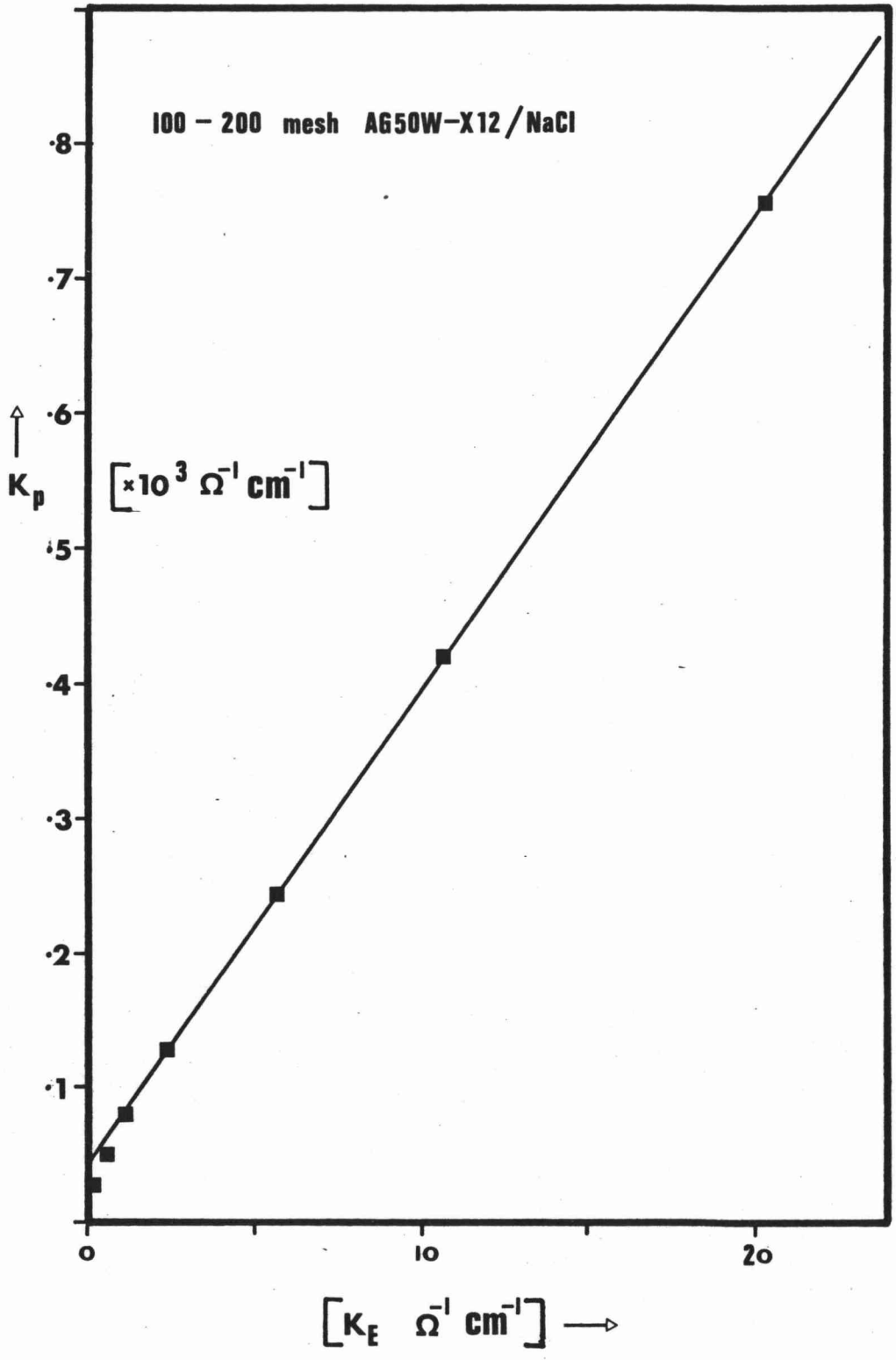

By a process of elimination, R_s must involve conduction within the resin particles, and there is experimental evidence to support this conclusion. Firstly, R_s is observed to increase with increasing particle size (Table 7.3). Since the volume fraction of resin decreases with increasing particle size, this observation is consistent only with a conduction mechanism within the resin phase and not with conduction in the electrolyte. If conduction occurs within the resin gel phase by a site "hopping" mechanism, the activation energy for conduction will be increased over the bulk electrolyte value by an amount related to the cation-site interaction energy (39 , 63 , 122). Such an increase is observed for R_s (Table 7.3). The small ($C^{-\frac{1}{2}}$) concentration dependence of R_s also is consistent with conduction within the resin phase. However, unlike R_p, R_s continues to rise with decreasing electrolyte concentration, even for C as low as 0.0002 M NaCl (Table 7.1.2), suggesting that the intrinsic resistivity of resin spheres is very large.

The above arguments suggest that R_s originates within the resin gel phase, but that the conduction mechanism predominantly involves cations arising from the electrolyte.

7.5 PHYSICAL REALISATION

The proposed electrochemical model on the scale of individual resin particles is extremely simple. A Warburg diffusional impedance occurs at the resin/electrolyte interface and is shunted by diffusion layer and an electrolyte conduction path normal to the interface. The resistance within the resin gel phase appears in series. Figure 7.11 shows this model for a particular resin particle for the impedance in the direction of the local electric field gradient.

Figure 7.11

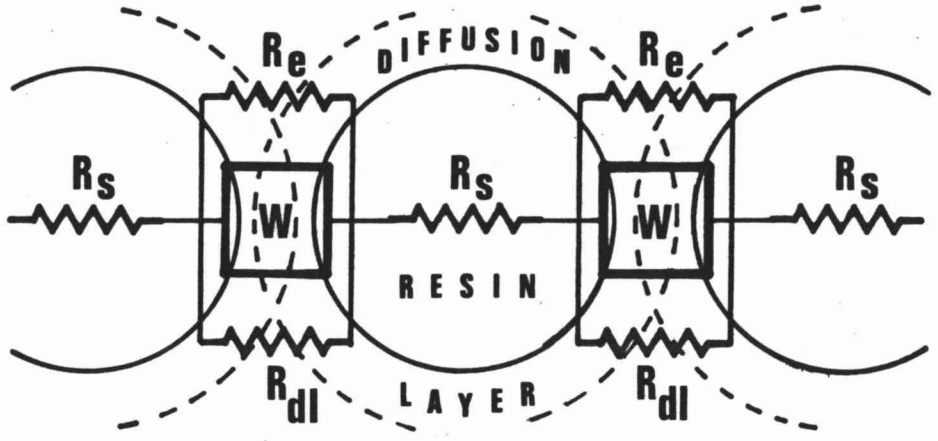

where $W = Z'' = \sigma(1-j)\omega^{-\frac{1}{2}}$

$$R_p = R_e R_{d.\ell}/(R_e+R_{d.\ell})$$

To transform this "microscopic" model into the macroscopic two terminal cell impedance, except for the very smallest number of resin particles, would require an assumption about the interconnection of impedance elements in the plane perpendicular to the field gradient. This problem is considered in Chapter 9.

CHAPTER 8 CLAY AND LATEX CELL DATA

8.1 COMPARISON WITH THE IMPEDANCE DISPERSION OF RESIN CELLS

8.1.1 The Impedance Locus

In order usefully to apply the data and conclusions derived from ion exchange resin cells, it is necessary to show that the mechanism and thus the equivalent circuit for the impedance dispersion of resins are the same as those for cells containing clay coated glass particles and for packed beds of polystyrene spheres (latex). In fact the form of the dispersion observed for these three cells is virtually the same with several significant exceptions as follows.

When represented as an impedance locus, data for clay and latex cells, as for resin cells, have the form of an arc of a circle with centre below the real axis. A best fit to this circle can readily be accomplished and R_s, R_p and ϕ determined (see section 7.1). For resin cells the phase angle is invariably close to 45° (i.e. -X" = R"), but for clay and latex cells ϕ is generally not 45°. For the admittance locus this effect appears as a slope not equal to 1, but the data is invariably a close fit to a straight line, and the routine shown in Fig. 7.5 can be utilised to yield R_s, R_p and Z", where

$$Z'' = (a-jb)\omega^{-\frac{1}{2}}$$

$a \neq b$ for clay and latex cells,

$a = b = \sigma$ for resins.

Values so obtained are presented in Table 8.1 which reveals the existence of three distinct types of behaviour determined by ϕ and ω_o, and the data has been grouped accordingly.

I: For a small number of experiments on Wyoming bentonite/ground pyrex cells two semi-circles are observed in the impedance loci. Provided the characteristic frequencies are sufficiently far apart that two circles can be resolved and solved for, then the impedance dispersion can be characterised by two sets of parameters related to an equivalent

Table 8.1

Clay and Latex Cell Data

8.1.1 Group I - Twin Dispersion (T=27°C)

Cell*	Electrolyte	Concentration (Molar)		R_s (Ω)	R_p (Ω)	a (Ω $s^{-\frac{1}{2}}$)	-b (Ω $s^{-\frac{1}{2}}$)	ω_o (rad s^{-1})	ϕ (degrees)
B	$CaCl_2$	0.01	High	9587	378	36100	109000	9.23×10^4	72
			Low		368	256	282	1.07	47
B	"	0.1	High	4606	71.3	2136	2245	1.89×10^3	46.4
			Low		173.8	379	332	8.40	41.2
3	NaCl	0.1	High	3228	15.3	1671	1921	2.77×10^4	49.0
			Low		102.8	79.8	56.3	0.90	35.2

8.1.2 Group II - Laponite

Cell*	Electrolyte	Concentration (Molar)	Temperature (°C)	R_s (Ω)	R_p (Ω)	a ($\Omega\ s^{-\frac{1}{2}}$)	-b ($\Omega\ s^{-\frac{1}{2}}$)	ω_o (rad s^{-1})	ϕ (degrees)	G_E ($x10^6\ \Omega^{-1}$)
7	$CaCl_2$	0.0002	26.59	51880	17616	44821	33149	14.5	36.5	26.14
"	"	0.0005	"	37734	11554	-	-	16.2	39.7	54.61
"	"	0.001	"	26413	8307	19012	15219	13.2	35.9	106.57
"	"	0.002	"	18858	4037	-	-	14.8	38.4	204.9
"	"	0.005	"	11411	1551	-	-	13.8	38.9	466.3
"	"	0.01	"	7216	681	1483	1105	13.5	36.0	899.5
"	"	0.02	"	4360	-	-	-	14.1	-	1709
"	"	0.001	14.3	35381	11112	-	-	11.7	34.8	-
"	"	"	26.6	26707	7843	-	-	14.0	36.2	121.5
"	"	"	39.9	20357	6115	-	-	19.7	35.6	156.9
"	"	"	49.9	17172	5093	-	-	20.2	37.1	184.9
8	"	0.001	26.59	24487	10392	-	-	0.039	29.3	-
"	"	0.01	"	7607	968	-	-	0.099	34.0	-
"	"	0.1	"	1347	0	0	0			-
"	"	0.001	14.3	28914	18613	-	-	0.0131	28.5	-
"	"	"	26.6	21518	12408	-	-	0.0342	29.1	-
"	"	"	39.9	16282	8952	-	-	0.0543	30.1	-
"	"	"	49.9	13717	6154	-	-	0.151	32.1	-

8.1.3 Group III - Wyoming bentonite

Cell*	Electrolyte	Concentration (Molar)	Temperature (°C)	R_s (Ω)	R_p (Ω)	a ($\Omega\ s^{-\frac{1}{2}}$)	-b ($\Omega\ s^{-\frac{1}{2}}$)	ω_o (rad s^{-1})	ϕ (degrees)	G_E ($x10^4\Omega^{-1}$)
1	NaCl	0.01	27	8823	343	24000	43000	$2.06x10^4$	60.7	-
2	"	"	"	9269	398	27000	51000	$2.10x10^4$	61.8	-
3**	$CaCl_2$	"	"	11001	499	32650	59715	$1.86x10^4$	61.3	-
3	"	"	"	11028	719	68100	106000	$3.07x10^4$	57.4	-
4	"	"	"	18660	1600	143400	231100	$2.89x10^4$	58.2	-
3	"	"	6.37	21607	1047	-	-	-	-	-
"	"	"	14.55	18379	860	-	-	-	-	-
"	"	"	21.12	15904	699	79765	127830	$4.65x10^4$	58.0	-
"	"	"	26.59	14157	592	74396	125356	$6.06x10^4$	59.3	-
"	"	"	26.59	14742	685	-	-	-	-	-
"	"	"	26.63	17450	757	90046	159979	$5.88x10^4$	60.6	-
"	"	"	35.0	14695	584	71291	128891	$6.36x10^4$	61.1	-
"	"	"	43.1	12335	449	51117	96481	$5.91x10^4$	62.1	-
"	"	"	50.1	10947	403	52383	88067	$6.47x10^4$	59.3	-
"	"	"	61.0	9475	360	56552	73653	$6.65x10^4$	52.5	-
"	"	"	69.6	8283	285	43313	59035	$6.60x10^4$	53.7	-

8.1.4 Group III - Polystyrene Latex

Cell*	Electrolyte	Concentration (Molar)	Temperature (°C)	R_s (Ω)	R_p (Ω)	a ($\Omega\ s^{-\frac{1}{2}}$)	-b ($\Omega\ s^{-\frac{1}{2}}$)	ω_o (rad s^{-1})	ϕ (degrees)	G_E (x10^6 Ω^{-1})
9	$CaCl_2$	0.01	27	51443	806	39000	111000	2.13×10^4	70.6	-
Latex	"	"	"	1250	312	39400	133000	1.98×10^5	73.5	-
Latex	NaCl	0.1	"	217.9	14.17	512	2566	3.41×10^4	78.7	-

* Cells are designated as follows:

B, 1, 2, 3 all contain 8% Wyoming bentonite/100-200 mesh ground pyrex.

7 contains 9% laponite/100-200 mesh ground pyrex.

8 contains 8% laponite/20-50 mesh soda glass spheres.

9 is a cell of the form shown in Figure 5.2.2, containing close-packed latex.

Latex is a cell of the form shown in Figure 5.2.3, containing close-packed latex.

4 contains 6% Wyoming Bentonite/100-150 mesh ground Pyrex.

** For this cell only, the clay and electrolyte were not homoionic.

The clay was (initially) in the sodium form.

circuit of the form

Figure 8.1

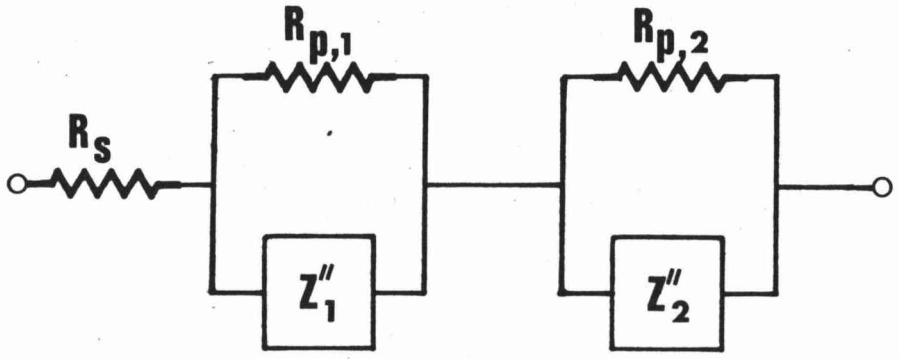

The two dispersion processes are assumed to occur independently of each other, and effectively in series.

II: All impedance measurements made on cells containing laponite/ground pyrex and laponite/soda glass spheres show a single semicircle for which,

$$\omega_o < 20 \text{ rad } s^{-1},$$

$$\phi < 45°.$$

With the exception of the phase angle the impedance dispersion of these cells is very similar to that for resin cells.

III: All measurement which display an impedance dispersion, for cells containing Wyoming bentonite/ground pyrex* show a response at high frequency, having

$$\omega_o > 10{,}000 \text{ rad } s^{-1}$$

$$\phi > 45°$$

Three cells show an additional low frequency dispersion of the form described in II.

For latex cells the impedance dispersion also occurs at high frequencies, with ω_o as high as 2×10^5 rad s^{-1}, and ϕ as high as 79°. Both latex and Wyoming bentonite cells however clearly show a component

---

* No impedance dispersion was observed for Wyoming bentonite/soda glass sphere cells.

of the cell impedance proportional to $\omega^{-\frac{1}{2}}$ (i.e. Warburg type).

8.1.2 Equivalent Circuit

For II and III above the observed impedance dispersion can be adequately characterised by the addition of a single parameter, α, to the equivalent circuit proposed for resins.

Figure 8.2

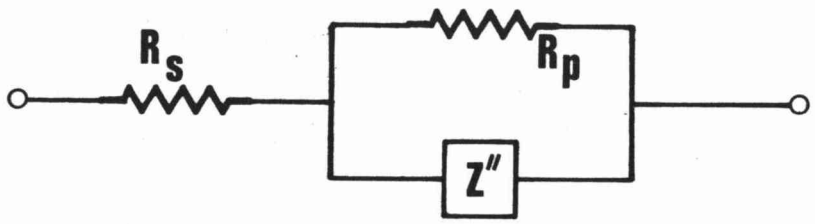

$$Z'' = (a-jb)\omega^{-\frac{1}{2}} = \sigma(1-\alpha j)\omega^{-\frac{1}{2}}$$

This circuit however has no theoretical significance since for a Warburg impedance or semi-infinite transmission line (163), α must equal 1. Buck (38) has proposed a model of a finite transmission line to explain an observed phase angle not equal to 45 , for the film of hydrolysed glass at the surface of a glass membrane electrode. He does not justify this theoretically and Brand and Rechnitz have shown that in this case the data is adequately explained by a shunted Warburg impedance.

Figure 8.2 is useful since the parameters are very easily determined and can be used to catagorise the types of impedance dispersion. It can be readily shown that,

$$\omega_o = (a^2 + b^2)/R_p^2 \qquad \text{(c.f. section 7.2.2)}$$

and $$\phi = \mathrm{Tan}^{-1}\,(b/a)$$

and the characteristic frequency and phase angle calculated in this way are included in Table 8.1.

8.1.3 Reduced Impedance Plots

Figure 8.3 shows plots of the reduced impedance versus reduced frequency for resin cells and groups II and III cells, and clearly demonstrates the differences between the impedance dispersion of these systems. Group III cells ($\phi > 45°$) display a greater maximum reactance and narrower spread for both $-X'/R_p$ and R'/R_p, which nevertheless remain symmetric. For group II cells ($\phi < 45°$) these plots are broader and flatter than for resin cells. Thus while resin, clay and latex cells display the same general form of impedance dispersion, the scale is slightly altered.

Since dispersions in non-resin systems fall into two distinct categories, then two distinct mechanisms must operate to modify the impedance spectra. One operates at high frequencies to increase the phase angle for Wyoming bentonite and latex cells. The other operates at low frequencies to decrease the phase angle.

The most effective way of examining these mechanisms is with the reduced impedance and this formalism will be used to elucidate the two processes in the following sections.

8.2 WYOMING BENTONITE AND LATEX (GROUP III) DATA

8.2.1 Equivalent Circuit

A phase angle greater than 45° indicates that the reactive component of Z" has increased. An increased phase angle is only observed at high frequencies suggesting a parallel capacitance is present. Since in the model proposed for resins a significant part of R_p is attributed to a double layer resistance, the presence of a parallel capacitance arising as a consequence of charge within the double layer, is to be expected.

For an electrical double layer at a metallic electrode/electrolyte interface, the capacitance per unit area, $C/A \approx 10^{-5}$ to 10^{-6} F cm^{-2}. Provided C/A for resin particles is not significantly greater than this, then for a 100 mesh resin particle ($A = 3 \times 10^{-3}$ cm^2), $C \approx 1 \times 10^{-8}$ F. If $R_p = 1$ kΩ, then $\omega_o \approx 10^5$ rad s^{-1}, and at 100 Hz the reactive component due to the double layer capacitance will be less than 0.1% of the

FIGURE 8.3 Reduced Impedance Plots for Resin and Clay Cell Data

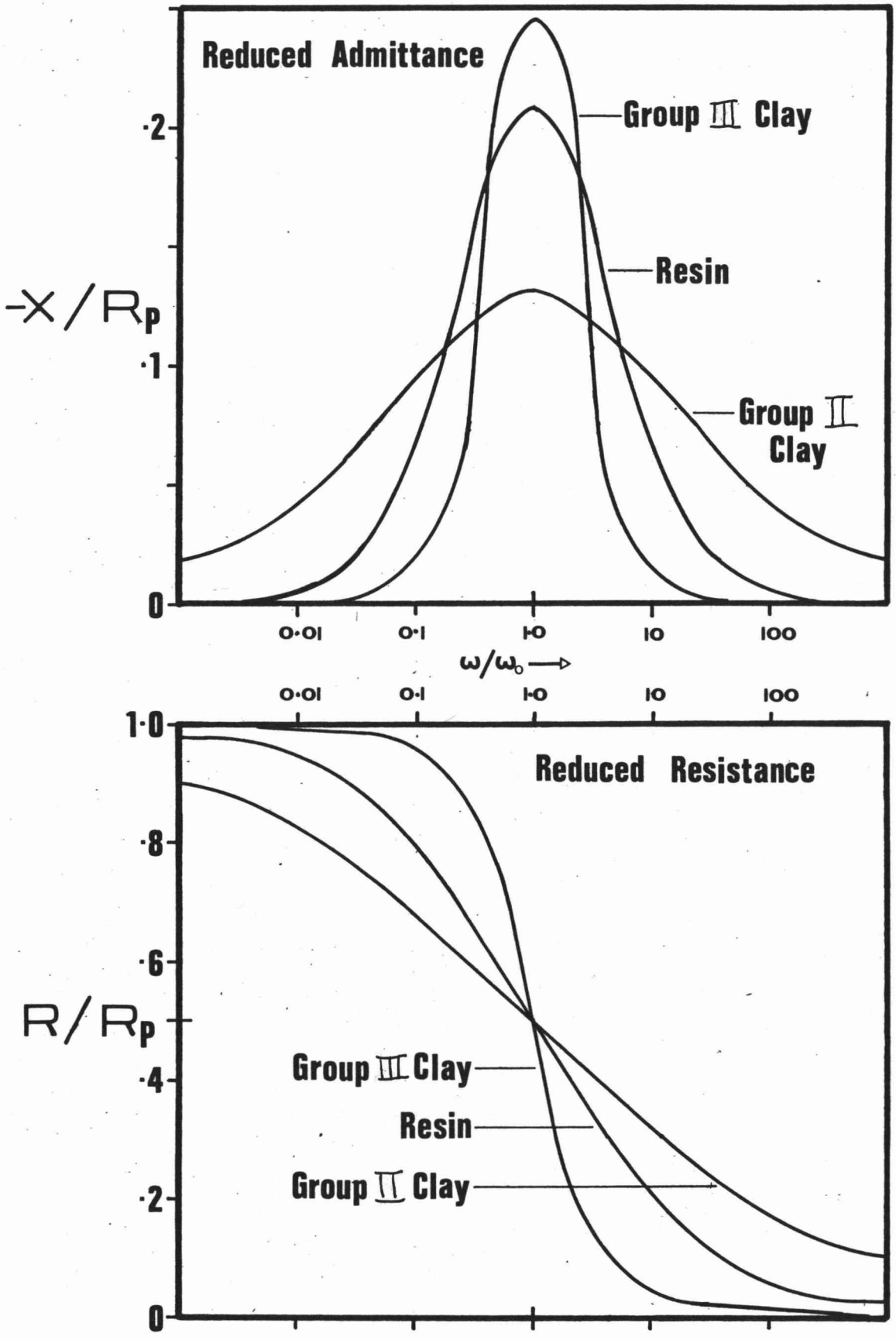

total impedance. It is not difficult to see therefore, why the double layer capacitance can be ignored for resin and low frequency (Group II) clay data, and becomes significant only when ω_o is high.

The form of the reduced impedance plots observed is also indicative of a parallel capacitance as they are intermediate between the form for a shunted Warburg impedance and a shunted capacitance (see Figure 7.6), as would be expected for the following equivalent circuit.

Figure 8.4

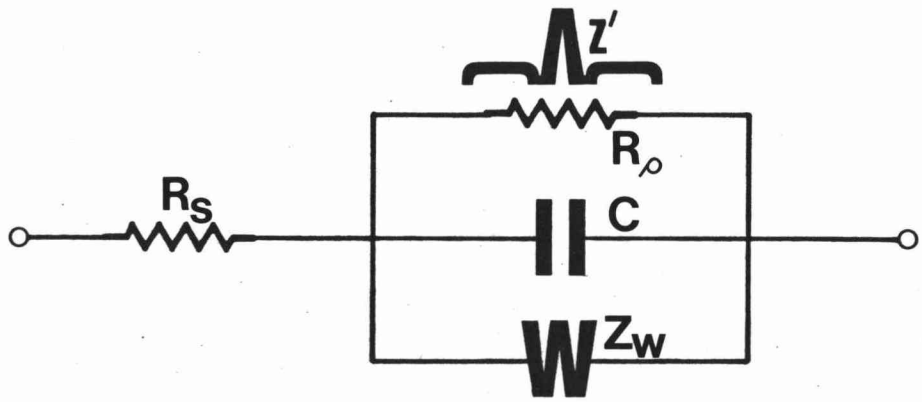

As for the circuit in Figure 7.2.1 the impedance dispersion is due to Z' alone and may be determined as follows.

Since the Z' is a parallel combination it is easier to work with the admittance,

$$Y' = 1/Z' = 1/(Z-R_s)$$

$$= 1/R_p + j\omega C + (1+j)\omega^{\frac{1}{2}}/2\sigma$$

$$= A + jB$$

$$A = 1/R_p + \omega^{\frac{1}{2}}/2\sigma \qquad [1]$$

$$B = \omega C + \omega^{\frac{1}{2}}/2\sigma \qquad [2]$$

A plot of A versus $\omega^{\frac{1}{2}}$ will thus be a straight line of slope $1/2\sigma$ and intercept $1/R_p$. Having determined R_p and σ, then a plot of,

$B - \omega^{\frac{1}{2}}/2\sigma \quad (=B')$ versus ω,

will be a straight line of slope C and intercept 0.

In practice R_p is more accurately determined than σ, and the second plot is made using (B'=) B-A + $1/R_p$.

The form of equations [1] and [2] is found to be extremely well obeyed for all group III cell data. R_p, σ and C are readily determined from a linear regression of A versus $\omega^{\frac{1}{2}}$, and B' versus ω, and Figure 8.5 shows data for a typical clay cell in this form, superimposed upon the best fit straight lines.

Table 8.2 gives the values of R_p, σ and C determined by this method together with the coefficients of determination (r^2) for A versus $\omega^{\frac{1}{2}}$ and B' versus ω.

It is worthwhile noting that for the equivalent circuit shown in Figure 8.4, the assumption of a constant phase angle for Z", necessary for the impedance locus to have a circular form, does not hold.

$$Y'' = 1/Z'' - j\omega C + (1+j)\omega^{\frac{1}{2}}/2\sigma$$

$$\text{Tan } \phi = (B''/A'')$$

$$= (\omega C + \omega^{\frac{1}{2}}/2\sigma)/(\omega^{\frac{1}{2}}/2\sigma)$$

$$\phi = \text{Tan}^{-1}(1 + 2\sigma C\omega^{\frac{1}{2}}).$$

In fact $2\sigma C\omega^{\frac{1}{2}}$ is typically much less than 1 and thus the departure of the impedance locus from a circular form is slight. However, the values of R_p shown in Table 8.2 are greater than those determined by a circular fit (Table 8.1) by 5 to 10% as a consequence of the dependence of ϕ on ω.

8.2.2 Physical Dependence of Parameters

Only a limited number of clay experiments display an impedance dispersion with a sufficiently high characteristic frequency to show a double layer capacitance. All these determinations were made on cells containing Wyoming bentonite/ground pyrex/0.01 M electrolyte. At higher concentration (0.1 M), clay cells display a twin dispersion, and the dispersion for lower concentrations (0.001 M) has moved to higher frequency, outside the effective measurement range of the bridge.

Table 8.2

Group III

8.2.1 Preliminary Experimentation, Wyoming bentonite

Cell	Electrolyte	Concentration (Molar)	Temperature (°C)	R_s (Ω)	R_p (Ω)	σ/r^2 ($\Omega\ s^{-\frac{1}{2}}$)	C/r^2 (F)
1	NaCl	0.01	27	8823±10	365±5	2.82×10^{4}/.9913	1.78×10^{-7}/.968
2	"	"	"	9269±10	409±3	3.97×10^{4}/.9915	1.80×10^{-7}/.992
3	$CaCl_2$	"	"	11001±10	543±6	3.76×10^{4}/.9968	1.22×10^{-7}/.999
3	"	"	"	11028±10	741±5	7.86×10^{4}/.9961	4.66×10^{-8}/.992
4	"	"	"	18660±20	1656±11	1.77×10^{5}/.9945	1.94×10^{-8}/.988

8.2.2 Temperature Dependence, Wyoming bentonite Cell 3

Cell	Electrolyte	Concentration (Molar)	Temperature (°C)	R_s (Ω)	R_p (Ω)	σ/r^2 ($\Omega\ s^{-\frac{1}{2}}$)	C/r^2 (F)
3	$CaCl_2$	0.01	6.37	21607±20	1088±7	1.31×10^{5}/.9964	2.20×10^{-8}/.953
"	"	"	14.55	18379±10	885±3	1.17×10^{5}/.9978	3.07×10^{-8}/.996
"	"	"	21.12	15904±10	720±2	9.78×10^{4}/.9986	3.21×10^{-8}/.990
"	"	"	26.63	14157±10	610±1	8.65×10^{4}/.9983	3.86×10^{-8}/.969
"	"	"	26.59	17450±10	771±1	1.20×10^{5}/.9991	3.48×10^{-8}/.990
"	"	"	35.0	14695±10	599±1	9.58×10^{4}/.9993	4.50×10^{-8}/.999
"	"	"	43.1	12335±10	460±1	7.91×10^{4}/.9980	5.89×10^{-8}/.989
"	"	"	50.1	10947±10	423±1	6.05×10^{4}/.9986	4.23×10^{-8}/.915
"	"	"	61.0	9475±10	384±1	4.39×10^{4}/.9990	2.19×10^{-8}/.957
"	"	"	69.6	8283±10	-	-	-

8.2.3 Polystyrene Latex

9	$CaCl_2$	0.01	27	51443±30	924±5	2.11×10^{5}/.9934	5.39×10^{-8}/.9932
Latex	"	"	"	1250±5	328±3	3.26×10^{5}/.9941	1.73×10^{-8}/.9996
Latex	NaCl	0.1	"	217.9±.5	13.96±.06	8.25×10^{3}/.993	1.54×10^{-6}/.989

FIGURE 8.5 Group III Linear Regression

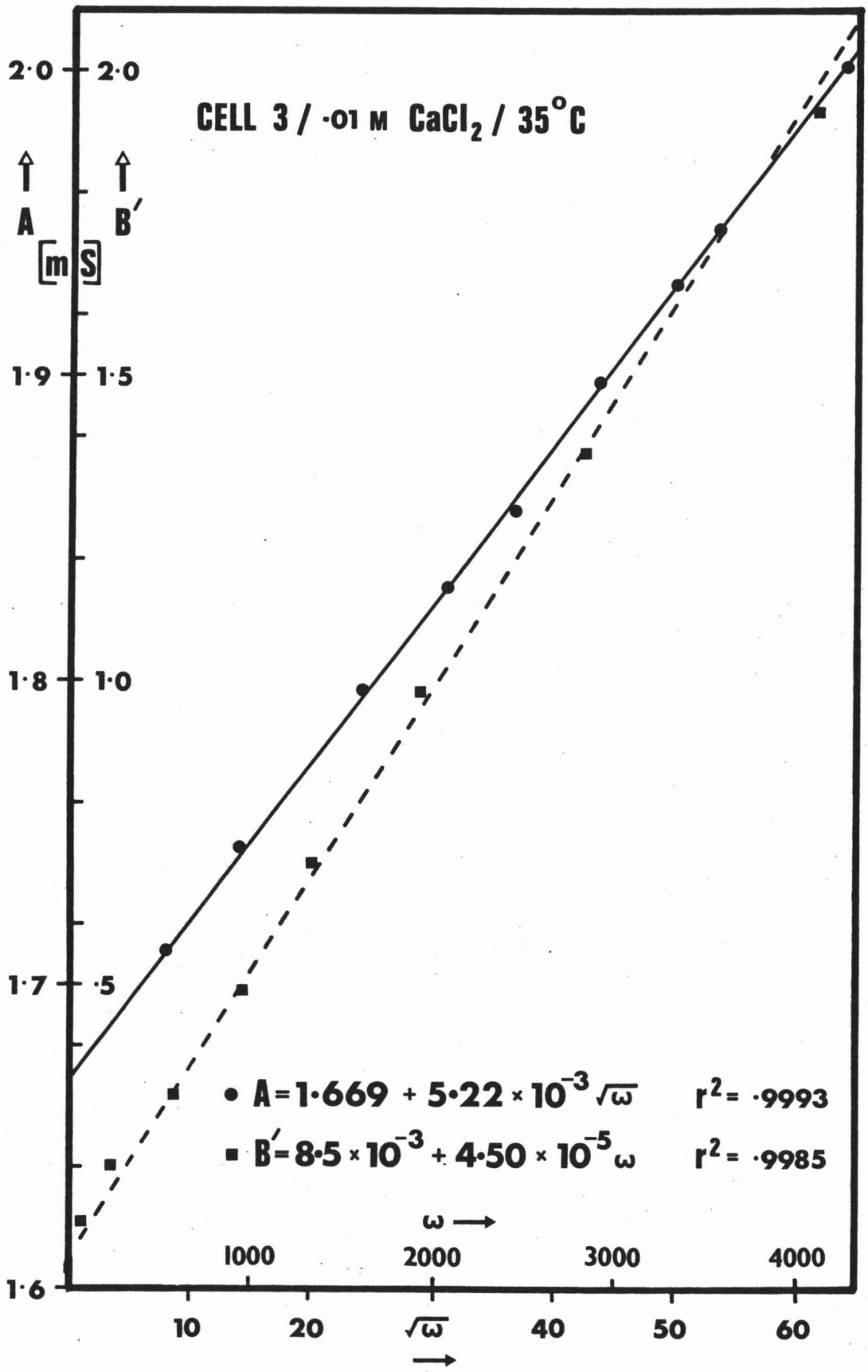

8.2.2.1 Reproducibility

Three identical cells (1, 2 and 3) were filled with samples of the same 8% sodium-Wyoming bentonite/50-100 mesh ground pyrex distilled water slurry. These cells were dried and equilibrated with electrolyte identically in all respects, except that cells 1 and 2 were equilibrated with 0.01 M NaCl, and cell 3 with 0.01 M $CaCl_2$.

As expected the observed impedance dispersion for cells 1 and 2 is very similar, and the parameters of the equivalent circuit are thus similar (Table 8.2.1), with the exception of σ which is 40% larger for cell 2.

The difference in σ observed for cells 1 and 2 highlights the difficulty in working with clay cells. An attempt to re-exchange or re-equilibrate Wyoming bentonite cells results in clay eluting with the electrolyte, with the attendent loss of reproducibility of clay configuration. New cells must be constructed in order to study the effects of electrolyte type and concentration, however cells 1 and 2 were prepared at the same time, in an identical fashion, with identical materials, and yet the measured value of σ for the two cells shows a 40% variation (see section 9.2.5).

8.2.2.2 Electrolyte

The difference between cells 1 and 2, and cell 3 is simply that of electrolyte, and in changing for NaCl to $CaCl_2$, significant trends in the equivalent circuit parameters are observed (Table 8.1.2). R_p and R_s increase, and C decreases, but because of the discrepancy in σ observed for cells 1 and 2, no trend can be assessed for this parameter. However, an increase in R_p and R_s between NaCl and $CaCl_2$ is not consistent with either being a pure electrolyte path, since for the same molarity, the conductivity of $CaCl_2$ is greater than NaCl (168).

8.2.2.3 Temperature

Cell 3 was exchanged into the calcium form and equilibrated with 0.01 M $CaCl_2$, and a number of experiments performed to determine the effect of temperature on the parameters of the equivalent circuit. The results are shown in Table 8.2.2.

Determinations made at 26.6°C before the high temperature measurements, and again before and after the low temperature measurements show a considerable discrepancy indicating that a significant change occurred in the cell as a result of heating and cooling. This change is probably due to a movement of clay within the cell caused by electrolyte expansion and contraction, as a consequence of the poor cementation of Wyoming-bentonite to the ground pyrex. This results in a significant systematic error in the electrical parameters obtained, but by taking values in two groups of increasing temperature as shown in Table 8.2.2, some quantitative information may be obtained.

R_s and R_p

Arrhenius plots give the following straight lines.

a) $\log R_s = 1.61 \pm .08 + (763 \pm 22)/T$ $\quad r^2 = .9983$

b) $\log R_s = 1.62 \pm .11 + (784 \pm 34)/T$ $\quad r^2 = .9942$

a) $\log R_p = -0.70 \pm .18 + (1045 \pm 52)/T$ $\quad r^2 = .9951$

b) $\log R_p = -0.14 \pm .42 + (900 \pm 133)/T$ $\quad r^2 = .939$

The following activation energies for conduction may be calculated.

	Electrolyte*	R_s	R_p	
E_A	14.0±.3	14.7±.3	19.4±.4	kJ mol^{-1}

The value of activation energy obtained for R_p is thus significantly larger than for bulk electrolyte conduction, although not as high as that determined for 100-200 mesh resin/0.001 M NaCl (E_A = 29.9 kJ mol^{-1}).

R_s on the other hand has an activation energy for conduction close to that of the electrolyte. This does not mean however, that R_s necessarily involves a conduction process within the bulk electrolyte (c.f. section 8.2.2.2).

---

* Calculated from data for 0.01 M $CaCl_2$ given in Robinson and Stokes (168).

$\underline{\sigma}$

As discussed in section 7.3.5, for a Warburg impedance a plot of log (σ^2/T) versus $1/T$ should be a straight line of slope proportional to the activation energy for the limiting equivalent conductivity ($\Lambda°$). For cell 3/0.01 M $CaCl_2$ straight lines are observed for the two groups of temperature data, with the following least squares fits.

a) $\log (\sigma^2/T) = 1.93\pm.59 + (1647\pm171)/T \qquad r^2 = .979$

b) $\log (\sigma^2/T) = 1.28\pm.46 + (2693\pm145)/T \qquad r^2 = .991$

The activation energy obtained by this analysis contains a large uncertainty,

$$E_{A,\Lambda°} = 41\pm10 \text{ kJ mol}^{-1},$$

but is in good agreement with the value obtained for 100-200 mesh resin/ 0.01 M NaCl (Table 8.3). This analysis is in fact good evidence that for both resin and Wyoming bentonite systems, σ is the coefficient of a Warburg diffusional impedance.

Table 8.3 Activation Energies for Conduction

Determined from		Wyoming bentonite/0.01 M $CaCl_2$	Resin/0.001 M NaCl	
σ	E_A =	41±10	42±1	kJ mol^{-1}
R_p	E_A =	19.4±.4	29.9±.9	"
R_s	E_A =	14.7±.3	20.5±.2	"
Electrolyte	E_A =	14.0±.3	13.8±.2	"

The significance of these activation energy values will be considered in Chapters 9 and 10.

C

The differential double layer capacitance for a Boltzmann distribution of point charges in a diffuse double layer is given by,

$$C_d = B(1/T)^{\frac{1}{2}}\cosh(\Psi/T) \qquad [3]$$

where B = a constant (see reference 50, Chapter 3.3).

Ψ = potential of the plane of charge.

Provided Ψ is not temperature dependent, then from equation [3], C should decrease monotonically with increasing temperature. However, from Table 8.2.2 it can be seen that C is not a single valued function of temperature, and passes through a maximum at about 41°C. This behaviour is not consistent with the theoretical capacitance of a diffuse double layer (equation [3]), although the observed magnitude is similar to that of a plane metallic electrode/electrolyte interface (50). A further consideration of C is presented in section 10.1.7.

An analogy between the clay/electrolyte interface which arises within clay cells and the diffuse double layer at a plane metallic electrode is clearly of limited value because of the many possible complicating features within a clay cell. A double layer capacitance is expected from the model and, at frequencies sufficiently high, a capacitance is observed.

8.2.3 Polystyrene Latices

In an attempt to clarify the impedance dispersion observed at high frequencies for Wyoming bentonite cells, experiments were conducted on a system containing a packed bed of polystyrene spheres of diameter 1250±50 nm (section 6.3), perfused with electrolyte. These particles are known to have a surface double layer but have effectively no conductance within the spheres. They thus more closely represent clay particles than do ion exchange resin particles.

The form of the impedance dispersion observed for polystyrene latices is the same as for Wyoming bentonite cells, having a phase angle between 70°and 80°, and a characteristic frequency greater than 10,000 rad s^{-1}. In all respects the observed impedance dispersion is consistent with the equivalent circuit shown in Figure 8.4 and the parameters of this circuit may be solved for as described in section 8.2.1. These values are shown in Table 8.2.3.

A measurable impedance dispersion was observed for only three cells - two containing latex/0.01 M $CaCl_2$, and one containing latex/0.1 M NaCl. No dispersion was observed for latex/0.001 M $CaCl_2$ or latex/0.1 M $CaCl_2$.

The initial investigations of latex/0.01 M $CaCl_2$ was performed using the cell shown in Figure 5.2.1, however the impedance of this was found to be too large for accurate measurement, and the cell shown in Figure 5.2.3 was constructed. This second cell which had an internal diameter of 2 cm and a potential electrode spacing of 3.5 cm has a cell constant of 1.1 compared with 16.6 for all other cells. The latex in the second cell was consolidated using an ultra-sonic bath, and an effective close packing was obtained.

8.2.4 Physical Dependence (Polystyrene Latices)

Because of the limited number of systems observed which displayed an impedance dispersion, little information can be obtained about the physical significance of the parameters of the equivalent circuit for polystyrene latex cells.

The most significant observation is that polystyrene latex/electrolyte cells display an impedance dispersion at all; and that the form of this dispersion is identical with that observed for Wyoming bentonite cells.

The system itself is an extremely simple one. Non-conducting plastic spheres of constant diameter, bearing a negative surface charge density are surrounded by electrolyte. Conduction can only occur within the bulk electrolyte, or in the polystyrene/electrolyte interfacial double layer. Since the bulk electrolyte is not expected to behave reactively any reactive component can only originate in the double layer. The observed Warburg type impedance, and the shunt

capacitance must therefore be associated with the diffuse double layer.

This argument may be extended to Wyoming bentonite cells which behave identically. A comparison of the parameters determined for Wyoming bentonite cell 3/0.01 M $CaCl_2$ with those for the two latex cells/0.01 M $CaCl_2$ (Table 8.2) reveals a strong similarity for R_p, σ and C. Considering the physical differences between these three cells this similarity is remarkable and suggests that R_p, σ and C are indeed microscopic parameters of the system, and specifically of the electrical double layer.

R_s on the other hand shows considerable variation, and for the latex determinations is markedly dependent on cell constant. This suggests that R_s is a property of the cell, but does not mean that R_s involves electrolyte conduction, since the conductance of the double layer parallel to the interface will also vary with cell geometry.

It is easily demonstrated that neither R_s nor R_p represents exclusively a bulk electrolyte path by considering the conductivity ratios determined from latex cells containing 0.01 M $CaCl_2$ and 0.1 M NaCl.

	Bulk Electrolyte	R_s	R_p
$\frac{\kappa \text{ (0.1 M NaCl)}}{\kappa \text{ (0.01 M } CaCl_2\text{)}}$	9.3	5.7	23.5

R_p is thus more strongly dependent on the electrolyte type than is the bulk electrolyte conductivity, and R_s is less strongly dependent.

The double layer capacitance is expected to be proportional to the surface charge density, and inversely proportional to the double layer thickness. A diffuse double layer is known to be compressed with increasing electrolyte concentration (192), and since the surface charge density will not change, the capacitance should increase with increasing concentration. This is observed for latex cells (Table 8.2.3).

8.3 LAPONITE (GROUP II) DATA

8.3.1 Distribution of Characteristic Frequencies

The general form of the impedance dispersion observed for laponite cells has been discussed in section 8.1. The phase angles are significantly less than 45°, and the characteristic frequencies less than 20 rad s^{-1}, at which frequencies any realistic value of a double layer capacitance would contribute insignificantly to the measured impedance and is hence not included in the evaluation of the data.

Reduced impedance plots for laponite data (Figure 8.3) show a broadening of the impedance spectrum as would be expected if Z' represented not a single shunted Warburg impedance, but a distribution of such circuits with a mean characteristic frequency $\overline{\omega_o}$. Since log symmetry is observed in all cases, this distribution also must be log symmetric.

8.3.2 Equivalent Circuit

Consider the contents of a cell to be a series-parallel combination of membrane impedances (relating to individual membrane zones) of the form shown by Figure 8.6.

Figure 8.6

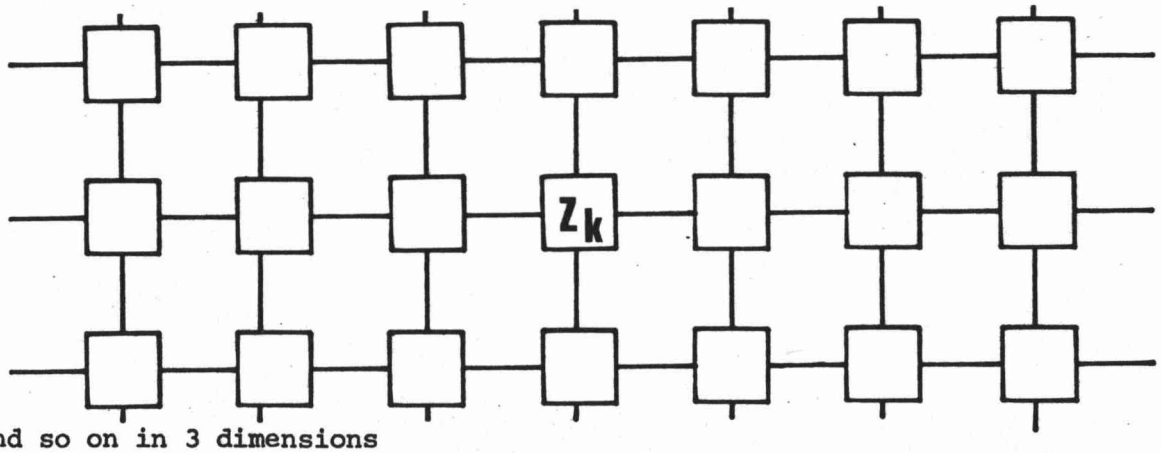

and so on in 3 dimensions

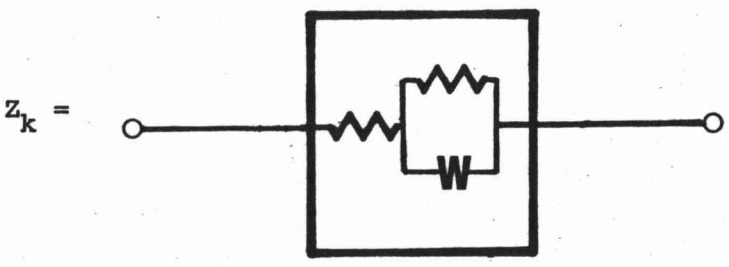

Since the cell impedance (Z) is measured as V_{cell}/I_{cell}, then V_{cell} will be the potential drop across any (and all) series combinations of say n elements between the potential electrodes. I_{cell} (defined to be in phase) is a function of the number of possible parallel paths (= m) and the current flow in each.

Provided n is sufficiently large then local impedance fluctuations will average out and the current through all elements in the direction of the field gradient will be the same (= i). Now

$$V_{cell} = \sum_{k=1}^{n} Z_k \, i$$

$$I_{cell} = m \, i$$

$$Z_{cell} = (1/m) \sum_{k=1}^{n} Z_k \qquad [4]$$

If there is no distribution of Z_k then,

$$Z_{cell} = (n/m) \, Z_k,$$

which is the form expected for a resin cell.

However, if Z_k must be described as a distribution of zone impedances, then equation [4] must be used. From the form of this equation, the non-reactive series component (R_s) may be treated separately.

$$Z_k = R_{s,k} + Z_k'$$

$$R_{s,cell} = (n/m) \, \bar{R}_{s,k}$$

The impedance dispersion is determined by Z_k' and for a shunted Warburg impedance (section 7.2.2),

$$\frac{Z_k'}{R_p} = \frac{1 + (\omega/2\omega_{o,k})^{\frac{1}{2}}(1-j)}{1 + (2\omega/\omega_{o,k})^{\frac{1}{2}} + \omega/\omega_{o,k}} \qquad [5]$$

$$Z_{cell} = \frac{n\bar{R}_{s,k}}{m} + \frac{R_p}{m} \sum_{k=1}^{n} \frac{1 + (\omega/2\omega_{o,k})^{\frac{1}{2}}(1-j)}{1 + (2\omega/\omega_{o,k})^{\frac{1}{2}} + \omega/\omega_{o,k}} \qquad [6]$$

The cell impedance may thus be determined at any frequency (ω) by a summation over all values of $\omega_{o,k}$ for a series combination of n elements. The geometric mean value of $\omega_{o,k}$ is defined as $\overline{\omega}_o$.

As a simple example a distribution involving only two values of $\omega_{o,k}$ is shown in Figure 8.7. Impedances are calculated from equation [6] for $\omega_{o,1} = 0.1$, $\omega_{o,2} = 10.0$, $R_{p,1} = R_{p,2} = 1000$, $\sigma_1 = 224$, $\sigma_2 = 2240$ and for simplicity, $\bar{R}_s = 0$.

Figure 8.7

ω	$-X_1$	R_1	$-X_2$	R_2	"$-X$"$_{cell}$	"R"$_{cell}$	ϕ
10^{-3}	61	930	7	993	34	962	43.5
10^{-2}	145	791	21	978	83	885	41.1
10^{-1}	207	500	61	930	134	715	35.8
1	145	209	145	791	145	500	32.3
10	61	70	207	500	134	285	35.8
10^2	21	22	145	209	83	115	41.1
10^3	7	7	61	70	34	38	43.5

The last column shows that the phase angle is reduced from 45° by this distribution. Figure 8.8 shows reduced impedance plots for Z_1, Z_2 and "Z_{cell}", and demonstrates the broadening caused by a distribution of ω_o. The geometric mean of $\omega_{o,k}$ is $\overline{\omega}_o = 1.0$ which is the frequency for which "$-X_{cell}$" is a maximum.

For any real system $n >> 2$ and a mathematical distribution function must be selected for $\omega_{o,k}$, which fits the observed impedance dispersion.

8.3.3 Types of Distribution

Two distribution functions were employed in order to fit observed laponite impedance data.

A logarithmic Gaussian (log normal) distribution is commonly employed to describe the distribution of time constants for dielectric relaxation (48), and a distribution of this form (equation [7]) was used to fit laponite cell data.

FIGURE 8.8 Distribution of ω_o

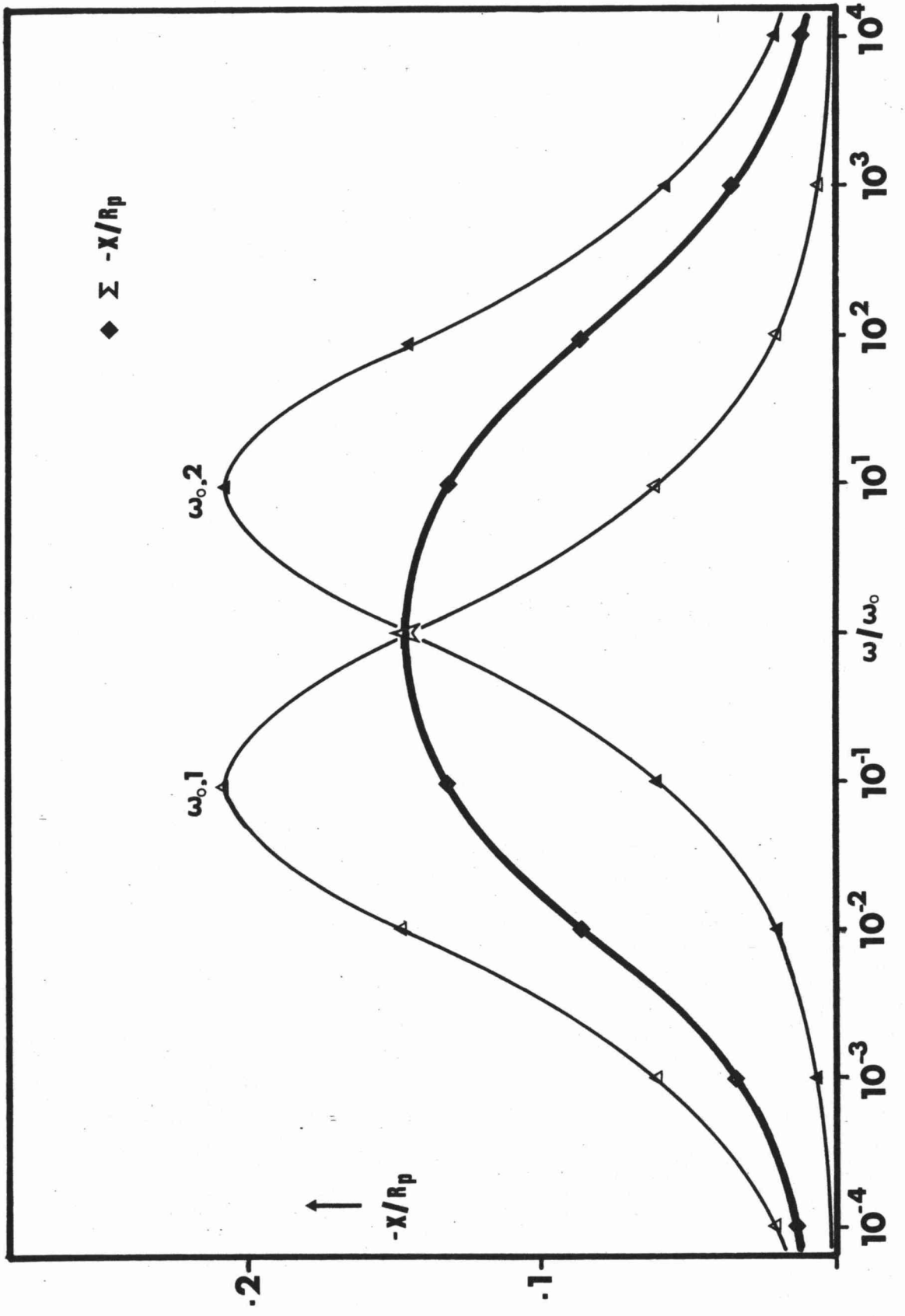

$$f(s) = (b^2/\pi)^{\frac{1}{2}} \exp(-b^2 s^2) \qquad [7]$$

where $s = \ln(\omega_{o,k}/\overline{\omega_o})$.

This equation describes the distribution of a random variable ($\ln \omega_{o,k}$) with geometric mean $\overline{\omega_o}$. The variance or distribution width is determined by b, which must be adjusted to give a best fit.

A distribution of the form of equation [7] was found to adequately describe the impedance dispersion measured for laponite cells for frequencies within two decades of $\overline{\omega_o}$. However, at frequencies higher than about 100 $\overline{\omega_o}$, the observed dispersion falls off more rapidly than that calculated from equations [6] and [7] . This is in part due to the asymptotic form of equation [7] since the contribution of elements for which $\omega_{o,k} >> \overline{\omega_o}$ and $\omega_{o,k} << \overline{\omega_o}$, is significant. Another limitation of equation [7] is its relative complexity*, and a second distribution was proposed to fulfill the requirements of log symmetry, a finite limit for $\omega_{o,k}/\overline{\omega_o}$ (i.e. truncation) and mathematical simplicity. This distribution is described by equation [8].

$$\log(\omega_{o,k}/\overline{\omega_o}) = \pm(4/\gamma_o)\gamma_i \qquad [8]$$

where γ_i varies linearly from $-\gamma_o$ to $+\gamma_o$.

The forms of the distributions described by equations [7] and [8] are shown in Figure 8.9.

Equation [8] is found adequately to represent the observed dispersion, with an improved fit over equation [7] at high frequencies. As such, this simpler distribution has been assumed and the experimental observations have been evaluated in terms of equations [6] and [8].

8.3.4 Data Fit

Reduced impedance plots were calculated using equation [6] and [8] for a distribution of characteristic frequencies, by taking a

---

* Summations were performed using an HP 65 programmable calculator with a limit of 100 program steps. Using equation [7], $\Sigma R/R_p$ and $\Sigma X/R_p$ cannot be calculated from the same summation.

FIGURE 8.9 Distribution Functions

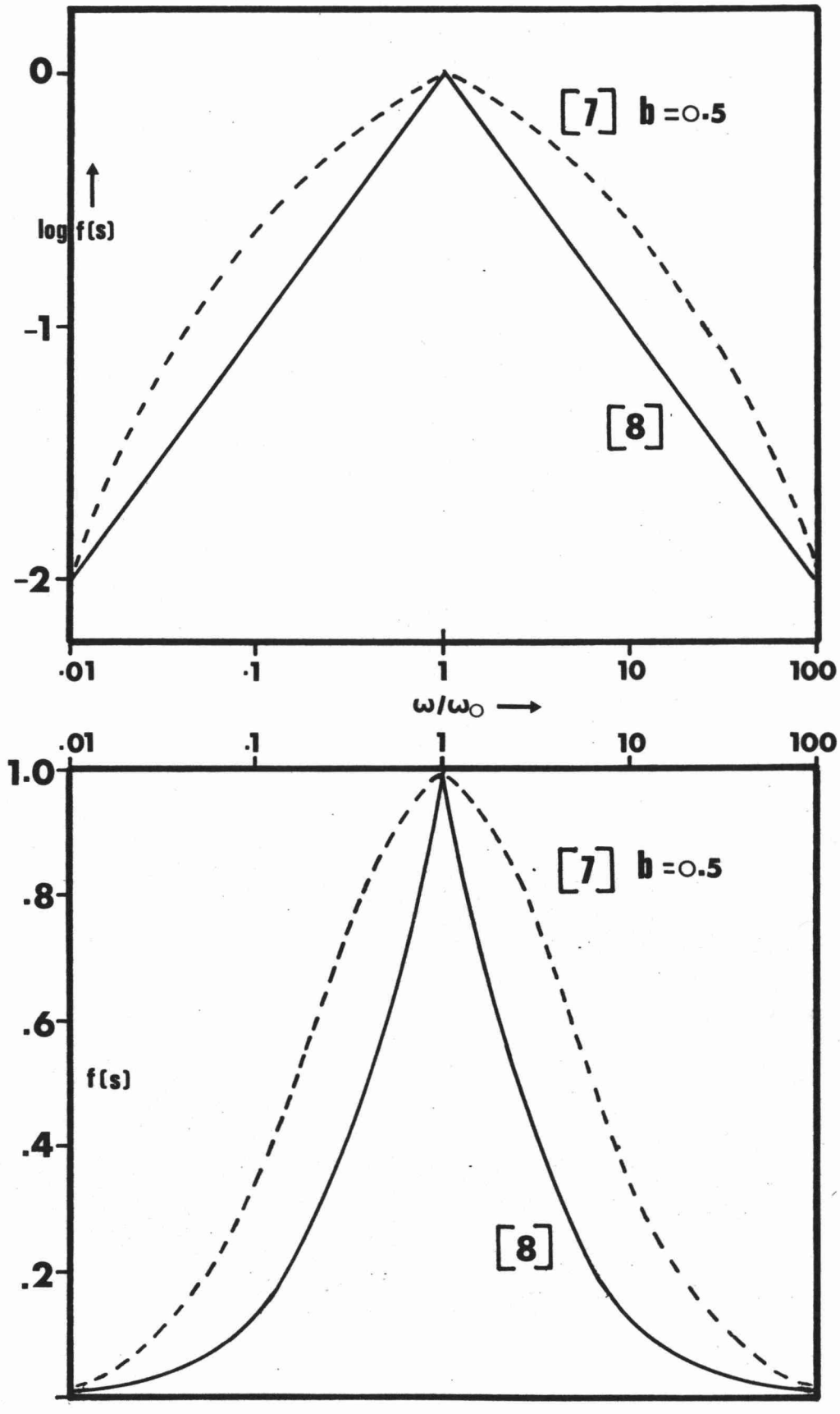

summation over (say) 100 values of $\gamma_{o,k}$ (derived from γ_i) for each value of ω^*. In this form the only adjustable parameter is γ_o, and a set of curves were calculated, to determine the effect of varying γ_o on reduced impedance (Figure 8.10) and impedance locus (Figure 8.11) plots.

The dependence of a number of parameters on γ_o has been determined from equations [6] and [8], and the results are summarised in Table 8.4.

Table 8.4

γ_o	ϕ	$-X_{max}/R_p$	$\omega_{2/3}$	$\omega_{1/3}$
0	45.00	0.207	11.6	76
1.0	44.59	0.205	12.0	80
1.5	43.33	0.199		
1.6			14.5	100
2.0	40.21	0.183	19.5	150
2.5	35.28	0.159	40.0	360
3.0	29.15	0.120	135	1500
3.3			360	4300
3.5	23.39	0.103		
3.7			1800	22500
4.0	18.63	0.082	7000	
4.5	14.88	0.065		

where ϕ = phase angle of Z" at $\omega=\overline{\omega_o}$

$-X_{max}/R_p$ = maximum value of $-X/R_p$

$\omega_{2/3}$ and $\omega_{1/3}$ = the frequency $(\omega/\overline{\omega_o})$ at which X has fallen to 2/3 or 1/3 of X_{max}.

Figure 8.12 shows $\omega_{2/3}$ and $\omega_{1/3}$ versus γ_o, and Figure 8.13 shows $-X_{max}/R_p$ versus γ_o, from which plots R_p and γ_o may be interpolated from experimental data.

Of the two clay systems which displayed a distribution of characteristic frequency (cells 7 and 8 - see Table 8.1.2), only for cell 7 is $\overline{\omega_o}$ at a sufficiently high frequency to fall within the lower limit of bridge measurement. Two different routines must therefore

---

* The HP 65 program used to perform this summation is shown in Appendix 8.1.

FIGURE 8.10 Reduced Impedance versus γ_o

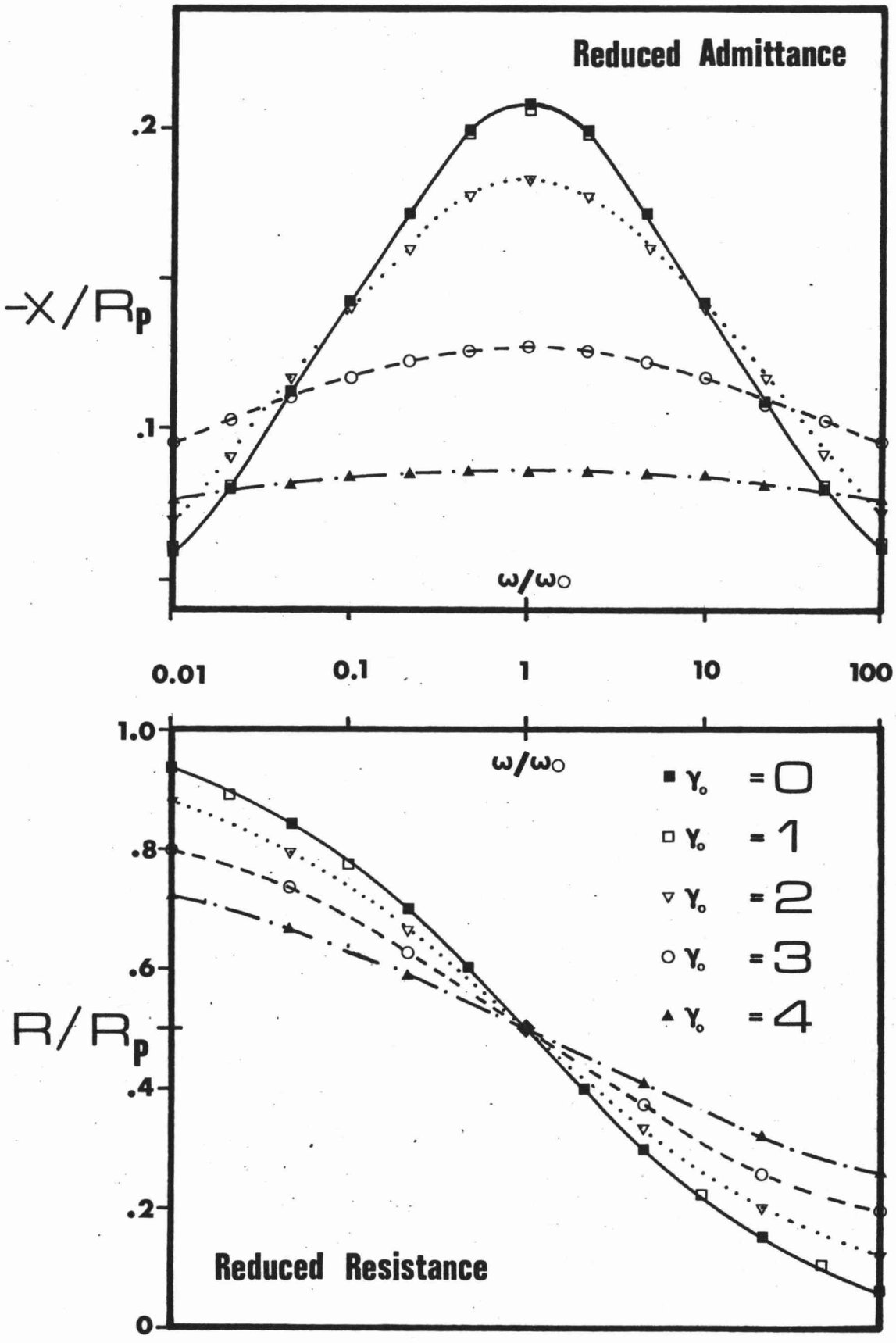

FIGURE 8.11 Impedance Loci versus γ_o

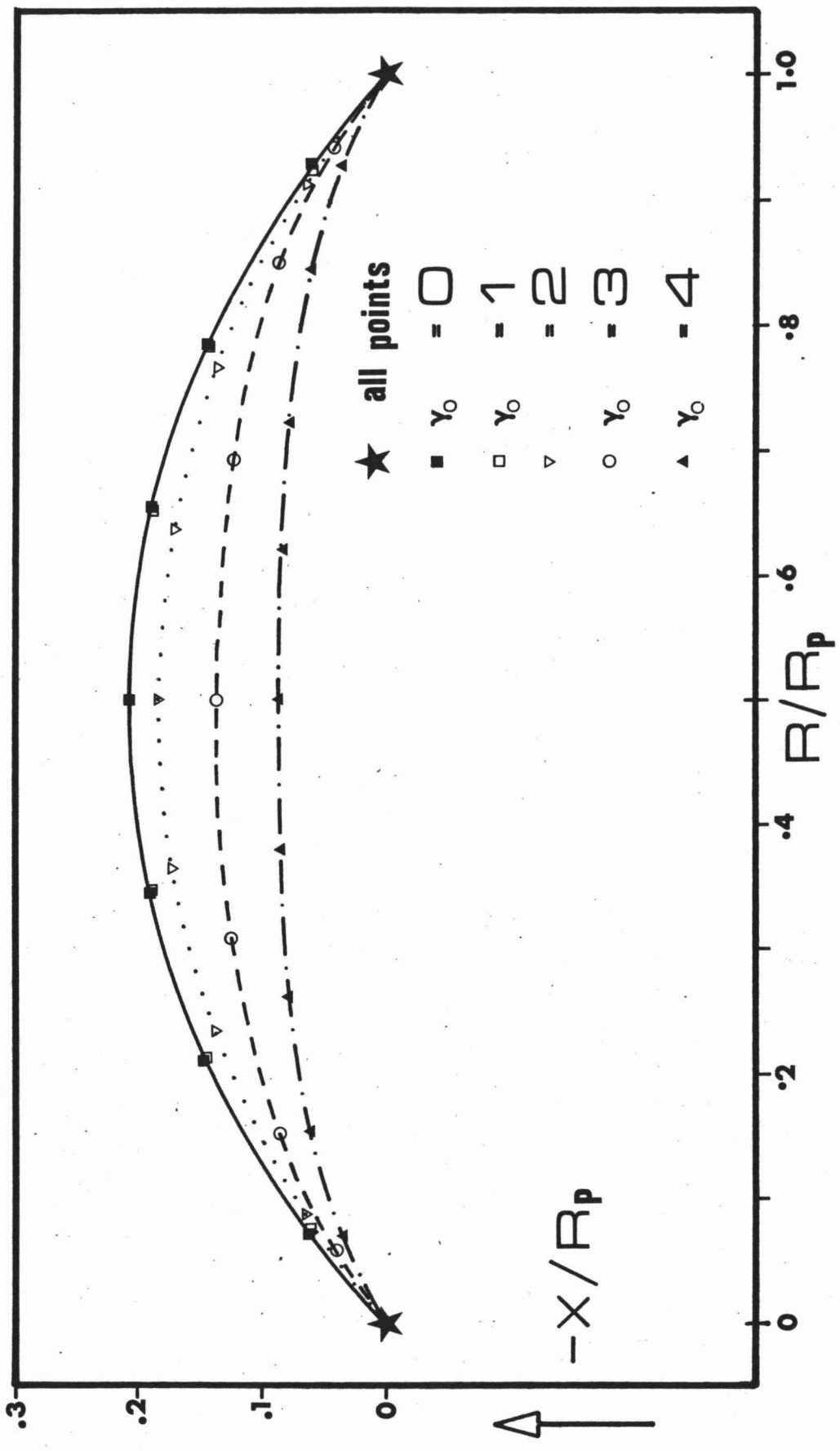

FIGURE 8.12 Dispersion Width versus γ_o

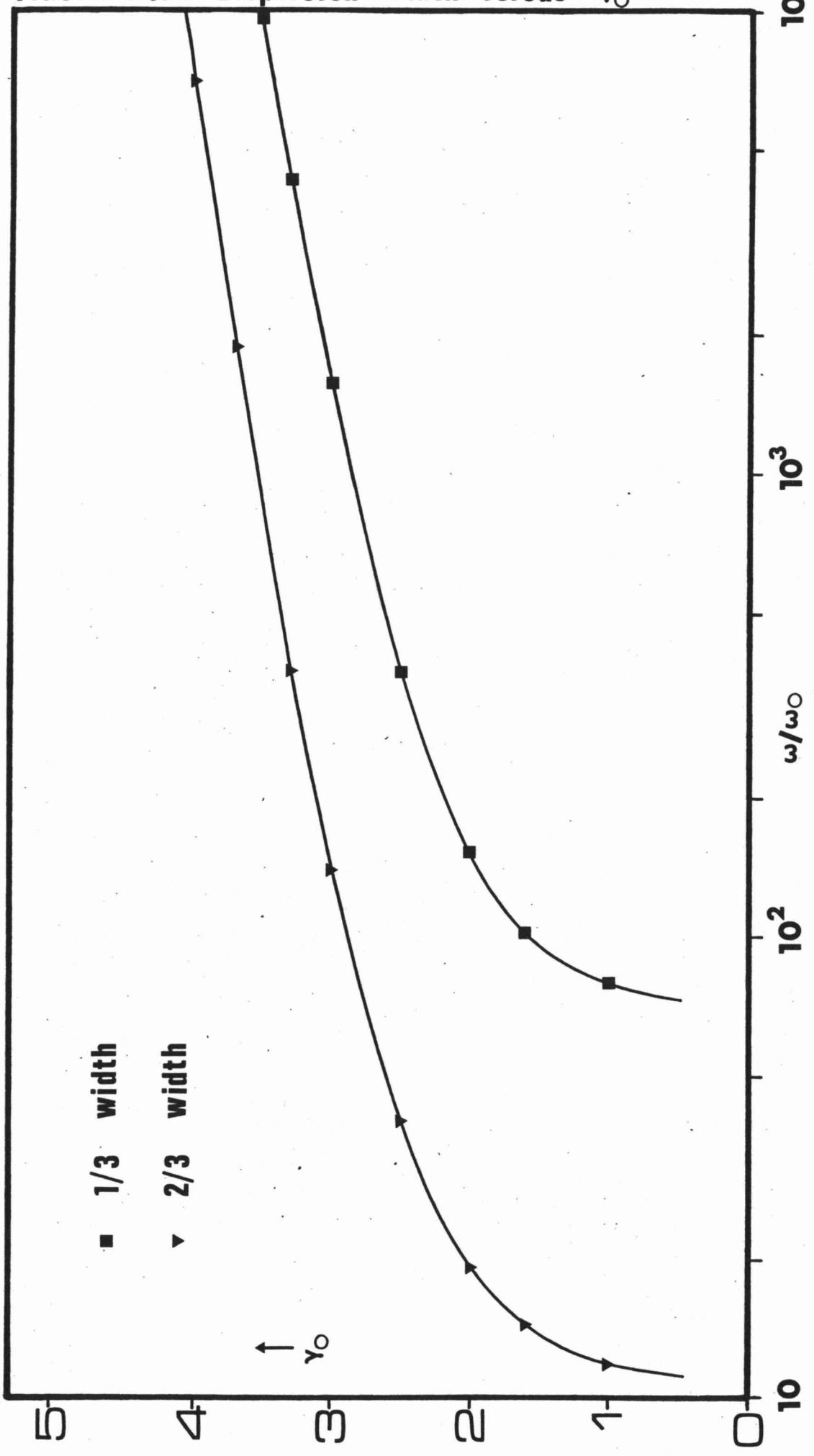

FIGURE 8.13 ∅ and $X_{max.}$ versus Y_O

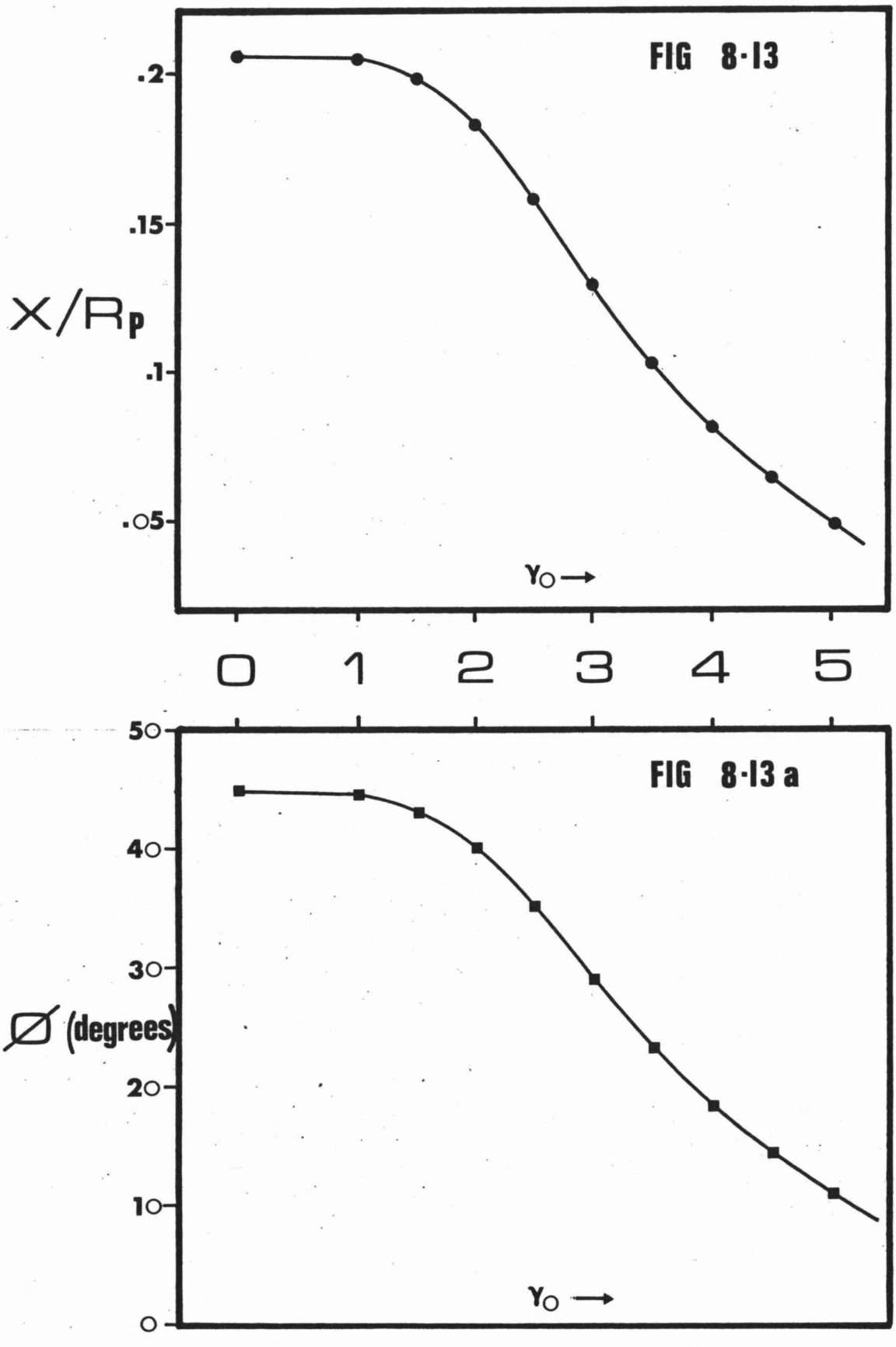

be utilised to fit cell 7 and cell 8 data to theory, and these are described separately.

8.4 CELL 7/$CaCl_2$

8.4.1 Description of Cell

Cell 7 contains 9% calcium form laponite/100-200 mesh ground pyrex, equilibrated with $CaCl_2$ electrolyte. Experiments were conducted varying the temperature at a concentration of 0.001 M $CaCl_2$, and the concentration from 0.0002 M to 0.02 M $CaCl_2$ at a temperature of 26.6°C.

In addition to the cell impedance, the electrolyte conductivity, G_E, was measured.

8.4.2 Determination of R_p, R_s, $\overline{\omega_o}$, γ_o and $\bar{\sigma}$.

For experiments using cell 7, a maximum is observed for the reactance at a frequency between 10 and 20 rad s^{-1}, which is significantly higher than the lower limit of bridge measurement. For these experiments the distribution parameters may be determined as follows.

1) X_{max} and $\overline{\omega_o}$ can be measured, and $\omega_{2/3}$ and $\omega_{1/3}$ interpolated from a plot of the measured reactance versus log ω.

2) γ_o can be obtained by interpolating values of $\omega_{2/3}$ and $\omega_{1/3}$ into Figure 8.12.

3) X_{max}/R_p can be obtained by interpolating γ_o into Figure 8.13, and since X_{max} is known, R_p may be calculated.

4) Since $\omega_o = 2\sigma^2/R_p^2$ (see section 7.2.1), then having determined $\overline{\omega_o}$ and R_p, the mean Warburg coefficient, $\overline{\sigma}$, may be calculated.

5) The experimental values of ω are now used to calculate values of X and R from equations [6] and [8], by using the values of $\overline{\omega_o}$, γ_o and R_p determined in steps 1, 2 and 3. At frequencies less than about 1000 $\overline{\omega_o}$, the values of X calculated are within ±0.1% of the experimental values. At higher frequencies, the measured reactance falls off less rapidly than calculated value.

6) The values of R obtained may be used to calculate R_s, since

$$R(\text{experimental}) = R_s + R(\text{theory}).$$

A number of frequencies are used and a mean value of R_s obtained.

The procedure outlined is necessarily complicated because a simple mathematical relationship between the experimental variables R, X and ω_o, and γ_o does not exist. Despite the accumulation of errors due to repeated interpolations however, a satisfactory fit to the measured impedance dispersion is obtained in all cases.

Figure 8.14 shows how the procedure described above is employed for a typical cell 7 experiment, and Figure 8.15 shows the correlation between the theoretical "best fit" and the experimental impedance loci.

8.4.3 Physical Dependence of Parameters

Table 8.5.1 summarises the values of R_p, R_s, γ_o, $\bar{\omega}_o$, and $\bar{\sigma}$ determined for cell 7, as a function of temperature and of electrolyte concentration.

8.4.3.1 Concentration

Figure 8.16 shows a log log plot of R_s, R_p and $1/G_E$ versus C. The electrolyte conductance shows the form expected for $CaCl_2$ at low concentrations (168) with the following straight line fit.

$$1/G_E = (11.76 \pm .13)C^{-1}$$

Both R_p and R_s however show a distinct curvature in Figure 8.16, indicating a non-simple power dependence, but for concentrations greater than 0.001 M, R_p approximates a C^{-1} dependence, and R_s a $C^{-\frac{1}{2}}$ dependence, with least squares fits.

$$R_p = -210\pm27 + (8.10\pm.10)C^{-1} \qquad r^2 = .9997$$

$$R_s = -2260\pm240 + (953\pm17)C^{-\frac{1}{2}} \qquad r^2 = .9994$$

Thus the series resistance has the same concentration dependence as that observed for resins. R_p on the other hand has the same

Table 8.5 Laponite Distribution Parameters

8.5.1 Cell 7/$CaCl_2$

Concentration (Molar)	Temperature (°C)	R_s (Ω)	R_p (Ω)	$\bar{\sigma}$ (Ω $s^{-\frac{1}{2}}$)	$\overline{\omega_o}$ (rad s^{-1})	γ_o
0.0002	26.7	52675	15750	4.24×10^4	14.5	2.07
0.0005	"	37781	11390	3.24 "	16.2	2.01
0.001	"	26746	7350	1.39 "	13.2	2.02
0.002	"	18956	3830	1.04 "	14.8	1.98
0.005	"	11450	1450	3.81×10^3	13.8	1.89
0.01	"	7244	574	1.99 "	13.5	1.80
0.02	"	4379	191	5.05×10^2	14.1	1.78
0.001	14.3	29480	9455	2.29×10^4	11.7	2.01
0.001	26.6	26984	7173	1.90 "	14.0	2.09
0.001	39.9	20641	5370	1.69 "	19.7	2.00
0.001	49.9	17323	4700	1.50 "	20.2	2.02

8.5.2 Cell 8/$CaCl_2$

0.001	26.6	25040	11593	1.99×10^3	0.039	3.21
0.01	"	7629	1097	4.88×10^2	0.099	2.87
0.1	"	1347	0	0	-	-
0.001	14.3	29699	20426	1.66×10^3	0.0131	3.24
0.001	26.6	21941	12980	1.70 "	0.0342	3.17
0.001	39.9	16590	9192	1.52 "	0.0540	3.09
0.001	49.9	13917	6542	1.80 "	0.151	2.95

FIGURE 8.14 Cell 7 Data Fit

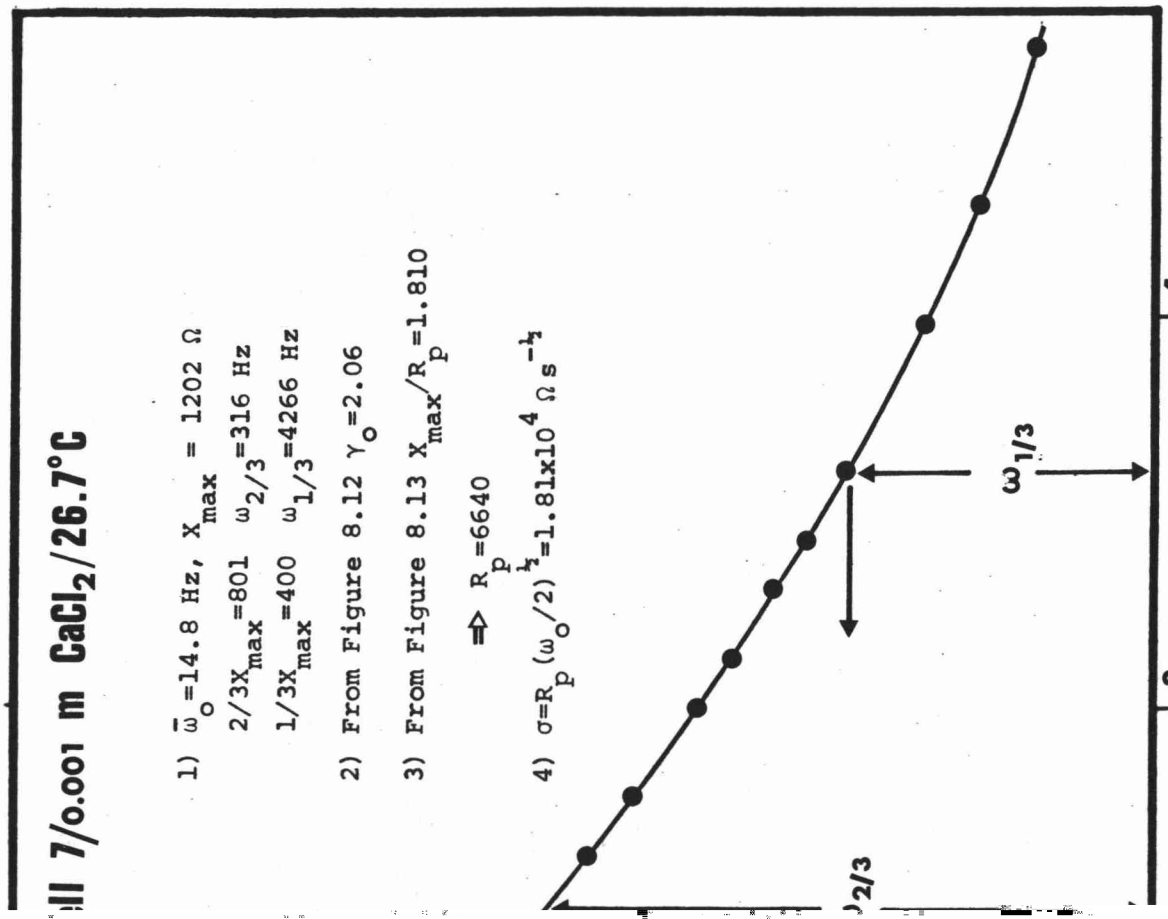

FIGURE 8.15 **Cell 7 Impedance Locus**

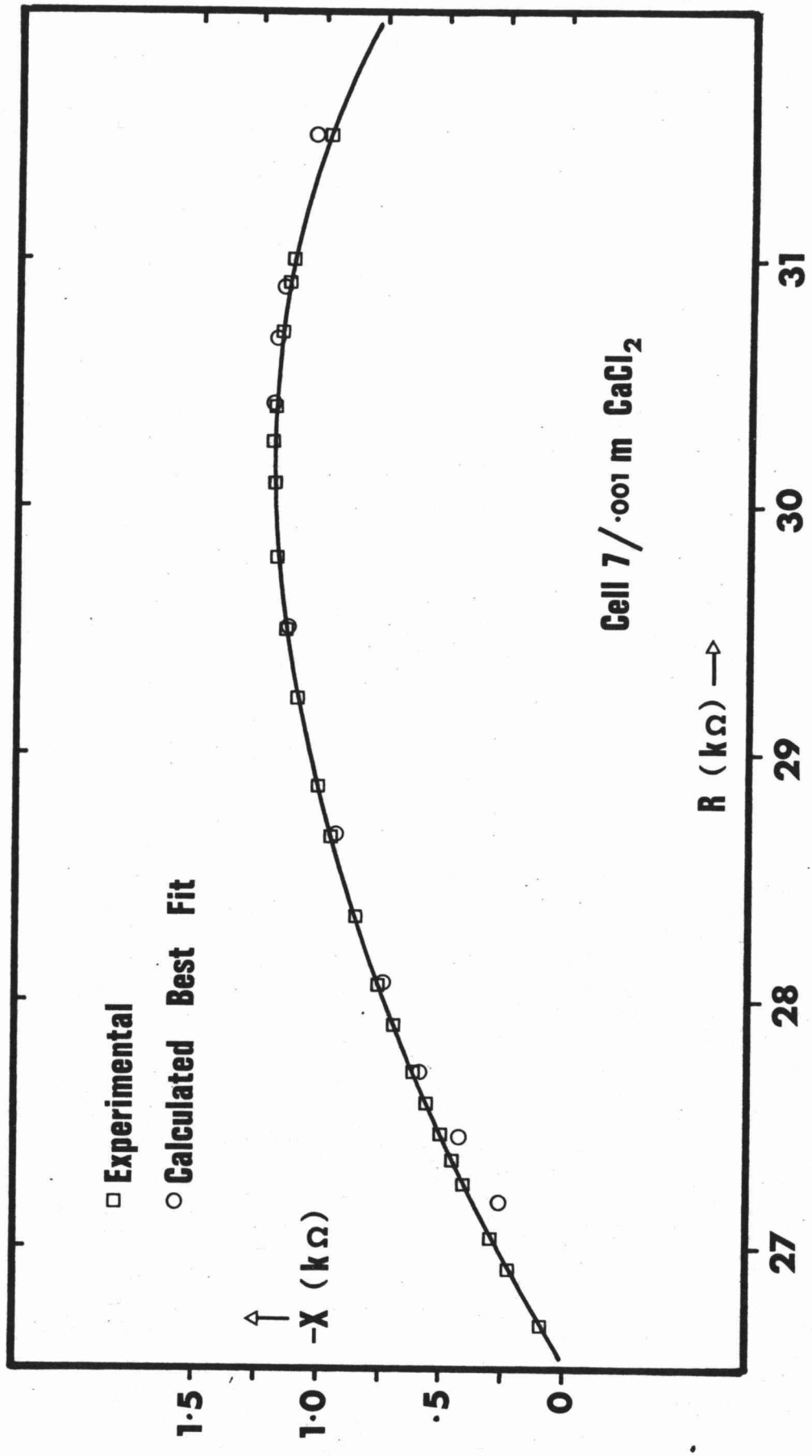

FIGURE 8.16 Log Log Resistance Versus Concentration Plots

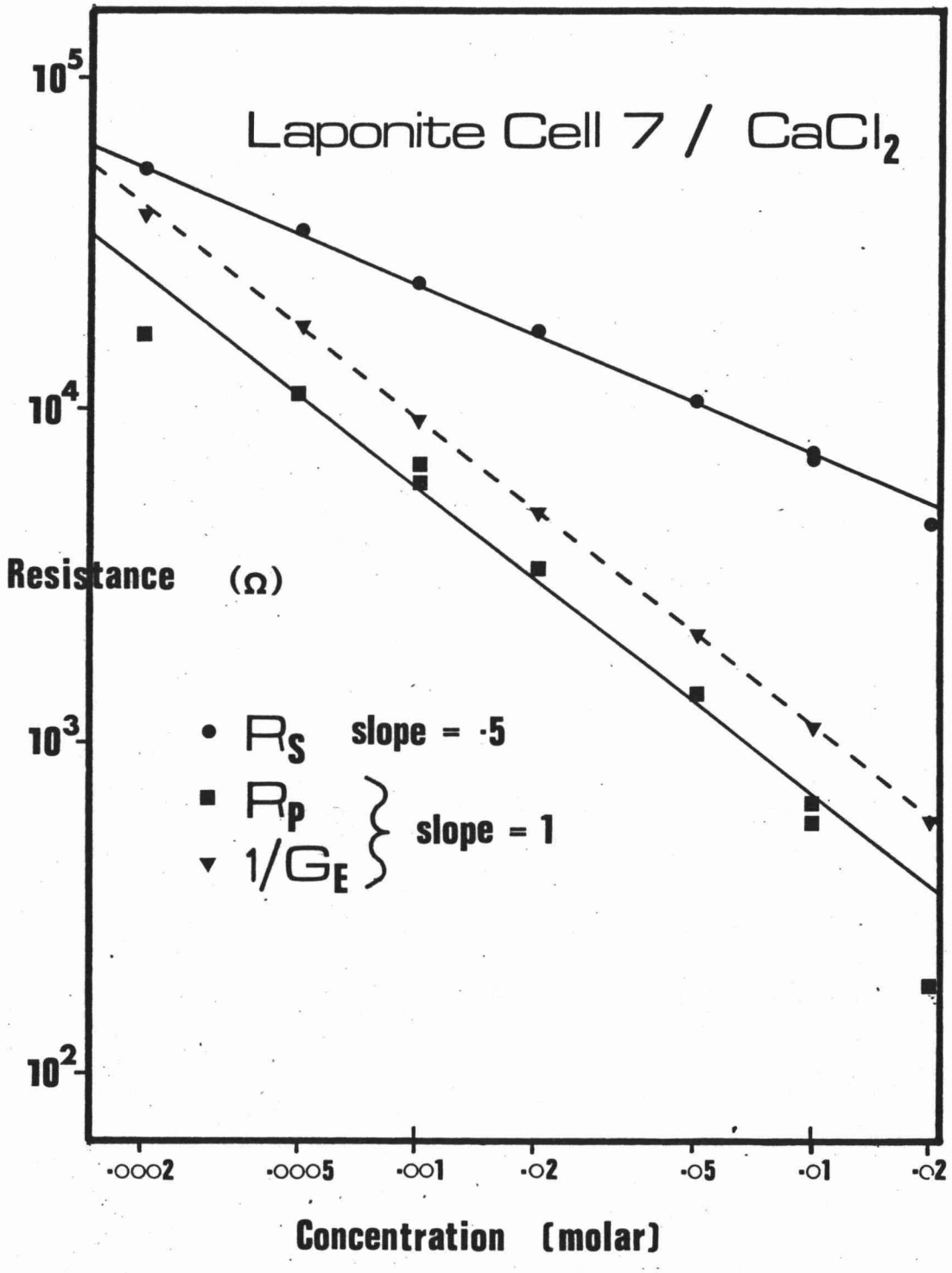

concentration dependence as the electrolyte, while for resin cells $R_p \propto C^{-3/4}$.

As expected for a Warburg impedance (equation [8], Chapter 7) σ is observed to be inversely proportional to C.

$$\bar{\sigma} = -191\pm380 + (19.49\pm.75)C^{-1} \qquad r^2 = .9992$$

The negative intercepts observed for R_p, R_s and $\bar{\sigma}$ are not significant and arise only because of the limited range of concentration observed. Clearly for finite concentrations all three must remain positive and thus at concentrations greater than 0.02 M the form of dependence of R_p, R_s and $\bar{\sigma}$ must change as does the concentration dependence of the electrolyte conductance (168).

Qualitatively it is observed that γ_o (and thus the spread of characteristic frequencies) decreases with increasing concentration, but there is no real trend in $\bar{\omega}_o$.

8.4.3.2 Temperature

Arrhenius plots for $1/G_E$, R_p and R_s all exhibit a straight line form over the temperature range 14.3 to 49.9°C measured.

$$\log(1/G_E) = 1.38\pm.05 + (759\pm17)/T \qquad r^2 = .9995$$

$$\log R_p = 1.17\pm.13 + (806\pm39)/T \qquad r^2 = .9953$$

$$\log R_s = 1.66\pm.39 + (1095\pm159)/T \qquad r^2 = .959$$

The activation energies for conduction are,

	$1/G_E$	R_p	R_s	
E_A	14.5±.3	15.4±.7	21±3	kJ mol^{-1}

Thus for 0.001 M $CaCl_2$, R_p behaves very similarly to the bulk electrolyte resistance, while R_s displays a significantly greater activation energy.

As expected for a Warburg impedance (section 7.3.5) a plot of $\log(\bar{\sigma}^2/T)$ versus 1/T is a straight line of slope proportional to the activation energy for the limiting equivalent conductivity.

$$\log(\bar{\sigma}^2/T) = 2.54\pm.18 + (1067\pm54)/T \qquad r^2 = .9949$$

$$E_A = 20.4\pm1.0 \text{ kJ mol}^{-1}.$$

Qualitatively γ_o is observed to be relatively independent of temperature, but $\bar{\omega}_o$ virtually doubles between 14.3 and 49.9°C.

8.5 CELL 8/$CaCl_2$

8.5.1 Description of Cell

Cell 8 contains 7% calcium form laponite/20-50 mesh soda glass spheres, equilibrated with $CaCl_2$ electrolyte. This is the only cell in which clay could be made to adhere to these large diameter smooth glass spheres, and 7% clay corresponds to an average clay thickness of 8×10^{-4} cm over all the glass surface within the cell. Assuming the clay to be in a relatively compact form in this surface coating, then the layer averages about 10^3 particles thick.

An impedance dispersion was observed for cell 8 for only 2 concentrations (0.01 and 0.001 M $CaCl_2$) at 26.6°C, and experiments were conducted at 4 temperatures using 0.001 M $CaCl_2$.

8.5.2 Determination of R_p, R_s, γ_o, $\bar{\omega}_o$ and $\bar{\sigma}$.

For all observations on cell 8, -X continues to rise at the lowest frequencies for which the impedance can accurately be measured (1 rad s^{-1}), and thus X_{max} and $\bar{\omega}_o$ cannot be obtained directly. Four independent variables (R_p, R_s, γ_o, $\bar{\omega}_o$) must thus be solved for from the observed variation of -X and R with ω, and an approximation must be employed as follows.

If the observed impedance data is fitted to a semicircle a value of R_s can be obtained, and admittance loci calculated from

$$A = \frac{R-R_s}{(R-R_s)^2 + X^2} \qquad B = \frac{X}{(R-R_s)^2 + X^2}$$

It is observed that as the frequency approaches zero, the admittance locus has the form

$$A = A_o + bB \qquad [9]$$

Admittance loci can be calculated for a distribution of time constant using equation [6] to obtain values of $-X/R_p$ (=x) and R/R_p (=r)

$$R-R_s = r\,R_p$$

$$X = x\,R$$

Thus,

$$A = \frac{r/R_p}{r^2 + x^2} \qquad B = \frac{x/R_p}{r^2 + x^2} \qquad [10]$$

Theoretical admittance loci were calculated for a distribution of the form shown in equation [8], as a function of γ_o. As $\omega \to \overline{\omega_o}$ *, admittance loci are found to be straight lines of the form,

$$A = A_o/R_p + bB \qquad [11]$$

and the linear regression parameters together with $\phi = \mathrm{Tan}^{-1}(B/A)$, are shown in Table 8.6.

Table 8.6

γ_o	A_o/R_p	b	r^2	ϕ
2.0	1.058±.020	1.112±.016	.9998	43.56°
2.3	1.082±.030	1.201±.027	.9995	42.03°
2.5	1.100±.036	1.280±.034	.9993	40.69°
2.7	1.111±.038	1.386±.041	.9991	38.73°
3.0	1.100±.036	1.630±.050	.9991	34.02°
3.2	1.103±.035	1.803±.055	.9991	31.46°
3.5	1.103±.035	2.112±.064	.9991	27.57°

Figure 8.17 shows A_o/A_p and b versus γ_o, and these may be used to determine R_p, R_s, $\overline{\omega_o}$ and γ_o from the measured impedance, as follows:

---

* This corresponds to the limiting frequency experimentally observed for cell 8.

FIGURE 8.17

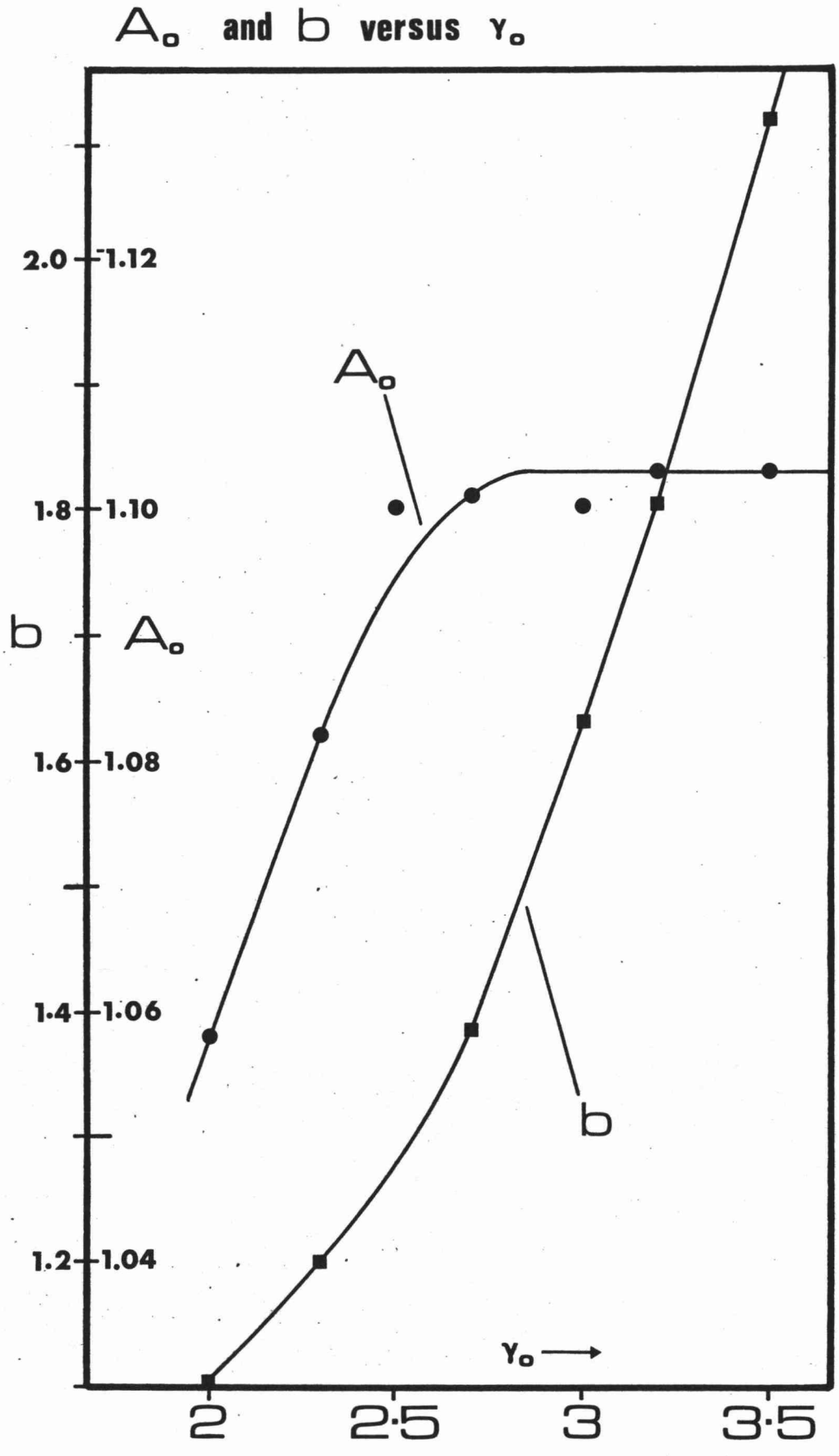
A_o and b versus γ_o
2.0
1.8
1.6
1.4
1.2
1.12
1.10
1.08
1.06
1.04
b
A_o
A_o
b
γ_o ⟶
2
2·5
3
3·5

1) An initial value of R_s can be estimated from the best fit of the measured impedance locus to a circle. Using R_s the admittance is calculated, and A_o and b obtained (equation [9]).

2) Using Figure 8.17, γ_o can be interpolated from b, and R_p calculated from the interpolated value of A_o/R_p, and A_o.

3) Values of R and X can now be calculated from equations [6] and [8] by setting γ_o and R_p at the values determined in step 2. X and R are calculated at values of $\omega/\overline{\omega_o}$ chosen to give impedances within the limits of those determined experimentally. Since a maximum is not observed for -X, an initial value of $\omega/\overline{\omega_o} = 100$ is usually selected.

4) The values of -X so calculated are interpolated into a plot of -X (experimental) versus log ω, and from the value of ω obtained, $\overline{\omega_o}$ can be calculated.

5) The value of ω determined in step 4 is interpolated into a plot of R (experimental) versus log ω, and from the value of R (experimental) obtained, and R (calculated), R_s may be calculated, since

$$R \text{ (experimental)} = R_s + R \text{ (calculated)}$$

6) Steps 3, 4 and 5 are repeated for different values of $\omega/\overline{\omega_o}$, and a mean value of $\overline{\omega_o}$ and R_s obtained.

7) As for cell 7, $\bar{\sigma}$ can be determined from R_p and $\overline{\omega_o}$, since,

$$\overline{\omega_o} = 2\bar{\sigma}^2/R_p^{\,2}$$

For cell 8 however $\overline{\omega_o}$ is known with little precision, and the estimated error in $\bar{\sigma}$ is probably not less than $\pm 30\%$.

The good fit to the measured impedance dispersion invariably obtained is a substantial verification of this rather cumbersome technique. Figure 8.18 shows -X and R versus log ω measured for a typical experiment, together with an outline of the procedure to find R_p, γ_o, $\overline{\omega_o}$ and R_s. Figure 8.19 shows the correlation between the experimental, and the calculated "best fit" impedance loci.

FIGURE 8.18 Cell 8 Data Fit

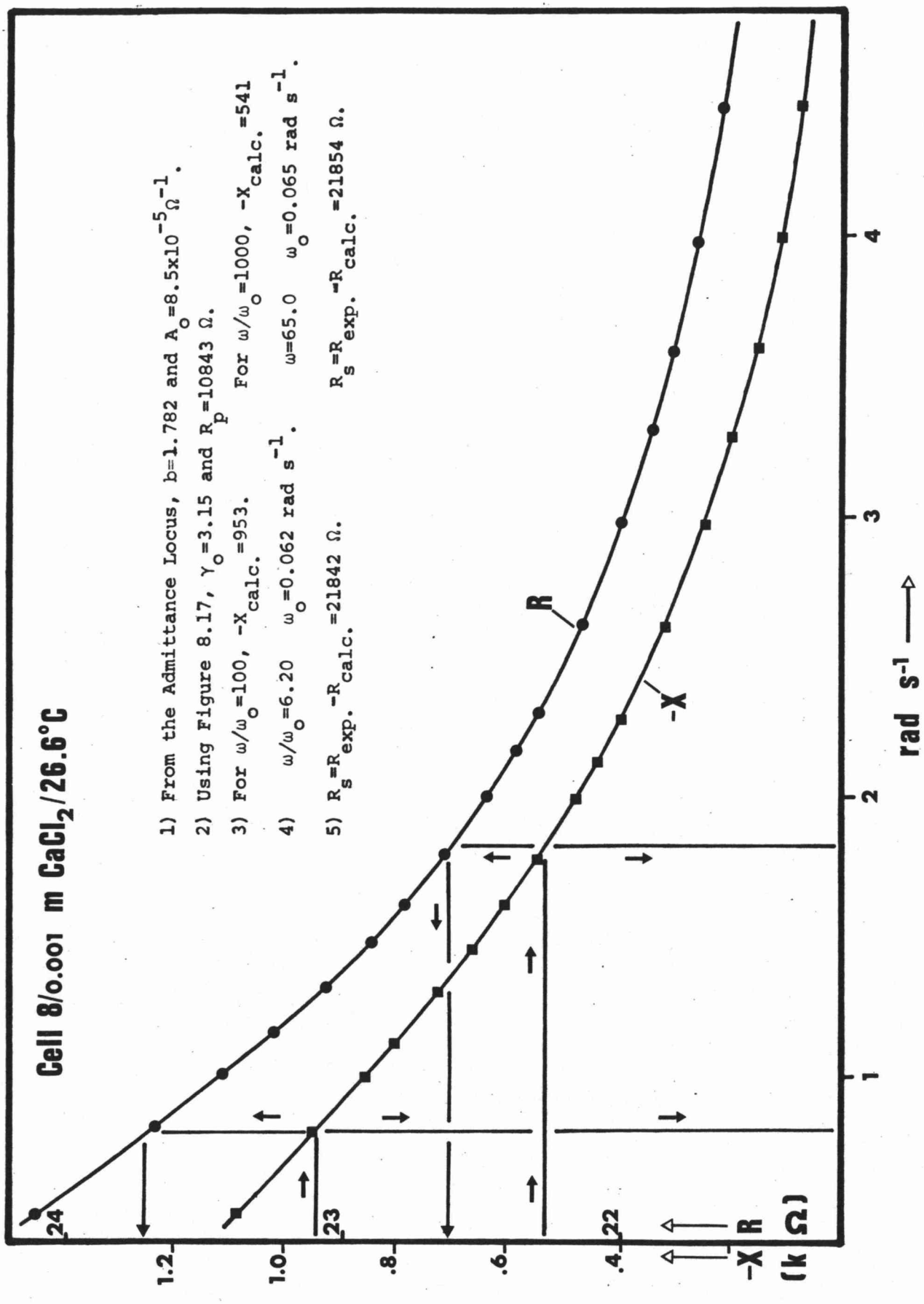

FIGURE 8.19 Cell 8 Impedance Locus

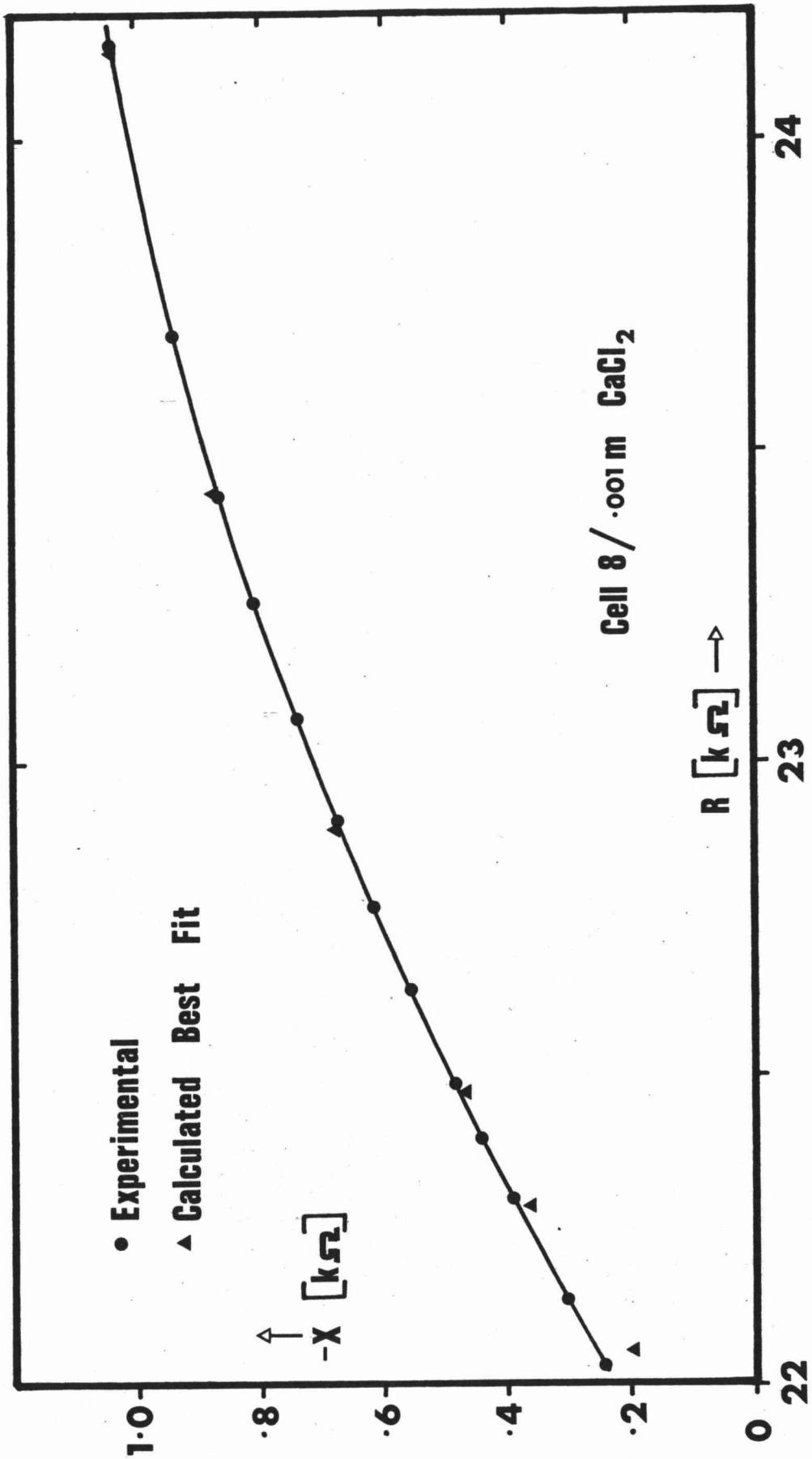

8.5.3 Physical Dependence of Parameters

The temperature and concentration dependence of R_p, R_s, γ_o, $\overline{\omega_o}$ and $\bar{\sigma}$ have been observed over a limited range, and the results are shown in Table 8.5.2.

8.5.3.1 Concentration

An impedance dispersion was observed for cell 8/0.001 M $CaCl_2$ and cell 8/0.01 M $CaCl_2$, and no dispersion was observed for cell 8/0.1 M $CaCl_2$. By assuming that the impedance tends to zero as 1/C goes to zero the concentration dependence may be determined to be as follows.

$$R_s = (794\pm10)C^{-\frac{1}{2}} \qquad r^2 = .9998$$

$$R_p = (11.62\pm.06)C^{-1} \qquad r^2 = .99997$$

$$\bar{\sigma} = (3.54\pm.10)C^{-1} \qquad r^2 = .9992$$

Thus $\bar{\sigma}$ behaves as a Warburg coefficient and the effects of concentration for cell 8 are the same as for cell 7.

8.5.3.2 Temperature

Four temperatures were examined between 14.3 and 49.9°C, at a concentration of 0.001 M $CaCl_2$.

Arrhenius plots for R_s and R_p yield the following straight lines.

$$\log R_s = 1.48\pm.07 + (860\pm21)/T \qquad r^2 = .9983$$

$$\log R_p = -0.08\pm.18 + (1260\pm54)/T \qquad r^2 = .9964$$

The activation energies for conduction are thus,

	R_s	R_p	$1/G_E$*
E_A	16.5±.4	24±1	14.5±.3 kJ mol^{-1}

The uncertainty in $\overline{\omega_o}$ is reflected in the values of $\bar{\sigma}$ which cannot be fitted meaningfully to the form expected for a Warburg impedance.

---

* Determined from cell 7.

8.6 TWIN DISPERSION (GROUP I) DATA

8.6.1 Introduction

For three cells containing Wyoming bentonite/ground pyrex, two sets of parameters relating to two distinct dispersion processes must be used to describe the impedance dispersion. These experiments were performed during preliminary studies and the effects of temperature and concentration were not studied. The two dispersion processes observed in each of these cells however, provides a strong link between the mechanisms proposed for Group II and Group III clay data.

The high frequency dispersion process is that expected for Wyoming bentonite cells (Group III) and may be adequately fitted using the procedure described in section 8.2.1 to obtain R_p, σ and C. The anomalous dispersion is that which occurs at low frequencies, and is found to be similar to the dispersion of laponite (Group II) cells. The low frequency dispersion can be adequately characterised using the procedures described in sections 8.4.2 and 8.5.2.

The theoretical best fit for twin dispersion data is shown in Table 8.7.

Table 8.7

Cell/Electrolyte		R_s (Ω)	R_p (Ω)	σ ($\Omega s^{-\frac{1}{2}}$)	ω_o (rad s^{-1})	γ_o	C (F)
B/0.01 $CaCl_2$	High	9587	423	3.27×10^{4}	9.23×10^{4}	-	2.66×10^{-7}
	Low		368	2.69×10^{2}	1.07	-	-
B/0.1 $CaCl_2$	High	4606	71.4	1.06×10^{3}	6.96×10^{3}	-	2.2×10^{-7}
	Low	4626	180	3.76×10^{2}	8.71	2.00	-
3/0.1 NaCl	High	3219	15.2	2.04×10^{3}	1.38×10^{4}	-	1.1×10^{-6}
	Low	3228	107	1.14×10^{2}	2.29	2.72	

Both cells B and 3 contain 8% Wyoming bentonite/50-100 mesh ground pyrex, the clay being homoionic with the electrolyte.

8.6.2 High Frequency Dispersion

It has previously not been possible to determine the concentration dependence for Wyoming bentonite cells (see section 8.2.2). For cell B two concentrations have been observed, and assuming the cell impedance tends to zero as 1/C goes to zero, the form of the concentration dependence is found to be as follows.

$$R_s = (922\pm174)C^{-\frac{1}{2}} \qquad r^2 = .967$$

$$R_p = (13.4\pm.1)C^{-3/4} \qquad r^2 = .9999$$

$$\sigma = (337\pm21)C^{-1} \qquad r^2 = .9961$$

Thus σ has the expected (Warburg) concentration dependence and R_s shows a rather poor fit to the form previously observed for all cells ($R_s \propto C^{-\frac{1}{2}}$). R_p is very closely proportional to $C^{-3/4}$ which is the form observed for resin cells, but for laponite cells $R_p \propto C^{-1}$.

Comparing the high frequency parameters for cell 3/0.1 M NaCl with the single dispersion data for cells 1 and 2 (which are identical in all respects to cell 3)/0.01 M NaCl (Table 8.2.1), the same concentration dependence as observed for cell B, holds.

$$R_s = (896\pm40)C^{-\frac{1}{2}} \qquad r^2 = .9981$$

$$R_p = (12.9\pm1.7)C^{-3/4} \qquad r^2 = .982$$

$$\sigma = (293\pm8)C^{-1} \qquad r^2 = .9992$$

It would seem therefore that the high frequency dispersion process is identical with the model proposed for Wyoming bentonite and latex cells in section 8.1.2.

8.6.3 Low Frequency Dispersion

An anomalous dispersion arises for high electrolyte concentrations as a consequence of some low frequency process not previously observed in Wyoming bentonite cells. Because of the limited number of observations little quantitative information is available, but the form of the low frequency dispersion is similar to that observed for laponite cells, and the parameters R_p, $\bar{\sigma}$ and γ_o are similar (Tables 8.5 and 8.7).

It is not unreasonable therefore to suppose that the mechanism for low frequency dispersion in Wyoming bentonite cells is the same as that proposed for laponite cells - that is, an assemblage of shunted Warburg impedances with a distribution of characteristic frequencies. The origin of such a dispersion will be discussed in section 9.2.

Section

IV

Conclusions

CHAPTER 9 DISCUSSION OF RESULTS

9.1 EQUIVALENT CIRCUIT

Four different types of cell have been investigated and found to display an effectively identical impedance dispersion.

1) Packed beds of ion exchange resin spheres/electrolyte.
2) A synthetic clay (laponite)/glass particles/electrolyte.
3) A natural clay (Wyoming bentonite/glass particles/electrolyte.
4) A packed bed of polystyrene latex spheres/electrolyte.

For all these systems the dispersion is due to a Warburg impedance which arises as a consequence of diffusional limitation at the interface between the solid and electrolyte phases. In all except latex cells two possible regions exist in which diffusional limitation can occur. One is immediately inside the resin (or clay)/electrolyte interface, and the other on the electrolyte side of this interface. It is not necessary that the precise nature of this interface be defined or that the two adjacent regions be separated, provided the electrical properties of the interfacial region as a whole are understood.

Associated with the diffusional impedance are a shunt resistance (R_p) and capacitance (C), and a series resistance (R_s). The equivalent circuit shown in Figure 9.1 can be used to describe the measured electrical properties of all cells studied.

Figure 9.1 Cell Equivalent Circuit

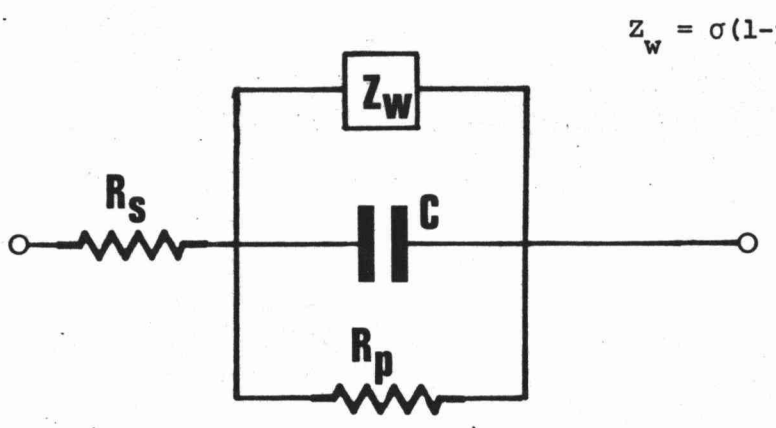

For resin and laponite cells, σ is relatively small and $Z_w \rightarrow 0$ with increasing frequency, before the capacitance can be observed. For Wyoming bentonite and latex cells σ is large and the capacitive term contributes significantly to the impedance, increasing the observed phase angle.

If all membrane zones within a cell are not identical, then the measured two terminal cell impedance may be characterised by considering a distribution of characteristic frequencies (ω_o) for the zone impedances. This is observed for laponite cells and results in a decreased measured phase angle. No distribution of ω_o is found for resin cells, and it is tacitly assumed that none occurs with Wyoming bentonite or latex cells, in order to solve for C. This assumption cannot be checked directly, but is a reasonable one for latex cells in which the individual particles are highly uniform.

9.2 PHYSICAL SIGNIFICANCE OF THE EQUIVALENT CIRCUIT

9.2.1 Introduction

Table 9.1 is a summary of the temperature and concentration dependence observed for resin and clay cells. For all cells studied, R_p, R_s and σ were found to display the Arrhenius temperature dependence expected for ionic conduction, and the derived activation energies are given in Table 9.1.1, together with E_A measured for the bulk electrolyte.

The form of the concentration dependence found for R_p, R_s, σ and the bulk electrolyte resistance ($1/G_E$), are shown in Table 9.1.2.

9.2.2 R_s

For resin cells R_s is associated with conduction by cations within the resin phase (see section 7.4.3). The value of the activation energy for conduction obtained (20.5±.2 kJ mol^{-1}) is close to that measured by Owen (160) for the limiting equivalent conductivity of Na^+ ions in a similar resin (E_A = 18.4 kJ mol^{-1}). The greater activation energy observed in the present study is probably due to the greater cross linkage of the resin (12% compared with 8.6% - see reference 189).

Table 9.1 Summary of Temperature and Concentration Dependence for Clay and Resin Cells

9.1.1 Activation Energy for Conduction

Parameter	$1/G_E$	R_s	R_p	σ
Resin/0.001 M NaCl	13.8±.2	20.5±.2	29.9±.9	42 ±1 kJ mol^{-1}
Laponite 7/0.001 M $CaCl_2$	14.5±.3	21 ±3	15.4±.7	20.4±1 "
Laponite 8/0.001 M $CaCl_2$	14.5±.3	16.5±.4	24 ±1*	- *
Wyoming bentonite/ 0.01 M $CaCl_2$	14.0±.3	14.7±.3	19.4±.4	41 ±10 "

9.1.2 Concentration Dependence

Parameter	$1/C_E$	R_s	R_p	σ
Resin/NaCl	C^{-1}	$C^{-\frac{1}{2}}$	$C^{-3/4}$	C^{-1}
Laponite 7/$CaCl_2$	C^{-1}	$C^{-\frac{1}{2}}$	C^{-1}	C^{-1}
Laponite 8/$CaCl_2$	C^{-1}	$C^{-\frac{1}{2}}$	C^{-1}	C^{-1}
Wyoming bentonite/$CaCl_2$	C^{-1}	$C^{-\frac{1}{2}}$	$C^{-3/4}$	C^{-1}

* The uncertainty expressed for cell 8 data represents only random scatter about the best fit line. Because only a small fraction of the total dispersion is observed at frequencies above 1 rad s^{-1}, there undoubtedly exists a large systematic error in R_p and σ. For σ this error is so large that a meaningful fit cannot be made to the expected Warburg dependence, and for R_p the error in E_A is probably >10 kJ mol^{-1}. A similar error does not arise for R_s, because this is determined at the high frequency limit, which may be observed directly.

The dependence of R_s on concentration and temperature observed for clay and resin cells is the same. From Table 9.1, for both systems $R_s \propto C^{-\frac{1}{2}}$ and $E_A \approx 20$ kJ. These observations suggest a similar mechanism for R_s in clay and resin cells. In the latter R_s arises within the resin gel and for clay cells such a membrane phase can only occur within the macroscopic clay layer adhering to the matrix of glass particles. For laponite cell 8/20-50 mesh glass spheres this clay coating is on average 1000 clay particles thick and might be expected to behave similarly to a resin gel. The layer contains a concentration of fixed (anionic) charges on the colloidal platelet surfaces, surrounded by diffuse counter ions. The structure of the clay is likely to be an open, edge to face (192) aggregation in which ions originating in both the electrolyte and the double layer, contribute to conduction.

For resin cells therefore R_s involves a conduction path through the bulk of the spherical particles. For clay cells R_s is the resistance of a membrane like layer of finite thickness. Latex cells represent the limiting case. There is no macroscopic conducting layer on the surface of individual polystyrene latex particles and it must be supposed that R_s involves a surface conduction mechanism parallel to the surface in the polystyrene/electrolyte interfacial region. It is not possible to assess directly the contribution of such a surface conduction, since the concentration dependence of R_s for latex cells is not known. However, even considering the very large surface area of these particles (5×10^4 cm^2 g^{-1}), in order to account for resistances as low as those observed for R_s in latex cells, the specific surface conductivity (λ_σ) would need to be 4 to 6 orders of magnitude larger than that calculated from the zeta potential and attributable to the diffuse double layer (see sections 5.3.5 and 7.4.3). This requirement is consistent with the known properties of polystyrene latex particles. Wright and James (210) measured the surface conductivity of suspensions of polystyrene latex particles as a function of concentration for a number of electrolytes. They observed an increase of surface conductivity with increasing concentration for KCl, $Ba(ClO_4)_2$, and $Al(ClO_4)_3$, and found that the measured surface conductivity was up to four orders of magnitude larger than that calculated for the diffuse double layer (i.e. from the zeta potential). Wright and James interpreted these results as indicating a large contribution to the

total surface conductivity from the fixed (Stern) layer, and it is presumably within this layer that R_s, for latex cells, originates.

For the same electrolyte, R_s should increase as the fraction of the particle cross section involved in conduction decreases, and this trend is observed in Table 9.2 for 0.01 M $CaCl_2$.

Table 9.2

System/0.01 M $CaCl_2$	R_s (Ω)
Resin 200-400 mesh	4,050
Laponite 7/100-200 ground pyrex	7,200
Wyoming bentonite 3/50-100 ground pyrex	15,000
Latex	51,443

9.2.3 R_p and σ

The origin of a shunted Warburg impedance will be discussed in section 10.1. However, from the frequency, concentration and temperature dependence observed for all cells, σ may be associated with the coefficient of a Warburg diffusional impedance having the form,

$$Z_w = \sigma(1-j)\omega^{-\frac{1}{2}}$$
$$\sigma = RT(n^2F^2AC)^{-1}(2D)^{-\frac{1}{2}} \qquad [1]$$

with $\sigma \propto C^{-1}$

and $\log(\sigma^2/T) \propto T^{-1}$.

The best fit of experimental data to the form expected from equation [1] is used to obtain information about the coefficients of this equation, in section 9.2.4.

R_p represents an ohmic shunt to Z_w. From the observed concentration and temperature dependence for Wyoming bentonite and laponite (Table 9.1), and latex cells (section 8.2.4), R_p cannot be attributed to a pure electrolyte shunt. However, at high concentrations the electrolyte contribution has been shown to be predominant (section 7.4.2), and from Table 9.1, for laponite cells R_p behaves similarly to the electrolyte resistance.

9.2.4 Area

From equation [1] the expected slope of a plot of σ versus 1/C is,

$$\sigma C = RT(n^2F^2A)^{-1}(2D)^{-\frac{1}{2}}$$

thus $$A = 1.89\times10^{-4}/n^2D^{\frac{1}{2}}(\sigma C)\ cm^2 \qquad [2]$$

where C is expressed in moles dm^{-3}.

A is the characteristic area of the membrane zones. When determined from the concentration dependence of the cell impedance (Z_w) this area is non-physical since it is a property of the geometrical configuration of the cell components, and of the individual membrane zones. In order to obtain a meaningful value of A therefore, it is necessary to determine Z_w for each particle/electrolyte interface from the measured two terminal cell impedance. Nevertheless information may be obtained about A by observing the dependence of the characteristic area (from equation [2]), on particle size.

The cation diffusion coefficient in the double layer normal to the surface is indeterminate, but using values for the bulk electrolyte, then equation [2] becomes,

$$A = 1.37\times10^{-2}/\sigma C \quad \text{for } CaCl_2 \qquad [3]$$

$$A = 4.80\times10^{-2}/\sigma C \quad \text{for NaCl} \qquad [4]$$

Table 9.3 gives measured values of σC and the characteristic area, A_{cell} calculated from equations [3] and [4].

Table 9.3 Characteristic Area from Cell Impedance

System	Electrolyte/Mesh	σC ($\Omega.s^{\frac{1}{2}}$mol dm^{-3})	A_{cell} (cm^2)	A_o* (cm^2)	A_{cell}/A_o
Latex	$CaCl_2$	2110	6.49×10^{-6}	4.91×10^{-8}	132
Resin	NaCl/200-400	78	6.17×10^{-4}	1.72×10^{-4}	3.59
Laponite	7,$CaCl_2$/100-200	19.5	7.03×10^{-4}	3.46×10^{-4}	2.03
Resin	NaCl/100-200	33	1.46×10^{-3}	8.04×10^{-4}	1.82
Wyoming bentonite	3,$CaCl_2$/50-100	293	4.67×10^{-5}	9.84×10^{-4}	0.047
	B,$CaCl_2$/50-100	337	4.06×10^{-5}	9.84×10^{-4}	0.041
Laponite	8,$CaCl_2$/20-50	3.54	3.87×10^{-3}	7.85×10^{-3}	0.49

* A_o is calculated from the mean mesh diameter, assuming the particles to be uniform smooth spheres.

With the exception of Wyoming bentonite cells the characteristic area increases with increasing particle size, as would be expected if the areas in which Z_w originates were the individual particle surface areas. However, A_{cell}/A_o shows a substantial variation up to 132 times A_o, indicating the need for an estimation of the microscopic zone impedance.

The cell impedance may be considered to be that of a three dimensional array of local membrane impedances, such as that shown in Figure 8.6. In section 8.3.2 an expression is derived for the cell impedance in terms of this three dimensional network, and

$$Z_{cell} = \frac{1}{m} \sum_{k=1}^{n} Z_k$$

where n = the number of series element.

m = the number of possible parallel conduction paths

Z_k = the impedance of the kth membrane zone.

A "typical" zone impedance $\bar{Z}_k$ may be defined such that

$$\bar{Z}_k = m\, Z_{cell}/n \qquad [5]$$

and n ≈ length of cell/mean particle diameter.

In order to calculate m it is necessary to make an approximation. It is assumed therefore that the number of parallel conduction paths is simply the number of particles in a cross section. This is equivalent to assuming that particles do not interact laterally, and particle to particle conduction occurs only with neighbours immediately up and down field.

Thus,

$$m \approx \text{Area of cell}/(\text{mean particle diameter})^2$$

and

$$\bar{Z}_k = Z_{cell}/b.d \qquad [6]$$

where b = cell constant (= 16.55)

d = mean particle diameter

It follows from equation [6] that the "typical" membrane zone Warburg coefficient,

$$\bar{\sigma}_k = \sigma_{cell}/16.55d$$

and the "typical" area of the membrane zone is

$$\bar{A}_k = 16.55d\ A_{cell} \qquad [7]$$

Areas of the membrane zones have been calculated from equation [7] and are presented in Table 9.4.

The last column of Table 9.4 gives the effective percentage of surface coverage of the membrane zone. These results are in substantial agreement with a model of zone polarisation associated with the individual resin, clay coated glass and latex particles. The areas calculated are realistic (i.e. not greater than 100% of A_o) with the effective area of the membrane zone varying between approximately 30% of A_o for latex and about 50% for resin particles. The area coefficient, A, in equation [1] may thus be seen to represent a physical area for individual particle membrane zones. The observation that σ behaves virtually identically for resin, laponite and latex cells is significant. Despite the obvious physical differences between these systems, and a factor of 400 difference in particle diameters between latex and laponite cell 8, it would appear that the origin of Z_w in all cases was the same.

Table 9.4

System	Electrolyte/Mesh*	d (cm)	$\bar{A}_k$ (cm^2)	$100\bar{A}_k/A_o$ (%)
Resin	NaCl/100-200	1.6×10^{-2}	2.54×10^{-4}	48.1
Resin	NaCl/200-400	7.4×10^{-3}	5.41×10^{-5}	43.9
Laponite	8,$CaCl_2$/20-50	5.0×10^{-2}	3.20×10^{-3}	40.8
Laponite	7,$CaCl_2$/100-200	1.1×10^{-2}	1.22×10^{-4}	35.3
Wyoming bentonite	3,$CaCl_2$/50-100	1.8×10^{-2}	1.37×10^{-5}	1.4
	B,$CaCl_2$/50-100	1.8×10^{-2}	1.19×10^{-5}	1.2
Latex	$CaCl_2$	1.25×10^{-4}	1.34×10^{-8}	27.3

* For resins the stated values 200-400 and 100-200 mesh are nominal size ranges only. For 200-400 mesh AG50W-X12 the geometric mean of the size distribution is about 200 U.S. wet mesh (corresponding to $d = 7.4\times10^{-3}$ cm) with half of the particles having diameters between 0.75 and 1.34 (i.e. ±34%) of this value (21).

Similarly for 100-200 nominal mesh, the geometric mean is about 90 ($d = 1.6\times10^{-2}$ cm) with half of the particles having diameters between 0.67 and 1.56 (i.e. ±50%) of this value.

For Wyoming bentonite/ground pyrex cells the fraction of the total particle surface contributing to the diffusional impedance is small. This observation is consistent with the known properties of the system. Ground pyrex particles are observed to have extremely irregular surfaces and Wyoming bentonite adheres very poorly and unevenly to this surface. It is probable that the clay lodges in small irregularities on the glass surface, having areas only of the order of a few percent of the total particle surface area.

9.2.5 Distribution of ω_o

The characteristic frequency (ω_o) is most easily calculated from the parameters of a semicircular fit of the impedance locus (see section 8.1.1).

$$Z'' = (a-jb)\omega^{-\frac{1}{2}}$$

$$\omega_o = (a^2+b^2)/R_p^2$$

$a=b = \sigma$ for resin cells

$a \approx b \approx \sigma$ for clay and latex cells

Thus $$\omega_o \approx 2\,\sigma^2/R_p^2. \qquad [8]$$

In order to explain the dispersion of cell impedance observed for cells containing laponite, it is necessary to propose a distribution of characteristic frequencies for the individual membrane zones. From equation [8] a distribution of ω_o may arise because either σ or R_p, or both vary from zone to zone. For mathematical convenience R_p has been assumed to be constant (see sections 8.3.2 and 8.3.3), and any distribution of ω_o is thus associated with σ. Examining equation [1], only A is likely to vary sufficiently to produce the distribution of σ and thus ω_o, calculated for laponite.

Resin cells are not observed to display a distribution of ω_o. The surfaces of resin particles are relatively smooth and the electrolyte/membrane interface can cover the entire surface. Assuming the distribution of ω_o to be associated only with A, γ_o can be calculated from the known size range of resin particles (21). For 100-200 mesh resin, $\gamma_o \approx 0.7$ and from Table 8.4 it is apparent that the expected decrease of ϕ below

45° for such a distribution is less than 0.2°, which is within the experimental uncertainty.

For laponite cells however the distribution of ω_o is large, with γ_o between 2 and about 3. Expressed in more conventional terms, $\gamma_o = 2$ implies that half of the membrane zones have characteristic frequencies between 0.1 and 10 times the (geometric) mean. Since $\omega_o \propto 1/A^2$, then half of the zones have areas within 0.56 and 1.78 (i.e. ±80%) of the mean. For $\gamma_o = 3$ then half of the membrane zones have areas between 0.18 and 5.62 of the mean.

Such a distribution cannot be explained in terms of the distribution of particle sizes, which is not significantly broader than for beds of resin spheres. For cells containing clay/glass particles however, the surface clay coating is not uniform or smooth, and a probable explanation of the observed distribution (of area) is that the effective fraction of the particle surface covered by a membrane-like layer, varies from particle to particle.

For clay/glass particle systems the effective area is between 1 and 40% of the total glass surface area. This is a clear indication that the interface at which the diffusional impedance arises is the macroscopic interface between clay aggregations and the electrolyte, and that the clay within these aggregations behaves as a homogeneous and non-reactive ion conducting phase. If this were not true, and a diffusional impedance appeared at the surface of each clay platelet then the total effective area would be large.* Nevertheless, the effects of local irregularity and surface roughness, and the extent to which the electrolyte phase enters the open clay structure, are not known. The calculated zone area may thus be the result of a significantly lower percent surface coverage, and the observed distribution may arise from microscopic cracks or inhomogeneity within the clay layer, or from uneven deposition of clay on the glass matrix surface.

This analysis provides an explanation for the high characteristic frequencies observed for Wyoming bentonite and latex cells. These relate

---

* For 7% laponite/20-50 mesh glass spheres, $A_{clay}/A_o \approx 3 \times 10^4$ (assuming a uniform distribution of clay, and an area of 350 $m^2\ g^{-1}$ for laponite.

simply to the small area of latex particles, and the small area of Wyoming bentonite aggregations on ground glass particles. Because of the presence of a parallel capacitance for systems having a high characteristic frequency (i.e. small characteristic membrane zone area), it is not possible to assess the size distribution of Wyoming bentonite aggregations. The analysis presented in sections 8.3 and 8.4 for laponite cells assumes the capacitive impedance contribution to be negligible and a considerably more complex procedure would be required to fit Wyoming bentonite data to a distribution equation.

The twin dispersion observed for Wyoming bentonite cells may also be explained in terms of the characteristic membrane zone area. Cells displaying two characteristic frequencies may be considered to contain both glass particles having surface clay aggregations of small area (ω_o high), and glass particles effectively uniformly covered with a layer of clay (ω_o low).

The discrepancy between σ for Wyoming bentonite cells 1 and 2, observed in section 8.2.2.1, may be explained in terms of a small change in the characteristic area of clay aggregations on the glass particle surfaces.

9.2.6 C

By using the characteristic area derived from σ, the capacitance per unit area (C') can be calculated from the measured values of C (Table 9.5).

It is clear that the capacitance is associated with the presence of a space charge but the precise region in which C is determined, is not known. If C arises simply as a consequence of the surface concentration of fixed charge, then the D.C. potential drop across the capacitor (V_c) can be calculated from the surface charge density (Q/A) and C'.

$$V_c = (Q/A)(1/C') \qquad [9]$$

For Wyoming bentonite Q/A may be calculated from the individual clay particle surface charge density, assuming the charge on the surface of clay aggregations to be due only to the outside layer of clay particles. The cation exchange capacity is 77 meq/100 g and the surface area is

700 $m^2\ g^{-1}$ (Table 5.1). Thus,

$$\text{Equivalents/unit area} = 1.10\times10^{-10}\ cm^{-2}$$

$$Q/A = 1.10\times10^{-10} \times \text{Faraday} = 1.06\times10^{-5}\ C\ cm^{-2}$$

Ottewill (159) has determined the number of surface carboxyl groups per unit area, for polystyrene latex particles as a function of particle diameter up to 423 nm. These values may be extrapolated to 1250 nm to give a value of $Q/A \approx 3.2\times10^{-5}$ C cm^{-2}, assuming all surface groups to be ionised.

Table 9.5 Double Layer Capacitance (0.01 M $CaCl_2$)

	C' ($F\ cm^{-2}$)	Q/A ($C\ cm^{-2}$)	$-\zeta$ (mV)	$-V_c$ (mV)
Wyoming bentonite Cell B	6.6×10^{-4}	1.06×10^{-5}	33	16.1
Wyoming bentonite Cell 3	7.8×10^{-4}	1.06×10^{-5}	33	13.6
Latex	8.3×10^{-3}	3.2×10^{-5}	18*	3.9

* Determined in 0.01 M $BaCl_2$ (111).

V_c is thus significantly less than ζ, indicating that the region in which C is determined incorporates little or none of the diffuse double layer, outside the plane of shear. This is consistent with the observation made in section 8.2.2.3, that the temperature dependence of C is different from that expected for a diffuse double layer capacitance.

CHAPTER 10 CONCLUSIONS

10.1 AN ELECTROCHEMICAL MODEL FOR INDUCED POLARISATION

10.1.1 Introduction

The experiments reported in this thesis have been devised and the results examined, in order to develop an electrochemical model for the membrane polarisation effect observed to be associated with clay/rock/electrolyte systems. The steps in the development of such a model may be summarised as follows.

1) Model systems including packed beds of ion exchange resin, clay/glass matrices and polystyrene latices, perfused with electrolyte, have been constructed to simulate the expected distribution of clay in an electrolyte-filled rock pore.

2) A precise low frequency impedance measuring system has been developed to measure accurately the impedance dispersion of such model systems between 10^{-1} and 10^{4} Hz.

3) From the form of the impedance spectra observed for all systems which display a measurable dispersion, a general electrical equivalent circuit (Figure 9.1) has been proposed.

4) In order to test and evaluate the parameters of this equivalent circuit a reduced impedance formalism has been developed and utilised extensively.

5) In addition to the characteristic ($\omega^{-\frac{1}{2}}$) form of the measured frequency dependence, observations of the dependence of equivalent circuit parameters on such physical variables as electrolyte type and concentration, temperature and particle size, suggest that the electrochemical origin of the impedance dispersion is associated with a shunted Warburg diffusional impedance.

6) By considering the measured cell impedance to arise from an assemblage of microscopic membrane zone impedances (which may or may not display a distribution of characteristic frequency), it has been demonstrated that Z_w is associated with individual membrane (resin, clay or latex)/electrolyte interfaces.

The form of the equivalent circuit developed is similar to that proposed by Cole et al. for biological membranes (see section 3.3.1), and by Buck and Brand et al. for ion selective glass and liquid exchanger electrodes (section 3.3.2). For biological membranes the reactive component has not as yet been associated with a diffusional impedance, and for ion selective electrodes no attempt has been made theoretically to justify the assignment of a Warburg impedance.*

The electrochemical origin of R_p remains to be explained. For a metallic electrode/electrolyte interface, the diffusional impedance which appears at low frequency is not shunted (6 to 10, 67, 68, 85). This is characterised on the impedance locus as a straight line of slope 45 , compared with the semicircular form observed for membrane systems due to the presence of R_p.

The origin of a shunted Warburg diffusional impedance at a membrane/electrolyte interface is most easily approached by comparing the steady state transport properties of such a system with those at a metallic electrode/electrolyte interface.

10.1.2 The Steady State Transport Properties of a Membrane/Electrolyte Interface

A Warburg diffusional impedance is historically associated with an electrode for which the reaction by which current crosses the interface is limited by diffusion of reactant to, or product away from, the electrode surface. The derivation of the impedance term associated with such an interface has been known for more than 70 years and has been comprehensively reviewed (85, 163, 201). However, substantial differences exist between packed bed membrane systems, and electrodes, and the Warburg derivation must be re-examined with regard to these dissimilarities (see section 10.1.4).

In this section the similarity between membrane and electrode systems will be demonstrated by considering D.C. conduction across a plane metallic electrode/electrolyte interface, and across a membrane

---

* The experimental evidence is simply the observed frequency dependence of the electrode impedance.

phase/electrolyte interface, perpendicular to the applied field gradient.

All membranes used in this work are cation selective* and thus anions are excluded from the membrane phase. Thus, while conduction in the electrolyte phase may involve both cations and anions, within the membrane phase the cation transport number is effectively unity. Depending upon the cell geometry, and on the membrane phase conductivity, a concentration deficit or excess will appear in the steady state on the electrolyte side of the interface.

This situation is analogous to an electrode reaction which involves only cations. Depending upon whether cations are depleted (e.g. the deposition of Ag^+) or generated at the electrode, a concentration deficit or excess will arise at the interface.

The transport properties for these two cases are shown in Figure 10.1. From Figure 10.1.1, deposition of cations at the electrode causes a concentration gradient. In order to maintain electroneutrality the concentration gradient for both ions must be identical, and is normally assumed to be linear (201). Diffusion occurs as a consequence of the gradient $\Delta C = C-C_0$, bringing cations to the surface where they react electrochemically (deposit). With the same concentration gradient anions also diffuse to the surface. However, since these ions are not deposited, the net anionic flux must be zero, and in the steady state the virtual fluxes due to anionic diffusion and migration, are equal and opposite. The total current flow (I) may be represented as follows.

$$I = \Sigma Z_i F|J_i|,$$

and provided there are only two species present

$$I = F[Z_+(J_+^{mig.} + J_+^{diff.}) + Z_-(J_-^{mig.} + J_-^{diff.})]$$

where $J_\pm^{mig.}$ = virtual flux due to cation/anion migration with the applied field.

$J_\pm^{diff.}$ = virtual flux due to cation/anion diffusion with the concentration gradient.

---

* Ion exchange resin AG50W-X12, Wyoming bentonite, laponite and latex, all are cation exchange materials having a fixed concentration of anionic sites.

FIGURE 10.1 Steady State Transport Properties

10.1.1 Electrode / Electrolyte Interface

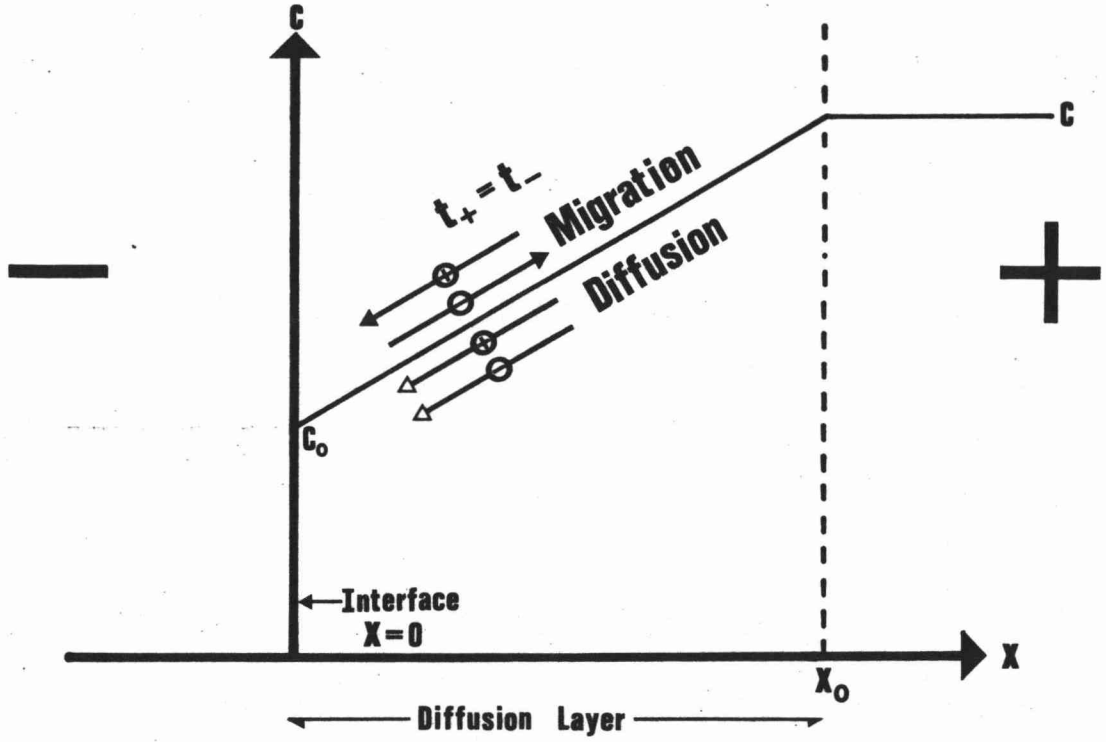

10.1.2 Membrane/Electrolyte Interface

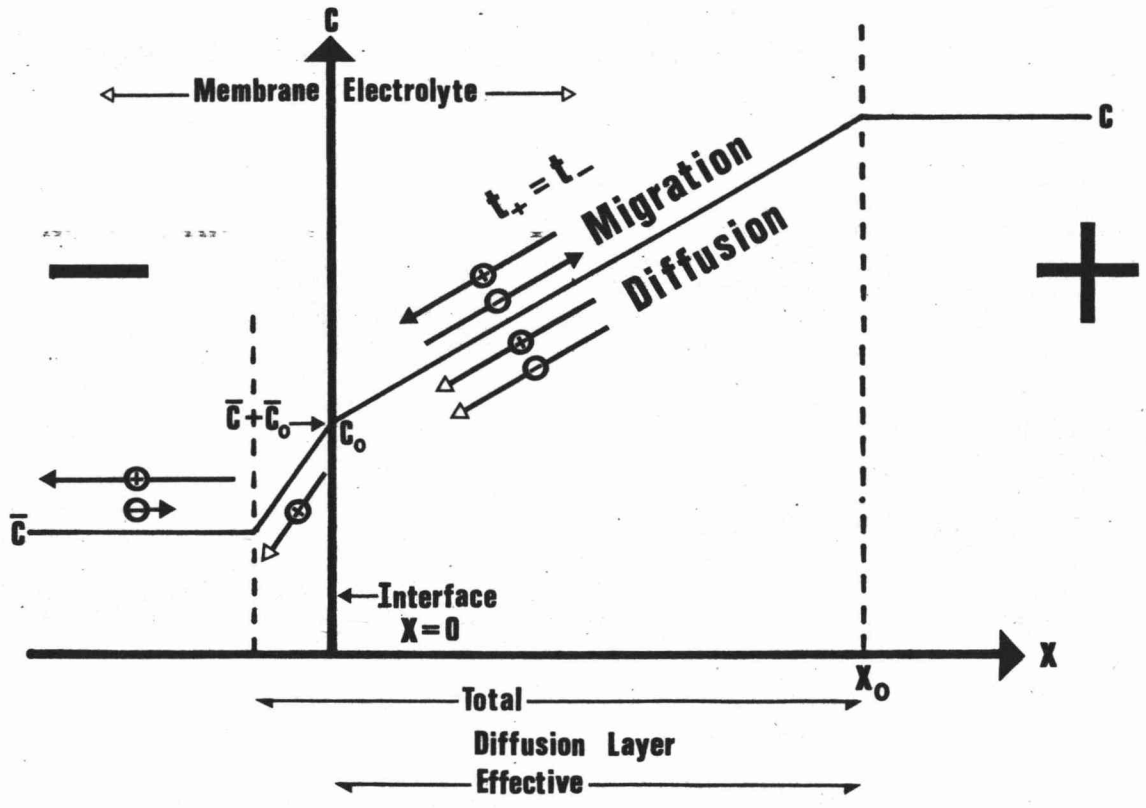

In the steady state $J_-^{mig.} + J_-^{diff.} = 0$, but cation migration contributes to the total current since $J_+^{mig.}$ and $J_+^{diff.}$ have the same sign. Migration is an ohmic process (168) and this effect may be represented as a shunt to the diffusional impedance. In the presence of a large excess of an electrolyte not involved in the electrode reaction* the migration effect is reduced since the transport number of the reacting component becomes very small.

Within the metallic electrode phase current is carried by electrons which have an effectively infinite mobility.

The analogous membrane/electrolyte situation is slightly more complex. If (as in Figure 10.1.2) the conductivity of the membrane phase is much greater than that of the electrolyte, then a concentration deficit will arise on the electrolyte side of the interface. The diffusion and migration processes within the electrolyte will be the same as those described above for a metallic electrode/electrolyte system. Both cations and anions will diffuse to the interface with the concentration gradient. Only cations may cross this interface and in the steady state the reverse migration flux of anions will balance forward anionic diffusion. As for a metallic electrode (in the absence of a supporting electrolyte), the increased cation flux to the interface will increase the total current, and this may be represented as an ohmic shunt resistance.

For membranes, unlike the metallic electrode case, the current carriers within the solid phase are cations, and have a finite mobility. Therefore, because of the flux of cations across the interface, a concentration gradient may arise also in the membrane phase. However, diffusional transport of cations within this phase can only arise if there is a concentration of mobile co-ions, since the electric field due to a concentration excess of cations will produce a migration flux many orders of magnitude larger than the expected diffusional term.

Figure 10.2 shows the equivalent circuits for electrode and membrane impedance. Since the diffusional term within the membrane phase is negligible, then in Figure 10.2.2, $Z_{w,2} \approx 0$.

---

* Often called a "supporting" electrolyte.

Figure 10.2 Equivalent Circuits

10.2.1 Electrode Impedance 10.2.2 Membrane Impedance

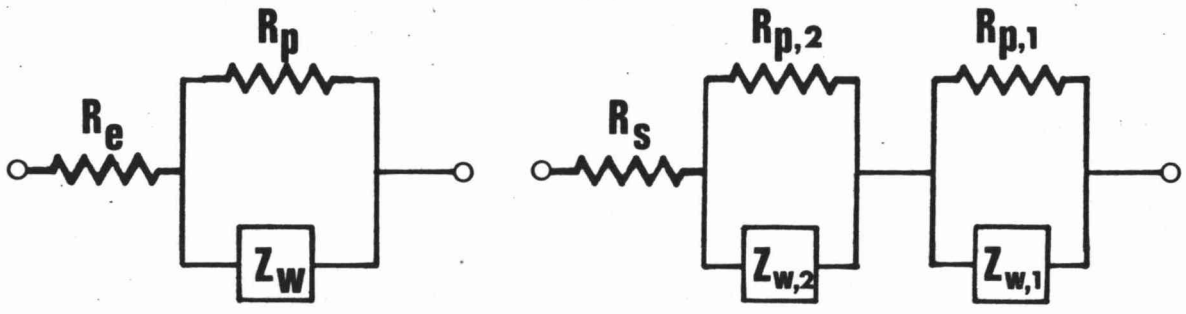

With the inclusion of a parallel capacitance (which does not contribute to the D.C. conductivity), Figure 10.2.2 has a form equivalent to that deduced for resin, clay and latex systems from experimental evidence in the previous chapters.

10.1.3 R_p

From the preceding steady state analysis, the calculated parallel resistance (R_p) for resin, clay and latex cells may be associated with a cation migration resistance within the electrolyte diffusion layer adjoining the membrane/electrolyte interface.

It is important to note that a migration term is necessarily associated with Z_w, if anions are excluded from the membrane phase and electroneutrality is maintained. These considerations ignore the presence of the electrical double layer formed by exchangeable cations, which also appears at the membrane/electrolyte interface. Since this double layer represents a significant modification to the nature of the electrolyte adjacent to the interface, its influence on R_p must be considered. However, since the microscopic field gradient across the interfacial layer cannot be measured, the conductivity associated with R_p and thus the effective thickness of the region in which it operates, cannot be assessed. Thus the extent to which double layer cations and

cations in the bulk electrolyte contribute to R_p cannot be determined directly. Some information is available from the measured concentration and temperature dependence for resin clay and latex cells.

Concentration

If the cation selectivity of the membrane phase is not complete ($\bar{t}_- \neq 0$)*, then the net anion migration and diffusion flux within the electrolyte will not be zero, and migration of anions will contribute to R_p. Since anion exclusion is dependent upon the fixed site concentration within the membrane phase being much greater than the external electrolyte concentration (99, 201), if C is large then there will be an anionic contribution to R_p.

This effect is observed for resin cells (section 7.4), for which an electrolyte (i.e. anion) contribution to R_p becomes significant at concentrations greater than about 0.1 M. Comprehensive data at high electrolyte concentrations is not available for clay or latex cells.

At lower concentrations R_p is observed to display the following (cation) concentration dependence.

Resin and Wyoming bentonite cells, $R_p \propto C^{-3/4}$.
Laponite cells 7 and 8, $R_p \propto C^{-1}$

For $C \lesssim 0.1$ M, a C^{-1} dependence is expected for cation migration within an electrolyte (168). Because the double layer contains a fixed number of cations, the resistance within this layer will display a reduced concentration dependence, being influenced only by the effective double layer compression at high electrolyte concentrations (192). Thus for laponite cells, the contribution of double layer cations is negligible, but for resin and Wyoming bentonite cells, a $C^{-3/4}$ dependence may be considered to reflect the migration of cations within the diffuse double layer.

---

* $\bar{t}_-$ is the anion transport number. The bar denotes the membrane phase.

Temperature

As expected for ionic migration, for all systems examined, R_p displays an Arrhenius temperature dependence over the narrow temperature range examined. The activation energies for conduction measured vary from slightly above the electrolyte value*, for laponite cell 7, to almost double, for resin cells (see Table 9.1). This increase is consistent with a mechanism for R_p involving both double layer and bulk electrolyte cations. The highly structured double layer known to be associated with clay surfaces (192) may be expected to occur also at a resin/electrolyte interface, and to increase E_A for those systems in which the migration of double layer cations contributes significantly to R_p.

10.1.4 R_s

In both the theoretically and experimentally determined equivalent circuits, R_s is associated with an ohmic conduction process within the membrane phase. In section 10.1.2 conduction is considered to be due to the migration of cations which cross the interface from the electrolyte phase. The concentration and temperature dependence of membrane phase conductance may be assessed from experimental results, as follows.

Concentration

For all systems examined in the present study, R_s displays a well characterised $C^{-\frac{1}{2}}$ dependence (Table 9.1). A similar dependence has been observed previously by this author (137) and by Schufle** (179) for packed beds of ion exchange resin spheres/NaCl, $NaNO_3$, $Ca(NO_3)_2$, $La(NO_3)_3$ and $Th(NO_3)_4$. The concentration dependence of R_s is thus similar for a range of electrolytes as well as for both resin and clay systems, and a general relationship of possible consequence in fields other than geophysics may be proposed.

---

* Determined for Na^+ and Ca^+ ions from data in Robinson and Stokes (168).

** R_s represents the limiting high frequency resistance, thus the resistance measured at frequencies $\gtrsim$ 1 k Hz (or short times), may be associated with R_s.

By extending the equivalent circuit for a single membrane zone to a three dimensional network, it is possible to calculate the resistance of individual particles. This provides a means by which the transport properties of the membrane phase may be calculated from the measured impedance of packed beds perfused with electrolyte (see section 9.2.5). These properties have been the subject of recent debate (90, 97, 122, 138) but the concentration dependence of R_s is of no geophysical significance, and will not be discussed further.

Temperature

For all systems measured, R_s displays the Arrhenius temperature dependence expected for ionic migration. From Table 9.1 the activation energy for conduction may be seen to vary from 14.7 kJ $mole^{-1}$ for Wyoming bentonite to 21 kJ $mole^{-1}$ for laponite cell 7. The value for AG50W-X12 resin (E_A = 20.5 kJ $mole^{-1}$) supports the hypothesis of Spiegler et al. (185a) that conduction in ion exchange resins occurs in part by a site-to-site translation mechanism. The increased activation energy compared with the electrolyte value is attributed to the cation-site interaction energy.

While exchange sites are not considered to occur within the open framework clay membrane phase, cations within this phase will be predominantly in the diffuse double layer of individual platelets. Thus E_A may be increased by a similar mechanism of downfield migration from platelet to platelet.

10.1.5 Z_w

Unlike migration resistance, the diffusional impedance is frequency dependent, and cannot be treated using a steady state D.C. analysis. However, the form of the experimentally determined equivalent circuit allows R_s and R_p to be removed explicitly, and Z_w may be treated mathematically in the absence of migration. This is analogous to the case of a metallic electrode/electrolyte interface, in the presence of a supporting electrolyte, for which the theoretical treatment is well known (85, 169, 205a). The following is based on

recent treatments by Vetter (201) and Clarkson (41), and is an attempt to relate these derivations to the case of diffusional limitation at a membrane/electrolyte interface.

Consider an interface of the form shown in Figure 10.1.2. Because of a high cation mobility within the membrane phase, upon application of an electric field with the polarity shown, a concentration gradient forms which drives cations (and anions) to the interface. Since anions are excluded from the membrane phase one need consider only the diffusion of cations.

Let the current density arising from the applied field gradient be

$$i = I \sin \omega t \qquad [1]$$

Following a variation in i, a steady state concentration gradient will be reached asymptotically with time. Therefore, a time dependent current density (e.g. [1]), will lead to a concentration gradient which also varies with time but which lags behind the applied field. Fick's second law must be used in order to obtain an expression for the resultant concentration wave in the electrolyte, as a function of distance from the interface (x) and time (t).

$$\frac{dC}{dt} = D \frac{\partial^2 C}{\partial^2 x} \qquad [2]$$

The solution of [2] considering [1] and the boundary condition [3] which is a form of Fick's first law for x=0,

$$\frac{\partial C}{\partial x}\Big|_{x=0} = - \frac{I \sin \omega t}{n F D} \qquad [3]$$

is,

$$C(x,t) = C + B \sin(\omega t - x/x_0 + \beta) \exp(-x/x_0) \qquad [4]$$

where C = mean concentration*

D = diffusion coefficient

---

* In the absence of an electrical double layer, mean concentration = bulk electrolyte concentration = C (see Figure 10.1).

n = cation valence

B, x_0 and β are coefficients to be determined.

[4] is the equation of a damped concentration wave with phase shift β at the interface (x=0). This is strictly applicable to both the electrolyte and membrane phases, but from the considerations in section 10.1.3, the contribution to the impedance due to diffusion within the membrane may be assumed to be zero.

x_0 can be determined by partially differentiating [4] and substituting into [2]. The result is,

$$x_0 = (2D/\omega)^{\frac{1}{2}} = \lambda/2\pi \qquad [5]$$

and x_0 represents the thickness of the diffusion layer, or the distance into the electrolyte at which the amplitude of the concentration wave is reduced to 1/e of its value at x=0. λ is the wavelength.

The subsequent derivation requires that the electrolyte within x_0 be stationary, and that the concentration gradient be reduced by diffusion only. However, a certain concentration equilibration will always occur by convection (201), and this effect will increase as x_0 increases. Since $x_0 \propto \omega^{-\frac{1}{2}}$, the effects of convection will increase with decreasing frequency, and for very low frequencies a separate analysis is needed (170). Within a packed bed system convection will be partly suppressed, but it is not possible to predict the minimum frequency for which its effects will be negligible. Measurements at frequencies less than 1 rad s^{-1} ($x_0 \approx 4\times10^{-3}$ cm) have shown that impedance loci depart from a semi-circular form. This may represent the practical lower limit of ω in packed bed systems.

B and β can be determined by evaluating $\partial C/\partial x$ at x=0 from [4], and comparing the coefficients with [3].

$$B = I/nF(\omega D)^{\frac{1}{2}} \text{ and } \beta = -\pi/4.$$

Thus [4] becomes,

$$C(x,t) = \frac{I \sin[\omega t-(\omega/2D)^{\frac{1}{2}}x-\pi/4]\exp[-(\omega/2D)^{\frac{1}{2}}x]}{nF(D\omega)^{\frac{1}{2}}} \qquad [6]$$

[6] describes the concentration of both ions as a function of distance from the interface, arising from an imposed A.C. field.

The potential drop Ψ_d within the diffusion layer due to the concentration gradient $C-C_{0,t}$ is,

$$\Psi_d = (RT/nF)\ln(C_0/C) \qquad [7]$$

In [7] it is assumed that the activity coefficient remains constant throughout the diffusion layer, so it is necessary that

$$|C - C_0| \ll C$$

Substituting [6] into [7] to calculate the potential drop between x_0 and the interface ($x=0$), noting that $\exp(0/x_0)=1$, and making the simplifying assumption that

$$I \ll nFC(\omega D)^{\frac{1}{2}},^*$$

$$\Psi_d = \frac{IRT\sin(\omega t-\pi/4)}{n^2F^2C(D\omega)^{\frac{1}{2}}} \qquad [8]$$

The magnitude of the diffusion layer impedance is given by,

$$|\Psi_d| / I.A = |Z_w| \qquad [9]$$

where A is the area of the zone in which the concentration gradient occurs.

Thus,

$$|Z_w| = \frac{RT}{n^2F^2A}\ \frac{1}{C(\omega D)^{\frac{1}{2}}} \qquad [10]$$

---

* In the present work the minimum value of $C \approx 10^{-6}$ mole cm^{-3}, and $\omega \approx 1$ rad s^{-1}. Thus,

$$nFC(\omega D)^{\frac{1}{2}} > (1)(96500)(10^{-6})(1\times10^{-5})^{\frac{1}{2}}$$
$$> 3\times10^{4}\ A\ cm^{-2}$$

Since the total current density for cells was kept below 2×10^{-6} A cm^{-2}, the assumption is justified.

From [8], the current lags the potential drop by $\pi/4 = 45°$, thus the real and imaginary components of Z_w have equal magnitude and opposite sign,

$$R_w = - X_w \qquad [11]$$

Thus,

$$Z_w = \frac{RT}{2^{\frac{1}{2}} n^2 F^2 A} \frac{1}{CD^{\frac{1}{2}}} (1-j)\omega^{-\frac{1}{2}} \qquad [12]$$

$$= \sigma(1-j)\omega^{-\frac{1}{2}} \qquad [13]$$

The form of equation [12] has been experimentally tested for resin, Wyoming bentonite, laponite and latex cells, and in all cases has been found to hold, for $\omega > 1$ rad s^{-1}, within the limits of experimental error. For all systems the frequency, concentration and temperature dependence predicted by equation [12] have been observed to be well obeyed.

The relative simplicity of the equivalent circuit determined experimentally, and the conformity of impedance observations with the form of equation [12], is a substantial justification for the assumption implicit in the above derivation - that migration and diffusion may be treated separately. These are not separate processes but different aspects of the same phenomenon. However, MacDonald (119,120) and others (16,74) have mathematically treated the case of a single-ion blocking electrode/electrolyte interface in the absence of a supporting electrolyte. These authors attempt to solve simultaneously for the diffusion, migration and double layer capacitive terms, but the equivalent circuits presented by MacDonald are much more complex than are necessary to characterise the present phenomenon.

10.1.6 Diffusion Layer Thickness

In the preceeding analysis, Z_w is considered to be determined in a region within the electrolyte, termed the diffusion layer and having a characteristic thickness x_0. From equation [5], $x_0 \propto \omega^{-\frac{1}{2}}$, and an estimation of the thickness of the diffusion layer for a particular

cell may be made from the measured characteristic frequency. As stated in section 8.1.1, the systems examined fall into two categories of dispersion.

1) Resin and laponite cells, $\omega_0 < 20$ rad s^{-1}, thus $x_0 > 1x10^{-3}$ cm.

2) Wyoming bentonite and latex cells, $\omega_0 > 10^4$ rad s^{-1}, thus $x_0 < 4x10^{-5}$ cm.

Thus for resins and laponite cells, the diffusion layer is of macroscopic extent, but for Wyoming bentonite and latex cells, x_0 is of the order of the double layer thickness. A double layer arises because of the fixed negative charge density on the surface of latex particles and Wyoming bentonite platelets (192, 193), and the extent of the diffuse layer may be estimated from the measured zeta potential (Table 5.1) to be of the order of 10^{-6} to 10^{-5} cm (64).

10.1.7 C

For systems in which the characteristic membrane area is small, and thus the characteristic frequency high ($A \propto 1/\sigma$, $\omega_0 \propto \sigma^2$), a parallel capacitive term must be included in the equivalent circuit (see section 8.2.1). This is observed only for latex and for Wyoming bentonite cells, and the properties of the measured capacitance have been discussed in section 9.2.6.

In the electrochemical model of the resin, clay or latex/electrolyte interface, used to describe R_p, R_s and Z_w, this interface is considered to have both membrane and surface double layer properties. For Wyoming bentonite aggregations and latex particles the diffuse double layer and the diffusion layer in which Z_w is determined, have a similar extent.

Figure 10.3 shows the distribution of charge, ion concentration and potential gradient for an electrical double layer, and for a membrane/electrolyte interface. Clearly both these systems involve a space charge, and thus either may contribute to the observed capacitance.

The origin and structure of the double layer at a charged solid/electrolyte interface is well known and expressions for the double layer capacitance are well established (see for example - 50).

FIGURE 10.3 Structure of the Interfacial Layer

10.3.1 Double Layer

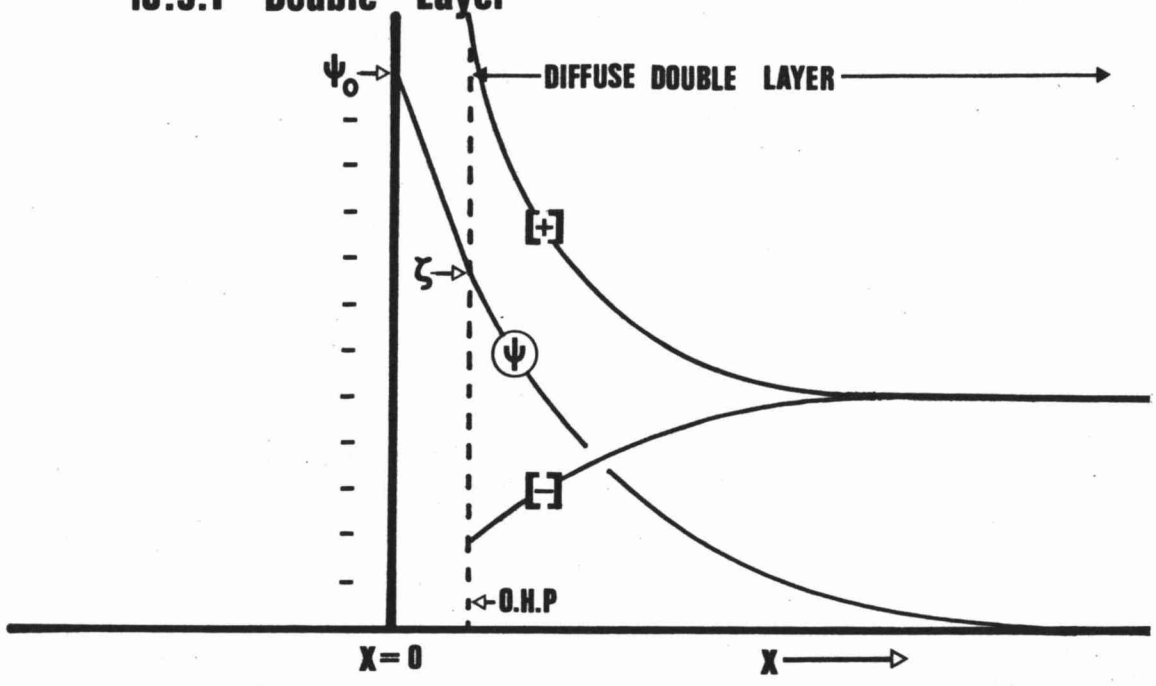

10.3.2 Membrane/Electrolyte Interface

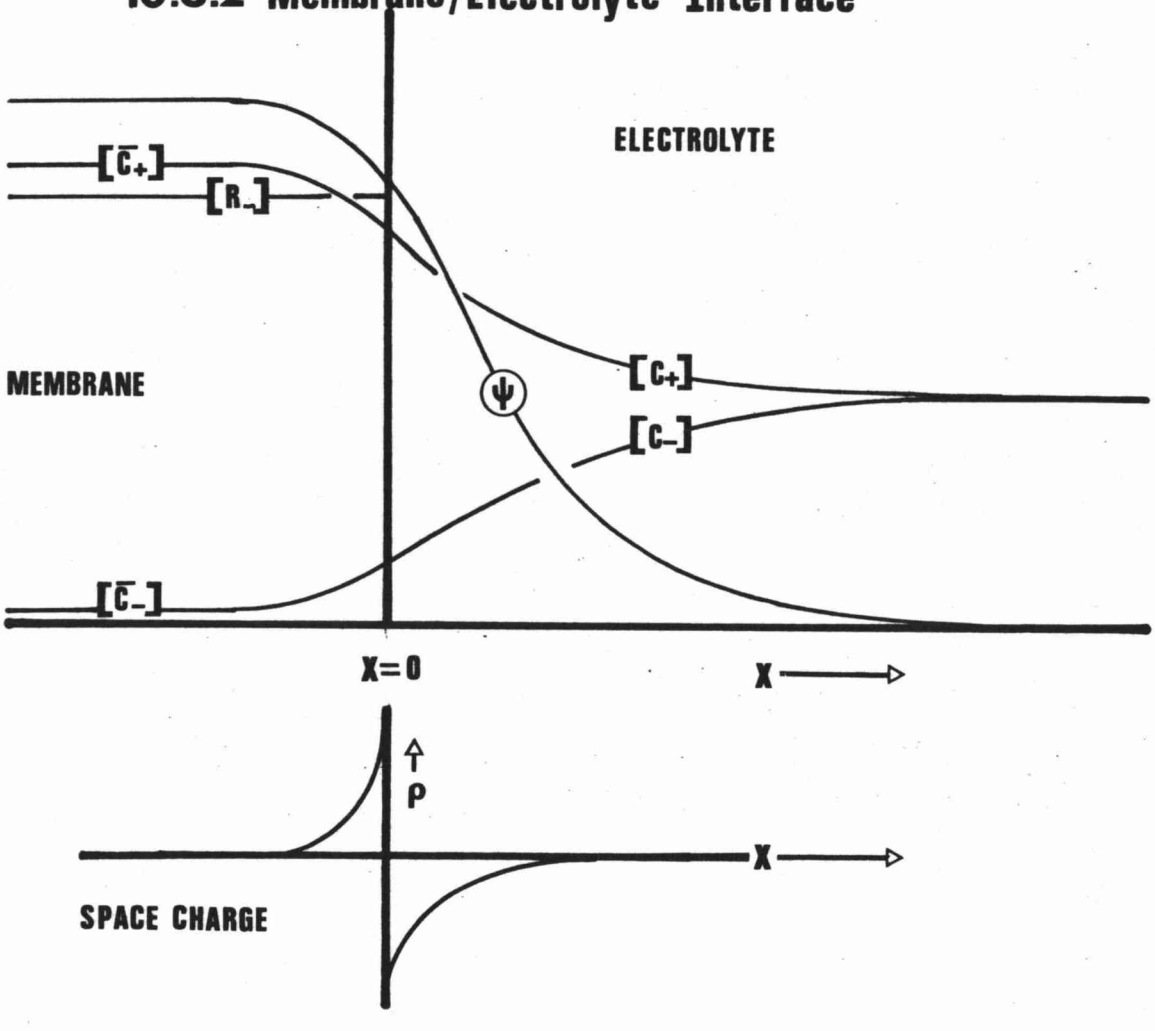

However, the observed properties of C for Wyoming bentonite and latex systems, are not consistent with this term arising within the diffuse double layer (see section 9.2.6).

Figure 10.3.2 shows the expected ion distribution and potential gradient arising from a Donnan equilibrium at a membrane/electrolyte interface. The theory of Teorell-Meyer-Sievers is well known (99, 132, 201) and will not be restated. A high concentration of fixed charge within the membrane phase results in a Donnan potential (Ψ_m), and the ion distribution shown in Figure 10.3.2. A space charge region appears in both phases, and it is important to note that these occur simply because there is a gradient of fixed charge. Mauro (132) has demonstrated that when the potential gradient accompanying such a junction is perturbed by a small applied field, the expanding and contracting of the space charge behaves as <u>though</u> it were a geometric capacitance. He derives an expression for the capacitance at a junction between membranes containing fixed positive and negative charges, but maintains that a single membrane/electrolyte interface should not display a capacitance, because there is no potential gradient at the interface. However, we have found an impedance, and thus potential gradient, clearly attributable to the membrane/electrolyte interface, and thus a membrane capacitance term is to be expected.

The establishment of a Donnan equilibrium, and thus effective separation of charge, requires only the presence of a discrete phase containing fixed charge. For clay aggregations this condition is fulfilled due to fixed charge on the clay platelet surfaces. For latex the measurements of R_s in this study, as well as the surface conductivity measurements of Wright and James (210), suggest that polystyrene latices have a discrete surface phase containing charged carboxyl groupings (see section 9.2.2).

Both Wyoming bentonite and polystyrene latex cells might be expected to display membrane and double layer capacitances. However, without further experimental evidence it is not possible to distinguish between these models, or estimate their respective contributions to the measured capacitance. Experiments by which this may be accomplished are discussed briefly in section 10.4.5.

10.2 COMPARISON WITH PREVIOUS MODELS

10.2.1 Membrane Polarisation

From the results in this work the Membrane Polarisation Effect may be seen to be well named. For four model clay/rock/electrolyte systems,

1) Ion exchange resins,
2) Natural clay (Wyoming bentonite),
3) Synthetic clay (laponite),
4) Polystyrene latices,

the measured impedance dispersion has been found to be associated with the following properties of a cation selective membrane/electrolyte system.

A) Diffusion of cations within the electrolyte → Z_w
B) Migration of cations within the electrolyte → R_p
C) Migration of cations within the double layer → R_p
D) Migration of cations within the membrane → R_s
E) The fluctuation of space charge arising from Donnan equilibria → C
F) The fluctuation of space charge within the electrical double layer → C.

Polarisation is expected, from the present model, when current is passed across a membrane/electrolyte interface in systems containing membrane zones of appreciable conductivity, in equilibrium with an electrolyte phase. Such a membrane zone need constitute only a discrete phase having a fixed concentration of ion sites, with mobile counter ions. These conditions apply not only to the systems,examined in this work, but to glass and liquid ion exchanger ion selective electrodes, which are observed to display a similar but less well characterised impedance dispersion (see section 3.3). Glass electrodes are considered (37) to be composed of a concentration of fixed anion sites (typically $\equiv SiO^-$), with mobile cations (e.g. Li^+, Na^+ or K^+). Liquid ion exchange systems contain a concentration of dissociated acid or base, dissolved in a phase poorly miscible with water. If one of the charged species (say R^- from a dissociated acid, $RH \rightleftharpoons R^- + H^+$) is unable to leave the supporting phase when this is brought into contact with an

electrolyte, then the conditions of the Teorell-Meyer-Sievers theory are met (172). Thus, both glass and liquid ion exchanger electrodes will establish a membrane/electrolyte interface when placed in an electrolyte, and the impedance of such systems may be expected to conform to the electrochemical model proposed in the present work.

It is probable also, that the biological membranes discussed in section 3.3.1 fulfill the requirements of a membrane necessary to produce membrane polarisation. Thus, although it has not been established in the literature, the polarisation observed for such materials probably arises from diffusional limitation at the membrane/electrolyte interface.

10.2.2 Dielectric Polarisation

The observed form of reduced impedance plots for all systems examined in the present work, is inconsistent with dielectric polarisation. In addition, the $\omega^{-\frac{1}{2}}$ dependence observed for Z" cannot arise from a dielectric system - even considering a distribution of time constants. We may therefore discount the models proposed in section 3.4. However, the process of Non Localised Diffusion* discussed in section 3.4 may be amenable to the type of treatment used here.

10.2.3 Geophysical Models

In section 2.3 the models which have been proposed to account for the Membrane Polarisation Effect of unmineralised material were discussed. Only two were shown not to be inconsistent with the results of previous studies.

1) The elementary clay conductor model (91).
2) The alternating transference zone model (5, 103, 104, 73, 127-131).

The first is significant in that polarisation is considered to be a property of a clay aggregation/electrolyte interface. In the model it is supposed that clay is an "electronic conductor" with a 90° phase

---

* NLD is considered to be associated with the diffusion of cations within a dry silicate membrane (121, 147, 152, 153).

shift of current occurring at the clay/electrolyte interface. No attempt is made to explain the origin of such a phase shift. From the results of the present study, a phase shift at this interface is seen to occur, but its magnitude is determined by σ, R_p and C, and always remains substantially below 90°.

Alternating transference zones are considered to arise by three separate mechanisms.

2a) Partial pore blockage by clay such that the double layer overlaps with that on the opposite wall, restricting the flow of anions. See Figure 2.2.2.

2b) Constriction within the rock pore such that the double layers on opposite walls of the rock itself, overlap. See Figure 2.2.2.

2c) Complete pore blockage by ion selective clays. See Figure 2.2.1.

2a and 2b may be dismissed immediately. Polarisation is observed to be only indirectly associated with the presence of a double layer, and is caused by diffusional limitation of cations as they enter the membrane phase, not as Keller and Fredricksberg suppose, concentration polarisation of anions entering the double layer.

The failure of Marshall and Madden's model (2c) is that polarisation is considered to occur across the length of the selective clay zone, rather than across an interfacial diffusion layer within the electrolyte. From measurements of the impedance dispersion and characteristic frequency of a packed bed of 20-40 mesh cation exchange resin, Marshall and Madden calculate from their model a selective zone length of 3×10^{-6} to 3×10^{-5} cm. They state that this value "does not correlate with any known property of the resin", but 10^{-5} cm is not an unreasonable estimation of the thickness of the diffusion layer (see section 10.1.6).

10.3 GEOPHYSICAL SIGNIFICANCE OF MODEL

10.3.1 Introduction

Since Chapter 2 the discussion in this thesis has strayed somewhat from the geophysical considerations outlined, to more fundamental electrochemical phenomena. It is proposed now to bring the model back to earth and consider the likely polarisation effects of a clay distributed in geological rock pore/electrolyte systems.

10.3.2 The Membrane Polarisation Effect of Clay/Rock/Electrolyte Systems

Under the conditions of partial or complete clay blockage of a rock pore, the resultant membrane/electrolyte interface will polarise in an applied field (see Figure 10.4). In an A.C. field an impedance dispersion will result which may be characterised by the equivalent circuit shown.

The real earth case will differ from that of a packed bed of resin, clay or latex particles, only in the significance of the series resistance. The parallel components R_p, C and Z_w are properties of the membrane/electrolyte interface and will be the same for clay in a packed bed as for clay in a rock pore, provided the cation type and concentration, temperature and interfacial area are the same. This is not so for R_s. In packed bed systems the membrane zones are effectively continuous, and no system has been observed for which electrolyte conduction contributes significantly to R_s. However, for any realistic concentration of clay aggregations in geological systems, the major contribution to the series resistance will arise from conduction processes within the electrolyte between membrane zones. This effect may be represented by including an electrolyte resistance term (R_e) in series with R_s in the equivalent circuit, as shown in Figure 10.4.2.

As for packed bed systems, dispersion for the circuit in Figure 10.4.2 is determined by the parallel combination of R_p, Z_w and C. Since the areas of clay aggregations within a rock pore system are likely to display a considerable distribution, the characteristic frequency of individual zones will also be distributed, and the measured impedance dispersion will be broad. However, it is probable that this impedance dispersion will be amenable to the type of analysis employed in section 9.2.5 for a distribution of characteristic frequencies.

10.3.3 Geophysical Parameters

By employing the equivalent circuit shown in Figure 10.4.2 the single valued geophysical parameters commonly used to describe the I.P. effect in the time and frequency domains may be assessed. These have been defined in section 2.2 and are shown in Figure 2.1.

FIGURE 10.4 Membrane Polarisation in a Clay/Rock/Electrolyte System

10.4.1 Section of Rock Pore

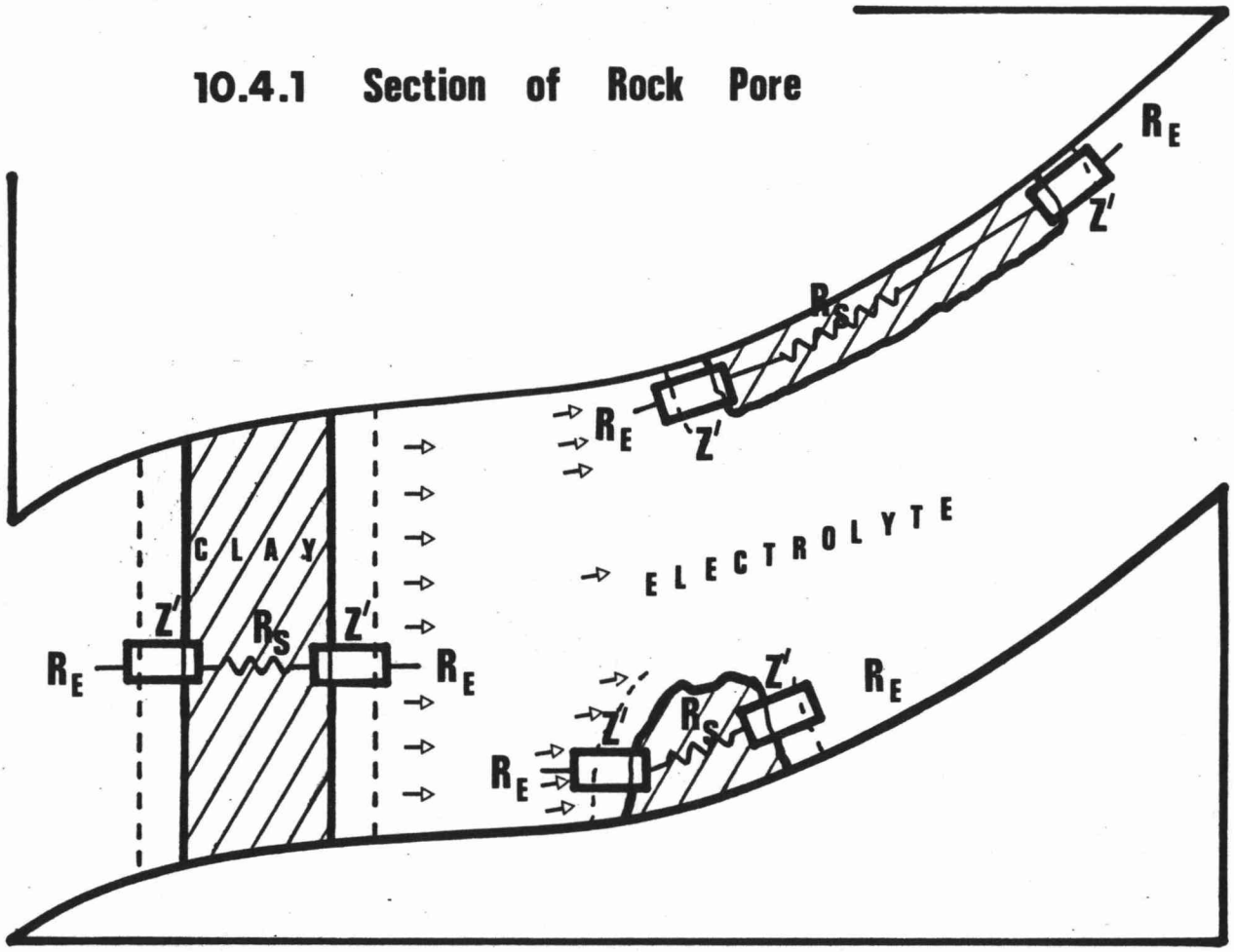

10.4.2 Equivalent Circuit

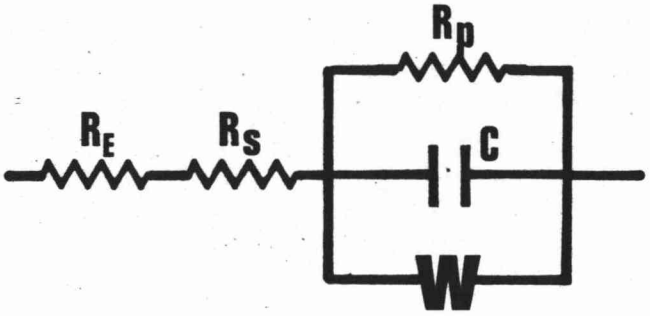

Frequency Domain

From Figure 10.4.2, the limiting high and low frequency resistances are

$$R_{High} = R_s + R_e$$

$$R_{Low} = R_s + R_e + R_p$$

Using the analysis employed in section 9.2.5 to relate the impedance measured between the potential electrodes at the surface (Z) to the individual membrane zone impedance,

$$Z = (n/m)\bar{z} \qquad [14]$$

where n = number of series elements between potential electrodes.

m = number of possible parallel conduction paths

$\bar{z}$ = mean membrane zone impedance.

n/m may be visualised as the equivalent of a "cell constant" for the earth between the potential electrodes of a linear four terminal I.P. survey.*

From [14], the measured impedances are,

$$R_p = (n/m)\bar{r}_p$$

$$R_s = (n/m)\bar{r}_s$$

$$R_e = (n/m)\bar{r}_e$$

$$Z_w = (n/m)\bar{z}_w$$

where $\bar{r}_p$, $\bar{r}_s$, $\bar{r}_e$ and $\bar{z}_w$ represent mean microscopic zone impedances.

Since r_p shunts the reactive component due to the presence of membrane zones, R_p must relate to the amount of cation selective material (i.e. clay) present. More specifically, the measured value of R_p ($= R_{Low} - R_{High}$) relates to the number of membrane/electrolyte interfaces. The frequency effect (F.E.) thus reflects the number of membrane zones, normalised (to

---

* The formalism of an "apparent resistivity" and the geometric factor related to electrode configuration, is well established for I.P. and resistivity surveying (see for example 106).

remove n/m) by the low frequency resistance

$$F.E. = \frac{R_{Low}-R_{High}}{R_{Low}} = \frac{R_p}{R_p+R_e+R_s} = \frac{\bar{r}_p}{\bar{r}_p+\bar{r}_e+\bar{r}_s}$$

If instead of dividing by R_{Low}, R_{High} is used, a simplified form results which, for convenience will be called the zone factor (Z.F.).

$$Z.F. = \frac{R_{Low}-R_{High}}{R_{High}} = \frac{R_p}{R_e+R_s} = \frac{\bar{r}_p}{\bar{r}_e+\bar{r}_s}$$

Except for very high electrolyte concentrations, $\bar{r}_e >> \bar{r}_s$, and

$$Z.F. \approx \bar{r}_p/\bar{r}_e \qquad [15]$$

Thus Z.F. is the resistance ratio of the membrane/electrolyte interfacial layer to the bulk electrolyte.

Since $\bar{r}_p = \rho_1 \ell/a_1$

and $\bar{r}_e = \rho_2 s/a_2$

where ρ_1 = interfacial layer resistivity (Ω cm).

ρ_2 = pore electrolyte resistivity (Ω cm).

a_1 = characteristic membrane/electrolyte interfacial area (cm^2).

a_2 = mean pore cross sectional area (cm^2).

ℓ = characteristic thickness of interfacial layer (cm).

s = mean spacing of membrane zones (cm).

Then,

$$Z.F. = \rho_1 \ell a_2/\rho_2 s a_1.$$

Unfortunately the properties of the interfacial layer are not well understood. ρ_1 strictly applies only to cations, the resistivity being modified from the bulk electrolyte value by the presence of a double layer. Similarly, ℓ cannot be quantified (see section 10.1.5), but from [15], Z.F. $\propto$ 1/s, and thus,

$(Z.F.)^3 \propto$ concentration of membrane zones (= number of zones per cm^3).

From field and laboratory I.P. measurements, $R_{Low}/R_{High} \approx 1$ and thus Z.F. ≈ F.E., and the above analysis is applicable to the frequency effect.

It is stated in section 2.2.3 that the advantage of the metal factor (M.F.) over the frequency effect, is its reduced dependence on the shunt resistance of unblocked pores.

$$M.F. = 2\pi x 10^5 \frac{(R_{Low} - R_{High})}{(R_{Low})(R_{High})} \qquad [16]$$

$$= (Z.F.)R_{Low} = (F.E.)R_{High}$$

$$= m\,\bar{r}_p/n\,(\bar{r}_e)(\bar{r}_e+\bar{r}_p) \qquad [17]$$

[17] assumes $\bar{r}_e >> \bar{r}_s$ but since this equation is not normalised and involves the factor n/m, it cannot easily be further simplified. It is difficult to see what, if any, physical significance the metal factor might have.

For both the metal factor and the frequency effect, if R_{High} or R_{Low} are measured at frequencies for which these have not attained their limiting values, no significance can be placed on the derived parameters. The magnitude of the impedance for an equivalent circuit of the form shown in Figure 10.4.2 is a complex function of applied frequency, and the significance of $|Z|$ measured at arbitrary frequencies is negligible.

In the present study the impedance spectra for clay systems are observed to be broad, and these are likely to be more so for real earth systems, due to a greater distribution of membrane/electrolyte interfacial area. As such, it is probable that R_{Low} should be measured at frequencies not above 0.1 Hz, and R_{High} not below 1 k Hz. Keller (106) states that "field measurements are usually made at two frequencies a decade apart, below 10 Hz" (e.g. 0.1 and 1.0 Hz). Clearly such measurements will have very little significance in characterising the polarisation, and will register less than 25% of the total impedance dispersion.

The results of the present study suggest also that D.C. may not be a suitable low frequency limit. Since the diffusion layer thickness is $\propto 1/\omega^{\frac{1}{2}}$, the effects of convection within this layer become increasingly significant with decreasing frequency (201). We observe the impedance

locus for both resin and laponite cells to depart from a semi-circular form at frequencies below 1 rad s^{-1} ($\approx$ 0.2 Hz), and it is probable that predictions from the model are applicable only above this frequency.

Time Domain

It is not intended to perform the complete transient analysis* on the circuit in Figure 10.4.2 necessary to examine fully the single valued time domain parameters. However, from inspection

$$\text{Primary voltage,} \qquad V_1 = I\,(R_s+R_e+R_p)$$
$$\text{Secondary voltage } (t=t_0), \qquad V_2 = I\,(R_p)$$

where I = total ground current.

Thus,

$$mV/V = 10^3 V_2/V_1 = 10^3 \bar{r}_p(\bar{r}_s+\bar{r}_3+\bar{r}_p)$$
$$= 10^3 (F.E.)$$

and
$$Z.F. = V_2/(V_1-V_2). \qquad [18]$$

The time constant (τ) is a function of the reciprocal of the characteristic frequency (ω_0). Since $\omega_0 \propto 1/A^2$ where A is the characteristic membrane/electrolyte interfacial area, large time constants will be associated with systems containing clay aggregations of large size.

The zone factor (obtained from equation [18]) is related to the concentration of membrane zones and the time constant to the size of these zones, and thus time domain I.P. surveys may be used to obtain information about clay in a rock pore/electrolyte system.

---

* Fourier analysis of comparable equivalent circuits for electrode systems, involving resistive, capacitive and diffusional impedance terms, have resulted in highly complex equations (14, 163) containing exponential and error function terms, which are not easy to handle mathematically, or to visualise.

10.3.4 Prospecting

Some of the practical justification for the present study involves the possible prospecting advantages which may accrue from an understanding of the mechanism of membrane polarisation. These advantages will be discussed in the order in which they were proposed in section 2.5.1.

1) Membrane and Electrode I.P. Effects

We have shown that the membrane polarisation effect in unmineralised material has the same electrochemical origin as that proposed for the I.P. effect of material containing disseminated electron conducting minerals (106, 130). In both cases, polarisation results from a diffusional impedance in the electrode phase adjacent to a pore blocking material, at which a discontinuity of conduction occurs. Therefore, unless the distribution of interfacial area (and thus σ*) for the clay and mineral particles within a geological material are significantly different, even the most precise impedance dispersion measurements will not distinguish between the effects of electrode and membrane polarisation.

2) Prospecting for Ground Water

Clearly, only clay situated in electrolyte filled pores (i.e. below the water table) will contribute to the measured membrane polarisation. Since clay is virtually ubiquitous in rock pore systems, I.P. surveys may readily be used to search for ground water or to establish the level of the water table (197).

3) Prospecting for Clays

Polarisation arises at a clay/electrolyte interface. Thus, provided clay aggregations remain disseminated in a rock pore structure, the polarisation effect (e.g. Z.F.) will increase with increasing clay zone concentration. However, the limiting cases for dissemination have been observed in the present study to display no measurable impedance dispersion.

---

* The derivation of a Warburg impedance for an electrode and a membrane interface yield similar expressions for the impedance, and the significance of σ for the two systems is the same.

These are

a) amorphous plastic clay equilibrated with electrolyte, and

b) clay dispersed in electrolyte.

$$\omega_0 = 2\sigma^2/\bar{r}_p^{\,2}$$

$$\bar{r}_p^{\,2} = A_1^{\,2} \exp(2E_{A,1}/RT)$$

$$\sigma^2 = A_4^{\,2} T \exp(E_{A,\sigma}/RT)$$

where $E_{A,\sigma}$ is the activation energy for the limiting conductivity determined for diffusion layer cations (see section 7.3.5).
Thus,

$$\omega_0 \propto T \exp[(E_{A,\sigma} - 2E_{A,1})/RT]$$

Since $E_{A,\sigma} \lesssim 2E_{A,1}$ (Table 9.1), the characteristic frequency will increase approximately linearly with temperature.

b) Increasing Concentration:

$\sigma \propto C^{-1}$ (equation [12]), and except at very high concentration (168) $\bar{r}_e \propto C^{-1}$. The concentration dependence of $\bar{r}_p$ varies between $C^{-3/4}$ for Wyoming bentonite and C^{-1} for laponite (Table 9.1). Thus Z.F. ($= \bar{r}_p/\bar{r}_e$) will be constant or increase slightly with increasing C, while ω_0 ($= 2\sigma^2/\bar{r}_p^{\,2}$) will be constant or decrease slightly.

c) Increasing Porosity:

Assuming an increased porosity to be due to an increased mean pore cross sectional area, the effect of increasing ϕ will be to increase the number of unblocked pores and thus the mean spacing of membrane zones (s), and Z.F. will decrease (see equation [15]).

However, $\bar{r}_p$ and σ are properties of the membrane/electrolyte interface and not the pore structure, and ω_0 will therefore be uninfluenced by ϕ.

In summary, Table 10.1 shows the expected variation of Z.F. and ω_0 with increasing T, C and ϕ, compared with the trends obtained from clay cell data.

Table 10.1 Variation of Z.F. and ω_0 with T, C and ϕ

	Z.F.			ω_0		
	T	C	ϕ	T	C	ϕ
Predicted	Small increase	Small increase	Decrease	Increase	Small decrease	No change
Laponite 7	No change	Small increase	-	Increase	No change	-
Laponite 8	No change	Small increase	-	Large increase	No change	-
Wyoming bentonite	No change	-	-	Increase	-	-

Thus, in the presence of a high temperature, high porosity, saline water reservoir, Z.F. will be relatively unchanged and may increase or decrease depending upon whether T and C, or ϕ dominate. On the other hand ω_0 will display a marked increase with temperature, and in conjunction with the resistivity may yield useful information in hydrothermal prospecting. However, it would be unwise to extrapolate these conclusions into the regions of temperature and pressure necessary for geothermal power production. The maximum temperature used in this study was 70°C and the effects of pressure have not been examined, and the properties of electrolytes are known to alter markedly at temperatures greater than the atmospheric boiling point (69a).

10.4 SUGGESTIONS FOR FURTHER WORK

10.4.1 Introduction

In Chapter 2 it was stated that experiments were to be conducted in order to determine the electrochemical origin of the Membrane Polarisation Effect, and that experimental results were to be analysed only to elucidate an electrochemical model. As such, a comprehensive mathematical analysis of the data has not been performed, and, as with any exploratory study, this thesis has raised more questions than have been answered. This section

is an attempt to do no more than itemise possible avenues of research. In doing this the application of a low frequency, high precision impedance measuring system to the field of electrodics, and the possible application of the reduced impedance formalism developed, in interpreting electrochemical impedance data, have been ignored.

10.4.2 Geophysical Systems and Clays

1) Before the model can be used to make substantive geophysical predictions, it must be tested by making high precision, wide band impedance measurements in the field. A system by which this may be accomplished has been designed by the author.

2) In order to assess the applicability of induced polarisation surveying to hydrothermal prospecting, laboratory experiments must be conducted in order to determine the pressure and temperature dependence of the impedance dispersion of model clay systems, particularly with regard to the characteristic frequency.

3) From the present study it would appear that of the single valued parameters used to characterise the I.P. effect, those determined in the time domain have substantially more significance than frequency domain parameters. As such, experiments should be performed on simple laboratory model systems in both the time and frequency domains. From a Fourier analysis of the results, the exact relationship between the time constant and characteristic frequency may be determined, and the significance of the polarisability assessed.

10.4.3 Ion Exchange Resins

1) The explanation for the reduced phase angle and broadened dispersion observed for laponite systems is based on the consideration of a distribution of membrane zone area, but this has not been the subject of a separate experimental test. One means by which this may be accomplished is to measure the impedance dispersion of a packed bed containing two widely different resin mesh sizes, uniformly distributed.

2) The transport processes of ions in exchange resins are not well understood. These may involve diffusion (189), and migration in microscopic electrolyte filled pores (15) or by a site-to-site "hopping" mechanism (63, 122, 185a). These processes will be effected by such properties as

a) cross-linkage, which influences the diameter of micropores (21, 189),
b) nature of exchange site, which influences the counter ion-site interaction energy, and
c) resin particle size which will influence the time taken to establish an exchange equilibrium, in non-homoionic systems.

By varying these properties together with electrolyte type, concentration and temperature, and measuring R_s, the mechanisms of ion transport and exchange kinetics may be investigated.

3) In addition, fundamental properties of the Donnan equilibrium and the membrane/electrolyte interface may be obtained from measurements of R_p and Z_w. In this work the activation energies for conduction within the diffusion layer (Z_w) are observed to be large, supporting the contention of Eckfeldt (66) and Soldano (189) that there is a macroscopic "film" of electrolyte at a resin/electrolyte interface, which has an increased activation energy compared with the bulk electrolyte.

10.4.4 Biological Membranes and Ion Selective Electrodes

1) By analysing the impedance dispersion of biological membrane systems, it will be possible to determine whether the observed polarisation is due to diffusional limitation at the membrane/electrolyte interface.

2) From measurements of the concentration and temperature dependence of the impedance of glass and liquid exchanger electrodes, properties similar to those outlined in 10.4.3.2 and 10.4.3.3 may be obtained.

10.4.5 Polystyrene Latices

Of the systems examined in this work, latices show the most promise for future studies. These may be prepared in a wide range of diameters but having a very narrow size distribution (13a, 84, 159), and the particles are highly spherical. Thus impedance measurements on packed beds may readily be subjected to a mathematical analysis, and the properties of individual zones accurately determined. The frequency range in which dispersion is observed ($> 10^4$ Hz) means that more conventional impedance measuring techniques may be used.

The following experiments are thought to be of particular significance.

1) To determine the effect of electrolyte concentration on the measured capacitive shunt to Z_w. From this experiment the contribution to the capacitance from the electrical double layer and from a membrane capacitance, may be assessed.

2) Polystyrene latices have been shown by Wright and James (210) to display anomalous conduction in a surface layer, and this has been associated here with R_s. Thus, measurements of R_s in packed bed latex systems may be used to determine the nature and extent of this layer.

3) By making measurements on systems of different particle diameters, the effect of area on Z_w may be determined directly.

4) The principle laboratory application for polystyrene latices is in experiments relating to interparticle forces. Measurements of R_s, R_p, Z_w and C for latex systems as the interparticles distance is decreased (with pressure - see 13a) could conceivably contribute to an understanding of these forces.

Appendix 4.1 Calibration of R_1

4.1.1 Sullivan Decade Resistance Box No. 671320

The resistance for the dial settings were measured* and are given as follows.

Dial x 1000	Resistance (Ω)	Dial x 100	Resistance (Ω)	Dial x 10	Resistance (Ω)
1	1000.0	1	100.0	1	10.00
2	1999.5	2	200.0	2	20.00
3	2999.0	3	300.0	3	30.00
4	3999.0	4	400.0	4	40.00
5	4999.0	5	500.0	5	50.00
6	5999.0	6	600.0	6	60.00
7	6999.0	7	700.0	7	70.00
8	7999.0	8	800.0	8	80.00
9	8999.0	9	899.9	9	90.00
10	9999.0	10	999.9	10	100.00

Dial x 1	(Ω)	Dial x 0.1	(Ω)	Dial x 0.01	(Ω)
1	1.002	1	0.100	1	0.010
2	2.001	2	0.199	2	0.020
3	3.001	3	0.299	3	0.030
4	4.001	4	0.399	4	0.040
5	5.002	5	0.499	5	0.050
6	6.001	6	0.599	6	0.059
7	7.002	7	0.698	7	0.069
8	8.002	8	0.798	8	0.079
9	9.002	9	0.898	9	0.089
10	10.002	10	0.998	10	0.099

* Department of Scientific and Industrial Research, Physics and Engineering Laboratory, Lower Hutt, New Zealand.

4.1.2 Sullivan Decade Resistance Box No. 3981

For higher resistance settings the reactive error becomes significant. The resistive and reactive percentage errors were measured using a Wayne Kerr B331 Autobalance bridge at 1592 Hz and these were as follows.

Dial x10^5	Resistive Error (%)	Reactive Error (%)	Dial x10^4	Resistive Error (%)	Reactive Error (%)	Dial x10^3	Resistive Error (%)	Reactive Error (%)
1	0.18	0.90	1	0.05	0.07	1	0.03	-0.01
2	0.30	1.56	2	0.06	0.16	2	0.05	-0.01
3	0.35	2.13	3	0.06	0.13	3	0.05	-0.01
4	0.41	2.60	4	0.07	0.22	4	0.04	0.00
5	0.41	2.69	5	0.08	0.23	5	0.04	0.00
6	0.44	3.05	6	0.09	0.27	6	0.05	0.02
7	0.45	3.43	7	0.09	0.31	7	0.05	0.02
			8	0.09	0.35	8	0.05	0.02
			9	0.08	0.39	9	0.04	0.02
			10	0.07	0.43	10	0.05	0.01

Appendix 4.2 Calibration of C

Hewlett Packard model 4440B Decade Capacitance (serial number 936-00433).

4.2.1 Variation with Frequency*

Setting	1 k Hz	10 k Hz	100 k Hz	1 M Hz	
40	40.03	40.03	39.99	40.35	pF
140	140.51	140.44	140.37	142.87	pF
1040	1039.5	1039.6	1040.2	1152.0	pF
10.04	10.030	10.022	10.109	-	nF
100.04	100.01	100.08	-	-	nF
1.00	0.9984	-	-	-	F

* Department of Scientific and Industrial Research, Physics and Engineering Laboratory, Lower Hutt, New Zealand.

4.2.2 Capacitive and Conductive Error at 1592 Hz

Setting	Capacitive Error (%)	Conductive Error (%)
40 pF	-0.64	0.04
100 pF	-0.70	0.02
200 pF	-0.13	0.04
500 pF	-0.01	0.04
1100 pF	-0.08	0.02
5100 pF	-0.04	0.02
10.10 nF	-0.14	0.02
50.10 nF	-0.02	0.02
100.10 nF	-0.01	0.04
500.10 nF	-0.11	0.04
1000.10 nF	-0.11	0.03

Appendix 4.3 Integrated Circuit Specifications

4.3.1 Analog Devices AD 520 K Instrumentation Amplifier.

			Units
Gain	Range	1-1000	V/V
	Linearity	±0.02	%
Output characteristics	Voltage	±10	V
	Current	± 5	mA
	Impedance	2	Ω
Input Impedance	Differential	$2x10^9$	Ω
	Common Mode	$2x10^9$	Ω
Noise 0.1 Hz to 10 Hz,	G = 1000	5	μV
10 Hz to 200 k Hz,	G = 1	1	mV
1 Hz to 5 k Hz,	G = 1000	2	μV
CMRR* D.C. to 100 Hz	G = 1	80	db
	G = 10	100	db
	G = 100	110	db
	G = 1000	110	db
Frequency Response, small signal,	G = 1	200	k Hz
	G = 10	175	k Hz
	G = 100	125	k Hz
	G = 1000	25	k Hz
Slew Rate** (all gain settings)		4.0	V/μs

* The common mode rejection ratio (CMRR) is defined as

Output Voltage/(Input Common Mode Voltage)(Gain)

where a common mode voltage is one applied equally to both inputs. Typical values are given, for a 1 kΩ input imbalance.

** The slew rate is the maximum rate of output voltage change (dV/dt).

4.3.2 National LM 310 D Voltage Follower

			Units
Gain, large signal, D.C. to 1 k Hz,		0.9999	V/V
Output characteristics	Voltage	±10	V
	Impedance	0.75	Ω
Input Impedance		10^{12}	Ω
Noise 10 Hz to 1 M Hz		<1	μV
Frequency Response	small signal	20	M Hz
	large signal	0.2	M Hz
Slew Rate		30	V/μs

Appendix 5.1 Preparation of Electrodes

5.1.1 Platinised Platinum

Platinised platinum electrodes were prepared by the method described by Vogel (202 - p.972) using a plating solution containing 3 g chloroplatinic acid (99 - p.107) and 0.025 g lead acetate in 100 ml double distilled water. The electrodes to be plated were made the cathode in this solution, and the current was not reversed. A plating current density of 100 mA cm^{-2} was passed for 5 to 10 minutes, the resultant coating in all cases being jet black.

5.1.2 Ag/AgCl

Chloridisation of silver wire electrodes was accomplished using the method of Brown and MacInnes (36), described in Ives and Janz (99 - p.206). Pairs of electrodes were prepared in series using a current density of 10 mA cm^{-2} applied for 30 minutes. The chloridising electrolyte was 0.1 M Analar HCl.

HP-65 Program Form

M 26

e Appendix 8.1 Reduced Impedance Summation for Distribution of Characteristic Frequency Page ____ of ____

SWITCH TO W/PRGM. PRESS [f] [PRGM] TO CLEAR MEMORY.

KEY ENTRY	CODE SHOWN	COMMENTS
	00 00	ENTER $\omega/\bar{\omega}_o$
L	23	
	11	INITIATE
D 1	33 01	
L 8	34 08	γ_o
S	42	
D	33 02	ω_k
	00	
D 4	33 04	
D 5	33 05	
D 6	33 06	
D	22	
	12	
N	24	
L	23	
	12	COMMENCE SUMMATION
L 8	34 08	
	04	
	81	
L 2	34 02	
	71	
S	42	
I	32	
G	08	
L 1	34 01	
x≷y	35 07	
	81	
O 3	33 03	γ
	02	
	71	
	31	
	09	
	01	
	61	
L 3	34 03	
	61	
L 3	34 03	
	02	
	81	
	31	
	09	
	81	
	35	
x	04	
L 4	34 04	
	61	
O 4	33 04	ΣR
L 3	34 03	
	02	
	71	

KEY ENTRY	CODE SHOWN	COMMENTS
f	31	
$x^{\frac{1}{2}}$	09	
1	01	
+	61	
RCL 3	34 03	
+	61	
STO 3	34 03	Re-set
2	02	
÷	81	
60 $f_{\frac{1}{2}}$	31	
$x^{\frac{1}{2}}$	09	
1	01	
+	61	
÷	81	
g	35	
1/x	04	
RCL 5	34 05	
+	61	
STO 5	33 05	$\Sigma(-X)$
RCL 8	34 08	
RCL 7	34 07	
÷	81	
RCL 2	34 02	
+	61	
STO 2	33 02	Re-set ω_k
RCL 6	34 06	
1	01	
+	61	
STO 6	33 06	Cycles Completed
RCL 8	34 08	Summations Requires
RCL 2	34 02	
g x≠y	35 22	Summation Complete?
GTO	22	No!
B	12	Re-cycle
RCL 5	34 05	Yes!
RCL 6	34 06	Terminate
÷	81	
R/S	84	Display $\Sigma R/R_p$
RCL 4	34 04	
RCL 6	34 06	
÷	81	
RTN	24	Display $\Sigma -X/R_p$
LBL	23	
E	15	
g x=y	07	
RTN	24	
100		

REGISTERS

- R_1 $\omega/\bar{\omega}_o$
- R_2 ω_k
- R_3 γ
- R_4 ΣR
- R_5 $\Sigma -X$
- R_6 Cycles completed
- R_7 n = summations required
- R_8 γ_o
- R_9 USED

LABELS

A INITIATE
B Compute
C –
D –
E g x≷y
0 –
1 –
2 –
3 –
4 –
5 –
6 –
7 –
8 –
9 –

FLAGS

1 –
2 –

TO RECORD PROGRAM INSERT MAGNETIC CARD WITH SWITCH SET AT W/PRGM.

Bibliography

1. Adamson, A. W. and Myers, L. S., J. Amer. Chem. Soc., 69, p.2836 (1947).
2. Adhikari, M., J. Indian Chem. Soc., 38, p.817 (1961) and 45, p.95 (1968).
3. Anderson, D. M., Soil Science Soc. Amer., Proc., 30, p.670 (1966).
4. Anderson, D. M. and Low, P. F., Soil Science Soc. Amer., Proc., 22, p.99 (1958).
5. Anderson, L. A. and Keller, G. V., Geophysics, 29, p.848 (1953).
6. Armstrong, R. D., J. Electroanal. Chem., 40, p.437 (1972).
7. Armstrong, R. D., Eyre, D., Race, W. P. and Ince, A., J. Applied Electrochem., 1, p.179 (1971).
8. Armstrong, R. D., Firman, R. E. and Thirsk, H. R., Electrochim. Acta., 18, p.927 (1973).
9. Armstrong, R. D. and Henderson, M., J. Electroanal. Chem., 39, p.81 (1972).
10. Armstrong, R. D., Race, W. P. and Thirsk, H. R., Electrochim. Acta., 13, p.215 (1968).
11. Arulanandan, K. and Mitchell, J. K., J. Soil Mech. and Foundations Div., Proc. Amer. Soc. Civil Eng., 94, p.447 (1968).
12. Arulanandan, K. and Smith, S. S., J. Soil Mech. and Foundations Div., Proc. Amer. Soc. Civil Eng., 99, p.1113 (1973).
13. Banwell, C. J. and MacDonald, W.J.P., 8th Commonwealth Mining and Metallurgical Congress, Aust. and N.Z., (1965), Paper No.213.

13a. Barclay, L., Harrington, R. H. and Ottewill, R. H., Kolloid Z. u. Z. Polymere, 250, p.655 (1972).

14. Barker, G. C., J. Pure and Aqplied Chem., 15, p.239 (1967).
15. Baumann, W. C. and Eichorn, J., J. Amer. Chem. Soc., 69, p.2830 (1947).
16. Beaumont, J. H. and Jacobs, P.W.M., J. Phys. Chem. Solids, 28, p.657 (1967).
17. Beers, Y., "The Theory of Error", Addison-Wesley Pub. Co., Mass. U.S.A. (1962).
18. Bentz, A. J., Sandifer, J. R. and Buck, R. P., Anal. Chem., 46, p.543 (1974).
19. Berberian, J. G. and Cole, R. H., Rev. Sci. Instrum., 40, p.811 (1969).
20. Bhattacharya, B. M., Geophysics, 22, p.905 (1957).
21. Bio Rad Laboratories, Richmond, California, U.S.A., "Ion Exchange Resin Catalogue", (1968, 1972).

22. Bleil, D. F., Geophysics, 18, p.636 (1953).

23. Borisov, N. P. and Gnusin, N. P ., Russian Journal of Phys. Chem., 48, p.2396 (1974).

24. Bose, S. J., J. Indian Chem. Soc. 37, p.465 (1960).

25. Boyd, G. E., Adamson, A. W. and Myers, L. S., J. Amer. Chem. Soc., 69, p.2840 (1947).

26. Boyd, G. E., Myers, L. S. and Adamson, A. W., J. Amer. Chem. Soc., 69, p.2854 (1947).

27. Boyd, G. E., Schubert, J. and Adamson, A. W., J. Amer. Chem. Soc., 69, p.2818 (1947).

28. Bradley, W. F., Clark, G. F. and Grim, R. E., Z. Krist., 97, p.216 (1937).

29. Bradley, W. F. and Grim, R. E., J. Phys. and Colloid Chem., 52, p.1404 (1948).

30. Brand, M.J.D. and Rechnitz, G. A., Anal. Chem., 41, p.1185 (1969).

31. Brand, M.J.D. and Rechnitz, G. A., Anal. Chem., 41, p.1788 (1969).

32. Brand, M.J.D. and Rechnitz, G. A., Anal. Chem., 42, p.304 (1970).

33. Brant, A. A., in "Overvoltage Research and Geophysical Applications", J. R. Wait, Ed., Pergamon Press (1959).

34. Brookdeal Electronics, "Signal Source type 741, Instruction Manual", Berkshire, England.

35. Brookdeal Electronics, "Phase Sensitive Detector type 9412, Instruction Manual", Berkshire, England.

36. Brown, A. S. and MacInnes, D. A., J. Amer. Chem. Soc., 57, p.1356 (1935).

37. Buck, R. P., J. Electroanal. Chem., 18, p.363 (1968).

38. Buck, R. P., J. Electroanal. Chem., 18, p.381 (1968).

39. Buck, R. P. and Krull, I., J. Electroanal. Chem., 18, p.387 (1968).

40. Caspari, W. A., Z. Physik. Chem., 30, p.89 (1899).

41. Clarkson, T. S., Ph.D. Thesis, Victoria Univ., Wellington, New Zealand (1972).

42. Cole, K. S., J. Gen. Physiol., 15, p.641 (1932).

43. Cole, K. S. and Curtis, H. J., J. Gen. Physiol., 22, p.649 (1939).

44. Cole, K. S. and Baker, R. F., J. Gen. Physiol., 24, p.535 (1941).

45. Cole, K. S. and Curtis, H. J., J. Gen. P-ysiol., 24, p.551 (1941).

46. Cole, K. S. and Cole, R. H., J. Chem. Phys., 9, p.341 (1941).

47. Cole, K. S. and Guttman, R. M., J. Gen. Physiol., 25, p.765 (1941).

48. Cole, R. H., J. Chem. Phys., 23, p.493 (1955).

49. Collett, L. S., in "Overvoltage Research and Geophysical Applications", J. R. Wait, Ed., Pergamon Press (1959).

50. Conway, B. E., "Theory and Principles of Electrode Processes", Ronald Press, New York (1965).

51. Cremers, A. and Laudelot, H., Soil Science Soc. Amer. Proc., 30, p.570 (1966).

52. Cremers, A., Van Loon, J. and Laudelot, H., Clays Clay Miner. (14th Conf.), p.149 (1966).

53. Cremers, A. and Thomas, H. C., J. Phys. Chem. 70, p.3229 (1966).

54. Cremers, A., Israel Journal of Chem., 6, p.195 (1968).

55. Dakhnov, V. N., Latyshova, M. G. and Ryopalova, V. A., Promyslovaya Geofizika, p.46 (1952).

56. Dakshinamurti, C., Soil Science, 90, p.302 (1960).

57. Davies, J. T., Rideal, E. K., "Interfacial Phenomena", Academic Press, New York (1961).

58. Davies, M., Quarterly Reviews, 8, p.250 (1954).

59. Debye, P. "Polar Molecules", Dover Publications, New York (1929).

60. Derjaguin, B. V., Kryolov, N. A. and Novik, V. F., Dokl. Phys. Chem., 193, p.501 (1970).

61. Department of Scientific and Industrial Research, Lower Hutt, New Zealand, Unpublished Report.

62. Dobrin, M. B., "Geophysical Prospecting" McGraw Hill, 2nd Edition (1960).

63. Doremus, R. H., J. Phys. Chem., 68, p.2212 (1964).

64. Dukhin, S. S. in "Surface and Colloid Chemistry", E. Matijevic, Ed.

65. Eisenmann, G., "Membranes" Volume 1, Marcell Dekker, New York (1972).

66. Eckfeldt, E. L. and Perley, G. A., J. Electrochem. Soc., 98, p.37 (1951).

67. Epelboin, I. and Keddam, M., J. Electrochem. Soc., 117, p.1052 (1970).

68. Epelboin, I., Keddam, M. and Takenouti, H., J. Appl. Electrochem., 2, p.71 (1972).

69. Falkenhagen, H., "Electrolytes", Clarendon Press, Oxford (1934).

69a. Fellows, K. S., Ph.D. Thesis, Victoria University, Wellington, New Zealand (1971).

70. Foscolos, A. E., Soil Science Soc. Amer. Proc., 32, p.350 (1968), and 33, p.242 (1969).

71. Foster, E. J., I.E.E.E. Trans., AU-13, p.104 (1965).

72. Fraser, D. C., Keevil, N. B. and Ward, S. H., Geophysics, 29 p.832 (1964).

73. Fredricksberg, D. A. and Cidarov, M. P., Vestnik of the Leningrad Univ. Geophysics and Chem., 4 (1962).

74. Friauf, R. J., J. Chem. Phys., 22, p.1329 (1954).

75. Fricke, H. and Morse, S., J. Gen. Physiol., 9, p.153 (1925).

76. Fricke, H. and Curtis, H. J., J. Phys. Chem., 41, p.729 (1937).

77. Fripiat, J. J., Jelli, A., Poncelet, G. and André, J., J. Phys. Chem., 69, p.2185 (1965).

78. Frische, R. H. and Von Buttlar, H., Geophysics, 22, p.688 (1957).

79. Fritsch, V. V. and Tauber, A. F., Acta Hydrophysica, 14, p.79 (1968).

80. Fuller, B. D. and Ward, S. H., I.E.E.E. Trans. Geoscience Electronics, GE-8, p.7 (1970).

81. Gammell, P., Chemistry Dept., Purdue Univ., Indiana, U.S.A., Personal Communication.

82. Girard, P., Trans. Farad. Soc., 30, p.763 (1934).

83. Goldman, D. E., J. Gen. Physiol., 27, p.37 (1943).

84. Goodwin, R. H., Hearn, J., Ho, C. C. and Ottewill, R. H. Brit. Polymer J., 5, 347, (1973).

85. Grahame, D. C., J. Electrochem. Soc., 99, p.370 (1952).

86. Grim, R. E., "Clay Mineralogy", McGraw Hill, 2nd Edition (1968).

87. Grimshaw, R. W., "The Chemistry and Physics of Clays and Other Clay Minerals", Ernest Benn, London, 4th Edition (1971).

88. Hasted, J. B. and El Sabah, S.H.M., Trans. Farad. Soc., 49, p.1003 (1953).

89. Hatherton, T., MacDonald, W.J.P. and Thompson, G.E.K., Bulletin Volcanologique, 29, p.485 (1966).

90. Helfferich, F. and Plesset, M. S., J. Chem. Phys., 28, p.418 (1958).

91. Henkel, J. H. and Collins, T. C., Geophysics, 22, p.205 (1961).

92. Henkel, J. H. and Van Nostrand, R. C., A.I.M.E. Trans., 9, p.355 (1957).

93. Hewlett Packard, "Electronic Counter type 5245L-Instruction Manual", Calif., U.S.A. (1972).

94. Hewlett Packard, "H.P.65 Calculator - Stat. Pac. 1 Manual", Calif. U.S.A., (1974).

95. Higgins, T. J., Boesch, L. P., Volterra, V., Moynihan, C. T. and Macedo, P. B., J. Amer. Ceram. Soc., 56, p.334 (1973).

96. Höber, R., Arch. ges. Physiol., 133, p.237 (1910), and 148, p.129 (1912).

97. Howery, D. G. and Tada, S., J. Macromol. Sci. Chem., A3, p.297 (1969).

98. Ilani, A., Biophys. J., 8, p.556 (1968).

99. Ives, D.J.G. and Janz, G. J., "Reference Electrodes, Theory and Practice", Academic Press (1961).

100. Jenny, H., J. Phys. Chem., 36, p.2217 (1932), and 40, p.501 (1936).

101. Jenny, H., J. Colloid Science, 1, p.2 (1946), and 1, p.33 (1946).

102. Jones, G. and Bradshaw, B. C., J. Amer. Chem. Soc., 55, p.1780 (1953).

103. Keller, G. V., U.S. Geological Survey Bulletins 1052-J (1959), and 1083-D (1960).

104. Keller, G. V. and Licastro, P. H., U.S. Geological Survey Bulletin 1052-H (1959).

105. Keller, G. V., Canadian Geological Survey, Economic Reports, 26, p.51 (1967).

106. Keller, G. V. and Frischknecht, F. C.m "Electrical Methods in Geophysical Prospecting", Pitman Press (1970).

107. Kelley, W. P., "Cation Exchange in Soils", Rheingold, New York (1948).

108. Kelley, W. P. and Jenny, H., Soil Science, 41, p.367 (1936).

109. Kemper, W. D., Soil Science Soc. Amer. Proc., 24, p.10 (1960).

110. Kemper, W. D., Maasland, D.E.L. and Porter, L. K., Soil Science Amer., Proc., 28, p.164 (1964).

111. Kotera, A., Furasawa, K. and Takeda, Y., Kolloid Z.u.Z. Polymere, 239, p.677 (1970).

112. Kressman, T.R.E. and Kitchener, J. A., Disc. Farad. Soc., 7, p.90 (1949).

113. Kunin, R. and Myers, R. J., "Ion Exchange Resins", John Wiley (1950).

114. Lakshminarayanaiah, N., "Transport Phenomena in Membranes", Academic Press (1969).

115. Low, P. F., Soil Science Amer., Proc., 22, p.395 (1958).

116. Low, P. F., Clays Clay Miner., 9, p.219 (1962).

117. Low, P. F., Clays Clay Miner., 8, p.170 (1960).

118. MacDonald, J. R., J. Chem. Phys., 36, p.345 (1962).

119. MacDonald, J. R., J. Chem. Phys., 54, p.2026 (1971).

120. MacDonald, J. R., J. Electroanal. Chem., 32, p.317 (1971).

121. Macedo, P. B., Moynihan, C. T. and Bose, R., Physics and Chemistry of Glasses, 13, p.171 (1972).

122. Mackey, M. C., Biophys. J., 11, p.75 (1971).

123. MacLeod, H. J., Phys. Rev., 21, p.53 (1923).

124. Mandel, P., Berg, J. W. and Cook, K. L., Geophysics 22, p.398 (1957).

125. Marshall, C. E. and Ayers, A. D., Soil Science Soc. Amer., Proc. 7, p.171 (1946).

126. Marshall, C. E., and Ayers, A. D., Soil Science Soc. Amer., Proc., 7, p.171 (1946).

127. Marshall, D. J., Fahlquist, D. A., Neves, A. S., Madden, T. R., U.S. Atomic Energy Commission RME-3156 (1958).

128. Madden, T. R. and Marshall, D. J. U.S. Atomic Energy Commission RME-3156 (1958).

129. Madden, T. R. and Marshall, D. J., U.S. Atomic Energy Commission RME-3157 (1959).

130. Madden, T. R. and Marshall, D. J., U.S. Atomic Energy Commission RME-3160 (1959).

131. Marshall, D. J. and Madden, T. R., Geophysics, 24, p.790 (1959).

132. Mauro, A., Biophys. J., 2, p.179 (1962).

133. Mattson, S., Soil Science, 33, p.41 (1932), and 49, p.109 (1940).

134. Mayper, V., in "Overvoltage Research and Geophysical Applications", J. R. Wait, Ed., Pergamon Press (1959).

135. McCardell, W. M. and Winsauer, W. O., A.I.M.M.E. Trans., 198, p.41 (1953).

136. McKelvey, J. G., Southwick, P. F., Spiegler, K. S. and Wylie, M.R.J., Geophysics, 20, p.913 (1955).

137. McKubre, M.C.H., M.Sc. Thesis, Victoria Univ., Wellington, New Zealand (1972).

138. Meares, P., Thain, J. F. and Dawson, D. G., in "Membranes" Vol. 1, G. Eisenmann, Ed., Marcel Dekker, New York (1972).

139. Mehran, M., Ph.D. Thesis, University of California, Davis, Calif., U.S.A., (1971).

140. Mering, J., Trans. Farad. Soc., 42B, p.205 (1946).

141. Mering, J. and Glaeser, R., Bull. Soc. Franc. Mineral. 77, p.519 (1954).

142. Mitra, R. P., Bagchi, S. N. and Ray, S. P., J. Phys. Chem., 47, p.549 (1943).

143. Mohomed, S. S., Geophys. Prosp., 18, p.654 (1970).

144. Mondriniak, N. and Studt, F. E., New Zealand Journal of Geology and Geophysics, 2, p.654 (1959).

145. Mooney, R. W., Keenan, A. G. and Wood, L. A., J. Amer. Chem. Soc., 74, p.1367 (1952).

146. Morgan, S. O., Trans. Electrochem. Soc., 65, p.109 (1934).

147. Moynihan, C. T., Bressel, R. D. and Angell, C. A., J. Phys. Chem., 55, p.4414 (1971), and 76, p.3287 (1972).

148. Mukherjee, J. N., Chatterjee, B. and Ray, S. P., J. Colloid Science, 3, p.437 (1948).

149. Murphy, E. J., Trans. Electrochem. Soc., 65, p.309 (1934).

150. Myers, R. J., Advances in Colloid Science, 1, p.317 (1942).

151. Nachod, F. C., "Ion Exchange", Academic Press, New York, (1949).

152. Namikawa, H., J. Non-Crystalline Solids, 18, p.173 (1975).

153. Namikawa, H., Yogyo-Kyokai-Shi, 83, p.500 (1975).

154. National Semiconductor Corporation, "Linear Integrated Circuits", Calif., U.S.A., (1973).

155. Neumann, B. S. and Sansom, K. G., Clay Minerals, 9, p.231 (1971).

156. Nikolaev, N. I., Chuvileva, G. G. and Popova, G. I., Russian Journal of Phys. Chem., 49, p.1566 (1975).

157. Olsen, H. W., Proc. 9th National Clay Conf., p.131 (1962).

158. Ottewill, R. H. and Shaw, J. N., Kolloid Z. Z. Polym., 215, p.161 (1967), and 218, p.34 (1967).

159. Ottewill, R. H. and Shaw, J. N., J. Electroanal. Chem., 37, p.133 (1972).

160. Owen, B. B., J. Chim. Phys., 49, p. C72 (1952).

161. Owen, A. E. in "Progress in Ceramic Science" Volume 3, J. E. Burke, Ed. (1962).

162. Pain, B. K., and Mukherjee, S. K., J. Indian Chem. Soc., 46, p.341 (1969).

163. Parsons, R., Adv. in Electrochem. and Electrochem. Eng., 7, p.177 (1970).

164. Perkins, R., Brace, R. and Matijević, E., J. Colloid and Interface Science, 48, p.417 (1974).

165. Pilla, A. A., J. Electrochem. Soc., 117, p.467 (1970).

166. Princeton Applied Research, "Lock-In Amplifier, Model 129A", Instruction Manual (1975).

167. Provenzano, V., Boesch, L. P., Volterra, V., Moynihan, C. T. and Macedo, P. B., J. Amer. Ceram. Soc., 55, p.492 (1972).

168. Robinson, R. A. and Stokes, R. H., "Electrolyte Solutions", Butterworths Publications, 2nd Edition (1959).

169. Randles, J.E.B., Disc. Farad. Soc., 1, p.11 (1947).

170. Rosebrugh, T. R., and Miller, W.L., J. Phys. Chem., 14, p.816 (1910).

171. Resnick, R. and Halliday, D., "Physics", John Wiley, New York (1966).

172. Sandblom, J., in "Membranes" Volume 1, G. Eisenman, Ed., Marcell Dekker, New York (1972).

173. Sandifer, J. R. and Buck, R. P., J. Phys. Chem., 79, p.384 (1975).

174. Sata, T., Yamane, R. and Mizutani, Y., Bull. Chem. Soc. of Japan, 42, p.279 (1969).

175. Sauer, M. C., Southwick, P. F., Spiegler, K. S. and Wylie, M.R.J., Ind. and Eng. Chem., 47, p.2187 (1955).

176. Scheidegger, A. E., "The Physics of Flow Through Porous Media", University of Toronto Press (1957).

177. Schlumberger, C., "Etude sur la Prospection Electrique du Sous-Sol", Gauthier-Villars (1930).

178. Schofield, R. K. and Sampson, H. R., Disc. Farad. Soc., 18, p.135 (1954).

179. Schufle, J. A., Geophysics, 24, p.164 (1959).

180. Schwan, H. P., Schwarz, G., Maczuk, J. and Pauly, H., J. of Physics and Chem., 66, p.2636 (1962).

181. Scott, W. J. and West, G. F., Geophysics, 34, p.87 (1969).

182. Segal, J. R., J. Theoret. Biol., 14, p.11 (1967).

183. Siegel, H. O., Canadian Geological Survey, Economic Report, 26, p.123 (1967).

184. Smyth, C. P. and Hitchcock, C. S., J. Amer. Chem. Soc., 54, p.4631 (1932).

185. Spiegler, K. S., Yoest, R. L. and Wylie, M.R.J., Disc. Farad. Soc., 21, p.174 (1969).

185a. Spiegler, K. S. and Coryell, C. D., J. Phys. Chem., 57, p.687 (1953).

186. Stone, R. L., Inst. Mining Metallurgical and Petroleum Eng., Trans., 238, p.284 (1967).

187. Street, N., Aust. Journal Chem., 10, p.207 (1957), and 9, p.333 (1956).

188. Studt, F. E., N.Z. Journal of Science and Technology, 38, p.595 (1957).

189. Soldano, B. A. and Boyd, G. E., J. Amer. Chem. Soc., 75, p.6091 (1954).

190. Soldano, B. A. and Boyd, G. E., J. Amer. Chem. Soc., p.6099 (1953).

191. Soldano, B. A. and Soldano, B. A., J. Amer. Chem. Soc., p.6105 (1953).

192. Swartzen-Allen, S. L. and Matijević, E., Chem. Rev., 74, p.385 (1974).

193. Swartzen-Allen, S. L. and Matijević, E., J. Colloid and Int. Sci., 50, p.143 (1974).

194. Taylor, C. D., Victoria University, Wellington, New Zealand, "Preparation of Sintered Pyrex Glass Filters", Unpublished.

195. Teorell, T., Progr. in Biophys., 3, p.305 (1953), Ed. Butler and Randall, Pergamon, London.

196. Touret, C. and Vestier, D., Silicates Industrieles, 36, p.205 (1971).

197. Vacquier, V., Holmes, C. R., Kintzinger, P. R. and Lavergne, M., Geophysics, 22, p.660 (1957).

198. Van Leeuwan, H. P., Kooijman, D. J., Sluyters-Rehbach, M., Sluyters, J. H., J. Electroanal. Chem., 23, p.475 (1969).

199. Van Olphen, H., J. Phys. Chem., 61, p.1276 (1957).

200. Van Valkenburg, M. E., "Network Analysis", Prentice Hall (1964).

201. Vetter, K. J., "Electrochemical Kinetics", English Edition, Academic Press, New York (1964).

202. Vogel, A. I., "A Text-Book of Quantitative Inorganic Analysis", Longmanns, 3rd Edition (1966).

203. Von Hippel, A. R., "Dielectrics and Waves", John Wiley, New York (1954).

204. Wait, J. R., "Overvoltage Research and Geophysical Applications", Pergamon Press (1959).

205. Wagner, K. W., Annals de Physik., 40, p.817 (1913).

205a. Warburg, E., Wied. Ann., 67, p.493 (1899).

206. Weigner, G., Trans. 3rd International Cong. Soil Science, 3, p.5 (1936).

207. White, A. H. and Morgan, S. O., J. Frank. Inst., 216, p.635 (1933).

208. Winsauer, W. O. and McCardell, W. M., Petroleum Trans. A.I.M.E., 198, p.129 (1953).

209. Wright, D. P., Physics Department, Victoria Univ., Wellington, New Zealand, Personal Communication.

210. Wright, M. H. and James, A. M., Kolloid-Z. and Z. Polymere, 251, p.745 (1973).

211. Wyllie, M.R.J. and Patnode, H. W., Trans. A.I.M.E., 189, p.47 (1950).

212. Wyllie, M.R.J. and Southwick, P. F., J. Petrol. Tech., 6, p.44 (1954).

Acknowledgements

I gratefully acknowledge the assistance in particular of Professor J. W. Tomlinson and Professor F. F. Evison, for introducing me to the fields of Electrochemistry and Geophysics, and for their continuing assistance and encouragement throughout the course of this work.

I must also acknowledge my debt to the professionalism and friendship of C. D. Taylor, I. C. Crighton, J. D. Wells, C. Heath and C. A. Snell, each of whom contributed immeasurably to the experimental aspects of this work.

Thanks also to my colleagues Dr T. S. Clarkson, Dr H. Wong, D. P. Wright and B. G. Pound for their practical assistance and stimulating discussion, and to P. Mackey for illustrations in this thesis and for his scientific encouragement.

Each of the above has contributed much in valuable discussion.

The bridge chassis was constructed by K. Whalon in the Mechanical Workshops, Victoria University. Clays were generously supplied by,

J. Linzey, Crown Lynn Potteries Ltd, Auckland, New Zealand,
- Wyoming bentonite,

Dr B. S. Neumann, Laporte Industries Ltd, Redhill, Surrey, England,
- laponite,

and, samples and suggestions for the preparation of latices, by Professor R. H. Ottewill, University of Bristol, England.

I wish to thank M. D. King for the photographs used in this work, and C. G. McKubre for assistance with the lettering of Figures.